

UNIVERSITÀ DEGLI STUDI DI SALERNO

Dipartimento di Medicina, Chirurgia ed Odontoiatria



Dottorato di Ricerca in
Medicina Traslazionale dello Sviluppo e dell'Invecchiamento Attivo
XXXIII ciclo

Curriculum: Tecnologie Innovative in Medicina Traslazionale

Tesi di Dottorato

DEVELOPMENT OF A BIOENGINEERED THREE-DIMENSIONAL SCAFFOLD ABLE TO COMMIT STEM CELLS TOWARD TENOGENIC PHENOTYPE

Coordinatore:

Ch.mo Prof. Palmiero Monteleone

Tutors:

Ch.mi Proff. Nicola Maffulli, Giovanna Della Porta

Candidato/a:

Maria Camilla Ciardulli

Matricola:

8800900027

Anno Accademico 2020/2021

*“Now this is not the end.
It is not even the beginning of the end.
But it is, perhaps, the end of the beginning.”*

Winston Churchill

Abstract

The term tendinopathy is a generic descriptor of tendon disorders. Spontaneous adult tendon healing results in scar tissue formation and fibrosis, with impaired biological and mechanical properties. Adult tendons have a limited natural healing capacity, and often respond poorly to current treatments, including exercise, drug delivery and surgical procedures. To treat tendon diseases and support tendon regeneration, cell-based therapy and tissue engineering approaches are considered options. None can however yet be considered conclusive in their restoration of a safe and successful long-term solution for full microarchitecture and biomechanical tissue recovery.

This thesis describes the work to develop an innovative bioengineered multiphasic three-dimensional scaffold, seeking to reproduce the complex microenvironment able to support tenogenic differentiation. Mesenchymal stem cells derived from human bone marrow (hBM-MSCs) are one of the main stem cells sources used in tissue-engineering protocols while extra-embryonic cord-derived, including from Wharton's Jelly (hWJ-MSCs), are emerging as useful alternatives.

To explore the tenogenic plasticity of hBM-MSCs and hWJ-MSCs, we first conducted a pilot study treating both cell types with different doses of human Growth Differentiation Factor-5 (hGDF-5), a growth factor which induces tenogenic differentiation, improving the outcome of tendon repair. hGDF-5 induced the expression of genes (SCX-A, COL1A1, TNC, DCN, TNMD) and proteins (type I collagen, tenomodulin) linked to the neo-tendon phenotype in a time and concentration-dependent manner. The concentration of 100 ng/mL was the most effective for both stem cells types, coupled with specific alignment and shape modification. However, compared to hBM-MSCs, hWJ-MSCs showed higher proliferation rate and earlier up-regulation of tenogenic markers. Since the modulation of the inflammatory response is reported to be necessary in tendon healing and regeneration, we analyzed the gene expression of pro-

inflammatory (IL-6, TNF, IL-12A, IL-1 β) and anti-inflammatory (IL-10, TGF- β 1) cytokines, observing an anti-inflammatory immunomodulatory response of both stem cells, related to their tenogenic commitment.

In a following study, we focused on a three-dimensional (3D) scaffold, which we named HY-FIB, incorporating a force-transmission band of braided hyaluronate embedded in a cell localizing fibrin hydrogel and poly-lactic-co-glycolic acid (PLGA) nanocarriers as transient components for growth factor controlled delivery. The tenogenic supporting capacity of HY-FIB on hBM-MSCs was explored under static conditions and under bioreactor induced cyclic strain conditions. Mechanical signaling, conveyed by HY-FIB to hBM-MSCs, promoted upregulation of tendon related genes (SCX-A, COL1A1, DCN) and proteins (type I collagen). Cells also showed pro-inflammatory (IL-6, TNF, IL-12A, IL-1 β) and anti-inflammatory (IL-10, TGF- β 1) cytokine gene expressions, with a significant increase of anti-inflammatory ones in dynamic conditions.

Since these results provided strong evidence in support of the HY-FIB system and its interaction with cells, we enhanced the system fabricating PLGA nanocarriers, engineered to ensure a controlled delivery of hGDF-5.

PLGA nanocarriers, with controlled size and suitable encapsulation efficiency, were produced using Supercritical Emulsion Extraction (SEE) technology and were added to the fibrin hydrogel to provide a controlled growth factor delivery. The effect of biochemical and mechanical stimuli was studied on hWJ-MSCs, showing a significantly increased expression of tenogenic markers.

The described approach opened exciting perspectives for future development of engineered tendon tissue substitutes. HY-FIB was an excellent system for the sustained release of biochemical signals and a strategic approach to develop *in vitro* 3D bioengineered models to understand specific behaviour of tendon healing and regeneration.

Contents

| | |
|--|----|
| <i>Chapter 1. Introduction: Going toward tendon tissue engineering strategies: the need of innovative solutions to support tendon regeneration</i> | 1 |
| 1.1 Tendon structure | 2 |
| 1.1.1 Tendon cells..... | 3 |
| 1.1.2 Tendon components..... | 4 |
| 1.1.3 Tendon vasculature..... | 5 |
| 1.1.4 Tendon innervation..... | 5 |
| 1.2 Tendon function..... | 6 |
| 1.3 Tendon biology..... | 9 |
| 1.4 The role of inflammation in tendon healing and regeneration | 10 |
| 1.5 Stem cells in tendon tissue engineering..... | 11 |
| 1.6 The role of BMPs | 14 |
| 1.7 Biomaterials for scaffolds fabrication | 15 |
| 1.7.1 Fibrin hydrogels: versatile scaffolds in tendon tissue engineering..... | 17 |
| 1.8 Mechanical stimuli and bioreactors | 18 |
| 1.9 The importance of combined <i>in vitro</i> studies in tendon tissue engineering | 21 |
| <i>Chapter 2. A pilot study to explore the tenogenic responsiveness of hBM-MSCs and hWJ-MSCs to hGDF-5</i> | 23 |
| 2.1 Introduction | 24 |
| 2.2 Aim | 26 |
| 2.3 Materials and Methods | 26 |
| 2.3.1 hBM-MSCs Isolation and Harvesting | 26 |
| 2.3.2 hWJ-MSCs Isolation and Harvesting | 27 |
| 2.3.3 Flow cytometry..... | 27 |
| 2.3.4 hGDF-5 treatment..... | 28 |
| 2.3.5 mRNA isolation and gene expression profiles | 28 |
| 2.3.6 Morphometric and proliferation analysis | 29 |
| 2.3.7 Immunofluorescence assay..... | 29 |
| 2.3.8 Statistical analysis..... | 30 |
| 2.4 Results | 30 |
| 2.4.1 Flow cytometry characterization of hBM-MSCs and hWJ-MSCs..... | 30 |

| | |
|---|-----------|
| 2.4.2 Effect of hGDF-5 on cells proliferation and morphology | 31 |
| 2.4.3 Gene expression of tenogenic markers | 34 |
| 2.4.4 Expression of COL1A1 and TNMD proteins | 36 |
| 2.4.5 Cells immunomodulatory activity | 38 |
| 2.5 Discussion..... | 39 |
| 2.6 Conclusions | 42 |
| <i>Chapter 3. Fabrication and Characterization of PLGA-NCs for hGDF-5 controlled delivery</i> | <i>43</i> |
| 3.1 Introduction | 44 |
| 3.2 Aim | 48 |
| 3.3 Materials and Methods | 48 |
| 3.3.1 Emulsions preparation | 48 |
| 3.3.2 Dense gas technology protocol..... | 49 |
| 3.3.3 Morphological and size distribution analysis | 50 |
| 3.3.4 GDF-5 release study and encapsulation efficiency | 51 |
| 3.3.5 Cells isolation and harvesting..... | 51 |
| 3.3.6 Cytotoxic activity | 52 |
| 3.4 Results | 52 |
| 3.4.1 Emulsion formulation optimization..... | 52 |
| 3.4.2 Release profile study | 54 |
| 3.4.3 Cytotoxicity studies on CHO-K1 and hPBMCs..... | 54 |
| 3.5 Discussion..... | 56 |
| 3.6 Conclusions | 58 |
| <i>Chapter 4. Development of HY-FIB 3D scaffold: effect of the mechanical signaling on the tenogenic commitment of hBM-MSCs</i> | <i>59</i> |
| 4.1 Introduction | 60 |
| 4.2 Aim | 61 |
| 4.3 Materials and Methods | 62 |
| 4.3.1 hBM-MSCs isolation and harvesting | 62 |
| 4.3.2 ihGDF-5 effect on hBM-MSCs | 62 |
| 4.3.3 Immunofluorescence and Immunohistochemical assays..... | 63 |
| 4.3.4 RNA isolation and gene expression profiles by qRT-PCR | 63 |
| 4.3.5 HY-FIB preparation and characterization | 64 |

| | |
|---|-----------|
| 4.3.6 Dynamic culture | 65 |
| 4.3.7 Statistical analysis..... | 65 |
| 4.4 Results | 65 |
| 4.4.1 Effect of ihGDF-5 on tenogenic commitment and immunomodulatory activity of hBM-MSCs | 65 |
| 4.4.2 Effect of ihGDF-5 on COL1A1 and COL3A1 proteins expression | 67 |
| 4.4.3 ihGDF-5 loaded PLGA-NCs | 68 |
| 4.4.4 hBM-MSCs cultivation in HY-FIB 3D microenvironment..... | 68 |
| 4.4.5 Gene expression profiles of tenogenic markers..... | 70 |
| 4.4.6 hBM-MSCs immunomodulatory activity | 72 |
| 4.4.7 Histological characterization of HY-FIB | 74 |
| 4.4.8 COL1A1 protein expression in dynamic culture | 74 |
| 4.5 Discussion..... | 75 |
| 4.6 Conclusions | 78 |
| <i>Chapter 5. Study of the effect of biochemical and mechanical stimuli on the tenogenic commitment of hWJ-MSCs</i> | <i>80</i> |
| 5.1 Introduction | 81 |
| 5.2 Aim | 82 |
| 5.3 Materials and Methods | 83 |
| 5.3.1 hWJ-MSCs isolation and harvesting | 83 |
| 5.3.2 Flow cytometry and gating strategy | 84 |
| 5.3.3 3D system preparation and characterization..... | 84 |
| 5.3.4 Cyclic strain bioreactor for dynamic culture and cytotoxicity | 85 |
| 5.3.5 Gene expression profiles by qRT-PCR | 86 |
| 5.3.6 Immunohistochemical assay..... | 87 |
| 5.3.7 Statistical analysis..... | 87 |
| 5.4 Results | 87 |
| 5.4.1 Cytotoxicity of 3D printed cyclic strain bioreactor elements..... | 87 |
| 5.4.2 3D scaffold assembly and its mechanical characterization | 88 |
| 5.4.3 Biomimetic system in dynamic culture coupled to hGDF-5 in the external medium | 92 |
| 5.4.4 Biomimetic system in dynamic culture coupled to hGDF-5 controlled delivery | 94 |

| | |
|---|------------|
| 5.4.5 hWJ-MSCs immunomodulatory activity within the biomimetic system | 96 |
| 5.5 Discussion..... | 97 |
| 5.6 Conclusions | 99 |
| <i>Chapter 6. Conclusions and future perspectives</i> | <i>100</i> |
| <i>References</i> | <i>102</i> |
| <i>Figures</i> | <i>125</i> |
| <i>Tables</i> | <i>126</i> |
| <i>Abbreviations</i> | <i>127</i> |
| <i>Publications in International Peer Review Journals</i> | <i>130</i> |
| <i>Book chapters.....</i> | <i>131</i> |
| <i>Oral presentations at International Conferences</i> | <i>131</i> |
| <i>Poster presentations at International Conferences</i> | <i>132</i> |
| <i>Awards</i> | <i>132</i> |
| <i>Acknowledgements.....</i> | <i>133</i> |

Chapter 1

Introduction

Going toward tendon tissue engineering strategies: the need of innovative solutions to support tendon regeneration

1.1 Tendon structure

Tendons are fibro-elastic structures that connect muscles to bones or other musculoskeletal structures, have a high resistance to mechanical loads, and allow the conduction, distribution, and modulation of the force exerted by the muscles to the structures to which they are connected. The area of union with the muscle is the myotendinous junction, whereas the area of union with the bone is the osteotendinous junction or enthesis¹.

Tendons are surrounded by a loose connective tissue called paratenon, whose main components are type I and type III collagen fibrils, elastic fibrils, and synovial cells lining the inner surface of the paratenon. The paratenon is elastic, and allows free movement of the tendon within the surrounding tissues. The epitenon is a thin connective tissue sheath that surrounds the entire tendon below the paratenon. The paratenon and epitenon together are often defined as the peritendon. The epitenon on its inner surface is in contact with the endotenon, which wraps around the collagen fibers themselves. The epitenon and the endotenon contain the vascular, lymphatic, and nervous structures².

Tendons are composed of millions of fascicles, which consist of twisted bundles of collagen fibrils, whose number and thickness determines the final size of the tendon. This organization provides resistance against the tensile stresses produced by muscles. Microscopically, in healthy tendons, closely packed collagen fibers are assembled with cells within a well-ordered extracellular matrix (ECM). Collagen is the major component (60% to 85% of the dry weight) of the ECM, type I collagen being the most abundant and responsible for the fibrous structure of tendons².

Collagen molecules are arranged in a hierarchical manner and are alternated with the ground substance, a less fibrous and highly hydrated matrix³ (Figure 1-1). Type I collagen molecules aggregate to form collagen fibrils, the basic nanostructural tendon unit. In particular, the soluble form of tropocollagen molecules crosslinks to produce insoluble collagen molecules that gradually aggregate into defined units, which are clearly visible at electron microscopy and referred to as collagen fibrils. Bundles of fibrils form fibers, which become fiber groups, which then form bundles or fascicles. Collagen fascicles are aligned in the direction of force application⁴.

The complexity of a tendon structure is very important, as its basic function is to transmit the force produced by the muscle to the bone to make joint movement possible. During the various stages of movement, tendons are exposed to longitudinal, transverse, and rotational forces. In addition, they must be able to withstand direct contusion and compression. The three-dimensional internal structure of the fibers forms a buffer system against the forces of various directions and thus prevents damage and breakage of the fibers. The alteration of the physical forces, that influence a tendon increasing or reducing stress or compressive loads, induces a marked and predictable change in the tendon composition and structure. In general, stress segments exhibit greater responsiveness and regeneration than pressure areas⁵.

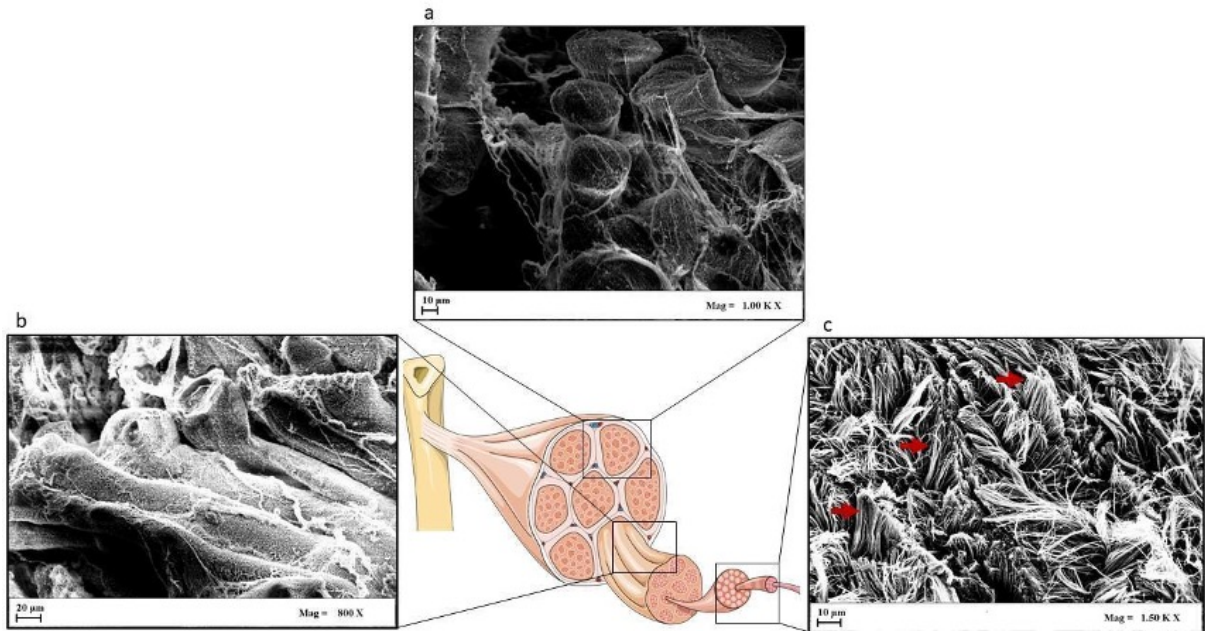


Figure 1-1. Hierarchical arrangement of the structure of tendons. (a) Field Emission-Scanning Electron Microscopy (FE-SEM) of a transverse section of collagen fiber bundles (scale bar = 10 μm); (b) FE-SEM image of longitudinal collagen bundles in which their parallel arrangement along the longitudinal axis of the tendon is clearly shown; each collagen bundle is surrounded by the endotenon (scale bar = 20 μm); (c) SEM image that shows the multiple collagen fiber bundles that make up the tendon. The sample has been cross-sectioned, but it is clearly evident the parallel orientation of the collagen fibers (red arrows) (scale bar = 10 μm). Tendon images were obtained by FE-SEM microscope (mod. LEO 1525; Carl Zeiss, Oberkochen, Germany). Samples were fixed in 4% paraformaldehyde (PFA), dehydrated with critical point dryer (mod. K850 Emitech, Assing, Rome, Italy), and sectioned before being coated with a gold (250 \AA thickness) using a sputter coater (mod.108 \AA ; Agar Scientific, Stansted, UK).

1.1.1 Tendon cells

Tendon cells, which are localized in the tendons ECM, are key players in growth, maintenance, ECM synthesis and turnover, homeostasis and remodeling. Mature tendons contain predominantly tenocytes and tenoblasts, which account for around 90–95% of the cell population⁶. There is no specific marker for these cells and the terms simply refer to cells of different shapes⁷.

Tenocytes are spindle-shaped, fibroblast-like cells with elongated nuclei and a thin cytoplasm that form a complex network of cytoplasmic processes that link adjacent cells via gap junctions^{8,9}. Gap junction communication is essential to form networks amongst tenocytes so that they can exchange ions and small molecules (<1 kDa), ensuring electrical coupling¹⁰ and facilitating the diffusion of signaling and nutrients in this poorly vascularized tissue¹¹. Gap junction communication in tendons allows also the coordination of synthetic responses to mechanical stimuli (i.e., mechanotransduction). Tenocytes are terminally differentiated cells typically anchored to the collagen fibers¹². The resident tenocytes finely regulate the anabolic and catabolic processes taking place in the

extracellular matrix, and they mediate tendon repair by a complex modulation of tendon homeostasis¹³.

Tenoblasts are relatively round cells with larger ovoid nuclei contained mainly in the endotenon⁷. They are immature tendon cells that give rise to tenocytes. Tenoblasts are dominant in young tendons and they transform into tenocytes during maturation and aging¹⁴.

Tendon stem/progenitor cells (TSPCs) have been recently characterized in tendon tissue of several species^{15,16,17,18}. TSPCs represent 1–4% of tendon resident cells, they mainly reside in the epitenon and exhibit the same characteristics as adult mesenchymal stem cells (MSCs)¹⁸. Their number and self-renewal potential decrease with age¹⁹. This could explain the low ability of adult tendons to spontaneous healing.

1.1.2 Tendon components

Tendons are fibrous connective tissues mainly formed by collagen fibers, which determine mechanical and physiological properties, and elastin fibers, which give it elasticity²⁰. Collagen and elastin are immersed in a matrix of proteoglycans and water, where the collagen is 60% to 85% of the dry mass of the tendon, while the elastin is just 2%²⁰. Type I collagen is the predominant protein, with small amounts (about 5%) of type III and type V collagen, probably involved in fibrillogenesis^{21,22}.

The basic unit of type I collagen consists in tropocollagen, a protein made by three polypeptide chains that give rise to a right-handed triple helix. The alpha chains of collagen are characterized by a specific repeating triplet of amino acids: glycine, proline and 4-hydroxyproline. The glycine residue, every three positions, allows the spiraling of the chains, while the other two amino acids stabilize the helix through the formations of hydrogen bonds. The presence of hydroxylysine is also essential for the formation of intermolecular cross-links, which are responsible for the high tensile strength of collagen fibers²³. The hydroxylation of proline and lysine residues, of fundamental importance to stabilize the tendon structure, takes place through specific enzymes (hydroxylase) utilizing as a cofactor vitamin C, an essential micronutrient for the health of the tendon.

Elastin, the most abundant and core protein of elastic fibers, is an essential structural constituent of tendons responsible for maintaining structural integrity and elasticity during normal function, allowing the tissue to return to its original shape once subjected to tensile force or strain, without energy input, which is extremely important during regeneration²⁴. Elastin is composed of amino acids glycine, valine, alanine, and proline, which form the basic units of tropoelastin, and they are joined together by covalent bonds to give a strong and elastic structure²⁰. Elastogenesis, the process responsible for the formation of elastin, is physiologically reduced with aging²⁵. Consequently, elastin content is lowered,

which may contribute to increasing tendon stiffness, leading to a complete tendon regeneration failure²⁶.

The most abundant tendon non-fibrous proteins are proteoglycans, accounting for 1–5% of the tendon dry weight. They have a core protein attached to one or more polysaccharides, the glycosaminoglycans (GAGs), which are negatively charged and attract water into the tendon³. Decorin (DCN) is the most abundant proteoglycan and represents 80% of the total proteoglycan content. DCN plays an important role in fibrillogenesis during development and maturation²⁷. DCN also influences the mechanical properties of tendons, transferring the load to collagen fibrils and promoting sliding between fibrils^{3,28}.

Glycoproteins are glycosylated proteins that have a similar structure to proteoglycans. These structural proteins produce a “bridge” between the molecules present in the ECM and the cell component present in the same matrix^{29,20}. The most represented glycoprotein in tendons is cartilage oligomeric protein (COMP). The role of COMP is uncertain, as knockout mice did not show any tendon defect³⁰. Another glycoprotein present in tendons in low quantity is Tenascin-C (TNC). It may have a role in tendon elasticity, as it is present in the tendon regions subjected to high tensile forces, and its levels are modulated by mechanical stresses³¹.

1.1.3 Tendon vasculature

Tendons are vascularized, but less so than muscles and ligaments, and the level of vascularization depends on their structure and site. Nutrients can also reach tendons thanks to the diffusion of synovial fluid that provides a significant amount of nutrients for many tendons³². The tissues enclosing and surrounding the tendon provide cellular and vascular factors that are useful for healing and nutrition of the internal tissue. During development, tendons are supplied with a rich capillary network and have high cellular and metabolic activity^{8,33}. However, mature tendons are poorly vascularized³⁴. Blood vessels are generally arranged longitudinally within the tendon, passing around the collagen fiber bundles in the endotenon^{8,35}.

Angiogenesis is regulated by a series of growth factors and cytokines the role of which is not yet well identified in normal, injured, and healing tendons^{36,37}. Vascular endothelial growth factor (VEGF) plays the key role in tendon healing, as it is expressed in early stages of the healing process³⁶. VEGF is also a key element of homeostasis restoration during regeneration, and it contributes to the biomechanical properties of the ECM³⁸.

1.1.4 Tendon innervation

Tendon innervation involves the surrounding structures that comprehend paratenon, endotenon, and epitenon: tendons proper have non-innervation. Nerves in tendons are characterized by a low degree of myelinated nerves fast transmitting A α - and A β -fibers and by a higher degree of unmyelinated, slow

transmitting $A\gamma$, $A\delta$ -, B- and C-fibers³⁹. The $A\alpha$ - and $A\beta$ - nerve fibers mediate mechanoreception, while the $A\gamma$, $A\delta$ -, and C- nerve fibers are nociceptors. Nociceptors mediate deep tissue pain and hyperalgesia, which is responsible for the pain in tendinopathy. The autonomic nerves ending with B-fibers are mainly localized in the walls of small arteries, arterioles, capillaries, and post-capillary veins exerting vasomotor actions³⁹.

Indeed, the nervous system plays an important role in pain regulation, inflammation, and tendon homeostasis. This neuronal regulation in healthy and damaged tendons is mediated by three major groups of molecules, including opioids, neuroregulators, autonomous, and excitatory glutamatergic neurotransmitters, which act on cell proliferation, the expression of cytokines and growth factors, inflammation and immune responses³⁹. Substance P (SP) and calcitonin gene-related peptide (CGRP) are stimulators of cell proliferation and stem cells recruitment during tendon healing^{40,41}.

However, damaged tendons may exhibit excessive and prolonged presence of sensory and glutamatergic neurotransmitters. This suggests an association with inflammatory and hypertrophic responses of the tissue, followed by triggering of pain signaling and hyper-proliferative/degenerative events associated with tendinopathy [64]. In the future, pharmacotherapy and tissue engineering strategies selective for neuronal mediators and their receptors could be used as selective therapies for tendon disorders⁴².

1.2 Tendon function

The primary function of the tendon is to transfer the forces produced by muscle contraction to the skeleton, facilitating movement around joints and positioning the limbs, playing an important role in locomotion^{43,44}. For efficient function, tendons must be strong and stiff under uniaxial tension, but also they have to retain viscoelastic properties^{45,46}. Tendon composition and the hierarchical organization of structural molecules in the ECM impart these properties to the tendon tissue.

The correct orientation of collagen molecules within the fibrils is responsible for the high mechanical strength of the tendon. The fibrils are stabilized by chemical cross-links between collagen molecules^{47,48,49}. These cross-links are formed by lysyl-oxidases which exert their enzymatic activity on specific lysine and hydroxylysine residues at the ends of the collagen molecules in the telopeptide regions, increasing the mechanical strength of the collagen fibrils⁵⁰.

The mechanical behavior of collagen depends on the number and types of intramolecular and intermolecular bonds⁵¹. At rest, the collagen fibers and fibrils show a curled configuration⁵². The initial concave portion of the curve (“start”), where the tendon is brought to a 2% level of stress, represents the lowering of the curled model. Beyond this point, tendons are deformed into a linear fashion as a result of intramolecular sliding of collagen triple helices, and the fibers become more parallel. With a mechanical stress below 4%, tendons behave in an

elastic fashion, returning to their original length. When stress is above 4%, microscopic damage can occur. Micro stress damage ranging from 8% to 10% occurs within the fibrils with a molecular slip⁵³. X-ray diffraction studies show that elongation of collagen fibrils initially occur as a result of molecular elongation, but the space between the molecules increases with the increase in stress, resulting in slippage of the adjacent lateral molecules⁵⁴. After this, the full damage occurs rapidly, and the fibers quickly entangle on themselves.

The breaking strength of tendons is related to their thickness and collagen content. A tendon with an area of 1 cm² can support a weight of 500 - 1000 kg⁵⁴. Some tendons are energy-storing structures, since they have the supplementary role of managing energy expenditure^{43,55}. Compared to positional tendons (i.e. human anterior tibialis tendon), energy-storing tendons (i.e. human Achilles tendon) are more elastic and extensible. Indeed, being subjected to high strains, they are required to stretch and recoil, therefore the maximum percentage of their *in vivo* failure strain is higher⁵⁶. Elastin, which is abundant in the endotenon of energy-storing tendons, reduces in quantity and becomes more disorganized with aging²⁶.

Furthermore, tendon is a viscoelastic tissue, exhibiting viscous and elastic behaviors. The viscoelastic behavior of tendons^{53,57} depends on age and activity, and it derives from a network of interactions that involves collagenous proteins, water, collagens, and proteoglycans. The unloading curve of a viscoelastic material/tissue does not proceed along the loading curve, and the material/tissue will not return to its initial shape and dimension immediately upon the removal of the applied deformation. Considering this behavior, known as hysteresis, the area between the loading and unloading curve represents the amount of energy lost during the cycle. In viscoelastic materials, the hysteresis is considerable, and much energy is lost during loading. Hysteresis seems to derive from the reorganization of the multilevel fibers composite structure, with water movement through the tissue³.

Mechanical *in vitro* tests on tendons involve separate clamps to grip the isolated tendon sample, ensuring it firmly. The tendon is loaded along its longitudinal axis, and the force and displacement are recorded at a constant speed until the tissue fails. The mechanical response of tendons is described plotting the applied extension and the resulting force as a stress–strain curve. The stiffness of the samples is represented by the slope of the curve: for a stiffer tendon, a steeper gradient indicates greater forces to extend the sample⁵⁸.

In a typical stress–strain curve, three distinctive regions can be identified (Figure 1-2). First, there is a toe region that indicates the stretching out of the crimped pattern of the collagen fiber bundles, which is visible by polarized light microscopy. This crimped configuration, not observable under tension, acts as a buffer against fiber damage and reappears only when the stress stops and the stretched collagen bundles return to their resting state, thanks to the elastin fibers in the ECM⁵⁹. The toe region is followed by a linear region. The slope of this region is constant and represents the stiffness, or Young's modulus. At this

point, the collagen fiber bundles have no longer a crimped configuration. Lastly, there is a failure region where the collagen fibers fail, leading tendon tissue to rupture. Therefore, the mechanical characteristics of the collagen fibers are directly correlated to the mechanical properties of the tendon⁶⁰. With elongation to 4%, a series of stretches reproduce the stress–strain curve, but, when this limit is exceeded, the crimped configuration undergoes subsequent deformations not reproducing the original curve. At 8% elongation or greater, caused by acute stress, human tendon tissue ruptures¹⁶.

Tendon tissue is not isolated communicates with both bone (enthesis) and muscle (by means of the myotendinous junction). In these transition regions, the tissue composition, material properties, and strain distributions can vary⁶¹, often constituting the initiation sites of tendon injury, with following modifications in the cellular/matrix response⁶². The precise loading levels required for tendon repair and the exact level of stimulation (magnitude, frequency, and duration) required for tendon homeostasis remain unknown, but the comprehension of these aspects is essential to understand and try to define the mechanobiological stimuli required to induce anabolic activity or reduce catabolic activity in tendon tissue⁶³.

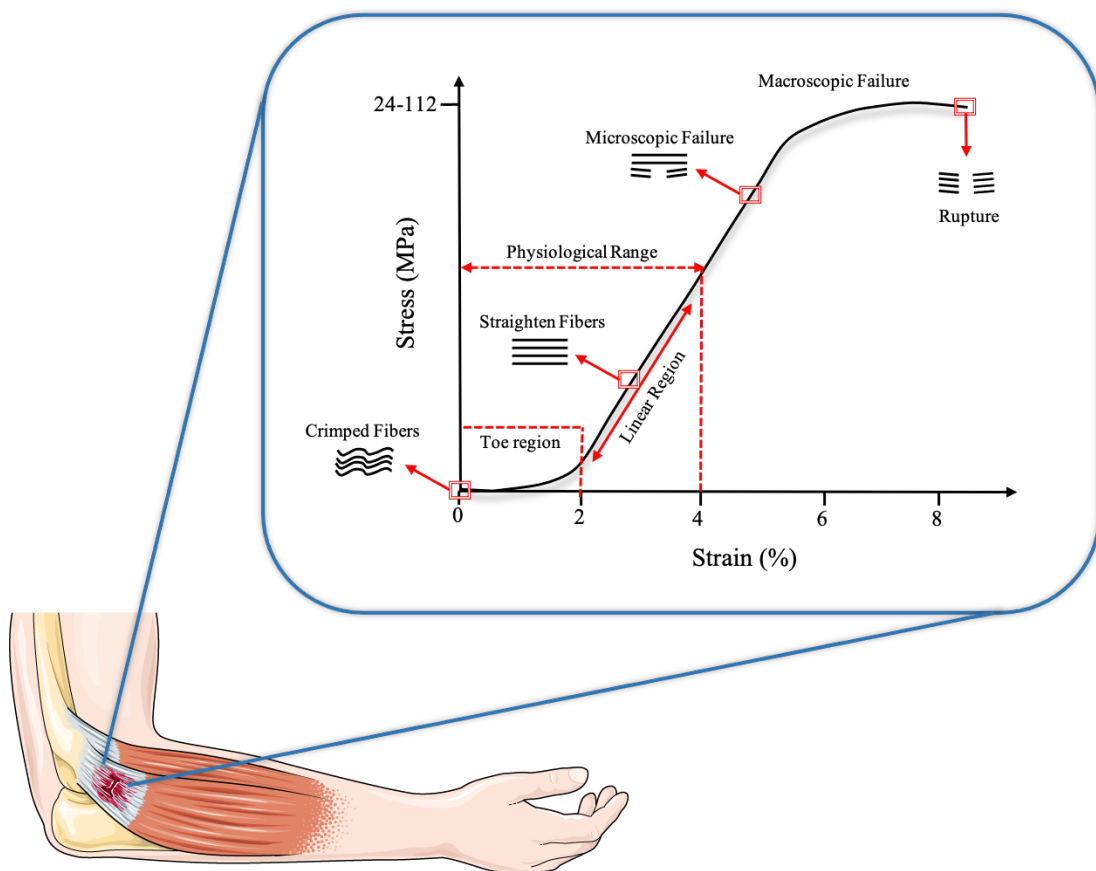


Figure 1-2. Typical stress–strain curve for tendon tissue. Schematics of the behavior of collagen fibers: under tensile strain, they stretch out absorbing shock. When the stimulus disappears, they return to their initial configuration. If the stretching limit is exceeded,

overcoming the physiological range, the tissue may suffer microscopic and macroscopic traumas. Adapted from Sensini *et al*⁶⁴.

1.3 Tendon biology

Tendon biology is essential to understand the mechanisms involved in tendon healing and differentiation.

Tendon formation occurs firstly with the appearance of progenitor cells and secondly with the commitment and differentiation as a consequence of a well ordained signaling cascade⁶⁵. Progenitor cells express the β helix–loop–helix transcription factor Scleraxis (SCX)^{66,67}, an early marker of tendon development and differentiation^{68,69}. Tendons differentiation combines the specialization of cellular compartment with the organization of the ECM, which is crucial to define tissue biomechanics properties such as elasticity and strength⁷⁰. ECM proteins deposition is led by the transcription factors.

In particular, SCX is involved in tendon ECM production, necessary for effective force transmission, triggering the transcription and the deposition of the structural collagens: collagen alpha-1(I) chain (COL1A1), collagen alpha-2(I) chain (COL1A2), collagen alpha-1(III) chain (COL3A1), and collagen alpha-1(XIV) chain (COL14A1)^{71,72}.

Early growth response 1 and 2 factors (Egr1/2) act as molecular sensors for mechanical signals⁷³ and are involved in collagen maturation and final tendon commitment^{74,75,76,77}. Both Egr1 and Egr2 are fundamental for tenocyte differentiation, regulating the tendon ECM and binding to tendon-specific enhancer elements of COL1A1 and COL1A2, which are also bound by SCX^{76,77,72}.

Recently, a new transcription factor, Mohawk (Mkx), was found to be responsible for the promotion of tendon lineage commitment and differentiation, influencing the expression of type I and XIV collagen^{74,78,79,80,81}.

A downstream signaling of Transforming Growth Factor- β (TGF- β), the protein kinase B-mammalian target of rapamycin (AKT–mTOR) axis, is essential for tenogenesis⁸². In addition to SCX, Egr1/2 and Mkx can function as transcriptional activators after the complexation with proteins receptors of TGF- β super-family Smad 2/3 to promote structural collagens and tendon late markers expression^{78,79}.

Mature tendons are characterized by the expression of Tenomodulin (TNMD) and Thrombospondin (THBS)⁸³. TNMD is the best-known mature marker for tendons^{84,85,86}; however, it has been found also in tendon progenitor cells, suggesting a role in tendon development⁸⁷. THBS is considered another late tendon marker⁸⁸; it plays a role in regulating ECM deposition and in the repair of myotendinous junction⁸⁹.

There are a series of pathological situations that affect tendons such as injury or tendinopathy⁶. Thanks to new technologies in proteomics, we know that when tendinopathy occurs, there are changes in the expression of many ECM tendon proteins^{6,90}.

TNC is an important component of the extracellular matrix, playing a role in collagen fibers orientation⁹¹. TNC is regulated by mechanic stimulation, and it is upregulated in the case of tendinopathy^{92,31,93}.

Glycoproteins, such as TBHS, play a role in tendon repair as they are highly expressed during tendon regeneration⁶. Proteoglycans enable the diffusion of water-soluble molecules and the migration of cells into areas of tendon injury. Type III collagen is overexpressed during repair, and it is replaced by type I collagen during post-injury remodeling⁹⁴. The ratio of type III to type I collagen can be used as an indicator of the tendon repair process⁹⁴.

Therefore, the transcription factors SCX, Egr1/2, Mxk, mTOR, and molecules TNMD, TBHS, TNC and type I and III collagen can be considered as the most important markers associated with tendons.

Tendon biology comprehends different factors that together produce a finely tuned balance which can be easily disrupted. Tissue engineering could be a solution to tendinopathy, because tendons are not able to fully repair themselves properly during aging or after injuries.

1.4 The role of inflammation in tendon healing and regeneration

The healing process is a prolonged and complex response of the host to injury and is crucial for the mechanisms of tissue regeneration⁹⁵. Because tendons possess a limited intrinsic regeneration capacity with low cellularity, low vascularization and poor innervation, their spontaneous healing results in healed tissues with impaired mechanical capabilities, fibrotic scarring and adhesion formation⁹⁶.

The mechanisms supporting tendon healing are still a subject of debate. Two mechanism of tendon healing are classically proposed: intrinsic and extrinsic. In intrinsic healing, tenocytes from the epitenon and endotenon migrate and proliferate into the site of injury, reorganizing the ECM and giving support to the internal vascular networking⁹⁷. Conversely, extrinsic healing is achieved by the invasion of cells from the surrounding sheath and synovium. Extrinsic healing is associated to greater scar formation and, consequently inferior biomechanics. Both intrinsic and extrinsic pathways are fundamental to the early stages of tendon healing⁹⁸.

The role of inflammation is a subject of debate. Several studies point a relation between inflammation and tendinopathy^{99,100,101,102}. Inflammation in itself may not be the cause of several tendinopathies, but the failure to resolve inflammation will likely contribute to tissue degeneration¹⁰³. Indeed, the tendon healing process typically includes three main phases: inflammation, proliferation and remodeling¹², all influenced by a temporally and spatially controlled array of mediators⁹⁶. The first phase is often rapid and characterized by the infiltration of inflammatory cells such as monocytes, macrophages, neutrophils and platelets. These cells release chemotactic factors that favor the migration and activation of tendon cells from nearby regions of the injury and from tendon

sheaths. In the next phase, tendon cells proliferate and produce a collagen rich ECM, re-establishing the alignment of tenocytes between collagen fibrils. Finally, during the remodeling phase, the ECM becomes more organized with axial arrangement of collagen fibers¹⁰⁴. The remodeling of the ECM is a crucial phase of tendon healing to regain biomechanical competence. Thus, inflammation is the physiological response to injuries and is part of tendon healing process. If the injury is not resolved, the response becomes chronic and pathologic. The magnitude and duration of the inflammatory response is adjusted by regulatory mechanisms at the injury site¹⁰⁵. Persistent inflammation contributes to scarred tendon healing and chronic matrix degradation^{99,106}. Scarred tissue results in poor rearrangement of collagen fibrils and separation of collagen bundles. Ruptures in collagen fibers may result in calcifications. Thus, modulation of the inflammatory response is necessary to restore and recover tendon function¹⁰⁷.

Cytokines constitute the major mediators of inflammatory response with a relevant role in cell signaling and communication, holding potent immunomodulatory properties. An endogenous expression of inflammatory cytokines, such as Tumor Necrosis Factor- α (TNF- α), Interleukin-1 β (IL-1 β), Interleukin-6 (IL-6), Interleukin-4 (IL-4) and Interleukin-10 (IL-10) has been demonstrated in human injured and healthy tenocytes^{108,109}. The biochemical profile within a tissue niche is of ultimate importance, as it can be indicative of homeostatic, inflammatory or pathological conditions. Thus, the biochemical relevance of soluble factors such as cytokines in tendon niches anticipates their application as therapeutic tools for repair and regeneration strategies.

The immunomodulatory action and trophic signaling on cytokine modulation are parameters to be taken in consideration in tendon tissue engineering studies. On the other hand, the crosstalk between inflammation cues and stem cells is important to elucidate the mechanisms of how stem cells respond to tissue damage. Growing evidence supports tendon stem cells, rather than tenocytes, as the main responsible for the healing response in acute injuries. Beyond the self-renewal capacity, proliferation and multilineage potential, stem cells are a secretory source of cytokines and growth factors with paracrine and autocrine activities. These soluble factors support the growth and differentiation of stem and progenitor cells, and have angiogenic, chemotactic, anti-apoptotic, anti-scarring or immunomodulatory activity¹¹⁰ in local environments. The secretion of a broad range of bioactive molecules with paracrine effects resulting from the dynamic communication between stem cells and niche environment is likely the main mechanism by which mesenchymal stem cells achieve their therapeutic effect¹¹⁰.

1.5 Stem cells in tendon tissue engineering

The first step in assessing an *in vitro* technique for tendon tissue engineering is the choice of the cell source. Different types of stem cells have been explored *in*

vitro to ascertain and quantify their capacity to differentiate into tenocytes for use in regenerative medicine. The literature generally describes the use of either tendon-derived stem cells, stem cells from fetal or adult origin, including embryonic stem cells, amniotic-derived stem cells, and mesenchymal stem cells from different tissue origins (bone marrow, adipose tissue). Many techniques have been used to induce tenogenic differentiation, but a validated protocol still does not exist¹¹¹.

Among pluripotent stem cells, both embryonic and induced pluripotent stem cells have been investigated. Embryonic stem cells (ESCs) could be suitable for tissue engineering because of their ability to differentiate into all tissues derived from the three germ layers¹¹². The proliferation capacity of ESCs is a clear advantage by providing sufficient cell numbers¹¹³.

The stepwise differentiation of human ESCs (hESCs) into tenocytes has been obtained through a mesenchymal transition stage. hESC-derived mesenchymal stem cells (hESC-MSCs), with fibroblast-like morphology, were induced to tendon differentiation with the combination of SCX overexpression and mechanical force stimulation. In particular, SCX overexpression led hESC-MSCs to a tenocyte commitment characterized by the expression of type I collagen and TNC^{114,115}. hESC-MSCs were also seeded onto a knitted silk-collagen sponge scaffold. When subjected to mechanical stimulation *in vitro*, hESC-MSCs exhibited tenocyte-like morphology and an expression of tendon-related gene markers such as type I and III collagen and SCX. When implanted *in vivo*, the engineered construct resulted in enhanced tendon regeneration *in situ* and superior mechanical performance characteristics¹¹⁶.

Induced pluripotent stem cells (iPSCs) can avoid the ethical concerns associated with hESCs^{117,118}. In principle iPSCs should have no biological difference to hESCs and should also be suitable for tenodifferentiative purposes, although to date, few studies have explored this^{119,120}.

Another category of stem cells includes fetal and adult multipotent stem cells derived from tendons or other systems. Fetal multipotent stem cells used to reproduce tenogenesis *in vitro* are amnion-derived and umbilical cord stem cells. Interestingly, these cells are emerging as a new resource for tissue engineering and regenerative medicine^{121,122}, since they marry remarkable plasticity with safety properties¹²¹.

Among amnion-derived stem cells, amniotic epithelial stem cells (AECs) are a relevant and promising resource for tissue engineering and regenerative medicine^{123,124}. They can be collected from human or animal amniotic membranes from the placenta as a discarded tissue with few ethical issues^{122,125}. Ovine AECs, by following a stepwise differentiation process, can develop a fully differentiated tendon phenotype. The protocol relied on exposing AECs to a co-culture microenvironment with ovine calcaneal fetal or adult tendon explant or tenocytes that resulted in AECs displaying a tenocyte morphology and a high level expression of tendon-related genes¹²⁶. AECs tenocyte differentiation was also tested on a poly(lactic-co-glycolyl) acid (PLGA)

electrospun tendon-mimetic scaffold. They displayed tenogenic markers expression (type I collagen and TNMD) after 28 days of culture¹²⁷.

Mesenchymal stem cells from the umbilical cord (UB) are also described as undergoing tenogenic differentiation when cultured with Bone Morphogenetic Protein-12 (BMP-12), resulting in the expression of Mx, COL1A1, SCX, TNMD and DCN at day 10 of culture¹²⁸.

Adult mesenchymal stem cells have a differentiation potential and paracrine effect playing a crucial role in their beneficial properties by promoting angiogenesis, stimulating local progenitor and mature cells, or regulating inflammation and immune cell functions¹²⁹.

Adult MSCs are mainly isolated from bone marrow (BM-MSCs) and adipose tissue (ADSCs).

BM-MSCs are the most widely used stem cell type. BM-MSCs are described as being tenocyte differentiation competent following exposure to growth factors, such as human Growth Differentiation Factor-5 (hGDF-5), and/or mechanical stimulation^{130,131,132}. However, BM-MSCs also have some limitations, such as painful harvesting procedures with frequently low cell yield, reduced MSCs quality with advanced donor age¹³³, ectopic ossification, and higher risk of adhesion formation when transplanted *in vivo*¹³⁴.

MSCs derived from adipose tissue (ADSCs) are attractive candidates given their easy isolation, multi-potentiality, and high responsiveness to distinct environment stimuli¹³⁵. The tenogenic ability of ADSCs has been shown when exposed to hGDF-5¹³⁶. Moreover, ADSCs seeded on a tropoelastin-coated biomimetic scaffold, after 21 days, showed an increased protein expression of tendon-related markers such as SCX and TNMD and were able to secrete extracellular matrix components such as type I and III collagen, TNC, and DCN¹³⁷.

Stem cells can also be genetically modified to either maintain a tenogenic phenotype or promote differentiation toward the tenogenic lineage¹³⁸. For example, hESCs transfected with SCX showed tenogenic commitment after mechanical stimulation. These cells expressed more TNMD gene expression and more ECM deposition compared to control cells or to those treated with only SCX overexpression or mechanical stimulation¹¹⁵.

Tendon-related somatic stem cells have created the possibility for tendons to use a pre-committed source of tissue specific stem/progenitor cells. Tendon progenitor stem cells (TSPCs) represent a particular category of multipotent stem cells with pro-tenogenic abilities. TSPCs express higher mRNA levels of tendon-related gene markers including the transcription factor SCX and the late differentiation factor TNMD¹³⁹. TSPCs spontaneously undergo tenocyte differentiation *in vitro*¹⁴⁰. However, as TSPCs are few, they need to be amplified *in vitro*, but their expansion leads to a loss of morphological characteristics^{141,142}.

Stem cells can be a solution to improve tendon healing and regeneration, but each of them have many advantages and disadvantages.

1.6 The role of BMPs

Growth Factors (GFs) involved in tenogenesis and able to control progenitor cell biology belong to a number of different families including Transforming Growth Factors β (TGF- β 1, TGF- β 2 and TGF- β 3), Bone Morphogenetic Proteins (BMPs: BMP-12, BMP-13 and BMP-14), Fibroblast Growth Factor (FGF-2), Vascular Endothelial Growth Factor (VEGF), Connective Tissue Growth Factor (CTGF), Platelet-Derived Growth Factor (PDGF), and Insulin-like Growth Factor 1 (IGF-1)^{143,144,145,146}. GFs with roles in driving regenerative and reparative tenogenesis are synthesized and secreted by a wide variety of cells. These include inflammatory cells, platelets, fibroblasts, epithelial cells, vascular endothelial cells, and tendon progenitor cells. The GFs released in response to tissue damage bind to external receptors on the cell membrane, leading to intracellular pathways involved in DNA synthesis and transcriptional expression directly affecting multiple cellular processes including proliferation, chemotaxis, matrix synthesis, and cell differentiation, all able to influence the healing cascade^{6,147}. In repair, tissue release of GFs is triggered, firstly, from the activated platelets straight after injury. This is followed by GF-driven initiation of the inflammatory cascade, recruiting inflammatory cells to the site of injury which, in turn, secrete additional GFs and amplify the inflammatory cascade. The stem/progenitor tendon cells next to the injury area are activated and themselves produce GFs. Further, mechanical loading placed on the injured tendon can further modulate GFs production and their paracrine release^{12,6,147,148}. This evidence seems to suggest that a physiological tendon-inductive microenvironment requires GFs over a specific temporal pattern and an optimized concentration^{6,143}.

Comparative studies of GFs teno-inductive capacity seem to suggest a central role of TGF- β superfamily GFs members. The TGF- β pathway is the most commonly recognized signaling pathway for tendon development¹⁴⁴. It is active in all stages of tendon healing, and its expression is upregulated in differentiated tendon cells^{149,146,150,151}. TGF- β induces extrinsic cell migration, regulates proteinases and cell proliferation, and stimulates collagen production. Moreover, its expression pathway in human tendons is crucial to tendon's adaptation to mechanical loading¹⁵².

BMP-12, -13, and -14 (also known as GDF-7, -6, and -5, respectively) are members of the TGF- β superfamily: each has individually been shown to play important roles in chemotaxis, proliferation, matrix synthesis, and cell differentiation¹⁵³. BMPs are elevated at the early stages of tendon healing and decrease gradually over time¹⁵⁴. The BMP-derived effect and relative mechanisms in modulating tenogenic differentiation were demonstrated in several preclinical settings^{155,156} and reproduced *in vitro* on different stem cells sources.

In vitro, BMP-12 supplementation promotes equine BM-MSCs differentiation inducing tendon-related markers, including TNMD and DCN¹⁵⁷. BMP-12 treatment has been evaluated as teno-inductive on BM-MSCs and ADSCs where

the upregulation of tendon markers including SCX, TNMD, type I collagen, TNC, and DCN, was recorded and confirmed *in vivo*¹⁴⁶. The BMP-12 teno-inductive role was also demonstrated in Rhesus BM-MSCs where transfection with BMP-12 was sufficient to induce differentiation into tenocytes by enhancing type I collagen and SCX, but not type III collagen mRNA expression¹³².

Analogously, BMP-13 seems to be involved in promoting *in vitro* tenogenic differentiation on BM-MSCs incorporated in an engineered tendon matrix, further confirmed by their effect on neotendon formation after implantation in an experimentally induced tendon injury model^{158,159}.

The teno-inductive influence of BMP-14 (also called GDF-5) has been evaluated on TSPCs. It has no effect on TSPCs proliferation but leads to a progressive loss in stemness by elevating the expression of DCN, SCX and osteonectin, and reduces TNC, type I collagen, and type II collagen¹⁶⁰. However, the effect of BMP-14 is highly stem cell-dependent. In multipotent adult adipose-derived rat MSCs, treatment with different concentrations of BMP-14 (0–1000 ng/mL) increased proliferation and induced more complete tenogenic differentiation with upregulation of tenogenic gene markers (SCX, TNMD, and TNC) and tendon-specific (type I collagen, DCN) markers codifying for ECM protein components¹³⁶.

hBMP-14 stimulation of hBM-MSCs maintained on a synthetic 3D microenvironment induced an early commitment toward the tenogenic lineage as a consequence of a combination biochemical and physical stimulation. In greater detail, using a multiphase 3D construct consisting of a braided hyaluronate elastic band merged with poly-lactic-co-glycolic acid GFs-loaded microcarriers, hBMP-14 was regularly delivered to hBM-MSCs stimulated with cyclic strain. A significantly increased expression of tenogenic markers, such as type I and III collagen, DCN, SCX, and TNC after 3 days of dynamic culture was reported¹³⁰.

The BMPs molecular signaling pathway involved in tendon differentiation is still unknown. BMPs can transduce the signal through the Smad pathway or through the mitogen-activated protein kinase (MAPK) pathway^{161,162}. However, a recent study demonstrated that BMP-14 promoted tenogenic differentiation in hBM-MSCs by activating cytoskeleton reorganization and extracellular matrix related signaling¹⁶³, demonstrating the involvement of alternative mechanisms of induction of *in vitro* tenogenic differentiation.

1.7 Biomaterials for scaffolds fabrication

The design of a tissue regeneration matrix is based on two essential aspects: the material that constitutes it and the structure that it should have. The ideal scaffold, acting as support matrix, should possess optimum cell compatibility and should not induce an inflammatory response or demonstrate immunogenicity or cytotoxicity^{164,165}. Moreover, the scaffold must be

bioresorbable, so that its by-products are eliminated through natural metabolic pathways in the human body with no residual side effects¹⁶⁴. In particular, the scaffold designed for tendon tissue engineering must mimic the architecture of the native healthy tissue and compensate for its mechanical properties¹⁶⁴.

Three features of the tendon-like scaffold are crucial for tendon tissue engineering; the scaffold should be teno-inductive (capable of inducing cell differentiation toward the tenogenic lineage), teno-conductive (support tendon growth and promote the ingrowth of surrounding tendon), and capable of teno-integration (integrate into surrounding tendon)¹⁶⁵.

Biomaterials play a pivotal role in scaffold fabrication providing three-dimensional templates and synthetic extracellular matrix environments for tissue regeneration. To fulfill the diverse needs in tissue engineering, various materials have been exploited. Polymers, materials widely used for scaffold design, are divided into two different categories: natural and synthetic.

Polymers of natural origin, such as collagen, silk and chitosan represent an interesting material choice to mimic the natural structure of a tendon and its properties. Collagen may be considered a good platform for tendon repair and reconstruction, since it represents the major component of the tendon and is characterized by its good biocompatibility properties¹⁶⁶. For this reason, many researchers have focused on producing scaffolds with collagen alone or mixed with other molecules such as proteoglycans^{167,168}. Despite the attraction offered by its biocompatibility, the main drawbacks of collagen scaffolds lie in their unsuitable mechanical properties linked to rapid degradation kinetics and poor structural stability, and potentially their immunogenic character from their animal origin¹⁶⁹. Alternative materials have been proposed for tendon reconstruction such as silk, which is a fibrous material secreted by spiders and by the caterpillars of certain butterflies (caterpillar of the mulberry bombyx)^{170,171}. Silk possesses exceptional mechanical properties in terms of strength, toughness, and elasticity, making it popular in the field of tendon tissue engineering¹⁷². However, when used alone, silk does not allow sufficient cellular attachment or growth^{171,172}, forcing its use in combination with other materials which share similarity with native tendon ECM to improve its bioactivity^{173,174}. Chitosan is another natural polymer identified as a promising candidate for tissue engineering, since it shares many structural similarities with the glycosaminoglycans (GAGs) present in native tendon ECM^{175,176}. Chitosan is characterized by its biocompatibility, biodegradability, antibacterial capacity, and non-toxicity¹⁷⁷. Despite these advantages, the high stiffness of chitosan membranes makes them challenging for applications in tendon tissue engineering given their low mechanical properties¹⁷⁶.

Another attractive material candidate for tendon tissue engineering is synthetic polymers, which have high flexibility and reproducible mechanical properties when compared to natural ones. The interest in bioresorbable synthetic polymers lies in the possibility of modulating their properties by varying their chemical composition and their structure, for example by choosing a particular molar

mass or crystallinity or by combining two polymers with different characteristics. These polymers are mostly inexpensive, can be scaled industrially, and are thermoplastic, making them moldable and allowing the development of a wide variety of different structures^{166,178,179}. Synthetic materials are common in tendon tissue engineering and belong mostly to aliphatic polyesters such as polyglycolic acids (PGA), polylactic acids (PLA), and polycaprolactones (PCL), as well as their copolymers poly (lactic-co-glycolic) acids (PLGA) and poly (lactic-co-caprolactone) acids (PLCL)^{178,180,181,182,183}. Other materials are also used such as poly (ester urethane) urea (PEUUR)^{184,185}, polyurethane (PU)¹⁸⁶, and polyethylene oxide (PEO)^{187,188,189}.

1.7.1 Fibrin hydrogels: versatile scaffolds in tendon tissue engineering

Hydrogels (such as collagen, chitosan, fibrin) are a class of biomaterials that have great scaffolding potential in many tissue engineering applications given their high tissue-like water content, high biocompatibility, mechanical properties that parallel the properties of soft tissues, efficient transport of nutrients and waste, powerful ability to uniformly encapsulate cells and/or nanocarriers, and ability to be injected as a liquid that gels in situ, since their cross-linking occurs at 37°C¹⁹⁰. Hydrogels, which are based on water-soluble components, are either chemically or physically cross-linked; depending on their chemistry, they can be either degradable or non-degradable¹⁹¹.

Fibrin hydrogels combine some important advantages such as high seeding efficiency and uniform cell/nanocarriers distribution¹⁹². In addition, fibrin has well defined adhesion capabilities and supports cells proliferation being remodeled and degraded over time¹⁹¹. Further, it can be produced from the patient's own blood and used as an autologous scaffold without the potential risk of foreign body reaction or infection¹⁹³.

Fibrin hydrogels are constructed from commercially purified allogeneic fibrinogen and purified thrombin¹⁹⁴ (Figure 1-3). Fibrin is a biopolymer of the monomer fibrinogen. The fibrinogen molecule is composed of two sets of three polypeptide chains named A α , B β , and γ , which are joined together by six disulfide bridges¹⁹⁵. Fibrin is formed after thrombin-mediated cleavage of fibrinopeptide A from the A α chains and fibrinopeptide B from the B β chains¹⁹⁶ with subsequent conformational changes and exposure of polymerization sites. This produces the fibrin monomer that has a great tendency to self-associate and form insoluble fibrin. Further, the blood coagulation factor XIIIa is a transglutaminase that rapidly cross-links γ chains in the fibrin polymer¹⁹⁷ by introducing intermolecular α -(γ -glutamyl) lysine covalent bonds between the lysine of one γ -chain and glutamine of the other. This covalent cross-linking produces a stable fibrin network that is resistant to protease degradation¹⁹⁸.

Fibrin hydrogels have been used as a biological scaffold for stem or primary cells in a variety of tissue engineering applications to regenerate adipose tissue,

bone, cardiac tissue, cartilage, liver, nervous tissue, ocular tissue, skin, tendons, and ligaments¹⁹².

However, fibrin hydrogels as a potential scaffold have three major disadvantages: the shrinkage of the gel that happens during the formation of flat sheets, its rapid degradation before the proper formation of tissue engineered structures and low mechanical stiffness. Gel shrinkage can be prevented by incorporating a fixing agent such as poly-L-lysine into the fibrin gel during the culturing period¹⁹². Fibrin rapid degradation (fibrinolysis), mediated *in vivo* by the serine protease plasmin, can be controlled through the addition of aprotinin, a small (58 amino acids) and potent competitive inhibitor for the active site of plasmin¹⁹⁹. To improve the low mechanical stiffness for some tissue engineering applications, fibrin hydrogels can be combined with other scaffold materials (such as synthetic polymers) to obtain constructs with desired mechanical strength.

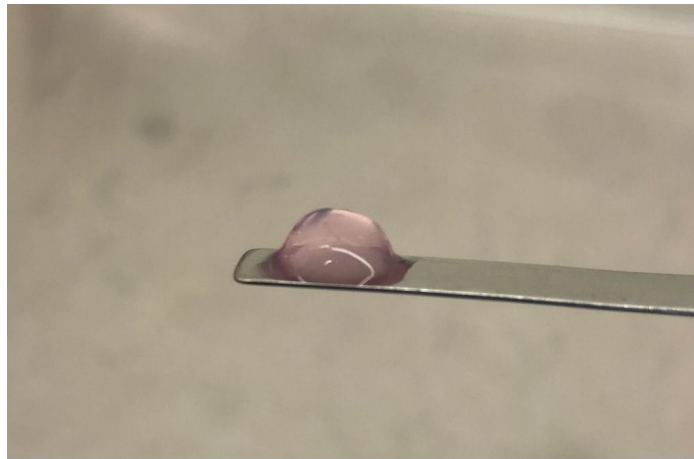


Figure 1-3. Image of a fibrin hydrogel. A mixture of 50 mg/mL of fibrinogen from human plasma, 15,600 U/mL of aprotinin and 100 U/mL of thrombin was placed at 37°C for 30 minutes allowing fibrin polymerization.

1.8 Mechanical stimuli and bioreactors

Tendon development, homeostasis, and regeneration following injury are based on the ability of tendon cells to biologically respond to externally applied forces. Tendons response to physiologic loading is strictly linked to its structure, cellular organization, and to the dynamic interactions between cells and their microenvironment⁶³.

Indeed, tendon cells are highly sensitive to mechanical inputs, and, according to the magnitude, frequency, direction, and duration of the applied loads, they can adapt to their extracellular matrix in a catabolic or anabolic fashion^{200,201,202}. Mechanical stimuli can also induce the activation of a biologic response that involves a complex set of pathways between the cell surface (ion channels, focal adhesion kinases, integrins, cytoskeleton) and the nucleus⁶³.

Just as physiologic loads are important to maintain tendon homeostasis^{203,204}, abnormal ones can cause injuries^{205,206,207}.

The study of tendon mechanobiology is essential to understand both the pathophysiology in tendon disease and the benefits of controlled applied loading during tendon healing and regeneration⁶³.

Tendon tissue engineering strategies are largely scaffold-based, relying on decellularized structures, polymers, and/or gels that, mimicking the extracellular matrix environment, are able to provide an initial supportive structure to which mechanical loads can be applied. Choosing the scaffold with an appropriate mechanical behavior, e.g., stiffness and elasticity, a given load is delivered to the seeded cells¹¹⁶.

In this context, a bioreactor can act as a system able to reproduce *in vitro* a suitable culture environment, which mimics the *in vivo* dynamics experienced by cells during tendon maturation, allowing cellular proliferation/differentiation and matrix production. Bioreactors for tendon tissue engineering require specific basic components such as an actuating system and a culture chamber, which provide, respectively, a construct's mechanical stimulation and a controlled culture environment; continuous loading monitoring plus a feedback actuating system have been also described²⁰⁸. In this sense, both biopolymer scaffolds and bioreactors are complementary paradigms of tissue engineering, both converging to develop highly predictive *in vitro* biomimetic systems to study tendon regeneration and healing strategies.

Bioreactors can provide a given physical stimulus by direct or indirect modes. Indeed, tensile strain can be delivered directly by applying a cyclic and programmable load to the scaffold system, aiming to mimic *in vitro* the biomechanical environment of tendon tissue. Alternatively, a given strain indirectly provided to cells can be achieved by using different physical stimuli such as magnetic fields or acoustic waves^{209,210}. Based on these concepts, several custom-made bioreactors have been developed^{203,204}. Two of these have become commercially available such as the LigaGen system (www.tissuegrowth.com/) or The Bose[®]ElectroForce[®]BioDynamic[®] system (www.bose-electroforce.com). Commercial bioreactors are well designed but they cannot meet all the specific requirements such as an easy and rapid scaffold fixation operation, adequate number of *in vitro* duplicates, or the necessity of a reduced amount of medium in the culture chamber²⁰⁸.

Several *in vitro* studies are described using custom-made bioreactor systems. Compared to static and planar culture, scaffold-based approaches that undergo specific strain stimulation display more elongated cellular morphology and increased cell density. Moreover, compared to a load-free culture environment, a bioengineered scaffold can show up to a 9-fold increase in the cell number after 2 weeks of cyclic stretching²¹¹. Tensile loads can deliver to the cells specific input to increase collagen synthesis, promoting the formation of bundles with parallel collagen fibrils and upregulating proteoglycans in the extracellular matrix^{212,213}. The formation of collagen fibers along the direction of loading also

results in an enhancement or optimization of the mechanical properties of the bioengineered tissue, such as stiffness, elastic modulus, maximum tensile stress, and maximum load^{214,215,216}.

The gene expression of tenogenic markers is also positively influenced by cyclic strain. For example, type I collagen expression under dynamic conditions has been reported to be three times higher than static conditions after 2 weeks of culture²¹⁷. Furthermore, mechanical stimuli orchestrate tenogenic differentiation upregulating SCX^{115,218,219,220}. Another study demonstrated the upregulation of type I collagen, type III collagen, and TNC in human marrow stromal cells encapsulated in an oligo (poly (ethylene glycol) fumarate (OPF) hydrogel and cultured under cyclic tensile strain (10%, 1 Hz, 3 h of strain followed by 3 h without) for 21 days²²¹. Additional data showed that only 24 h of moderate cyclic axial stretching (2% strain, 1 Hz) promoted the tenogenic differentiation and tendon matrix synthesis by equine adipose-derived mesenchymal stromal cells seeded on decellularized tendon matrix scaffolds, upregulating type III collagen, DCN, SCX and TNC²²². Moreover, an intermittent cyclic tensile strain (10% applied strain, 1 Hz, 10 min every 6 h) enhanced the proliferation and tenogenic differentiation of hBM-MSCs cultured in anisotropic collagen–glycosaminoglycan scaffolds, via time-dependent activation of ERK 1/2 and Smad 2/3 pathways. Cyclic strain promoted the activation of tendon-related (TNC, Mxk and SCX) and extracellular matrix biosynthesis-related genes (type III collagen, Decorin, COMP)²²³.

However, the frequency of stimulation²¹⁵ and the strain applied can have different effects on tenogenic differentiation. For instance, tenocytes cultured for 12 days upon poly(glycerol-sebacate) (PGS) sheets at 6% cyclic strain exhibited a tendon-like gene expression profile compared to 3% and 0% strain groups²²⁴, while uniaxial cyclic tensile stretching at 8% strain exclusively induced tenogenic differentiation of human bone marrow-derived mesenchymal stem cells, with protein and gene expression comparable to primary tenocytes²²⁵. On the other hand, constant strain negatively affects tendon diameter²²⁶, inhibiting cell proliferation and increasing apoptosis²²⁷.

In conclusion, maximum load, frequencies and cyclic strain are all parameters that have to be taken into account to achieve a highly predictive *in vitro* tendon-like bioengineered system. However, despite the importance of the choice of proper bioreactor devices and operative parameters, this aspect has to be strictly merged with the scaffold mechanical properties. Indeed, any mechanical input can only be effectively delivered to a scaffold (and to the cells on board) by taking into account the mechanical behavior such as the stiffness and elasticity of the specific scaffold chosen. In this sense, scaffold characteristics and mechanical performances have to be strictly selected and adapted to the bioreactor device.

1.9 The importance of combined *in vitro* studies in tendon tissue engineering

In vitro teno-differentiation strategies represent a fundamental step prior to *in vivo* tendon disorder treatment with tissue engineering approaches. Tissue engineering refers to a multidisciplinary field that aims to induce tissue repair or regeneration. Therefore, it involves the use of a combination of key factors, such as cells, scaffolds, biochemical inputs, and mechanical inputs to produce a functional tissue-like construct (Figure 1-4). Nowadays, a combination of two or more than one techniques seems to be the best way to induce tendon differentiation in stem cells²²⁸.

Cells represent the building blocks of the engineered tissue. Undifferentiated, pre-differentiated, or differentiated stem cells can be used in tissue engineering. Several studies displayed the involvement of various types of stem cells (embryonic, fetal, and adult stem cells) from different sources with promising results. Scaffolds supply mechanical stability and provide a 3D support for cell growth and differentiation. Mechanical inputs with different loading features, provided by bioreactors, can dynamically affect the cell behavior within the scaffold, mimicking the physiological environment of the tendon. On the other hand, biologically active molecules (such as growth factors) can be used in synergy with the other factors to drive the process of cells maturation and differentiation.

Taken together, all these elements contribute to the formation of a tissue-engineered substitute to be used as an *in vitro* model or to be applied in tissue replacement techniques *in vivo*. Several studies are recently focusing on a combined approach as a novel method for tendon tissue engineering, demonstrating how the cooperative effect of different factors improves the properties of the engineered tissue, compared to those obtained using a single factor^{130,229,230}.

In vitro studies are fundamental to: (i) identify and/or compare the tenogenic plasticity of different stem/progenitor cell sources, (ii) define and drive cell mechanism and environmental conditions leading tenogenesis, (iii) test teno-inductive properties of new scaffolds, (iv) validate biomechanical teno-inductive stimuli. At this time, *in vitro* differentiation techniques are not yet validated, but only with a successful *in vitro* model will we will have a clearer view of tendon biology and pathology to translate the knowledge matured in controlled laboratory conditions to the treatment of tendon disorders *in vivo*.

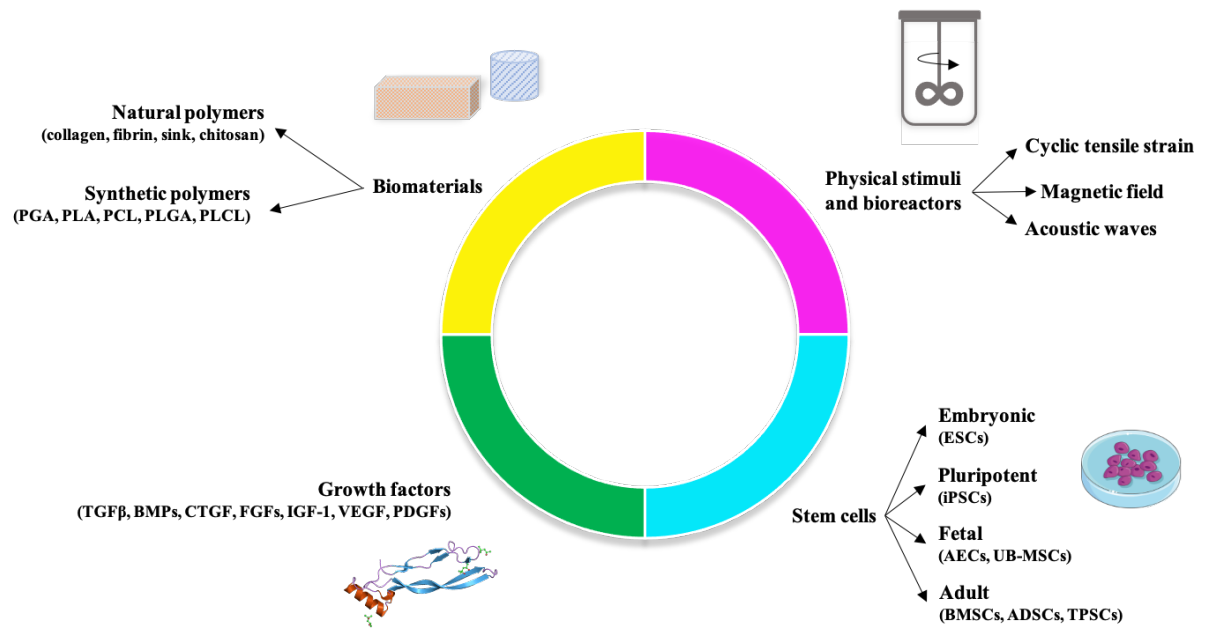


Figure 1-4. *In vitro* strategies for tendon tissue engineering. Tendon tissue engineering refers to a multidisciplinary field that aims at the inducement of tissue repair or regeneration, involving the combination of several key factors to produce a functional tendon-like construct.

Chapter 2

A pilot study to explore the tenogenic responsiveness of hBM-MSCs
and hWJ-MSCs to hGDF-5

Ref: Ciardulli MC, Marino L, Lamparelli EP et al. Int J Mol Sci. 21(16):5905. 2020.

2.1 Introduction

As discussed in Chapter 1, the management of tendon injuries is challenging, given their limited healing capability, and propensity for a failed healing response¹⁴⁷. Anti-inflammatory drugs are frequently used, but they may actually hinder recovery²³¹, while in clinical practice tissue grafts or prostheses are used for severe injuries¹⁶⁴. Since the present therapeutic modalities are only partially effective, cell therapies are proposed for future applications²³². They aim to induce tendon healing and regeneration, focusing on the role of mesenchymal stem cells therapy and their derivatives²³².

Multipotent Mesenchymal Stem Cells (MSCs) are considered a promising therapeutic tool to manage tendon conditions in clinical applications²³³. Both *in vivo* and *in vitro* studies evidenced that MSCs can contribute to accelerate and improve the quality of tendon healing⁶.

Human bone marrow MSCs (hBM-MSCs) have been extensively characterized. hBM-MSCs are multipotent cells able to differentiate into various types of mesenchymal cell phenotypes, including osteoblasts, chondroblasts, myoblasts and tenocytes under specific conditions *in vitro*²³⁴. hBM-MSCs have been also applied within 3D *in vitro* models of tendon healing and regeneration^{130,230}. However, given the limited number of hBM-MSCs available for autologous use, donor site morbidity, and their limited proliferative capacity, it is important to identify alternative MSCs sources for clinical use and application in tissue-engineered protocols of tendon regeneration.

An alternative tissue source of MSCs is the connective tissue (Wharton's Jelly) of the human umbilical cord (hWJ-MSCs)^{235,236}. MSCs derived from extra-embryonic tissue, including hWJ-MSCs, share several characteristics with adult MSCs, but also retain some features of developmentally immature stem cell populations, such as broad germ layer-spanning differentiation potential, but do not induce teratomas formation and have a potential application in regenerative medicine that is not impeded by ethical or legal issues²³⁷. Moreover, hWJ-MSCs display high proliferation rates, wide multipotency, hypoimmunogenicity and, unlike hBM-MSCs, require a painless collection procedure and have faster self-renewal properties, all important features in cell-based therapies^{238,239}. hWJ-MSCs have been induced to form neurons, myocytes, bone, cartilage and adipose cells²⁴⁰, but, except few recent studies *in vivo*^{241,242}, very little is known about their tenogenic commitment.

The use of MSCs, in combination with specific growth factors (GFs), is proposed as an innovative treatment for tendon healing and regeneration²⁴³.

Given the huge gap of knowledge regarding the biology of tendon healing and the sequence of events and biomolecules involved, several growth factors are used for tendon research¹². Among these, GDF family members, and especially Growth Differentiation Factor 5 (GDF-5), have been used successfully to drive tenogenic differentiation. GDF-5 belongs to the TGF- β superfamily, and it is highly expressed in mesenchymal condensations during skeleton development. GDF-5 is also called cartilage-derived morphogenetic protein-1 (CDMP-1) or

bone-derived morphogenetic protein-14 (BMP-14). BMPs are deeply involved in the development of endochondral bones²⁴⁴ and joints²⁴⁵, inducing the expression of type I collagen in connective tissue²⁴⁶, with a consequential important role in tendon healing²⁴⁷. Indeed, GDF-5 induces the expression of genes linked to the neo-tendon phenotype^{248,249,131}, and its administration seemed to improve the outcome of tendon repair¹⁵⁹.

Little is known about the effect of GDF-5 on BM-MSCs transcriptional regulation and differentiation, and, to our knowledge, WJ-MSCs have never been studied in this sense. GDF-5 supplemented (100 ng/mL) culture media enhanced extracellular matrix (ECM) and tenogenic marker gene expression in adipose-derived mesenchymal stem cells (ADMSCs) over 12 days¹³⁶. GDF-5 also appeared to induce tenogenic differentiation of human BM-MSCs when used at a concentration of 100 ng/mL, with significant increases in total collagen expression and tenogenic marker gene expression (SCX, TNC and type I collagen at Day 7)¹³¹. Further, BMP-14 (50–100 ng/mL) significantly increased tendon marker expression (SCX and TNMD) at mRNA and protein level potentially via the Sirt1-JNK/Smad1-PPAR signaling pathway and enhanced by TGF- β 3 and VEGF. The association of BMP-14 with TGF- β 3 and VEGF enhanced the tenogenic differentiation of BM-MSCs^{250,251}. Pathway analyses on hBM-MSCs treated with GDF-5 highlighted that the potential molecular pathways involved in GDF-5 induced tenogenic differentiation included cytoskeleton reorganization, cell adhesion, and extracellular matrix signaling¹³¹. The repair process in injured tendons consists of three overlapping phases reported as the inflammatory, proliferative and remodeling stages²⁵². Several cell types are involved in tendon healing. Pro-inflammatory (M1) and anti-inflammatory (M2) macrophages directly orchestrate tendon remodeling and by secreting cytokines and growth factors, activate the epithelial-to-mesenchymal transition (EMT) signaling cascades in the epithelial cells that surround tendon tissue, providing a source of mesenchymal cells able to repair the injured tissue²⁵². Indeed, preclinical and clinical studies have demonstrated the anti-inflammatory and immunomodulatory potential of MSCs, even though the mechanisms behind the MSC-based immunomodulation remain a challenge. For example, MSCs can have different immunomodulatory effects, even on the same types of immune cells, depending on the disease status. However, both hBM-MSCs and hWJ-MSCs display immunomodulatory properties and produce large amounts of cytokines and growth factors, connected to the differentiation processes^{237, 253, 254}. A correlation between GDF-5 and cytokine expression has been noted in human annulus cells in *in vitro* disc degeneration models where high levels of two pro-inflammatory cytokines (IL-1 β and TNF- α) leads to a significant down-regulation of GDF-5²⁵⁵.

To date, there is no single growth factor (or a cocktail of growth factors) and protocols which efficiently induce tenogenic differentiation of stem cells. Given this challenge, determining stem cells responses to specific dosages of GDF-5

treatment is a fundamental step in addressing tendon regeneration strategies, tissue-engineering models, and protocols.

2.2 Aim

To explore the possible use of hWJ-MSCs, instead of the gold standard hBM-MSCs, in tissue-engineering protocols for tendon healing and repair, we studied the effect of a range of human GDF-5 (hGDF-5) concentrations (1-10-100 ng/mL) on tendon and cytokine gene expression of hWJ-MSCs. hBM-MSCs were included to enable direct comparison with the research standard. Markers, such as type I collagen (COL1A1), Decorin (DCN), Scleraxis-A (SCX-A), Tenascin-C (TNC) and Tenomodulin (TNMD), and both pro-inflammatory (IL-6, TNF, IL-12A, IL-1 β) and anti-inflammatory (IL-10, TGF- β 1) cytokines, were monitored by quantitative Real-Time Polymerase Chain Reaction (qRT-PCR). Type III collagen (COL3A1) was chosen as a negative marker because it is basally expressed by stem cells. Morphometric analysis with cells alignment, shape and length/width ratio coupled with type I collagen and tenomodulin proteins detection by quantitative immunofluorescence (qIF) completed the study.

2.3 Materials and Methods

The protocol of the study and the written informed consent were reviewed and approved by the Institutional Review Board of San Giovanni di Dio e Ruggi D'Aragona Hospital (Review Board prot./SCCE n. 24988, March 2015).

2.3.1 hBM-MSCs Isolation and Harvesting

hBM-MSCs were obtained from the bone marrow of two male donors (age 37 and 39). Donors provided written informed consent in accordance with the Declaration of Helsinki to use their filter residual bone marrow aspirate for research purposes. Briefly, total bone marrow aspirate was directly seeded at a concentration of 50,000 total nucleated cells/cm² in T75 plastic flask (BD Falcon, Bedford, MA, USA) in Minimum Essential Medium Alpha (α -MEM; Corning Cellgro, Manassas, VA, USA) supplemented with 1% GlutagroTM (Corning Cellgro, Manassas, VA, USA), 10% Fetal Bovine Serum (FBS; Corning Cellgro, Manassas, VA, USA), and 1% Penicillin/Streptomycin and incubated at 37°C in 5% CO₂ atmosphere and 95% relative humidity. After 72 h, non-adherent cells were removed by media change, and the adherent cells were further fed twice a week with new medium. On day 14, colonies of adherent cells were detached and re-seeded at 4 x 10³ cells/cm² in the same culture conditions. Once cultures reached 70–80% confluence, cells were detached using 0.05% trypsin-0.53 mM EDTA (Corning Cellgro, Manassas, VA, USA) and washed with Phosphate-buffered saline (PBS) 1x (Corning Cellgro, Manassas, VA, USA), counted using Trypan Blue (Sigma-Aldrich, Milan, Italy)

and sub-cultured at a concentration of 4×10^3 cells/cm². Flow Cytometry analysis was performed on cell samples obtained at Passage 1.

2.3.2 hWJ-MSCs Isolation and Harvesting

hWJ-MSCs were isolated from two donors (both age 28, unrelated to the male donors) who gave written informed consent in accordance with the Declaration of Helsinki to use their umbilical cord for research purposes. hWJ-MSCs were prepared from fresh human umbilical cord obtained during normal spontaneous vaginal delivery. Briefly, umbilical cord sections, approximately 7.5 cm long, were placed in 0.9% NaCl physiological solution supplemented with Ampicillin-Sulbactam 1 g + 500 mg, stored at 4°C, and processed within 4h of collection. The umbilical cord was cut into 2.5 cm segments, and washed in fresh transport media to remove blood and debris. Each umbilical cord segment was sectioned longitudinally with sterile scissors, and the visible arteries and veins removed. Each piece was transferred to a tissue culture flask 175 cm² (BD Falcon, Bedford, MA, USA) containing α -MEM (Corning Cellgro, Manassas, VA, USA) supplemented with 10% FBS (Corning Cellgro, Manassas, VA, USA), GlutaGro™ (Corning Cellgro, Manassas, VA, USA), and Penicillin-Streptomycin solution. Cultures were incubated at 37°C in a humidified atmosphere containing 5% CO₂. Cell growth was monitored daily with changes in media twice a week. Upon reaching 100% confluence, cells were detached using 0.05% trypsin-0.53 mM EDTA (Corning Cellgro, Manassas, VA, USA) and were washed with PBS 1x (Corning Cellgro, Manassas, VA, USA), counted using Trypan Blue (Sigma-Aldrich, St. Louis, MO, USA), and sub-cultured at a concentration of 300 cells/cm². For hWJ-MSCs immunophenotype characterization flow cytometry analysis was performed on cell samples obtained at Passage 1.

2.3.3 Flow cytometry

hBM-MSCs and hWJ-MSCs were detached and counted; 1×10^5 cells were incubated at room temperature (RT) for 20 min with the following directly conjugated mouse-anti human antibodies: CD90 FITC (Beckman Coulter, Fullerton, CA, USA), CD73 APC (Miltenyi Biotec, Gladbach, Germany), CD105 PE (Beckman Coulter, Fullerton, CA, USA), CD45 PC7 (Beckman Coulter, Fullerton, CA, USA), HLA class-II FITC (Beckman Coulter, Fullerton, CA, USA), CD14 PC7 (Beckman Coulter, Fullerton, CA, USA), and CD34 PE (Beckman Coulter, Fullerton, CA, USA). The isotype-matched immunoglobulins IgG1 FITC (Beckman Coulter, Fullerton, CA, USA), IgG1 PE (Beckman Coulter, Fullerton, CA, USA), IgG1 APC (Beckman Coulter, Fullerton, CA, USA), and IgG1 PC7 (Beckman Coulter, Fullerton, CA, USA) were used as negative controls under the same conditions. At least 15,000 total events were acquired with a BD FACSVerser flow cytometer (Becton Dickinson,

BD, NJ, USA). Further analysis and plots were produced using the BD FACSuite analysis software.

2.3.4 hGDF-5 treatment

Each experiment was performed with $n = 3$ replicates, using both individual donor cells and pooling the source. hBM-MSCs and hWJ-MSCs (passage 3) were seeded on coverslips in 12 well-plates at a concentration of 4×10^3 cells/cm² and 300 cells/cm², respectively. The different seeding densities were used to normalize for the different cell proliferation times; seeding hWJ-MSCs at a density higher than 300 cells/cm² saw them reach 90% confluence in less than three days followed by detachment from the flask surface. Once the cell cultures reached 60% confluence, cells were treated with 1 mL of culture media supplemented with three different concentrations of recombinant human GDF-5 (PeproTech; UK): 1 ng/mL, 10 ng/mL, and 100 ng/mL. Cells were fed twice a week with new media and fresh growth factor supplementation. As a consequence of the different proliferation times, hBM-MSCs were treated for 16 days, and hWJ-MSCs for seven days. Untreated cells for matched time-points were used for control purposes.

2.3.5 mRNA isolation and gene expression profiles

Samples were collected at Day 1, 8 and 16 for hBM-MSCs and at Day 1, 3 and 7 for hWJ-MSCs. Total mRNA was extracted using QIAzol[®] Lysis Reagent (Qiagen, Hilden, Germany), chloroform (Sigma-Aldrich, Milan, Italy), and the RNeasy Mini Kit (Qiagen, Germany). For each sample, 1 μ g of total mRNA was reverse-transcribed using the iScript[™] cDNA synthesis kit (Bio-Rad, Milan, Italy). Relative gene expression analysis was performed in a LightCycler[®] 480 Instrument (Roche, Italy), using the SsoAdvanced[™] Universal SYBR[®] Green Supermix (Bio-Rad) with validated primers for COL1A1, COL3A1, DCN, SCX-A, TNMD, TNC, IL-6, TNF, IL-12A, IL-1 β , IL-10 and TGF- β 1 (Bio-Rad), and following MIQE guidelines²⁵⁶. Amplification was performed in a 10 μ L final volume, including 2 ng of complementary DNA (cDNA) as a template. The specificity of the amplification products was addressed via melting curve analysis. Data were normalized to glyceraldehyde-3-phosphate dehydrogenase (GAPDH) expression (reference gene), applying the geNorm method²⁵⁷ to calculate reference gene stability between the different conditions (calculated with CFX Manager software; $M < 0.5$). Fold changes in gene expression were determined by the $2^{-\Delta\Delta C_t}$ method, and are presented as relative levels versus untreated cells at each time-point explored. All normalizations were obtained using untreated control samples cultivated along the investigated time points.

2.3.6 Morphometric and proliferation analysis

Nuclei aspect ratio of hBM-MSCs and hWJ-MSCs was determined at different time points (Day 1, 8 and 16 for hBM-MSCs; Day 1 and 7 for hWJ-MSCs) in culture by analyzing optical microscope images processed using ImageJ software. Nuclei aspect ratio was determined by measuring and dividing the length by the width of each nucleus; a total of 50–80 nuclei was measured in each condition using a minimum of 10 microscope images. Proliferation of hBM-MSCs and hWJ-MSCs was quantified by counting the number of nuclei in each time point (Day 0 and 16 for hBM-MSCs; Day 0 and 7 for hWJ-MSCs) and in each condition of treatment (1 ng/mL, 10 ng/mL and 100 ng/mL of hGDF-5) using a minimum of 10 microscope images.

2.3.7 Immunofluorescence assay

Samples were collected at Day 1, 8 and 16 for hBM-MSCs and at Day 1 and 7 for WJ-MSCs. Cells were fixed with 3.7% formaldehyde for 30 min at RT followed by permeabilization with 0.1% Triton X-100 for 5 min and blocking with 1% BSA for 1 h. For type I collagen and tenomodulin staining, cells were incubated overnight at 4°C with a mouse monoclonal anti-type I collagen antibody (1:100, Sigma-Aldrich, Milan, Italy) and a rabbit polyclonal anti-TNMD antibody (1:100; Abcam, Cambridge, United Kingdom). Following incubation with the primary antibody, cells were incubated for 1 h at RT with the DyLight 649 anti-mouse IgG (1:500, BioLegend, CA, USA) antibody and the Alexa Fluor™ 488 goat anti-rabbit IgG (1:500; Thermo Fisher Scientific, Waltham, MA, USA). Cell nuclei were stained with DAPI solution (1:1000) for 5 min. Images were acquired at 63x magnification using an inverted Leica laser-scanning confocal microscope (TCS SP5; Leica Microsystems, Wetzlar, Germany) equipped with a plan Apo 63x/1.4 NA oil immersion objective. Image quantification was performed in a blinded manner using image analysis software (ImageJ, National Institutes of Health, Bethesda, MD, USA) by measuring the red and green areas where type I collagen and TNMD, respectively, are expressed [74,75]. Original images were converted from RGB format into a gray scale (16-bit). Then, the average value of pixel intensity (within a range from 0-dark to 255-white) was calculated for each image. Signal intensity was normalized by the cell number (e.g., by the amount of cell nuclei revealed by DAPI staining). A minimum of 10 image fields (with a comparable number of cells in each image) were used for the analysis at each time point for each experiment. Data were expressed as fold change relative to untreated cells at matched time-points.

2.3.8 Statistical analysis

Statistical analysis was performed using GraphPad Prism software (6.0 for Windows). For phenotypic analysis, data obtained from multiple experiments (n = 3) are calculated as mean +/- SD and analyzed for statistical significance using ANOVA test, for independent groups. Differences were considered statistically significant when $p < 0.05$.

2.4 Results

2.4.1 Flow cytometry characterization of hBM-MSCs and hWJ-MSCs

hBM-MSCs and hWJ-MSCs were isolated and harvested as described in sections 2.3.1 and 2.3.2. The expression of stemness surface markers was analysed using flow cytometry. All samples were positive for CD90, CD105, CD73 and negative for CD14, CD34, CD45, HLA-DR in accordance with previously published data²⁵⁸. Detailed flow cytometry characterization is reported in Table 2-1 and data acquisition profiles illustrated in Figure 2-1.

| Sample Name | # of Total Events | % Parent (Gated on P1) | % Total (No Gate) |
|----------------------------|-------------------|------------------------|-------------------|
| hBM-MSC all events | 15,000 | *** | 100.00 |
| hBM-MSC: P1 | 13,364 | 89.09 | 89.09 |
| hBM-MSC: HLA-DR+ | 72 | 0.54 | 0.48 |
| hBM-MSC:CD34+ | 87 | 0.65 | 0.58 |
| hBM-MSC:CD14+ | 258 | 1.93 | 1.72 |
| hBM-MSC all events | 15,000 | *** | 100.00 |
| hBM-MSC: P1 | 13,555 | 90.37 | 90.37 |
| hBM-MSC:CD90+ | 13,494 | 99.55 | 89.96 |
| hBM-MSC:CD105+ | 13,538 | 99.87 | 90.25 |
| hBM-MSC:CD73+ | 13,537 | 99.87 | 90.25 |
| hBM-MSC:CD45+ | 35 | 0.26 | 0.23 |
| Sample Name | # of Total Events | % Parent (Gated on P1) | % Total (No Gate) |
| hWJ-MSC all events | 15,000 | *** | 100.00 |
| hWJ -MSC: P1 | 11,619 | 77.46 | 77.46 |
| hWJ -MSC: HLA-DR+ | 41 | 0.35 | 0.27 |
| hWJ -MSC:CD34+ | 31 | 0.27 | 0.21 |
| hWJ -MSC:CD14+ | 21 | 0.18 | 0.14 |
| hWJ -MSC all events | 15,000 | *** | 100.00 |
| hWJ -MSC: P1 | 12,465 | 83.10 | 83.10 |
| hWJ -MSC:CD90+ | 12,368 | 99.22 | 82.45 |
| hWJ -MSC:CD105+ | 12,379 | 99.31 | 82.53 |
| hWJ -MSC:CD73+ | 12,369 | 99.23 | 82.46 |
| hWJ -MSC:CD45+ | 104 | 0.83 | 0.69 |

Table 2-1. Flow cytometry statistics data of all the main events considered for the population of hBM-MSCs and hWJ-MSCs used in the experiments. All samples were positive for CD90, CD105, CD73 and negative for CD14, CD34, CD45, HLA-DR.

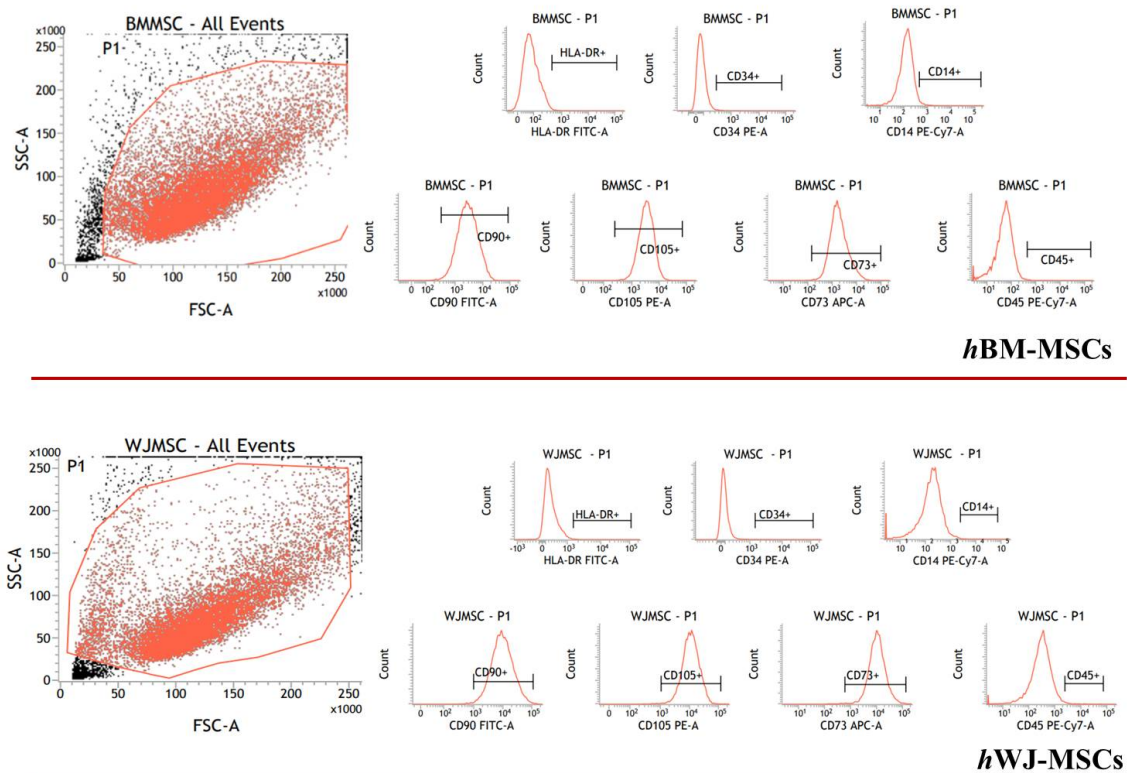


Figure 2-1. Flow cytometry events illustrate hBM-MSCs and hWJ-MSCs characterization. The panel shows the representative flow cytometry event of forward scatter (FSC) vs. side scatter (SSC).

2.4.2 Effect of hGDF-5 on cells proliferation and morphology

The proliferation of both cell types was examined during the experimental time course both with and without hGDF-5 supplementation and determined counting the number of nuclei in each time point. No statistically significant differences in proliferative potential were noted for hBM-MSCs (at Day 16 for untreated cells -NT- it looks like cells number decreased though) for all the hGDF-5 concentration explored. hWJ-MSCs displayed a generally higher proliferation rate (Figure 2-2) with respect to hBM-MSCs (see NT at Day 7) which was also positively affected by the concentrations of the growth factor.

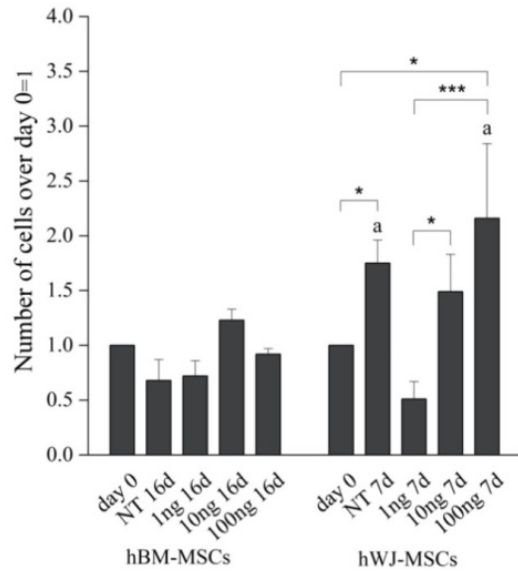


Figure 2-2. Proliferation rate of hBM-MSCs and hWJ-MSCs with the human Growth Differentiation Factor 5 (hGDF-5) dose-dependent effect. The proliferation rate was calculated over different culture time points and for both untreated cells and hGDF-5 treated cells. Statistically significant differences are shown as * = $p \leq 0.05$; ** = $p \leq 0.01$; *** = $p \leq 0.005$; a = $p \leq 0.05$ compared to hBM-MSCs (NT 7d hWJ-MSCs vs. NT 16d hBM-MSCs; 100 ng 7 d hWJ-MSCs vs. 100 ng 16 d hBM-MSCs); $n = 3$. (NT = untreated cells; 1 ng = 1 ng/mL of hGDF-5; 10 ng = 10 ng/mL of hGDF-5; 100 ng = 100 ng/mL of hGDF-5; d = days).

Moreover, nuclei aspect ratio of hBM-MSCs and hWJ-MSCs was determined at different time points (Day 1, 8 and 16 for hBM-MSCs; Day 1 and 7 for hWJ-MSCs) measuring and dividing the length by the width of each nucleus (length/width: L/W) (see section 2.3.6). Compared to tenoblasts, whose nucleus is ovoid (nuclei length/width ratio < 1.5), the overall tenocytes shape and their nucleus appears elongated with a nuclei length/width ratio > 1.7 (Figure 2-3a)^{183,7}. Therefore, hBM-MSCs and hWJ-MSCs phenotype commitment was evaluated by nuclear aspect ratio evolution. hBM-MSCs showed a specific alignment and shape modification (tenoblast-like) with an L/W ratio ≥ 1.5 when 100 ng/mL were supplemented at Day 8 and at Day 16 (Figure 2-3b and Figure 2-4). Extending our examination of hGDF-5 induction of tenogenic gene expression into hWJ-MSCs, we noted that cells displayed an aligned phenotype with a tenocyte-like shape, coupled to the L/W ratio value > 1.7 , at Day 7 with 100 ng/mL of hGDF-5 supplementation (Figure 2-3c and Figure 2-4).

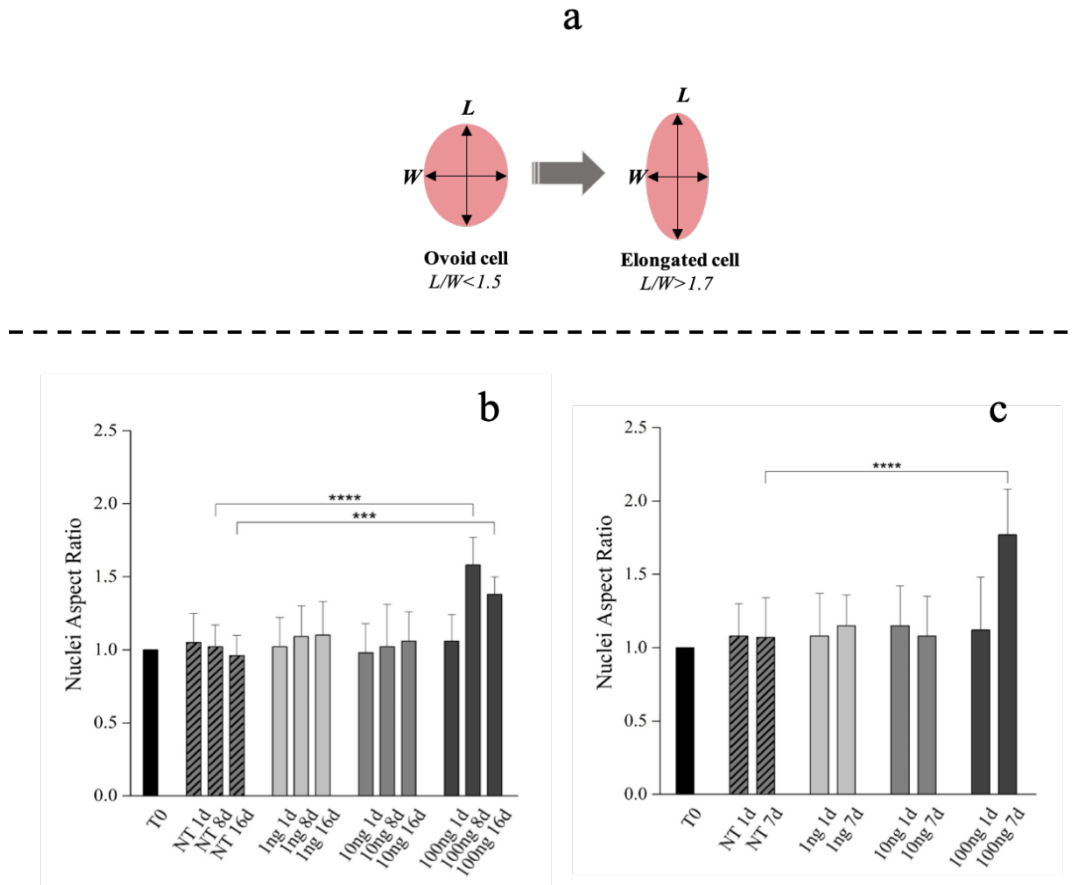


Figure 2-3. Morphometric analysis of hBM-MSCs and hWJ-MSCs with the hGDF-5 dose-dependent effect. Shape modification analysis illustrated the hGDF-5 concentration-dependent effect on cells (**a**). Nuclei aspect ratio vs. treated cells are reported for hBM-MSCs (**b**) and hWJ-MSCs (**c**); data on untreated cells are also reported for comparison purpose. Statistically significant differences are shown as *** = $p \leq 0.005$; **** = $p \leq 0.001$. (T0 = day 0; NT = untreated cells; 1 ng = 1 ng/mL of hGDF-5; 10 ng = 10 ng/mL of hGDF-5; 100 ng = 100 ng/mL of hGDF-5; d = days).

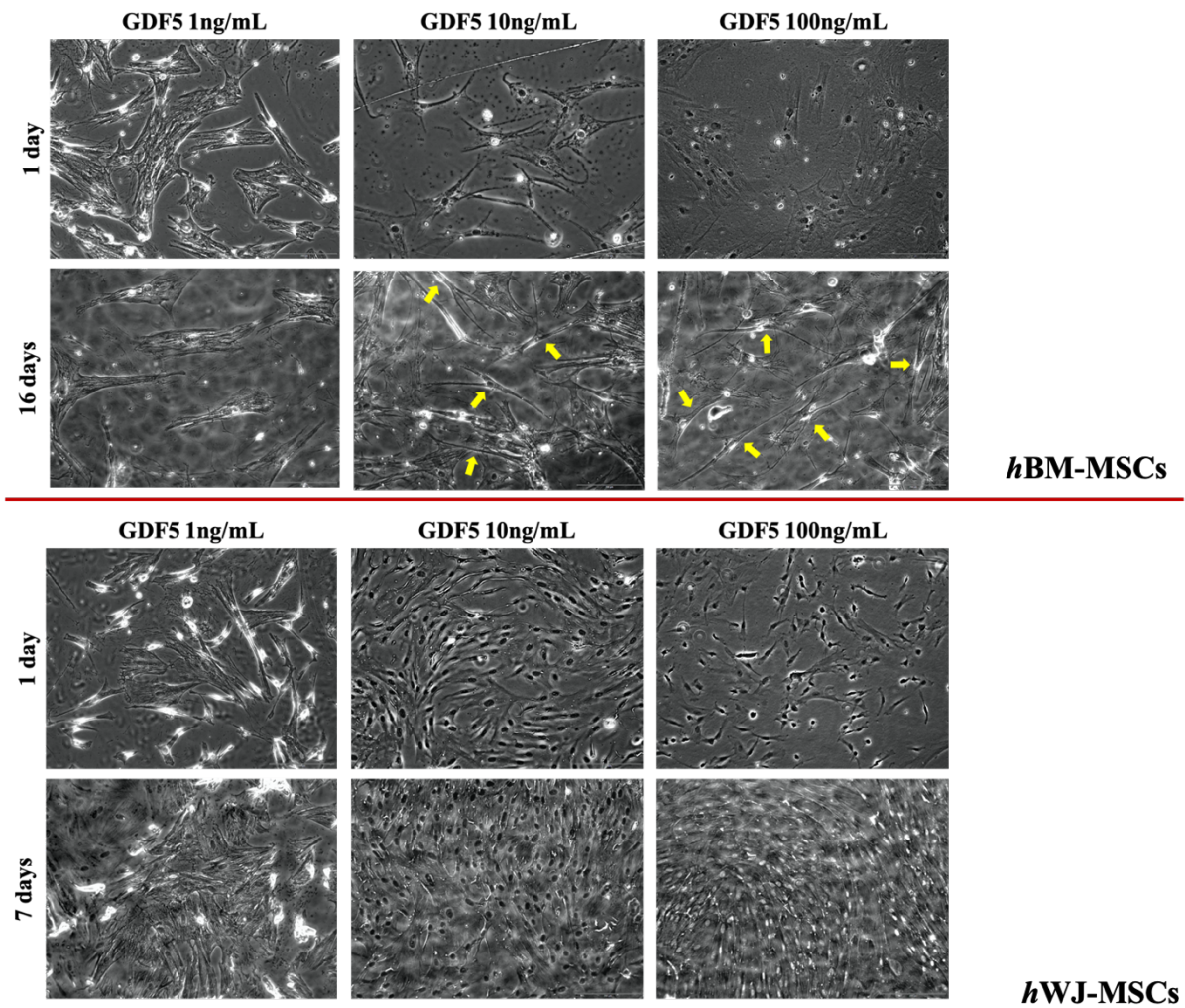


Figure 2-4. Brightfield images of hBM-MSCs and hWJ-MSCs with the hGDF-5 dose-dependent effect. Both cells showed cells specific alignment and their shape modification; hWJ-MSCs exhibited always higher proliferation rate positively affected by 100 ng/mL of GDF-5 dose.

2.4.3 Gene expression of tenogenic markers

hBM-MSCs and hWJ-MSCs commitment was also evaluated monitoring the mRNA expression for different tenogenic markers (COL1A1, DCN, SCX-A, TNC, TNMD). COL3A1, being basally expressed by cells, was chosen as negative marker.

Transcriptional analysis of hBM-MSCs supplemented with 1ng/mL of hGDF-5 revealed up-regulation of SCX-A (1.3-fold), COL1A1 (1.3-fold), COL3A1 (1.5-fold), DCN (1.2-fold) and TNC (1.2-fold) after 8 days of culture. Up-regulation was transient, and expression returned to baseline levels or less by Day 16 (Figure 2-5a). An hGDF-5 concentration of 10 ng/mL resulted in a similar transcriptional up-regulation pattern as before, but that peaked at Day 1 and decreased thereafter (Figure 2-5b). With 100 ng/mL hGDF-5 supplementation, SCX-A was overexpressed at Day 1 with an up-regulation of 1.7-fold and at

Day 8 TNMD (12-fold), DCN (1.4-fold), TNC (1.3-fold), COL1A1 (1.3-fold), and COL3A1 (1.2-fold) were observed (Figure 2-5c). All transcripts were down-regulated thereafter at Day 16.

Examining qRT-PCR data concerning the expression of tenogenic markers by hWJ-MSCs, 1 ng/mL was associated with up-regulation of SCX-A (2-fold) and COL1A1 (1.3-fold) at Day 3, and DCN (1.5-fold) only at Day 7 (Figure 2-5d). Similarly, 10 ng/mL had little effect on tenogenic gene expression with the exception of TNC, which increased 1.3-fold at Day 3 (Figure 2-5e). In contrast to the above, and similar to hBM-MSCs, 100 ng/mL hGDF-5 induced significant up-regulation of SCX-A (3.8-fold), COL1A1 (3-fold), TNC (2.3-fold), DCN (2.7-fold), and COL3A1 (2.9-fold) at Day 3 (Figure 2-5f).

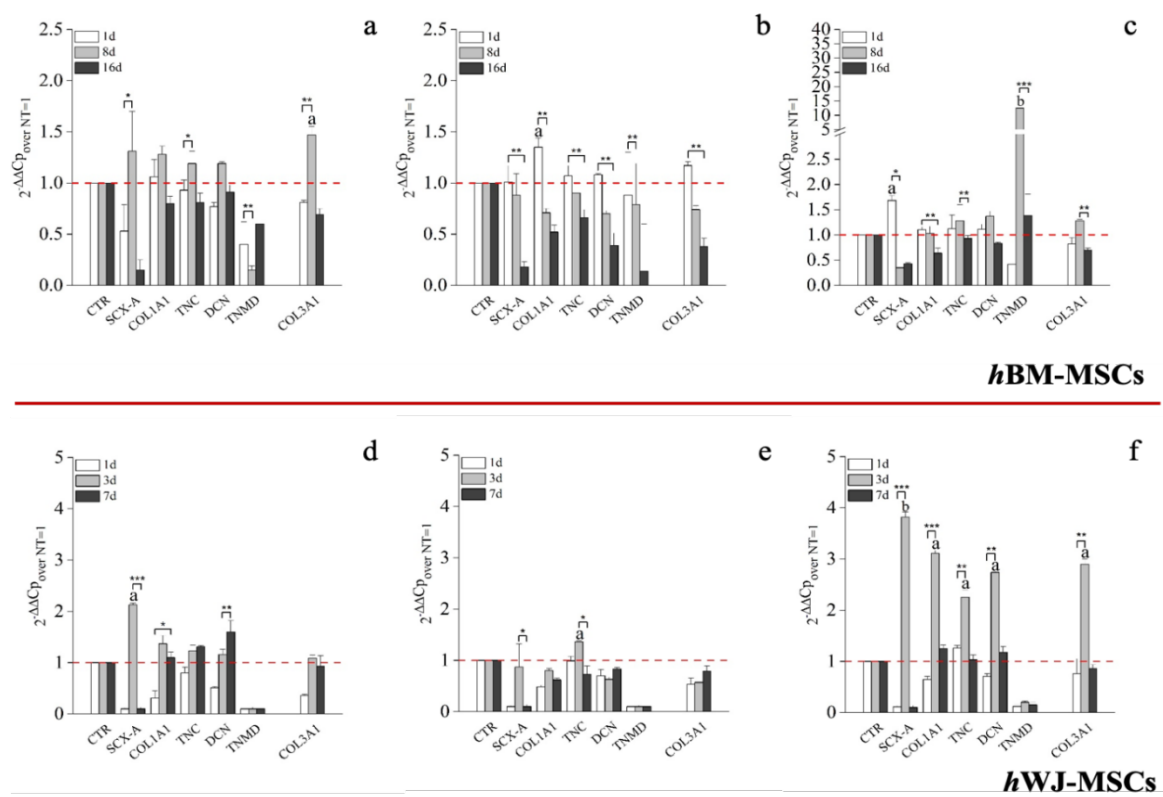


Figure 2-5. Quantitative Real-Time Polymerase Chain Reaction (qRT-PCR) on the expression of tenogenic markers by hBM-MSCs and hWJ-MSCs with the hGDF-5 dose-dependent effect. The mRNA levels of tenogenic markers (Type 3 collagen: COL3A1, type 1 collagen: COL1A1, Decorin: DCN, Scleraxis-A: SCX-A, Tenomodulin: TNMD, Tenascin-C: TNC) were monitored; three different concentration of hGDF-5 were tested: (a, d) 1 ng/mL, (b, e) 10 ng/mL and (c, f) 100 ng/mL. Untreated cells for matched time-points selected were used for control purposes. Statistically significant differences are shown as * = $p \leq 0.05$, ** = $p \leq 0.01$, *** = $p \leq 0.005$, **** = $p \leq 0.001$; a = $p \leq 0.05$, b = $p \leq 0.01$ compared to NT.

2.4.4 Expression of COL1A1 and TNMD proteins

COL1A1 and TNMD proteins expression were investigated by quantitative immunofluorescence assay across both hBM-MSCs and hWJ-MSCs populations. Representative images and their quantification are shown in Figures 2-6, 2-7 and 2-8, respectively. The protein expression by hBM-MSCs and hWJ-MSCs was similar even if the time points explored were necessarily different, given the proliferation rate.

With regard to hBM-MSCs, 1 ng/mL of hGDF-5 was associated with no up-regulation of either protein. The expression of type I collagen increased by 1.5-fold and 2-fold after treatment with 10 and 100 ng/mL of hGDF-5, respectively, at Day 1 (Figure 2-6b), and was accompanied by tenomodulin increase (1.5-fold) after treatment with 10 and 100 ng/mL of hGDF-5 at Day 1 (Figure 2-6c). No cells aggregates were detected along the culture.

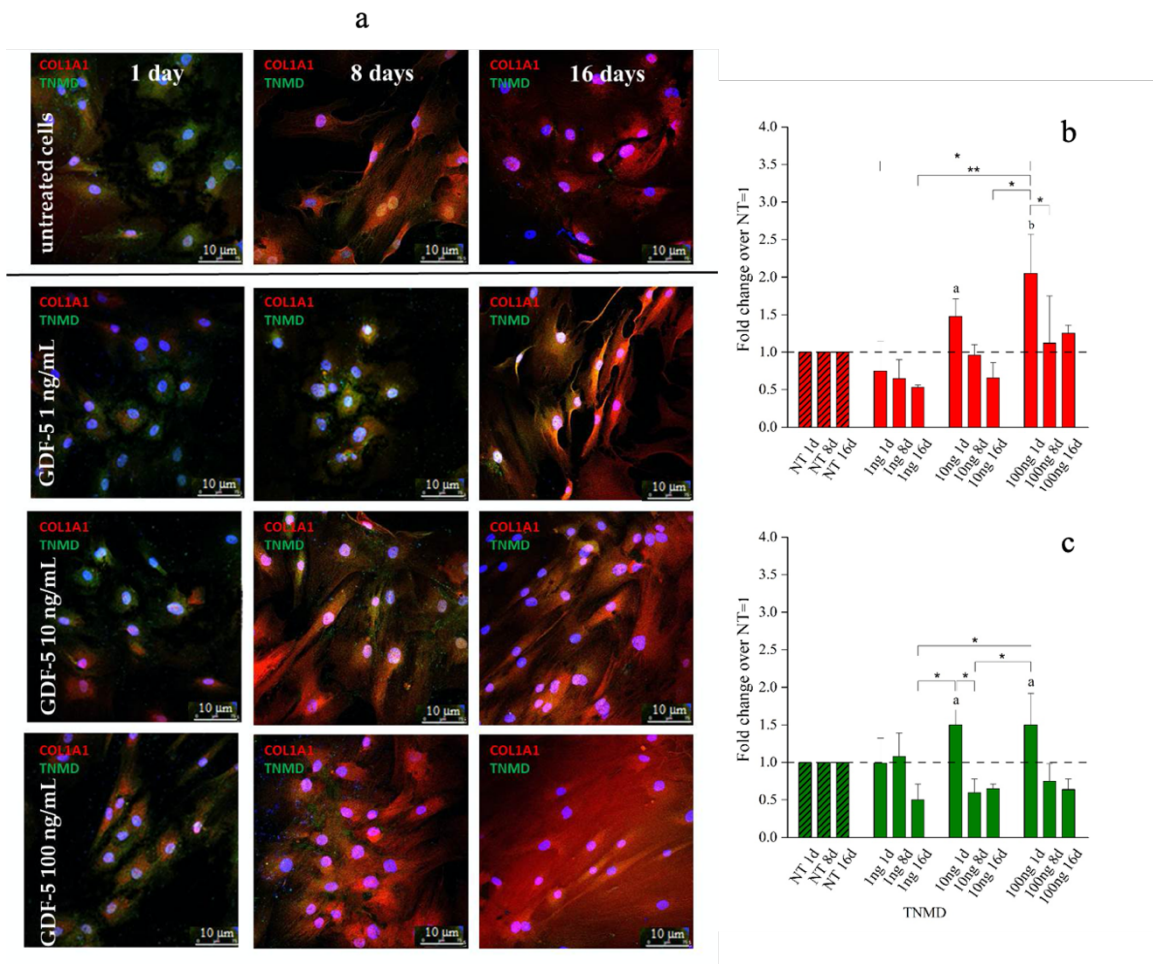


Figure 2-6. Immunofluorescence (IF) images and quantitative immunofluorescence (q-IF) data illustrating the effect of different hGDF-5 dose on hBM-MSCs. Panel (a) shows type I collagen (red staining) and tenomodulin (green staining) proteins up to 16 days of culture. Quantitative data on type I collagen (b) and tenomodulin (c) proteins were also reported; untreated cells (NT) are illustrated for comparison purpose. Statistically significant differences are shown as * = $p \leq 0.05$; ** = $p \leq 0.01$; *** = $p \leq 0.005$; **** = $p \leq 0.001$; a = $p \leq 0.05$, b = $p \leq 0.01$ compared to NT. (T0 = day 0; NT = untreated cells; 1ng = 1 ng/mL of hGDF-5; 10 ng = 10 ng/mL of hGDF-5; 100 ng = 100 ng/mL of hGDF-5; d = days).

Similar to hBM-MSCs, untreated hWJ-MSCs showed an increase in basal type I collagen over time; however, the protein was only largely overexpressed when 100 ng/mL of hGDF-5 were supplemented. Moreover, these cells achieved an extremely ordinate alignment in a specific direction and showed an elongated shape (Figure 2-7).

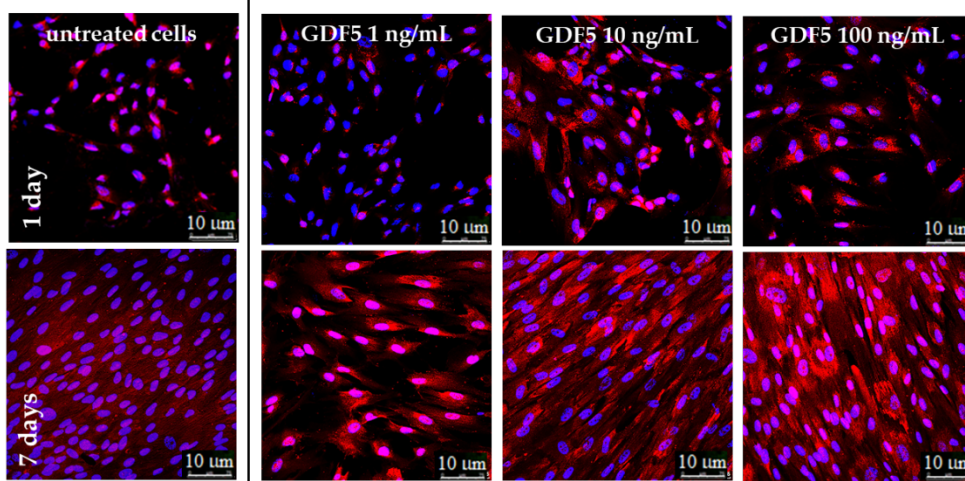


Figure 2-7. IF images illustrating the type I collagen expression at different hGDF-5 dose on hWJ-MSCs. Protein was stained in red and monitored up to seven days of culture.

Aggregation into 3D spindle-like structures was observed when cells were treated with 1 ng/mL of hGDF-5, while tubular-like 3D structures were observed when 100 ng/mL of growth factor was used after seven days of treatment. This tubular structure was already reported by Barboni *et al.*, and is considered an early organization of cellular 3D structure¹²⁶. TNMD was present within these spindle-shaped and tubular-shaped aggregates (Figure 2-8a). Quantification of immunofluorescence in hWJ-MSCs images indicated that the type I collagen signal was significantly increased by 1.5-fold and 2.0-fold after treatment with 100 ng/mL of hGDF-5 at Day 1 and Day 7, respectively (Figure 2-8b). TNMD staining showed a significant increase of 1.5-fold with 100 ng/mL of hGDF-5 at Day 7 (Figure 2-8c).

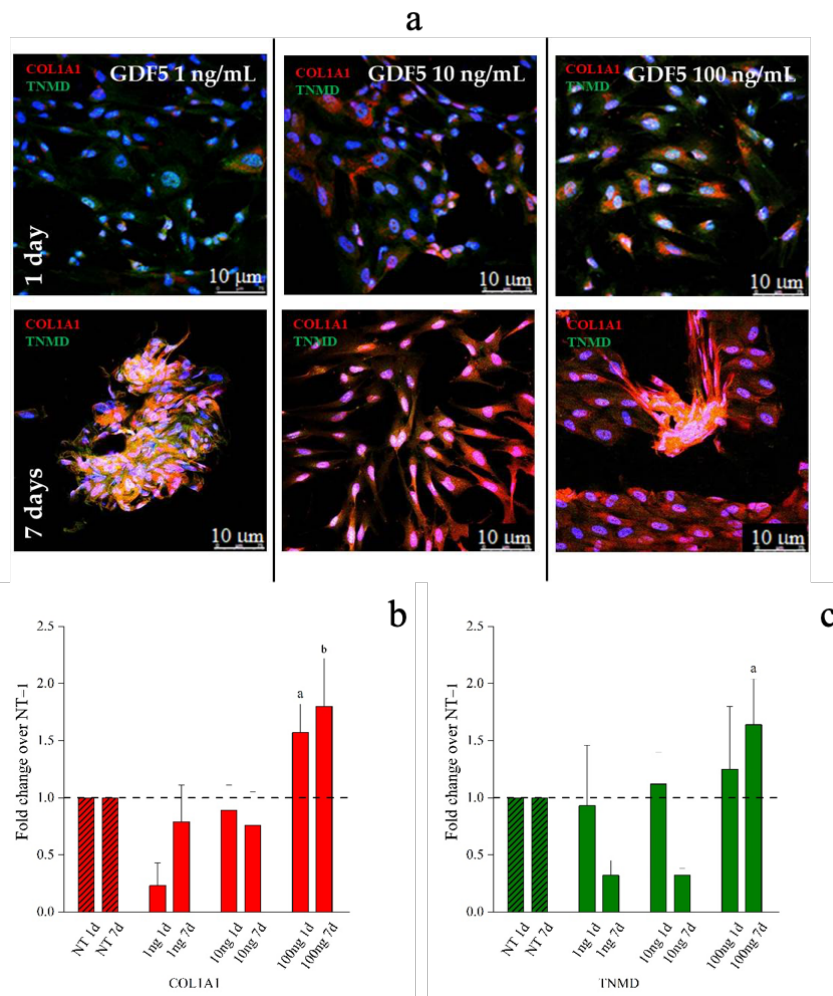


Figure 2-8. Immunofluorescence (IF) images and quantitative immunofluorescence (q-IF) data illustrating the effect of different hGDF-5 dose on hWJ-MSCs. The panel (a) shows type I collagen (red staining) and tenomodulin (green staining) proteins up to seven days of culture. Quantitative data on type I collagen (b) and tenomodulin (c) proteins were also reported; untreated cells (NT) are illustrated for comparison purpose. Statistically significant differences are shown as * = $p \leq 0.05$; ** = $p \leq 0.01$; *** = $p \leq 0.005$; **** = $p \leq 0.001$; a = $p \leq 0.05$, b = $p \leq 0.01$ compared to NT. (T0 = day 0; NT = untreated cells; 1ng = 1 ng/mL of hGDF-5; 10 ng = 10 ng/mL of hGDF-5; 100 ng = 100 ng/mL of hGDF-5; d = days).

2.4.5 Cells immunomodulatory activity

A key correlator with tendon repair and MSCs function is immunological responsiveness and modulation. Supplementation of 1 ng/mL of hGDF-5 on hBM-MSCs up-regulated both pro-inflammatory (IL-6: 4-fold; TNF: 4-fold; IL-12A: 6-fold and IL-1 β : 11.5-fold) and anti-inflammatory (IL-10: 3-fold and TGF β 1: 2.5-fold) cytokines, at Day 8, but not thereafter (Figure 2-9a). Conversely, with 10 ng/mL, up-regulation of IL-1 β (3-fold), only, was noted at Day 8 (Figure 2-9b). The highest dose of hGDF-5, 100 ng/mL, was accompanied by significant up-regulation of IL-1 β (11-fold) and IL-10 (10-fold) only at Day 8 (Figure 2-9c).

With regard to hWJ-MSCs, evaluation of pro- and anti-inflammatory cytokine expression following on from hGDF-5 supplementation revealed up-regulation of TNF (~1.5-fold) at Day 3 with 1 ng/mL (Figure 2-9d). With 10 ng/mL hGDF-5 supplementation, we again noted up-regulation of TNF (2-fold) at Day 3 (Figure 2-9e). Finally, with 100 ng/mL hGDF5 supplementation, we noted significant up-regulation of IL-12A (1.5-fold), and again, IL-10 (2.5-fold) at Day 3 (Figure 2-9f).

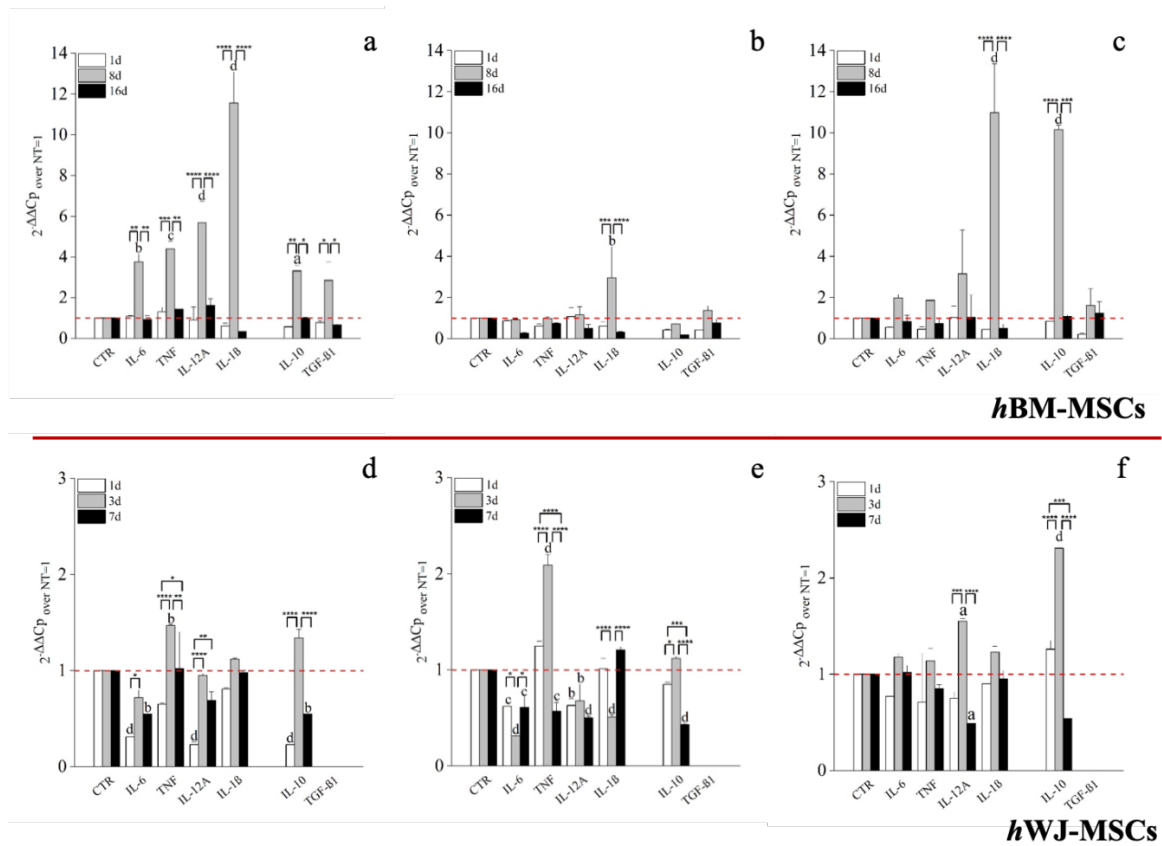


Figure 2-9. RT-PCR on the expression of cytokine by hBM-MSCs and hWJ-MSCs with the hGDF-5 concentration-dependent effect. The mRNA levels of both pro-inflammatory (IL-6, TNF, IL-12A and IL-1 β) and anti-inflammatory (IL-10 and TGF- β 1) cytokines were monitored at hGDF-5 concentrations of 1 ng/mL (a, d), 10 ng/mL (b, e) and 100 ng/mL (c, f). Untreated cells for matched time-points selected were used for control purposes. Statistically significant differences are shown as * = $p \leq 0.05$, ** = $p \leq 0.01$, *** = $p \leq 0.005$, **** = $p \leq 0.001$; a = $p \leq 0.05$, b = $p \leq 0.01$, c = $p \leq 0.005$, d = $p \leq 0.001$ compared to NT.

2.5 Discussion

We hypothesized that, as reported in the literature, supplementation of hGDF-5 to hBM-MSCs would result in up-regulation of genes and proteins consistent with tenogenic differentiation, and consequently, synthesize and secrete these into the extracellular environment. We further hypothesized a correlation between hMSCs differentiation and their immunomodulatory activity, through cytokines expression. We utilized hWJ-MSCs to determine their comparability

and behavior in the same conditions (three different concentrations of hGDF-5) and their possible *in vitro* use in tendon tissue-engineering. Different doses of hGDF-5 (1 ng/mL, 10 ng/mL and 100 ng/mL) were selected to explore a dose-response effect with regard to tenogenic commitment and cytokine profile behaviors. As reported in the introduction, the dosage range explored exerts have a biological action *in vitro* within tenogenic commitment studies^{249,131,136}. MSCs derived from adult sources have a very low proliferation potential²⁵⁹, and proliferation is reported to be inversely correlated to differentiation²⁶⁰. Therefore, we were able to explore hBM-MSCs behavior for up to 16 days, observing a lack of proliferation during hGDF-5 treatment. hWJ-MSCs showed several similarities, but also some differences. First, given their faster population doubling levels^{237,238,239}, treatment time longer than seven days was not possible, even though several and considerably lower seeding densities were explored. Our data are in strong agreement with previous literature in confirming the dose of 100 ng/mL as optimal for cells commitment toward a tenogenic phenotype. This observation was confirmed by morphometric analysis, which evidenced nuclei elongation with an increase of nuclei L/W ratio. hBM-MSCs showed specific tenoblast-like phenotype with an L/W ratio ≥ 1.5 when 100 ng/mL of hGDF-5 were supplemented at Day 8 and at Day 16. Instead, a tenocyte-like shape, coupled to the L/W ratio >1.7 was achieved by hWJ-MSCs after only seven days of treatment when 100 ng/mL of hGDF-5 was supplemented. In the case of hWJ-MSCs, we have not acquired images for intermediate time points, but, examining the results of the morphometric analysis in Figure 2-3c, cells supplemented with 100 ng/mL of GDF-5 were significantly more elongated than untreated cells at Day 7. This was not observed in the control; therefore, it cannot be considered an effect of confluency. Moreover, we noticed specific tenogenic markers overexpression by hWJ-MSCs at progressively earlier time points when increasing the dose of the growth factor administered. We elected to monitor the gene expression of TNC and SCX-A because TNC is an ECM glycoprotein considered an early marker of tenogenic differentiation, responsible of collagen fiber orientation³. At the same time, SCX-A is a tendon-specific basic helix-loop-helix transcription factor responsible for the transition of MSCs into tendon progenitors²¹⁸. These markers were up-regulated 1.3-fold at Day 8 with 1 ng/mL of hGDF-5, suggesting an activation of the tenogenic commitment pathway after 8 days of treatment. The same activation occurred earlier and was more pronounced when 100 ng/mL were supplemented, with SCX-A overexpressed 1.7-fold at Day 1 and TNC 1.3-fold, at Day 8. DCN was monitored because is the small leucine-rich proteoglycan involved in the regulation of fibrillogenesis, and is a fundamental component of the tendon extracellular matrix (ECM), binding to type I collagen fibrils²⁷. This protein was not really overexpressed by hBM-MSCs, except at Day 8 using 100 ng/mL (1.3-fold); this slight increase can be probably explained because the cells do not reach the complete organization of the ECM in all the experiments considered.

Type I collagen is the major component of tendon tissue (75–85% of the dry mass of tendon), and is responsible for its mechanical strength²⁶¹. The up-regulation of COL1A1 gene by hBM-MSCs reached 1.5-fold, even when a dose of 100 ng/mL of GDF5 was used. Nevertheless, the expression of TNMD was significantly increased, up to 12-fold, at the concentration of 100 ng/mL of hGDF-5 after eight days of treatment, suggesting cell commitment versus the specific tendon phenotype. Indeed, TNMD is a type II transmembrane protein, commonly detected in differentiated tenocytes, and is responsible for the organization of the collagen fibers in the late phase of tendon development⁸⁴. Furthermore, at 100 ng/mL of hGDF-5, the COL3A1 up-regulation was reduced to only 1.3-fold after eight days; indeed, this gene is basically overexpressed by hBM-MSCs, and is the main responsible for fibrotic and scar tissue arrangement, and has been reported at the site of rupture of human tendons²⁶¹. Since an early expression of SCX-A is reported to be a highly specific marker for tenocyte progenitor cell populations [36] and TNC up-regulation intervenes at the very beginning of tendon development [11], PCR data about hWJ-MSCs were favorable with a clear statistically significant overexpression of SCX-A (3.8-fold), COL1A1 (3-fold), TNC (2.3-fold) and DCN (2.7-fold) observed with 100 ng/mL of hGDF-5 at Day 3. However, hWJ-MSCs, in these conditions, also overexpressed COL3A1, which increased 2.8-fold, compared to the control, at Day 3. The overexpression of COL3A1 was always higher compared to hBM-MSCs. Nevertheless, we have to take into account that an early tenogenic commitment can be manifest by over-expression of SCX-A and COL1A1, an expected outcome of the tenogenic differentiation process, as stated before, because SCX-A regulates tendon formation and several other characteristics gene expression²⁵⁹. SCX-A also regulates the expression of TNMD²⁵⁹, but, since TNMD is a marker of mature tenocytes, we suspect that the expression of this gene was not observed in the case of hWJ-MSCs because it would be further up-regulated if our experiments were extended to a longer period of time.

The commitment of hBM-MSCs was confirmed by quantitative immunofluorescence assay. This investigation showed a basal level of type I collagen protein which was also evident in control cells, as largely documented²⁶², but a great overexpression of this protein was evident when 100 ng/mL were supplemented, while tenomodulin was evident only at the highest hGDF-5 dose tested. Immunofluorescence (IF) observations confirmed that cells showed an ordinate aligned pattern along a specific direction at an hGDF-5 dose of 100 ng/mL at Day 16 with evident shape change in the cells, which became ovoid. The overall data are in good agreement with the literature, and confirmed that hBM-MSCs are the gold standard to set *in vitro* protocols to study tenogenesis or tendon differentiation and healing.

In the case of hBM-MSCs, the overall trend of type I collagen is in agreement with published data, suggesting that the initial phases of tenogenic commitment occurred with different timelines in MSCs, though sharing similar characteristics^{131,136}. In the case of hWJ-MSCs, it is difficult to put our result in

the context of published data, because no similar study has been reported to date on hWJ-MSCs. However, under these experimental conditions, they seem to respond by activating tenogenic commitment events.

Regarding the mRNA levels of pro-inflammatory and anti-inflammatory cytokines, we noticed in hBM-MSCs a strong up-regulation of pro-inflammatory cytokines when the lowest concentration of hGDF-5 was used, above all IL-1 β , which reached an 11.5-fold increase at Day 8. However, the strong up-regulation of IL-1 β was better balanced by IL-10 (10-fold increase) when 100 ng/mL of hGDF-5 were used, suggesting that a differentiation process occurs and it could be accompanied by the immunomodulatory activity of hBM-MSCs in an anti-inflammatory fashion, as reported in the literature²⁵⁴. However, the early tenogenic commitment of hWJ-MSCs observed with 100 ng/mL at Day 3 was accompanied, similarly to hBM-MSCs, by an adjustment of their immunomodulatory response up-regulating the anti-inflammatory cytokine, such as IL-10 (2.5-fold). Unfortunately, to the best of our knowledge, this particular aspect of the behaviour of hWJ-MSCs have never been studied, so the hypothetic correlation between hWJ-MSCs and their immunomodulatory activity needs further investigations.

2.6 Conclusions

hGDF-5 induces cellular events of tenogenic differentiation that can be time and concentration-dependent. The concentration of 100 ng/mL is more effective in this sense, correlating with an anti-inflammatory immunomodulatory response of cells. This behavior was observed on both stem cells, bone marrow and umbilical cord derived. While the proliferation of hBM-MSCs is only slightly promoted during hGDF-5 treatment, the hWJ-MSCs population maintained a high proliferation rate. After seven days and at the dose of 100 ng/mL of hGDF-5, hWJ-MSCs manifested the up-regulation of tenogenic markers and showed L/W ratio > 1.7.

Although the use of autologous stem cells for tendon healing and regeneration has been described and all tissue-engineering studies indicated hBM-MSCs as the gold standard to promote tendon regeneration, hWJ-MSCs have never been studied in this sense and may be an interesting option. Our data suggest that, given their properties, hWJ-MSCs could be potentially used in more complex *in vitro* tendon tissue-engineering strategies, as described in Chapter 5.

Chapter 3

Fabrication and Characterization of PLGA-NCs for hGDF-5 controlled delivery

Ref: Palazzo I, Lamparelli EP, Ciardulli MC et al. Int J Pharm. 592:120108. 2021.

3.1 Introduction

As described in Chapter 1, tissue engineering strategies have relied on engineered 3D scaffolds to provide architectural templates that can mimic the native cell environment. Among the technologies proposed for the fabrication of 3D scaffolds, hydrogel moulding or plotting has been largely described, because a predefined microstructural organization can be easily obtained by stratifying a 3D structure, layer by layer²⁶³. Particularly, 3D hydrogels prepared with both moulding or biplotting strategies, can contain cells and microadditives dispersed within them, in a specific concentration per unit volume, to achieve given predesigned functional characteristics. Among all the additives, biopolymer micro/nano-carriers, conventionally described in controlled drug delivery formulations, have been recently proposed. These microdevices/nanodevices are able to deliver specific molecules in a controlled manner and, therefore, can be used to fabricate an organized 3D microenvironment in which several biosignals can be delivered with a spatial and/or temporal design to stimulate the living cells hosted within²⁶⁴. This last aspect becomes critical in tissue engineering applications that involve musculoskeletal soft tissues such as tendons, ligaments, cartilage, and their interfaces because, in these tissues, cells would have a more pronounced fibrous cytoskeletal organization²⁶⁵.

As hMSCs can differentiate into multiple tissue-forming cell lineages under stimulation by different GFs, the strategy is to deliver specific GFs during the hMSCs cultivation; hence, they can be guided toward different tissue types²⁶⁶. The conventional way to add GFs within *in vitro* cell culture is by adding them into the external medium; this solution has several drawbacks, including the short half-life of the molecule, but a major one is the reduced bioavailability caused by the mass transfer barrier to diffusion within the 3D structure²⁶⁷. Thus, it has often been suggested to use an excess of GFs in the external medium; a fine tuning of the GF concentrations delivered to the cells still seems challenging^{268,269}. Indeed, in some approaches of bone and cartilage regeneration, both *in vitro* and *in vivo*, the GFs are reported to be adsorbed to the scaffolds. In these cases, a strong “burst effect” in the first few days of cultivation is always described, often followed by poor bioavailability of the same factor in the subsequent days of cultivation^{270,271,272}. Moreover, the recent literature shows that the spatial and temporal distribution concentrations of the GF within a 3D scaffold system has been poorly investigated. Also their effective dosage to be delivered in the microenvironment near the cells has not been really optimized to a minimum effective dosage^{273,274,275}.

In this sense, the use of biopolymer micro/nano-carriers for the controlled delivery of selected molecules or peptides within a 3D predesigned structure could be an interesting approach. Indeed, attempting to influence cell phenotype, a sustained release of GFs, by means of devices such as micro/nano-spheres, supplies a higher level of control, compared with simple medium supplementation (Figure 3-1).

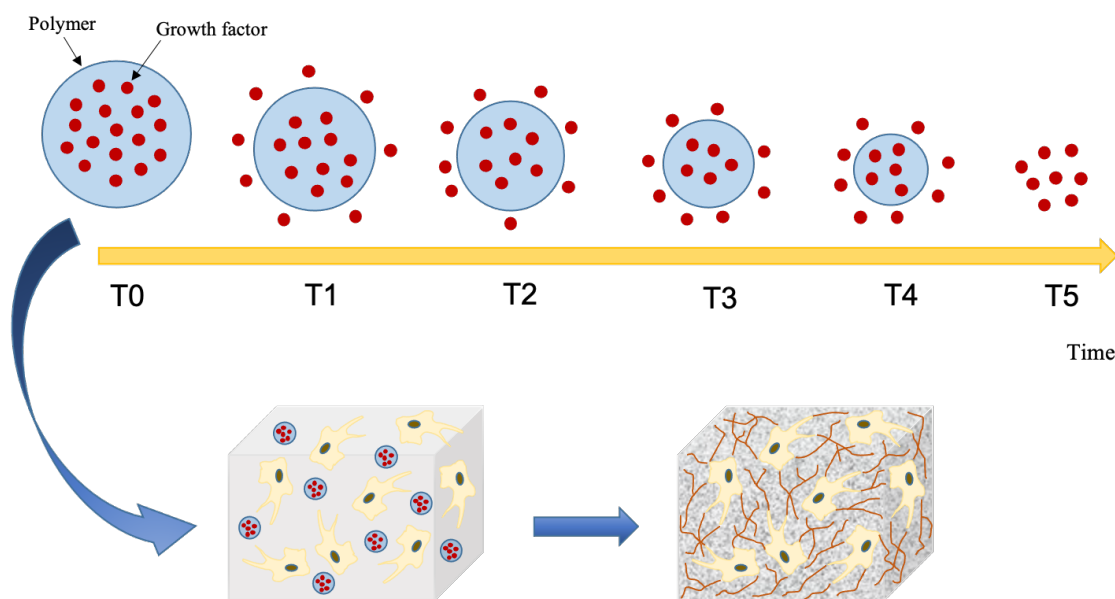


Figure 3-1. Biopolymer microspheres for controlled drug delivery. As the biopolymer degrades, biomolecules are released, with sustained delivery over time. Because of this feature, microspheres can be supplemented to 3D scaffolds, where they can deliver specific biosignals close to the cells, to direct and promote their differentiation.

Poly-lactic-co-glycolic acid (PLGA) are FDA-approved bioresorbable carriers^{276,277} capable of bulk degradation without swelling and with a recognized capacity of ensuring controlled release rates of loaded drugs^{278,279,280,281,282}. Several techniques are available to prepare biopolymer-based micro/nano-carriers, but the solvent evaporation/extraction (SE) of emulsions (single, double or multiple) is the most widely used (Figure 3-2). In the most common case (the double water-oil-water emulsion processing), the process involves the formulation of an oil-in-water emulsion, wherein the biopolymer is dissolved in a water immiscible, volatile organic solvent. The bioactive molecule is solubilized in water plus surfactant medium and then added to the polymer solution to produce the primary water-in-oil formulation. The primary emulsion is, then, emulsified (with appropriate stirring and temperature conditions) in a larger volume of water in the presence of an emulsifier, such as poly-vinylalcohol (PVA) or Tween 80/20, to yield a water-oil-water emulsion. The emulsion is subjected to solvent removal by either an evaporation or extraction process to harden the oil droplets. In the former case, the emulsion is maintained at a reduced pressure or at atmospheric pressure, with a low stir rate, to enable the volatile solvent to evaporate. In the latter case, the emulsion is transferred into a large quantity of water or other quench medium, in which the solvent associated with the oil droplets is diffused out. The solid microspheres obtained are then washed and collected by filtration or centrifugation; thereafter, they are dried under appropriate conditions or lyophilized²⁸³. The rate of solvent removal by the evaporation method strongly

influences the characteristics of the final microspheres, and it depends on the temperature and pressure, whereas the rate of solvent removal by the extraction method depends on the temperature of quench water or other medium, and ratio of emulsion volume to quench water/medium volume²⁸⁴. Solvent evaporation requires relatively high temperatures or reduced pressures, and shows batch-to-batch reproducibility disturbances. Solvent extraction uses relatively large amounts of a second solvent with the subsequent problem of solvent mixture recovery. Both processes also require long processing times (several hours), and, as a consequence, aggregation phenomena may occur between the droplets, producing microspheres with a larger polydispersity, with respect to the droplets in the starting emulsion²⁸⁵. Another disadvantage of the above-described methods is the poor encapsulation efficiencies of moderately water-soluble and water-soluble compounds. Indeed, these molecules could diffuse out from the dispersed oil phase into the aqueous continuous phase, and their microcrystalline fragments can deposit on the microsphere surface and/or outside of the biopolymer matrix²⁸⁶.

Recently, a dense gas has been proposed as a quenching medium, leading to a novel technology named supercritical extraction of emulsion: the oily phase is extracted by carbon dioxide compressed up to its critical point (Figure 3-2). Temperature and pressure variations can induce changes in the physical state of a substance, and, above the critical pressure (P_c) and temperature (T_c), a substance exists as a supercritical fluid. For a supercritical fluid, dynamic viscosities are close to those found in normal gas, and the diffusion coefficient is more than ten times larger than that of a liquid. These properties depend on temperature and pressure: diffusivity increases with an increase in temperature, whereas viscosity decreases (unlike gases) with a temperature increase. This behavior allows the use of supercritical fluids as solvents in chemical processes with an adjustable solvent power easily variable by changing the operative pressure and temperature in different parts of the plant. Supercritical carbon dioxide (SC-CO₂) is extremely attractive for several industrial applications because it is considered a “green” solvent; indeed, carbon dioxide is not flammable, and is nontoxic and inert. In addition, the supercritical regime of CO₂ is readily accessible because of its critical temperature (37°C) and pressure (74 bar)²⁸⁷. Several supercritical technologies described the use of SC-CO₂ to produce microparticles²⁸⁸. Indeed, the use of SC-CO₂ has been described as a ground-breaking solvent for biopolymer micro/nanodevices manufacturing, starting from emulsion. Particularly, SC-CO₂ is used as the extracting agent of the oily phase of emulsions to lead to solvent-free microparticles^{289,290,291}. In details, the described advantage of using SC-CO₂ are the reduction of micro/nanoparticle aggregation (typical of traditional technologies) because of the fast processing that occurs in 2/3 min against the several hours required by conventional evaporation/extraction^{292,293,294}. Greater product uniformity, higher throughput with smaller plant volumes, and elimination of batch-to-batch repeatability problems were other relevant advantages observed^{295,296,297}.

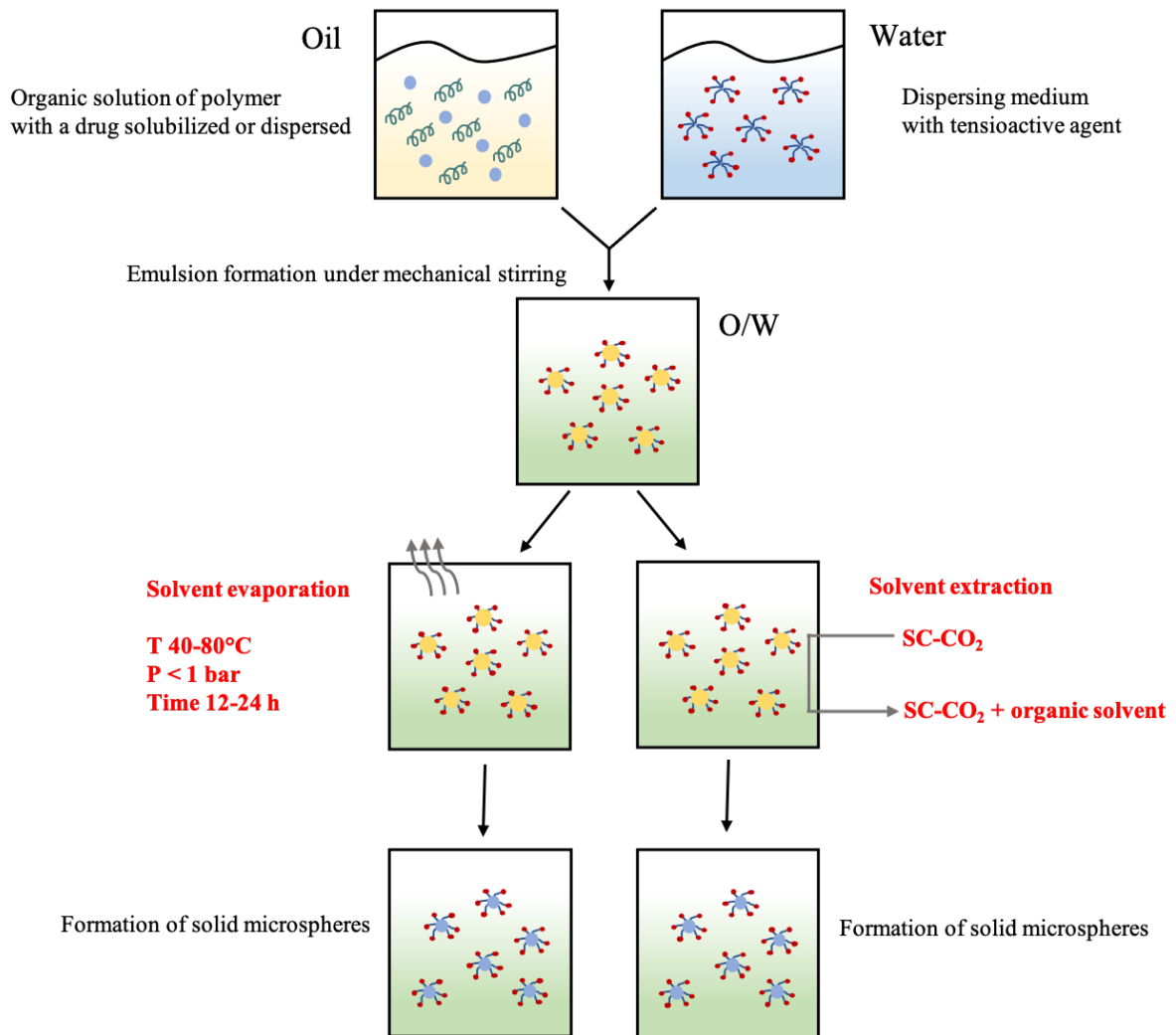


Figure 3-2. Schematic comparison between solvent evaporation (SE) and supercritical emulsion extraction (SEE) technologies. After emulsion formulation [oil-in-water (o/w) or water-oil-water (w1/o/w2)], the solvent of the oily phase can be removed by evaporation at 40/50°C temperature or reduced pressure and stirring for several hours (solvent evaporation), whereas in the SEE process the solvent is extracted in few minutes using supercritical carbon dioxide (SC-CO₂). In both cases, the result is the formation of solid microspheres that, once collected, are dried or lyophilized. SEE technologies prevent any aggregation phenomena, ensuring a precise control of the micro/nano capsule size distribution, and provide higher encapsulation efficiency because of faster and more effective extraction.

Supercritical extraction of emulsion technology has been described as an effective technology to fabricate microcarriers of different biopolymers such as PLGA, PLA, and PCL loaded with several bioactive molecules²⁹⁸. However, despite the large investigation on SEE carrier formulation in term of size distributions²⁹⁹ and drug loading optimization³⁰⁰, to date few investigations described the cytotoxicity of the produced particles. Particularly, *in vitro* cytotoxicity tests, including cell viability and proliferation studies are considered important screening assays, capable of evaluating the reaction of living cells to the implant and to assess safety characteristics of the produced carriers. Up to now, very few cytotoxicity characterizations have been described

for the micro/nano materials fabricated by dense gases, while several assays have been performed for carrier fabrication using conventional technologies^{301,302}. Different cell models can be used to assess the cytotoxic activity of biomaterials. For example, Chinese Hamster Ovary cells (CHO-K1) are mitotic primary cells and, therefore, they may provide indications on genotoxicity³⁰³. Human-Peripheral Blood Mononuclear Cells (hPBMCs), isolated from human healthy donors, can provide indications of the immune reaction to the biopolymer devices and can better mimic *in vivo* conditions^{304,303}.

3.2 Aim

Several emulsion formulation protocols were processed by SEE using PLGA with different molecular weights or co-polymer ratios to fix carrier size and distribution. Then, hGDF-5 was added to the formulation to provide data about the drug loading and related release profiles. Cytotoxicity was monitored using two different cell types, from both animal and human sources, CHO-K1 and hPBMCs. These data are extremely important for the use of carriers in *in vitro* (and *in vivo*) tissue engineering applications. Micro and nano-carriers, with controlled size and suitable encapsulation efficiency, may act as micro-environmental regulators within a 3D bioengineered scaffold, providing a wide range of spatio-temporally controlled bio-molecule delivery to trigger differentiation processes, as described in Chapters 4 and 5.

3.3 Materials and Methods

3.3.1 Emulsions preparation

Emulsions were obtained using a ratio of 1:19:80 water-oil-water (w1/o/w2). Oily phase was prepared by solubilizing a given amount of PLGA (RESOMER 504H, ratio 50:50 Mw 38,000–54,000 Da, indicated as high Mw-PLGA and RESOMER 752H, ratio 75:25, Mw 4,000–15,000 Da, indicated as low Mw-PLGA, Evonik Industries, Essen, DE). A variable amount of PBS solution 1X (Corning Cellgro, Manassas, VA, USA) containing Human Serum Albumin 1% w/v ($\geq 98\%$, HSA, Aldrich Chemical Co., Milan, IT) and PVA 0.06% w/w (Mol wt: 30,000–55,000, Aldrich Chemical Co., Milan, IT) was used as water internal phase. Recombinant hGDF-5 (PeproTech; UK) was reconstituted in Milli-Q water to a final concentration of 1 $\mu\text{g}/\mu\text{L}$. w1 was mixed with the oily phase to form a primary w1/o emulsion by sonication with a digital ultrasonic probe operating at 30% of its amplitude (mod. S-450D; Branson Ultrasonic Corp. Danbury, Connecticut, USA). When active growth factors were added, the inner water phase was mixed with the oily phase by vortexing (mod. Velp Scientifica, Monza, IT) at maximum speed for 30 sec. The primary emulsion was then slowly added into Ethyl Acetate (99.9%, Aldrich Chemical Co., Milan, IT) saturated aqueous Tween80 solution (Sigma-Aldrich, Milan, IT) by high-speed stirring (mod. L4RT, Silverson Machines Ltd., Waterside, Chesham, Bucks,

UK). In some cases, 15% w/w of glucose (Sigma-Aldrich, Milan, IT) was added in the water external phase. A constant temperature of 10°C was assured during emulsion phase mixing. All emulsions were processed by SEE immediately after their preparation.

3.3.2 Dense gas technology protocol

SEE is a continuous process which involves the continuous countercurrent extraction of solvent in the oily phase of emulsion by supercritical carbon dioxide. The prototype apparatus consists of a packed column with stainless steel pickings (1889 m⁻¹ specific surface and 0.94 voidage; Pro-Pak, Scientific Development Company, State College, PA, USA) where gaseous and liquid phases are in contact counter-current. The main apparatus system is formed by three extraction cascades in which the emulsion is introduced at the top, and CO₂ from the bottom, so counter-current flows are obtained²⁹⁵. The three stages are formed by AISI 316 stainless steel cylindrical sections of 30 cm height, connected by four cross-unions. A refrigerated cyclonic separator is located downstream the top of the column for oily phase recovery through a micrometric valve. Another separator is located at the bottom of the column to collect the water external phase with carriers. The high-pressure diaphragm pump (mod. Milroyal B, Milton Roy, Pont Saint-Pierre, FR) is used to deliver the dense-CO₂ at a selected flow rate (1.4 kg/h); a high pressure piston pump (mod. 305, Gilson, FR) is used to feed the emulsion at a constant flow rate (2.4 ml/min). A rotameter and a dry test meter, located at the exit of the separator, measure the CO₂ flow rate and the total amount delivered, respectively. The column is thermally isolated by ceramic cloths, and temperatures profiles are controlled by six controllers, located at different heights of the column²⁹⁴. The SEE process scheme with a continuous counter-current operation is shown in Figure 3-3.

To optimize performance, it is necessary to reach a steady state condition in the apparatus with proper gas/liquid mixing and complete wetting of the packing element of the column. This pre-conditioning operation was performed using a w1/o/w2 emulsion formed by only solvents and surfactant. Finally, a washing step is performed to recover the carriers still retained in the column packing elements. Normally, 70% of the overall polymer used in the emulsion is recovered for each run as a result of the loss of emulsion/suspension caused by dead volumes of SEE apparatus. The organic solvent recovered is less than 50% in weight of the solvent loaded in the emulsion, from partial loss in the gas stream at the exit of the separator located at the top of the column.

PLGA carriers are not amenable to conventional sterilization methods such as ethanol washing, gamma irradiation or steam because of biopolymer oxidation³⁰⁵ and further degradation of peptide payload. To overcome these challenges, a specific SEE operational protocol was set. Carriers, collected from each run, were always washed in sterile conditions with a

penicillin/streptomycin 1% w/v (Life Technologies Inc., USA) and amphotericin 1% w/v (Life Technologies Inc., USA) solution to ensure removal of the surfactant and ensure cell culture-grade preparation, centrifuged for 50 min at 6500 rpm at 4°C (model IEC CL30R Thermo Scientific, Rodano, Milan, IT), recovered using a membrane filtration (filter 0.2 μm HA Millipore, Sigma Aldrich, Milan, IT). All experiments were repeated twice ($n = 2$).

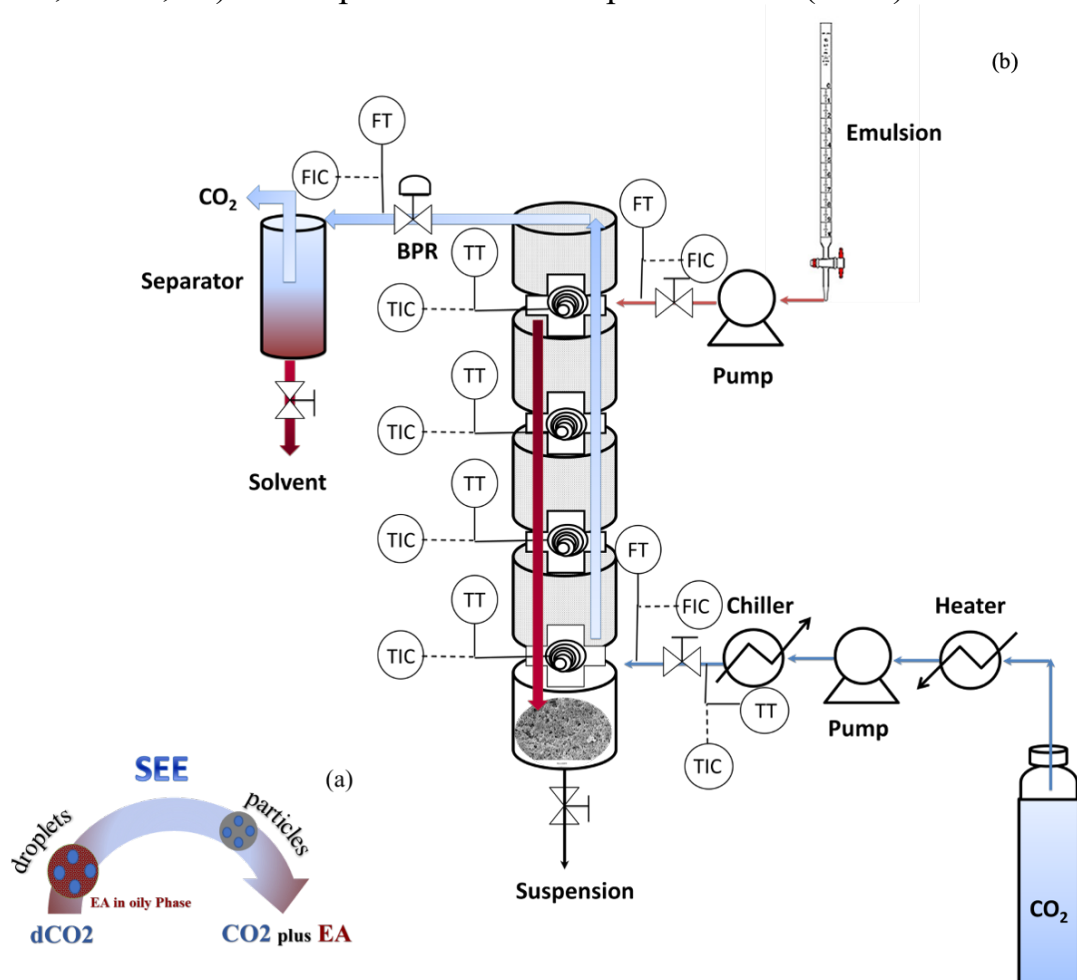


Figure 3-3. Schematic illustration of SEE process. Representation of droplet (in emulsion) shrinkage and polymer particle formation after the oily phase extraction by dense- CO_2 (a). SEE apparatus layout with the packed column operating in counter-current mode; other legends: CO_2 supply; chiller used for CO_2 cooling; diaphragm pump used for high pressure CO_2 ; heater used for SC- CO_2 heating; emulsion supply; piston pump used for the emulsion; TT-TIC, temperature control; FT-FIC, flow rate control; BPR, back pressure regulator; separator used for CO_2 and solvent recovery; suspension recovery (b).

3.3.3 Morphological and size distribution analysis

The droplets of the emulsions were observed using an optical microscope (mod. BX 50 Olympus, Tokyo, JP) equipped with a phase contrast condenser. Droplet size distributions (DSDs) and Particle Size distributions (PSDs) were measured by dynamic light scattering (DLS, mod. Mastersizer S, Malvern Instruments Ltd., Worcestershire, UK). Analyses were performed using several milligrams of each sample (corresponding to more than one million droplets or particles).

Size evaluation analyses were performed in triplicate. Mean and standard deviation were calculated for all data. The shrinkage factor percentage (SF%) was calculated as indicated in equation (1):

$$\% \text{Shrinkage} = (1 - \text{carriersmeansize}/\text{dropletsmeansize}) \times 100 \quad (1)$$

Carrier morphology was observed using a Field Emission-Scanning Electron Microscope (FE-SEM mod. LEO 1525, Carl Zeiss SMT AG, Oberkochen, DE). Powder samples of each test were placed on a double sided adhesive carbon tape previously glued to an aluminum stub and coated with a gold film (250 Å thickness) using a sputter coater (mod.108 A; Agar Scientific, Stansted, UK).

3.3.4 GDF-5 release study and encapsulation efficiency

GDF-5 release profiles were monitored *in vitro* by suspending approximately 5 (± 0.3) mg of carriers in 0.5 mL of Minimum Essential Medium Alpha (α -MEM) (Corning Cellgro, Manassas, VA, USA) plus 0.1% w/w Tween 20 (Sigma-Aldrich, Milan, IT), which was placed in an incubator at 37°C, and stirred continuously at 100 rpm. Every 24 h, the samples were centrifuged at 12,000 rcf for 10 min and the supernatant completely removed and replaced with fresh media to maintain sink conditions. The concentration of the released peptides were then measured with an Enzyme Linked Immunosorbent Assay (ELISA, Cloud-Clone Corp., USA). Release experiments were performed in duplicate ($n = 2$) and the curve describes the mean profile calculated as ng of growth factor released from 100 mg of polymer versus time. Encapsulation Efficiency (%) was defined as the ratio between loaded peptides in the emulsion and recovered per g of polymer; this value is expressed as a percentage.

3.3.5 Cells isolation and harvesting

Chinese Hamster Ovary Cells sub-clone K1 (CHO-K1, ATCC® CCL-61™) were seeded in 96-well plates at a density of 10.000 cells/well and cultured in HAM's F12 medium supplemented with 10% FBS (Life Technologies Inc.) and 1% penicillin/streptomycin (50 U/mL) (Life Technologies Inc., USA). Cells were then incubated in a humidified atmosphere containing 5% CO₂ and 95% air. Human Peripheral Blood Mononuclear Cells (hPBMCs) were obtained from three healthy donors (age 25–40 years) and separated by Ficoll-Hypaque gradient density (Sigma-Aldrich, Milan, IT) following standard techniques³⁰³. All donors gave their written informed consent in accordance with the Declaration of Helsinki for the use of their residual blood for research purposes, with approval from the University Hospital of Salerno Institutional Review Board. After isolation, cells were re-suspended in Roswell Park Memorial Institute medium (RPMI, Life Technologies Inc., USA), supplemented with 10% heat-inactivated FBS (Life Technologies Inc.), 10 mg/mL L-glutamine (Life Technologies Inc., USA), and penicillin/streptomycin (50 U/mL) (Life Technologies Inc., USA). Cells were then seeded in 96-well plates at a density

of 10.000 cells/well and incubated in a humidified atmosphere containing 5% CO₂ and 95% air.

3.3.6 Cytotoxic activity

Cell metabolic activity was analyzed using the MTT assay. Briefly, cells were treated with decreasing amounts of growth factor loaded and unloaded PLGA carriers; pure growth factor were also tested at different concentrations for 24 and 48 h. All carriers were suspended in culture medium using ultrasound in ice-cold (Elmasonic P, Elma Schmidbauer GmbH, DE). Following treatment, 3-(4,5-Dimethylthiazol-2-yl)-2,5-diphenyl-tetrazolium bromide (MTT, Sigma-Aldrich, Milan, IT) was added (1 mg/mL) to each well and incubated at 37°C for an additional 4h. Plates were centrifuged at 300 g for 10 min and the supernatants completely removed. Formazan products were dissolved in 100 µL of dimethyl sulfoxide (DMSO, Sigma-Aldrich, Milan, IT). Absorbance was determined at 490 nm using a microplate reader (Infinite F200 PRO, Tecan Group Ltd., SW). All assays were performed in triplicate (m = 3). For the MTT assay on hPBMCs, three independent experiments were performed in triplicate, each one on a single subject (n = 3). Cell metabolic activity, a surrogate of viability, was calculated as the percentage of the control group, considered as 100%. The percentage viability of cells was calculated according to equation (2):

$$\%Cellviability = (Absofsample - Absblank)/(Absofcontrol - Absblank) \times 100 \quad (2)$$

3.4 Results

3.4.1 Emulsion formulation optimization

A summary of all tested emulsion compositions and results in terms of mean diameter, polydispersity, and loading are summarized in Table 3-1.

The polymer concentration was fixed at 5% w/w in the oily phase. Several tests were performed using low Mw-PLGA (75:25) with a surfactant concentration of 0.6% w/w, and mixing the secondary emulsions at 2800 rpm for 6 min. In these conditions, PLGA emulsions had an average droplet diameter of 1388 ± 259 nm, and the related particles showed a mean size of 205 ± 32 nm.

Shrinkage was observed between the droplets and the solid particles in all experiments performed (see Table 3-1).

Preliminary tests of GDF-5 encapsulation were performed using the inactive epitope of growth factor (ihGDF-5). The surfactant concentration of 0.6% w/w was selected for ihGDF-5 encapsulation using low Mw-PLGA (75:25) biopolymer. Emulsion with a droplet mean size of 1453 ± 63 nm was obtained and related carriers with a mean size of 193 ± 19 nm were fabricated. The SF was coherent with previous data (88%). However, low encapsulation efficiency was obtained, which was of 22%, with ihGDF-5 loading of 2.2 µg/g (Table 3-1).

For the active peptide (hGDF-5) encapsulation, milder conditions were adopted. The emulsion preparation protocol was modified and the primary emulsion was obtained using vortex at maximum speed for 30 sec, instead of ultrasound. Moreover, to improve encapsulation performance, larger particles were fabricated reducing the surfactant concentration at 0.1 %w/w in the external water phase and downgrading the rotational speed of emulsifier to 2000 rpm for 5 min. Also the emulsion water phases were modified aiming to reduce the osmotic gradient switched from external phase to internal water phase, therefore PBS 1X solution was adopted as inner water phase, whereas, external water phase was prepared using 0.1% w/w of Tween 80 plus glucose (15% w/w). Additionally, a PLGA co-polymer ratio of 50:50 with higher molecular weight (3,8000–54,000 Da) was selected, to increase oily phase dynamic viscosity. Adopting these new conditions, larger droplet mean sizes were obtained with a consequent increase of derived carriers that showed a size of 2073 ± 94 nm. However, the encapsulation efficiency was increased to 64%, with carrier loading of 3.2 $\mu\text{g/g}$ (see Table 3-1 and Figure 3-4).

| Polymer | Tween80 % w/w | Emulsion composition | DSD (\pm SD) nm | PSD (\pm SD) nm | SF % | Load $\mu\text{g/g}$ | EE % |
|---|---------------|---|--------------------|--------------------|------|----------------------|------|
| low Mw-PLGA, 75:25 | 0.6% | w1: 0.5mL water plus 0.06% PVA o: 1 g PLGA in 19.5 mL EA w2: 80 mL of EA _{sat} -W plus Tween80 | 1388 \pm 259 | 205 \pm 32 | 85 | -- | -- |
| low Mw-PLGA 75:25 plus ihGDF-5 | 0.6% | w1: 0.5mL W plus 0.06% PVA plus 10 μg ihGDF-5 o: 1 g PLGA in 19.5 mL EA w2: 80 mL of EA sat-W plus Tween80 | 1653 \pm 63 | 193 \pm 19 | 88 | 2.2 | 22% |
| <i>Mixing by sonicated plus mixing 2800 rpm for 6 m</i> | | | | | | | |
| high Mw-PLGA 50:50 plus hGDF-5 | 0.1% | w1: 250 uL PBS plus 0.06% w/w PVA plus 5 μg hGDF-5 o: 500 mg polymer in 5 mL EA w2: 50 mL of EA _{sat} -W plus 15% w/w glucose | 3391 \pm 1196 | 2073 \pm 94 | 84 | 3.2 | 64 |
| <i>Mixing by vortex and emulsifier 2000 rpm for 5 m</i> | | | | | | | |

Table 3-1. A summary of emulsion formulations processed with SEE technology. Internal water phase was always added with Human Serum Albumin (1 % w/w); the proteins was used as growth factor stabilizer.

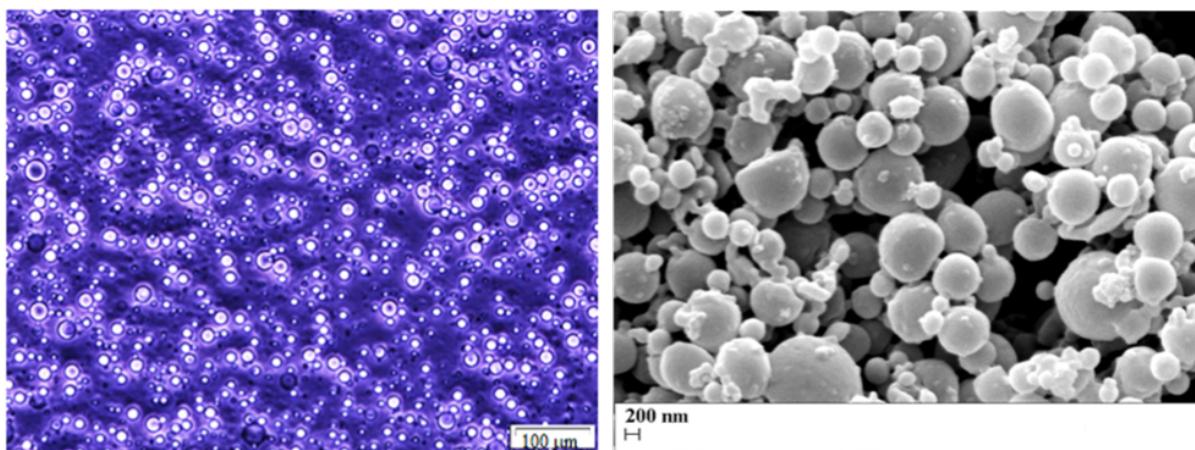


Figure 3-4. Optical image of emulsions and SEM image of carriers loaded with growth factor. High Mw-PLGA (50:50) loaded with hGDF-5.

3.4.2 Release profile study

The release profiles are related to the amounts of peptide (ng) released from 100 mg of carriers. In the case of hGDF-5 loaded carriers, loading of 3.2 $\mu\text{g/g}$ (high-Mw PLGA 50:50) provided a linear release profile over 25 days into α -MEM medium at 37°C (Figure 3-5), ensuring about 1.5 ng/mL released each day for the first 25 days.

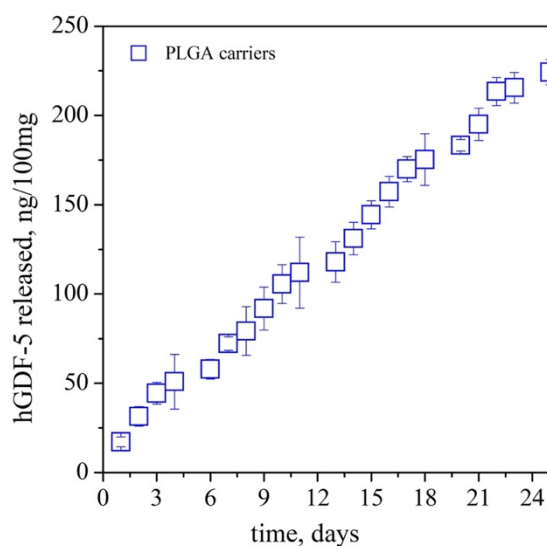


Figure 3-5. Release profiles of growth factors measured in α -MEM at 37°C for up to 25 days. The data are expressed as amounts (ng) of hGDF-5 released from 100 mg of carriers fabricated with high-MW PLGA (50:50).

3.4.3 Cytotoxicity studies on CHO-K1 and hPBMCs

The cytotoxicity of carriers was determined using CHO-K1 cells. Cells were incubated for 24 and 48 h using 10 $\mu\text{g/uL}$, 5 $\mu\text{g/uL}$, 2.50 $\mu\text{g/uL}$ and 1.25 $\mu\text{g/uL}$

concentrations of carriers (unloaded and loaded with growth factor) and their viability was analyzed using MTT assay.

PLGA carriers seemed to affect cell viability at lower, but not higher, concentrations (Figure 3-6). At 24 h, in the lowest concentrations, cell viability decreased up to a maximum of 50% with PLGA unloaded treatments, while the higher concentration seems to be less toxic with the highest (but not statistically significant) cell viability at 10 µg/uL, where cell viability reached about 60% at 48 h. On the other hand, treatment with pure growth factor, at the concentrations of 0.8 µg/uL; 0.6 µg/uL; 0.1 µg/uL, did not affect cell viability, stimulating cell viability and proliferation (Figure 3-6). At 24 h, 0.1 µg/uL of hGDF-5 induced the highest percentage of cell viability. At 48 h, the highest percentage of cell viability was obtained after pure hGDF-5 treatment at a concentration of 0.8 µg/uL (Figure 3-6).

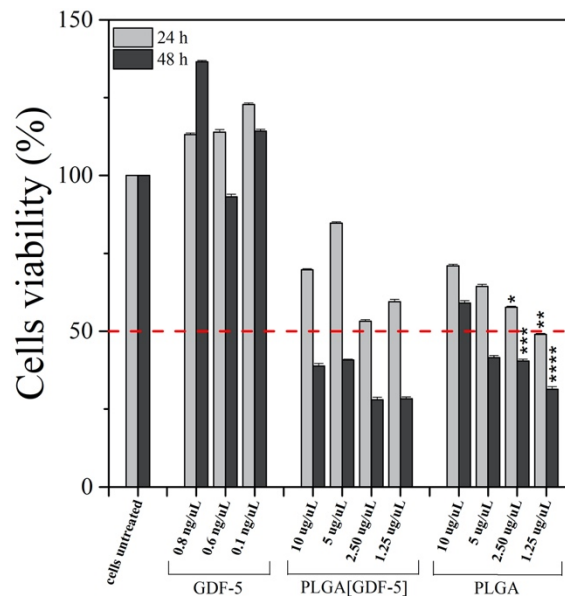


Figure 3-6. Carriers cytotoxicity evaluated using Chinese Hamster Ovary cell line (CHO-K1) that were treated with empty and loaded PLGA carriers for 24 h and 48 h. Empty PLGA carriers, free hGDF-5 and hGDF-5 loaded PLGA carriers were tested. The histograms report the mean percentage of viable cells compared to controls (untreated cells, 100%). The experiments were analyzed by two-tailed Student's t-test, * $p \leq 0.05$, ** $p < 0.01$, *** $p < 0.001$ and **** $p \leq 0.0001$; $n = 3$.

The cytotoxicity of high-Mw PLGA carriers loaded with hGDF-5 was also explored with hPBMCs. Cells were incubated for 24 and 48 h with decreasing concentrations of unloaded and hGDF5-loaded carriers, and viability analyzed by MTT assay as in the CHO-K1 cell system.

No cytotoxicity was detected in hPBMCs versus controls at either 24 h or 48 h of treatment with empty carriers. However, lower concentrations significantly improved cell viability (see Figure 3-8).

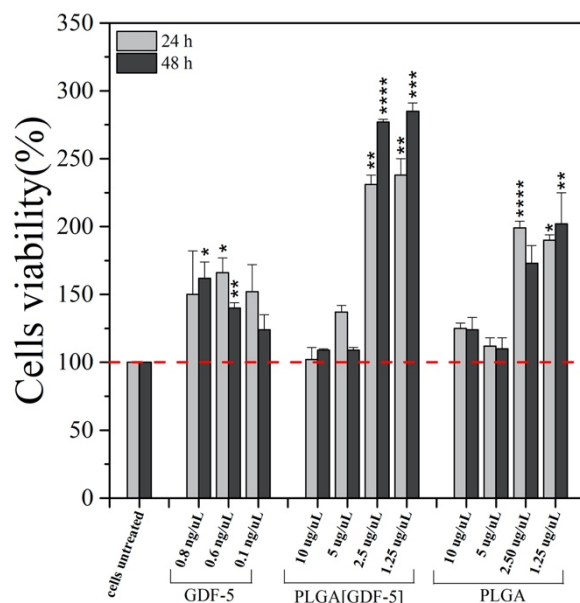


Figure 3-7. Carrier cytotoxicity evaluated using human peripheral blood mononuclear cells (hPBMCs). Cells were treated with decreasing amounts of empty and loaded high-Mw PLGA carriers for 24h and 48h: empty high-Mw PLGA carriers; free hGDF-5 and hGDF-5 loaded carriers. The histograms report the mean percentage of viable cells compared to controls (untreated cells, 100%). The experiments were analyzed by two-tailed Student's t-test * $p \leq 0.05$, ** $p < 0.01$, *** $p < 0.001$ and **** $p \leq 0.0001$; $n=3$.

3.5 Discussion

SEE pressure and temperature operating conditions were selected to extract the solvent from the oily phase, as illustrated in the schematic representation (Figure 3-3a). Pressure and temperature conditions were chosen at 8 MPa and 312 K and Liquid/Gas flow rate ratio was fixed at 0.1 (with CO₂ flow rate of 1.4 kg/h), according to the previous optimization^{295,296,300}. In these condition, the water suspension recovery displayed a solvent residue less than 100 ppm²⁹⁴.

The surfactant concentration in the external water phase was fixed at 0.6% for ihGDF-5 and at 0.1% for hGDF-5, as previously optimized³⁰⁶. The extremely low amount of growth factor used in the internal water phase was assumed not to exert any influence on carrier's morphology and size. GDF-5 was loaded in the emulsion formulation previously optimized, to observe its encapsulation efficiency and release profiles as well as carrier cytotoxicity.

The average diameter of droplets and carriers decreased when the concentration of surfactant increased. These data are in agreement with those previously reported²⁹⁹, confirming that higher surfactant concentrations lead to a higher number of micelles, which may stabilize smaller droplets in emulsion, and produce smaller particles. Lowering the surfactant concentration beyond 0.1% w/w of Tween 80, agglomerated droplets/particles were observed, from emulsion instability, probably induced by extremely low amount of micelles. This observation is in agreement with previous reports³⁰⁷.

Preliminary tests of hGDF-5 encapsulation were performed using the inactive epitope of growth factor (ihGDF-5) given high cost of the active recombinant form. However, the differences between the two epitopes were not relevant from the process point of view. The explored emulsion formulation conditions delivered anticipated carrier morphology and size control, but ensured low encapsulation efficiencies.

It is suggested that active peptide encapsulation requires milder conditions in terms of mixing times and velocity during the emulsion formulation. Moreover, the use of vortex (instead of ultrasound) was strongly recommended for emulsion phase mixing to avoid peptide denaturation. Sonication can induce changes in the structural and thermal properties of proteins and increase the enthalpy of denaturation from protein aggregation³⁰⁸.

Following these considerations, the emulsion preparation protocol was modified and the primary emulsion was obtained using vortex. Moreover, to improve encapsulation performance, larger particles were fabricated reducing the surfactant concentration and the rotational speed of emulsifier; to reduce the osmotic gradient switched from external phase to internal water phase³⁰⁹, the emulsion water phases were modified, adopting PBS 1X solution as inner water phase³¹⁰, whereas external water phase was supplemented with glucose. Additionally, a PLGA co-polymer ratio of 50:50 with higher molecular weight (3,8000–54,000 Da) was selected, to increase oily phase dynamic viscosity, which may also help the encapsulation efficiency²⁹⁹. Adopting these new conditions, larger droplet and carrier mean sizes were obtained, with higher encapsulation efficiency and loading.

The release profile studies are related to the amounts of peptide (ng) released from 100 mg of carriers. The linear profile obtained with the absence of a burst effect, a typical characteristic of these PLGA systems, may result from the nature of the growth factor or from the low amount loaded.

The cytotoxicity of carriers was studied on CHO-K1 cells. Cells were incubated with 10 µg/uL, 5 µg/uL, 2.50 µg/uL and 1.25 µg/uL of carriers (unloaded and loaded with growth factor) for 24 and 48h. Higher cytotoxicity was induced by lower concentrations of carriers. This was potentially a result of an interference of carrier material with specific cellular receptors and/or internal proteins involved in cell viability and proliferation together with a better internalization of carriers, when diluted. Efficient internalization of carriers by cells has been already reported by Ciaglia *et al.*, where the increasing granular appearance of gated monocytes supports the uptake of carriers³¹¹. We hypothesize that CHO-K1 cells might phagocytose carriers, affecting the relative viability. On the other hand, treatment with pure hGDF-5, at the concentrations of 0.8 µg/uL; 0.6 µg/uL; 0.1 µg/uL, did not affect cell viability, stimulating cell viability and proliferation (Figure 3-6). At 24 and 48 h, all hGDF-5 treatments increased cell viability compared to untreated cells. The treatment of proliferating CHO-K1 cells with hGDF-5/PLGA carriers exhibited a cytotoxic effect which did not exceed the effect observed for the empty carriers used at the same

concentrations. This suggests that the effect probably resulted from PLGA and not the hGDF-5 loaded carriers.

The cytotoxicity of high-Mw-PLGA carriers loaded with hGDF-5 was also explored at 24 h and 48 h on hPBMCs isolated from healthy donors to provide further evidence on toxicity of the encapsulated carriers directly on human primary cells. Lower concentrations significantly improved cell viability, suggesting a better uptake of the carriers with a significant enhancement of cell metabolism consistent with previous reports³¹². However, in contrast to CHO-K1 cells, PLGA carriers did not affect negatively cell survival, but instead resulted in modest increases (Figure 3-7). This suggests that both empty and loaded carriers, especially at lower concentrations, could stimulate cell proliferation by acting as mitogens or at a minimum improving mitochondrial metabolism. Therefore, the observed effects could be explained by either a stimulating effect on mitochondrial activity of the carriers and hGDF-5 or by a more general action of these compounds on hPBMCs survival, ultimately leading to an improvement of hPBMCs metabolism.

3.6 Conclusions

SEE technology can successfully encapsulate peptides, such as growth factors, into PLGA carriers, providing advanced control of carrier size and morphology, ensuring sustained growth factor release over 25 days. SEE-fabricated carriers do not present intrinsic toxicity, and they can be safely introduced within biomedical device structures as they are unlikely to pose a risk for human health. The present investigation opens new perspectives for the use of SEE fabricated carriers for the development of 3D bioengineered microenvironments where biological molecules can be released under controlled conditions stimulating tissue regeneration and healing (see Chapters 4 and 5).

Chapter 4

Development of HY-FIB 3D scaffold: effect of the mechanical signaling on the tenogenic commitment of hBM-MSCs

Ref: Ciardulli MC, Marino L, Lamparelli EP et al. Int J Mol Sci. 21(16):5905. 2020.

4.1 Introduction

As outlined in Chapter 1, tissue engineering strategies for tendon healing and regeneration are designed to improve existing therapies or provide new treatment possibilities. 3D bioengineered systems have the potential to promote our understanding of the physiopathology of tendinopathy and the role of stem cells in tendon regeneration. In this sense, 3D scaffold design and fabrication coupled to specific bioreactor arrangements could develop highly predictive 3D *in vitro* culture and differentiation systems to explore cell behaviors in response to defined external biochemical and mechanical stimuli³¹³. The 3D scaffold provides a model of fidelity via its provision of a microenvironment with defined stiffness and elastic modulus as well as the necessary surfaces for cell attachment^{314,315}.

Detailed understanding of cell behavior when incorporated into specific biomaterials allows to develop designs with specific functionalization. These functionalization may, for instance, stimulate local stem cells, attract specific circulating nucleated blood cells, such as macrophages, and induce their polarization into M2 phenotype to accelerate tissue regeneration and healing following the implantation of biomaterials *in vivo*³¹⁶. For example, human Mesenchymal Stem Cells (hMSCs) are largely used in tissue engineering strategies, and their immunomodulatory activity in the development of tendon pathologies have been explored, but the precise mechanisms involved remain undetermined^{317,102,318,319,320}. Neutrophils and macrophages infiltrate injured tendons, potentially interacting with MSCs and stimulating cytokine release at the site of repair and promoting degradation of the extracellular matrix (ECM), inflammation, apoptosis, and, in the later stages of acute tendon healing, they release anti-inflammatory cytokines to alleviate inflammation and promote tendon remodeling^{321,322}.

Among the biomaterials described for tendon tissue engineering³²³, a promising emerging strategy is the use of a complex biomimetic matrix with a hydrogel component and extracellular matrix mimicking properties^{232,324}. To overcome the intrinsic poor mechanical properties of the hydrogel, they can be merged with more force resistant biopolymers. Cells and biomaterials alone are not sufficient to achieve optimal levels of differentiation and matrix organization. Mechanical stimulation plays a key role in tenogenic differentiation induction²²¹. Scaffolds are therefore required to display an appropriate elastic behavior to deliver strain¹³⁰ or compression³²⁵ inputs. Strain is a tenogenic differentiation signal^{326,327,328,329}, and several bioreactors have been used to impart tenogenic mechanical stimuli to cells in culture^{221,203,330,229,215,230,225}. For example, Rinoldi *et al.* designed and fabricated 3D multilayered composite scaffolds, where an electrospun nanofibrous substrate was coated with a thin layer of GelMA-alginate composite hydrogel carrying MSCs. MSCs were subsequently differentiated by the addition of bone morphogenetic protein 12 (BMP-12) and, to mimic the natural function of tendons, the scaffolds were mechanically stimulated using a custom-built bioreactor²³⁰. Grier *et al.* described an aligned

collagen-glycosaminoglycan scaffold able to enhance tenogenic differentiation of MSCs via cyclic tensile strain within a bioreactor, in the absence of growth factor supplementation³³¹. Another protocol, proposed by Youngstrom *et al.*, promoted tenogenic differentiation of MSCs cultivated on decellularized tendon scaffolds with the application of 3% cyclic strain for one hour per day for 11 days³³⁰. Additionally, several growth factors (such as Growth Differentiation Factor-5^{248,249,163}) and other small molecules can stimulate transcriptional activation of genes involved in tenogenic differentiation^{232,332,333}.

Tendinopathies associated with physical activity and age-related degeneration are a major medical issue³³⁴, and recent healing and regeneration studies include the use of human Bone Marrow Mesenchymal Stem Cells (hBM-MSCs)^{335,336,337}. hBM-MSCs are a multipotent population present in bone marrow that can be readily differentiated *in vitro*^{338,339} into cells of three mesodermal lineages, namely adipocytes, chondrocytes and osteoblasts under appropriate conditions^{339,340,341,342}. MSCs-based therapies include direct transplantation of MSCs populations, growth factor-loaded scaffolds for local MSCs recruitment or implantation of scaffolds containing *in vitro* culture-expanded MSCs populations^{343,344}.

Proff. Maffulli and Della Porta and colleagues previously described an engineered multiphase 3D scaffold as an *in vitro* model for tendon regeneration studies. The multiphase 3D construct was totally absorbable and consisted of a braided hyaluronate elastic band merged with a fibrin hydrogel containing hBM-MSCs and poly-lactic-co-glycolic acid nano-carriers (PLGA-NCs) loaded with human Growth Differentiation Factor 5 (hGDF-5)¹³⁰. In that work, the PLGA nano-carriers were transient scaffold components to ensure sustained and controlled delivery of hGDF-5 with benefits beyond those associated with standard culture medium supplementation. The study reported an early tenogenic commitment of hBM-MSCs after three days of cultivation under dynamic conditions. Starting from these results, the same system was used for further investigations.

4.2 Aim

In the present study, we describe the use of the same scaffold (named HY-FIB here) to investigate the effects of the 3D environment on hBM-MSCs for 11 days with or without mechanical stimulation and in the absence of any specific biochemical differentiation signal. HY-FIB was assembled with hBM-MSCs as previously described¹³⁰ including PLGA-NCs stratified within the 3D fibrin structure. Importantly, the PLGA-NCs carried an inactive form of hGDF-5 (ihGDF-5) enabling the overall 3D scaffold structure to be safely evaluated with or without mechanical input. Gene expression of type I collagen, Decorin, Scleraxis-A, and Tenomodulin were considered; type III collagen was also monitored, being used as negative control. Histology and quantitative immunofluorescence were used to monitor cell behavior and their interaction

with the synthetic extracellular matrix. Moreover, to understand whether HY-FIB microenvironment configuration would stimulate any cell inflammation responses, the cells expression of cytokine markers was also monitored, including pro-inflammatory and anti-inflammatory cytokines.

4.3 Materials and Methods

4.3.1 hBM-MSCs isolation and harvesting

Human bone marrow mesenchymal stem cells (hBM-MSCs) were obtained from the bone marrow of three unrelated healthy donors (age 36, 38, 44 years). The donors gave written informed consent in accordance with the Declaration of Helsinki to the use of their filter residual bone marrow aspirate for research purposes, with approval from the University Hospital of San Giovanni di Dio e Ruggi d'Aragona (Salerno, IT). Review Board authorization number: (prot./SCCE n. 24988 achieved on April 9, 2015). Briefly, total bone marrow aspirate was directly seeded at a concentration of 50,000 total nucleated cells/cm² in T75 plastic flask in Minimum Essential Medium Alpha (α -MEM) supplemented with 1% GlutagroTM, 10% Fetal Bovine Serum (FBS), and 1% Pen/Strep and incubated at 37 °C in 5% CO₂ atmosphere and 95% relative humidity³⁴⁵. After 72h, non-adherent cells were removed by medium change, and the adherent cells were further fed twice a week with new medium. On day 14, colonies of adherent hBM-MSCs were detached and re-seeded at 4×10^3 cells/cm² in the same culture conditions. Once the cell cultures reached 70–80% confluence, cells were detached using 0.05% trypsin-0.53 mM EDTA and washed with PBS 1x (Corning Cellgro, Manassas, VA, USA), counted using Trypan Blue (Sigma-Aldrich, Milan, IT) and subcultured at a concentration of 4×10^3 cells/cm². Flow Cytometry analysis was performed on hBM-MSCs obtained at Passage 1 examining levels of CD90, CD105, CD73 CD14, CD34, CD45, and HLA-DR expression (Miltenyi Biotec, DE).

4.3.2 ihGDF-5 effect on hBM-MSCs

These sets of experiments were performed to ensure the absence of any effect of inactivated human GDF-5 (ihGDF-5, Cloud-Clone Corp., USA) on both tenogenic markers stimulation and cytokines expression by hBM-MSCs. Cells were seeded on coverslips in 12 well plates at a concentration of 4×10^3 cells/cm². Once the cultures reached 60% confluence, cells were treated with either 1.6 ng/mL or 100 ng/mL of ihGDF-5. Cells were fed twice a week with new medium and fresh ihGDF-5 supplementation for up to 16 days. Untreated cells for matched time-points studied were used for control purposes. Passage 3 cells were seeded in the 3D environment ($\sim 8 \times 10^5$ cells/mL) and were fed twice a week with new medium, without any growth factor added.

4.3.3 Immunofluorescence and Immunohistochemical assays

Cells were fixed with 3.7% formaldehyde for 30 min at room temperature (RT) followed by permeabilization with 0.1% Triton X-100 for 5 min and blocking with 1% Bovine Serum Albumine (BSA) for 1h. For type I and type III collagen staining, cells were incubated overnight at 4 °C with a mouse monoclonal anti-type I collagen antibody (1:100, Sigma-Aldrich) and a rabbit polyclonal anti-type III collagen antibody (1:100, Santa Cruz Biotechnology). Following incubation with the primary antibody, cells were incubated for 1h at RT with the DyLight 649 anti-mouse IgG (1:500, BioLegend, CA) and the Alexa Fluor™ 488 goat anti-rabbit IgG (1:500; Thermo Fisher Scientific, USA). Cell nuclei were stained with DAPI solution (1:1000) for 5 min. Images acquisition was at 20X magnification on a fluorescent microscope (Eclipse Ti-E Inverted Microscope; NIKON Instruments Inc., USA).

For 3D scaffold immunohistochemical analysis, slices were permeabilized with 0.1% Triton X-100 for 5 min, and non-specific staining blocked with 1% BSA for 1h at RT. For type I collagen staining, slices were incubated overnight at 4 °C with a rabbit polyclonal anti-type I collagen antibody (1:200, AbCam). Following incubation with the primary antibody, slices were incubated for 1h at RT with Alexa Fluor™ 488 goat anti-rabbit IgG (1:400, Thermo Fisher Scientific, USA) antibody. Subsequently, cell nuclei were stained with DAPI solution (1:1000) and incubated for 5 min. Images were acquired as described above. Image quantification was performed using image analysis software (ImageJ, National Institutes of Health, USA) [56,57] measuring the red and green areas where type I and type III collagen, respectively, were expressed. A minimum of 10 image fields was used for the image analysis at each time point. Signal intensity at each time point was normalized by the cell number (e.g., by amount of cell nuclei revealed by DAPI staining).

Sirius red staining was performed using the Picosirius Red Stain Kit (Polysciences, Inc., USA). Sections of 15 µm of thickness were stained in hematoxylin for 8 min, then washed in water for 2 min. The sections were dipped into phosphomolybdic acid for 2 min, then washed in water for 2 m. Then they were dipped into Picosirius Red F3BA Stain for 60 min and dipped into HCl 0.1M solution for 2 min. The sections were dehydrated in increasing ethanol gradient solutions (70–75–95–100%) and finally dipped into xylene for 5 min. Eukitt medium was used to mount the samples.

4.3.4 RNA isolation and gene expression profiles by qRT-PCR

Total RNA was extracted from hBM-MSCs seeded into the 3D construct of each experimental group using QIAzol® Lysis Reagent (Qiagen, DE), chloroform (Sigma-Aldrich, Milan, IT) and the RNeasy Mini Kit (Qiagen, DE). For each sample, 300 ng of total RNA was reverse-transcribed using the iScript™ cDNA synthesis kit (Bio-Rad, Milan, IT). Relative gene expression analysis was performed in a LightCycler® 480 Instrument (Roche, IT), using the

SsoAdvancedTM Universal SYBR[®] Green Supermix (Bio-Rad) with the validated primers for COL1A1, COL3A1, DCN, IL-1 β , IL-6, IL-10, IL-12A, SCX-A, TGF- β 1, TNF, and TNMD (Bio-Rad), and following MIQE guidelines²⁵⁶. Amplification was performed in a 10 μ L final volume, including 2 ng of complementary DNA (cDNA) as template. Specificity of the formed products was addressed via melting curve analysis. Triplicate experiments were performed for each condition explored, and data were normalized to glyceraldehyde-3-phosphate dehydrogenase (GAPDH) expression (reference gene), applying the geNorm method²⁵⁷ to calculate reference gene stability between the different conditions (calculated with CFX Manager software; M < 0.5). Fold changes in gene expression were determined by the $2^{-\Delta\Delta C_p}$ method, and are presented as relative levels versus hBM-MSCs just loaded within the HY-FIB system.

4.3.5 HY-FIB preparation and characterization

ihGDF-5 loaded PLGA-NCs were fabricated as described in Chapter 3. For each sample, a mixture of 50 mg/mL fibrinogen from human plasma (Sigma-Aldrich, Milan, IT), 15,600 U/mL aprotinin (Sigma-Aldrich, Milan, IT), and α -MEM (Corning, NY, USA) supplemented with 10% FBS (referred to as growing media, GM) was added at a 1:1:1 ratio to 100 mg of PLGA-NCs (ihGDF-5 loading: 350 ng/g) and, then, to an average of 8×10^5 cells. A homogeneous cells/PLGA-NCs/fibrinogen suspension was then embedded into a mold (30 \times 20 \times 4.5 mm) where the braided band had been previously positioned. Free ends were left to enable HY-FIB fixing into the bioreactor. Upon addition of 100 U/mL thrombin (Sigma-Aldrich, Milan, IT), the mold was placed in a 37°C humidified incubator for 30 min to allow fibrin polymerization. When the hydrogel was formed, the band was entrapped inside a uniformly distributed hydrogel. The construct was then transferred from the mold to either a standard polystyrene culture plate or to the bioreactor culture chamber, each containing 30 mL of the culture media, and placed in an incubator at 37 °C in a 5% CO₂ atmosphere and 95% relative humidity.

HY-FIB morphology was observed by field emission-scanning electron microscopy (FE-SEM; mod. LEO 1525; Carl Zeiss, Oberkochen, Germany). Samples were fixed in 4% PFA (4 °C, overnight) and then dehydrated by multiple passages across ethanol:water solutions (10 min each) with increasing concentrations of ethanol (10%, 20%, 30%, 50%, 70%, 90%), ending in a 100% dehydrating liquid (3 changes, 10 min each). Samples were then lyophilized in a Critical Point Dryer (mod. K850 Emitech, Assing, Rome IT), placed on a double-sided adhesive carbon tape previously glued to an aluminum stub and coated with a gold film (250 Å thickness) using a sputter coater (mod.108 Å; Agar Scientific, Stansted, United Kingdom) before observation.

HY-FIB mechanical characterization was performed according to the ASTM 1708 by a CMT 6000 dynamometer (CMT 6000 SANS, Shenzhen, China)

equipped with a 1 kN load cell. The sample was conditioned in Dulbecco's Modified Essential Medium (DMEM) for 1 h, and then shaped to obtain a specimen with gauge length (L_0) of 22 mm and width (W) of 5 mm. Sample thickness (S) was measured with a thickness gauge brand at three different averaged points. Monoaxial deformation was applied to the sample at a speed of 10 mm/min, and force (F) and elongation (L) during traction were recorded. The elastic modulus and ultimate tensile strength (both expressed in MPa) were calculated from the stress/strain plot.

For the immuno-histochemical analysis, at different time points, a portion of HY-FIB was fixed in 4% PFA (4 °C, overnight), cryo-protected in 30% sucrose overnight, mounted in OCT embedding compound, frozen at -20°C and then cut in slices of 10 μm of thickness using a cryostat. The remaining portion of HY-FIB was placed in QIAzol[®] Lysis Reagent for total RNA extraction.

4.3.6 Dynamic culture

HY-FIB was clamped at both free ends, one motionless and one sliding (operated by a linear motor actuator) arm, into the bioreactor system culture chamber, described in detail elsewhere³⁴⁶. A maximal load, set by pre-tensioning, was relaxed to a minimum value cycling at 1 Hz of frequency. In addition, continuous feedback signals, provided by strain gauges located onto the fixed arm, allowed the maintenance of a defined load on the scaffold in response to physical system modifications, by automatic adjustment of the pre-tensioning position.

4.3.7 Statistical analysis

Statistical analysis was performed using GraphPad Prism software (6.0 for Windows). Data obtained from multiple experiments are expressed as mean \pm SD and analyzed for statistical significance using ANOVA test, for independent groups. Differences were considered statistically significant when $p \leq 0.05$ ³⁴⁷.

4.4 Results

4.4.1 Effect of ihGDF-5 on tenogenic commitment and immunomodulatory activity of hBM-MSCs

hBM-MSCs were cultivated in a two-dimensional (2D) monolayer environment with medium supplemented with either 1.6 ng/mL or 100 ng/mL of inactive human Growth Differentiation Factor 5 (ihGDF-5) for up to 16 days. These two concentration conditions (two order of magnitude of difference) were chosen to ascertain the absence of any effect of the inactive hGDF-5 form on cells expression of tenogenic markers (COL3A1, COL1A1, DCN, SCX-A and

TNMD) and of cytokines (pro-inflammatory: IL-6, TNF, IL-12A, IL-1 β ; anti-inflammatory: IL-10, TGF- β 1) by qRT-PCR (Figure 4-1a to 4-1d).

Transient and slight, though significant, upregulation of COL3A1 (0.4-fold), DCN (0.2-fold), and COL1A1 (0.5-fold) was observed at Day 1 in cultures supplemented with 100 ng/mL ihGDF-5 (Figure 4-1b). The reduced dose of 1.6 ng/mL induced low-level transient expression at Day 1 for only COL3A1 (0.3-fold) and DCN (0.2-fold) only (Figure 4-1a). No significant upregulation was noted for TNF, IL-12A, IL-1 β , IL-10, or TGF β at any time point or ihGDF-5 concentration tested (Figure 4-1c,d). Compared to controls, IL-6 displayed significant levels of elevation at Days 8 (0.8-fold) and 16 (0.5-fold) with 100 ng/mL ihGDF-5 (Figure 4-1d).

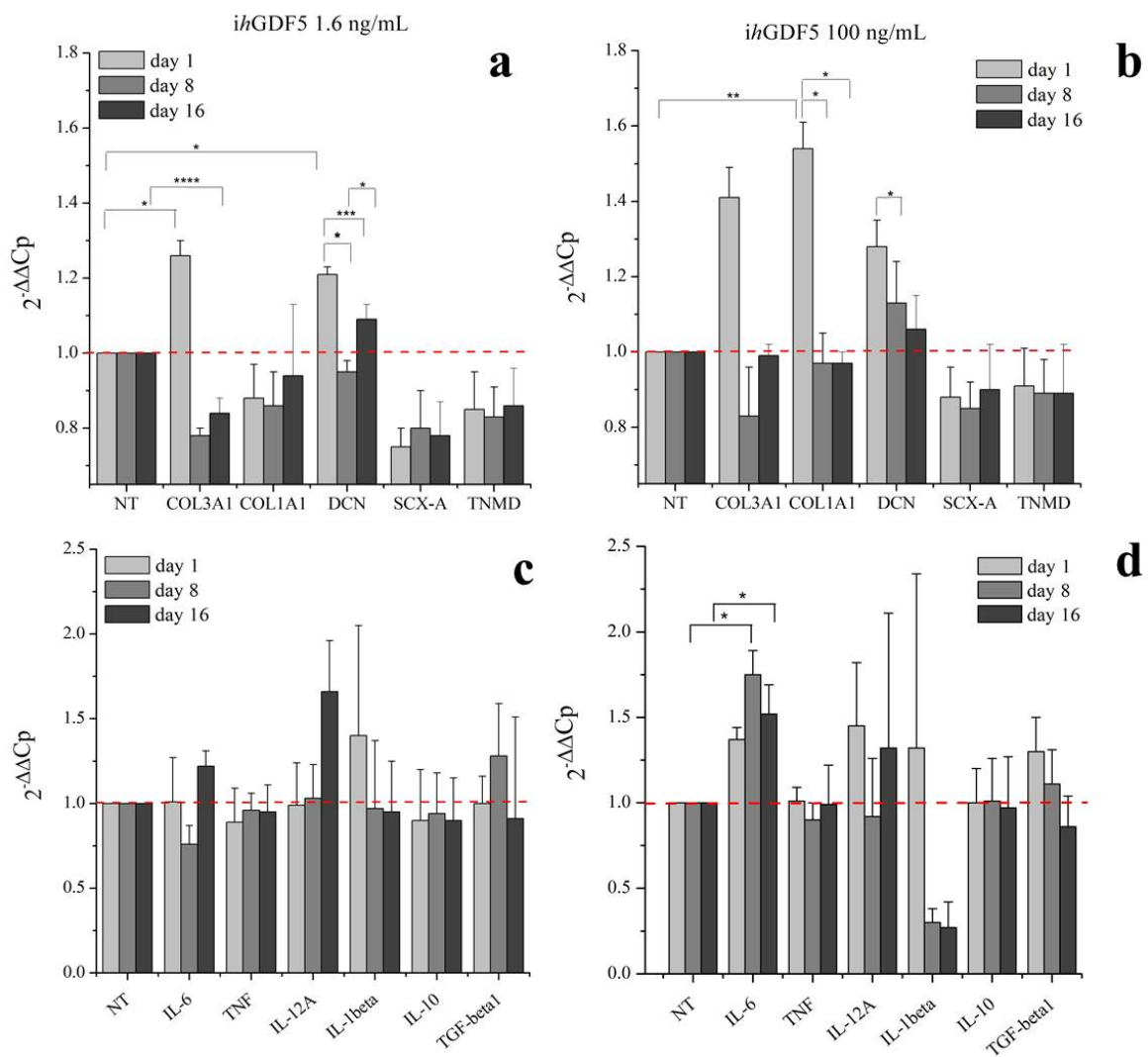


Figure 4-1. Gene expression profiles for tenogenic markers and pro-inflammatory and anti-inflammatory cytokines. hBM-MSCs treated with 1.6 ng/mL (a, c) and 100 ng/mL (b, d) of ihGDF-5 in monolayer 2D culture up to 16 days. mRNA levels of COL1A1, DCN, SCX-A, and TNMD were considered as tenogenic markers and COL3A1 selected as negative ones; pro-inflammatory (IL-6, TNF, IL-12A and IL-1 β) and anti-inflammatory (IL-10 and TGF- β 1) cytokines were monitored. Untreated cells for matched time-points were used as

control. * ≤ 0.05 ; ** <0.01 ; *** <0.005 ; **** <0.001 ; N = 3 (biological replicates); n = 3 (technical replicates).

4.4.2 Effect of ihGDF-5 on COL1A1 and COL3A1 proteins expression

Types I and III collagen expression levels were monitored by immunofluorescence during the 16 day culture period, as illustrated in Figure 4-2a,b. Immunofluorescence quantitative data by image analysis were congruent with qRT-PCR outputs when 1.6 ng/mL ihGDF-5 was supplemented: in this case, both proteins signals were not significantly elevated, compared to untreated cells (Figure 4-2c).

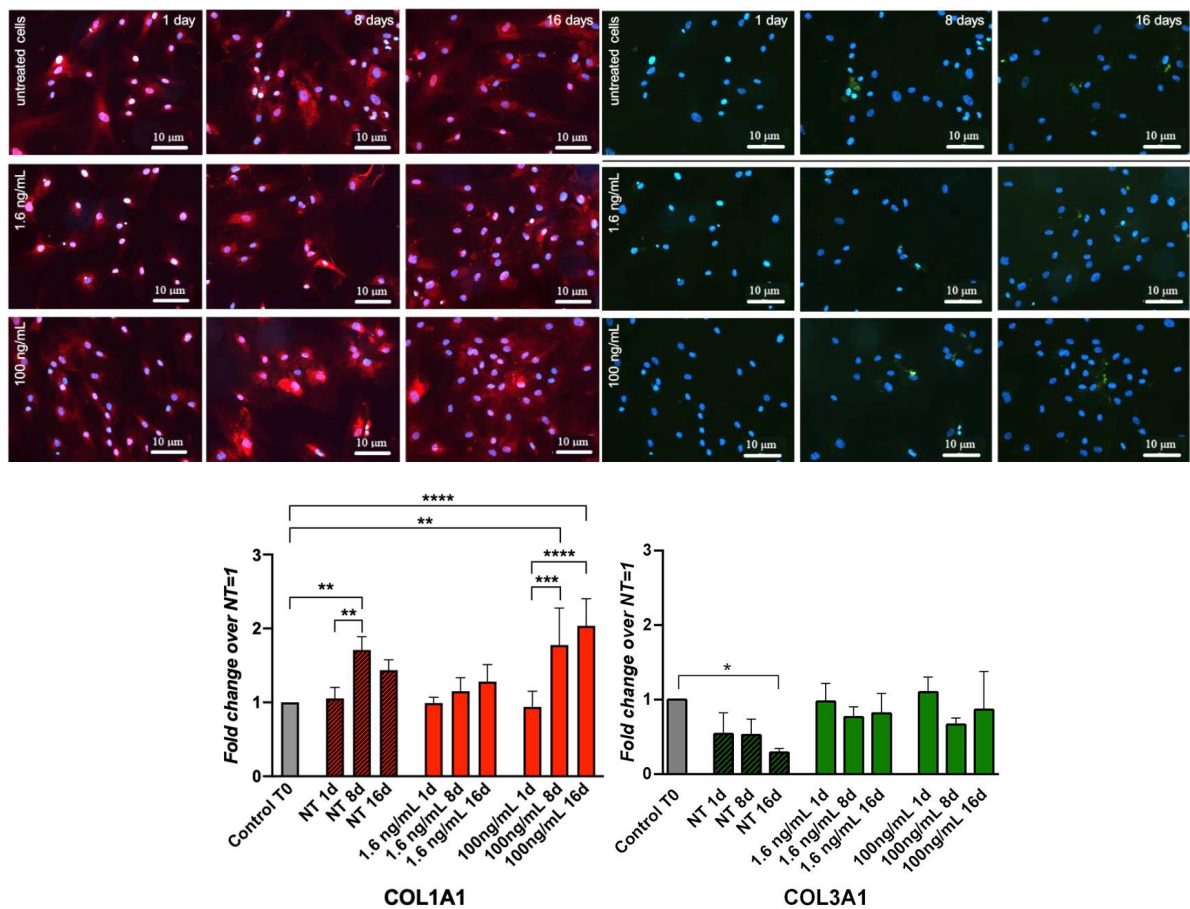


Figure 4-2. IF and quantitative-IF assays of type I collagen (COL1A1) and type III collagen (COL3A1) monitored along hBM-MSCs treatment with 1.6 ng/ and 100 ng/mL of ihGDF-5 for 16 days. Type I collagen was stained in red; type III collagen was stained in green; cell nuclei highlighted with DAPI in blue (a,b). Quantitative signal detection was performed via ImageJ software (c). Color intensity in each time point was normalized by the cell number. * ≤ 0.05 ; ** <0.01 ; *** <0.005 ; **** <0.001 ; n = 10 (image fields for each time point).

Quantitative image analysis displayed COL1A1 signal increase (1 fold) at Day 16 only with 100 ng/mL ihGDF-5 supplementation. These last data are in contrast with gene expression ones. COL1A1 and COL3A1 are the major components of the extracellular matrix in connective tissues, and their slight up-

regulations was reported when hBM-MSCs had been in routine culture for 16 days²⁶¹. However, in our case, ihGDF-5 seemed not to impact on their production, especially at the lower concentration tested. This preliminary information is important to confirm the inactivity of the biochemical input in regards to the gene expression and proteins that will be monitored in the 3D experiments.

4.4.3 ihGDF-5 loaded PLGA-NCs

Poly-lactic-co-glycolic-acid nano-carriers (PLGA-NCs) displayed a spherical morphology with a mean size of 230 ± 80 nm (Figure 4-3a). PLGA-NCs had an ihGDF-5 loading of 350 ng/g and provided a daily released peptide mean concentration of 1.6 ng/mL/day (Figure 4-3b), when an amount of 100 mg were inserted within HY-FIB over 11 days of culture (see Figure 4-3a to 4-3c). As highlighted above, these ihGDF-5 concentration levels did not stimulate sustained impacts on hBM-MSCs gene expression in 2D monolayer culture. Therefore, by excluding any non-specific ihGDF-5 induction (released within the 3D scaffold by the NCs), we could now observe cell behaviors arising from the HY-FIB microenvironment in both static and dynamic conditions.

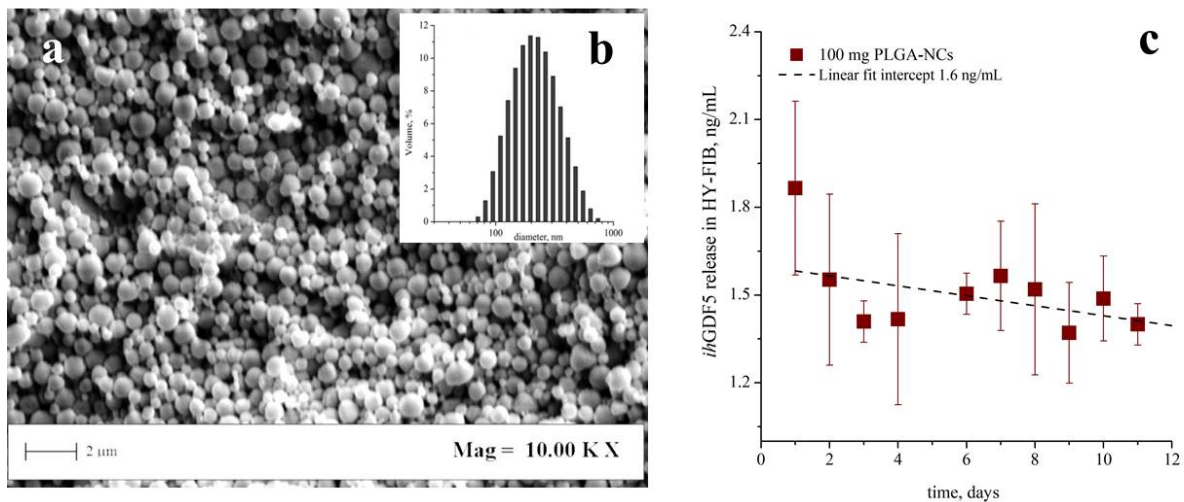


Figure 4-3. ihGDF-5 loaded PLGA-NCs characterization. Poly-lactic-co-glycolic-acid (PLGA) transient carriers field emission-scanning electron microscopy (FE-SEM) image (a), particle size distribution (b), and ihGDF-5 release profile (c).

4.4.4 hBM-MSCs cultivation in HY-FIB 3D microenvironment

The HY-FIB assembly featured a braided band (3×10 cm) joined to a fibrin hydrogel (on a band surface of 6 cm^2) containing 8×10^5 hBM-MSCs and 100 mg of ihGDF-5/PLGA-NCs. The picture and schematic representation of the 3D system is shown in Figure 4-4a,b. Field Emission Scanning Electron Microscopy (FE-SEM) images of the scaffold illustrate hyaluronate fibers,

embedded within a fibrin hydrogel (Figure 4-4c), which provided an entrapment surface for both NCs and hBM-MSCs (Figure 4-4d).

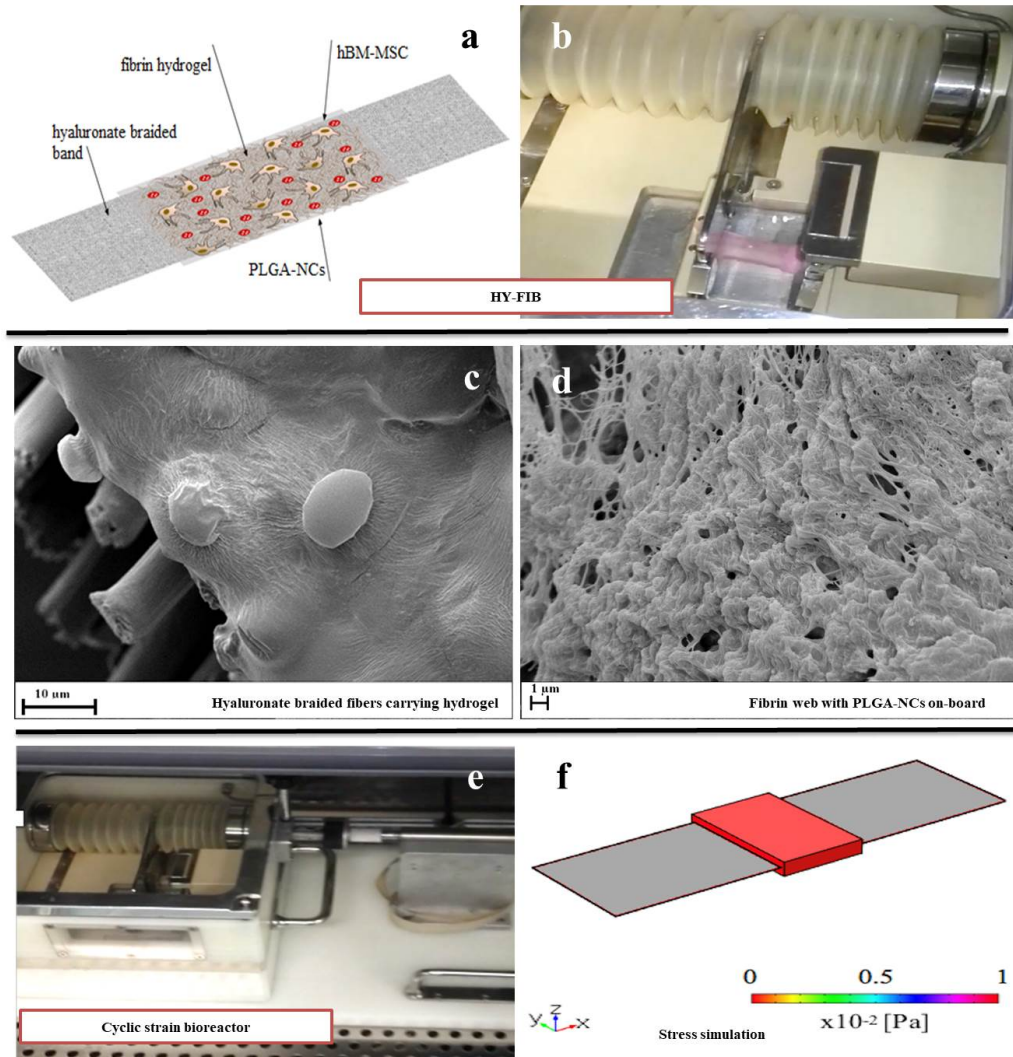


Figure 4-4. HY-FIB three-dimensional (3D) scaffold features and cyclic strain bioreactor. Schematic HYFIB representation (a) and image of 3D scaffold (b). FE-SEM images of hyaluronate braided fibers (10 μm mean diameter size) (c) joined to a fibrin web which entrapped both NCs and hBM-MSCs (d). Cyclic strain bioreactor (e) and in-silico study of stress distribution over HY-FIB upon mechanical strain of 10% (f). The simulation involved only the stress of the fibrin 3D environment, neglecting any further contribution^{348,203,130}.

HY-FIB was exposed to 10% deformation over a 1 Hz frequency for 4 h per day during the dynamic culture experiments via a cyclic strain bioreactor³⁴⁶, illustrated in Figure 4-4e. In greater detail, a HY-FIB braided band was held at one end by a motionless arm and at the other end by a sliding one. Motion was driven by a linear motor and transmitted through the braided band to cells embedded within the fibrin hydrogel. The motionless arm comprises a base, attached to the side wall of the culture chamber, housing the electronic components for load monitoring, and from which extended a cantilevered shelf whose deformation is measured by four strain gauges. The whole system was

housed within an incubator to ensure the appropriate CO₂ gaseous environment to control the pH of the cell culture media and 37 °C operational temperature. The stress delivered to the cells immobilized within the system was explored via computational analysis that estimated a mean shear stress value at 9×10^{-2} Pa within the fibrin 3D environment (Figure 4-4f)^{348,203,130}. This order of magnitude of stress value was reported for tenogenic induction²⁰³; larger deformation for longer times were excluded to focus the study on 3D environment assembled.

4.4.5 Gene expression profiles of tenogenic markers

HY-FIB samples were collected at Day 1, 2, 5, and 11 to monitor tenogenic marker expression. Time points at Day 1 and Day 2 were added for 3D culture to monitor the effect of HYFIB on cells behavior alone or in combination with cyclic strain culture. Indeed, in static conditions, both COL1A1 and DCN displayed significant upregulation of 3.8 fold (COL1A1) and 2.6-fold (DCN) at Days 1 and 2 before dropping progressively to elevated but non statistically significant levels (Figure 4-5a and Figure 4-6), confirming an HY-FIB effect on this gene expression in the first days of culture. In dynamic conditions, COL1A1 levels displayed responses similar to the static culture in the first two days but progressively rising thereafter to statistically significant levels (2.9 fold) at Day 11, probably from strain input. DCN expression levels in response to dynamic culture were to be elevated throughout, achieving statistical significance at Day 11 (3-fold) (Figure 4-5b and Figure 4-6).

SCX-A displayed significant upregulation (~340-fold) in both static and dynamic conditions at Day 1, suggesting an effect of HY-FIB system, on the expression of this gene. SCX-A levels were substantially elevated in both static and dynamic conditions at all following time points studied, even though a larger and significant increase was observed in dynamic conditions; an increase of 800-fold in static and of 1600-fold in dynamic culture conditions was seen at Day 11 (Figure 4-5a,b and Figure 4-6). Tenomodulin gene expression was also tested by qRT-PCR, but no expression was detected, probably because it is an event occurring during late differentiation³⁴⁹. Sustained, significant, downregulation of COL3A1 was observed in either static or dynamic conditions which instead either decreased progressively (static) or decreased through to Day 5 before reestablishing Day 0 levels at Day 11 (dynamic).

The data suggested an overall effect of the 3D environment on cells behavior clearly visible along the first two days of culture; furthermore, a statistically significant COL1A1, DCN, and SCX-A overexpression was observed after 11 days when mechanical strain was provided (Figure 4-6).

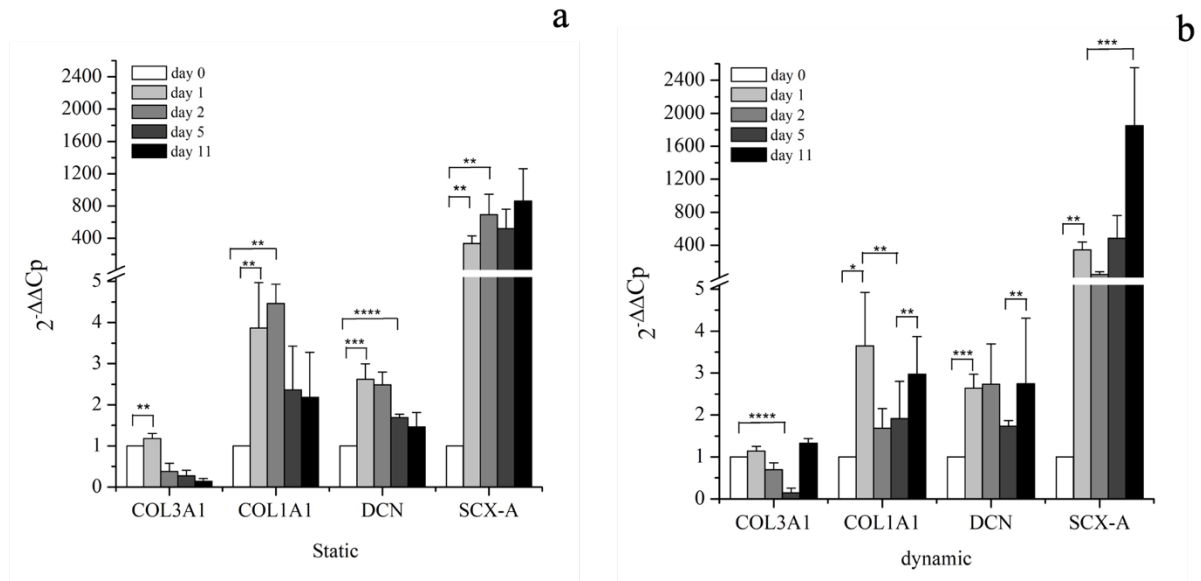


Figure 4-5. Gene expression profiles of tenogenic markers. hBM-MSCs within HY-FIB environment in static (a) and dynamic (b) culture up to 11 days. Days 1, 2, 5, and 11 were selected as time points to study the mRNA levels of positive tenogenic markers (COL1A1, DCN, SCX-A, and TNMD) and negative one (COL3A1). hBM-MSCs within HY-FIB at time zero were used as control. * < 0.05; ** < 0.01; *** < 0.005; **** < 0.001. N = 3 (biological replicates); n = 3 (technical replicates).

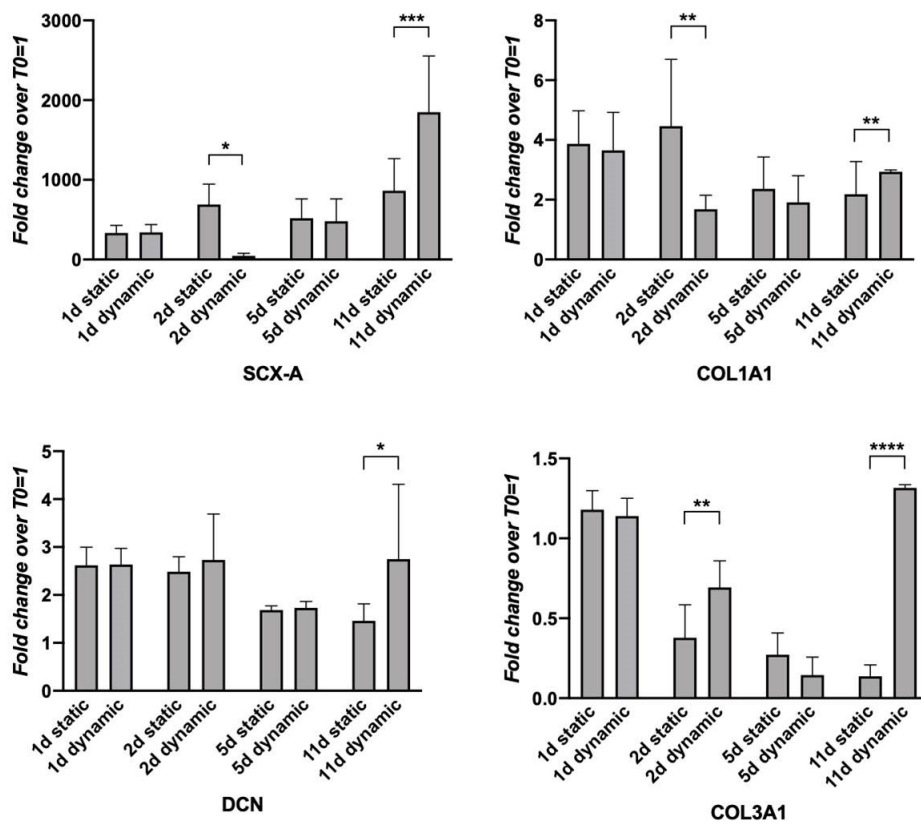


Figure 4-6. Tenogenic markers expression in static vs dynamic culture. Gene expression profiles of positive (SCX-A, COL1A1, DCN) and negative (COL3A1) tenogenic markers of HY-FIB static vs. dynamic culture. * < 0.05; ** < 0.01; *** < 0.005; **** < 0.001.

4.4.6 hBM-MSCs immunomodulatory activity

Cytokine transcript expression data are illustrated in Figure 4-7a,b, for static and dynamic culture, respectively. The HY-FIB system has an effect also on cytokines gene expression, as observed at all time points monitored with respect to Day 0, within static culture. Indeed, pro-inflammatory cytokines IL-6 (~6-fold), TNF (~10-fold), IL-12A (≤ 600 -fold), and IL-1 β (~200-fold) displayed rapid and significant upregulation that was maintained for the entirety of the experimental duration. Anti-inflammatory TGF- β 1 on the other hand displayed either no change (Day 11) or significant down-regulation (other time points) while IL-10 exhibited an overall similar profile to IL-1 β culminating in marked upregulation at day 11 (~300-fold) (Figure 4-7a).

Dynamic culture conditions had a distinct and significant effect on IL-6 with expression levels achieving a peak upregulation of 1.5-fold at Day 1 and decreasing to undetectable levels by Day 11 (Figure 4-8). TNF and IL-1 β were both gradually upregulated before achieving ~200-fold and ~300-fold, respectively, upregulation at day 11 (compared to 10-fold and 100-fold in static conditions). IL-12 displayed a similar profile of upregulation in dynamic vs. static culture conditions while achieving maximal levels that were 3X less in dynamic. Anti-inflammatory IL-10 expression levels were consistent across both dynamic and static conditions. In contrast to static culture, TGF- β 1 was significantly downregulated until day 5, and it underwent a 5-fold increase at Day 11 in dynamic culture conditions (Figure 4-7b and Figure 4-8).

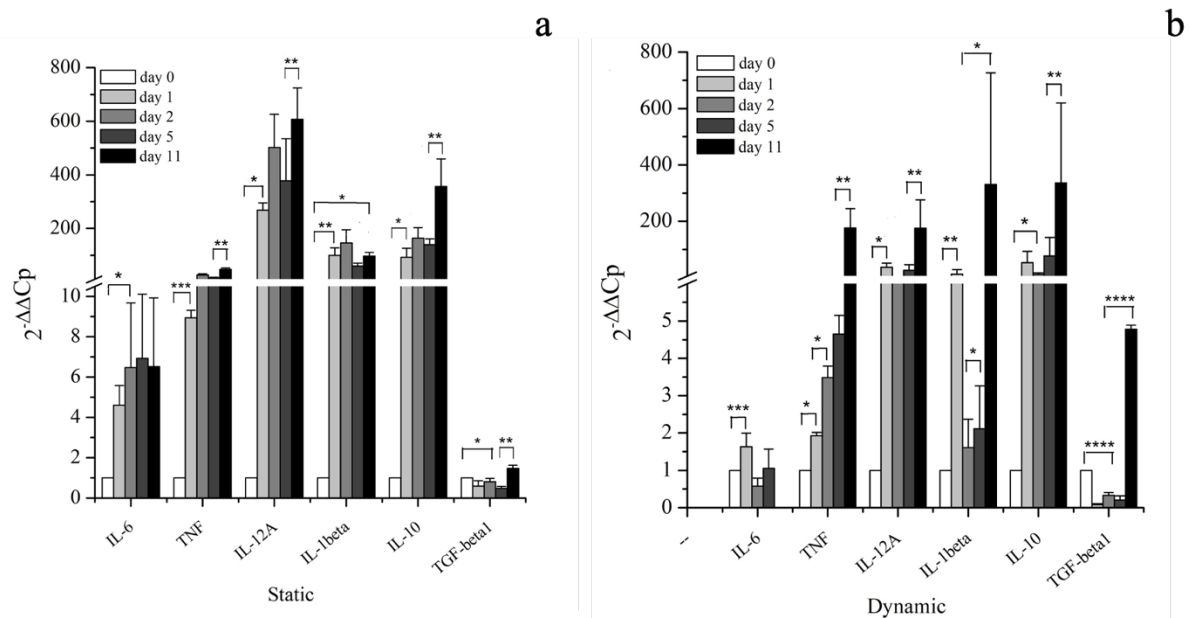


Figure 4-7. Gene expression profiles of pro-inflammatory and anti-inflammatory cytokines. hBM-MSCs within HY-FIB environment in static (a) and dynamic (b) culture up to 11 days. Days 1, 2, 5, and 11 were selected as time points to study the mRNA levels of pro-inflammatory (IL-6, TNF, IL-12A and IL-1 β) and anti-inflammatory (IL-10 and TGF- β 1) cytokines. hBM-MSCs within HY-FIB at time zero were used as control. * <0.05; ** <0.01; *** <0.005; **** <0.001. N = 3 (biological replicates); n = 3 (technical replicates).

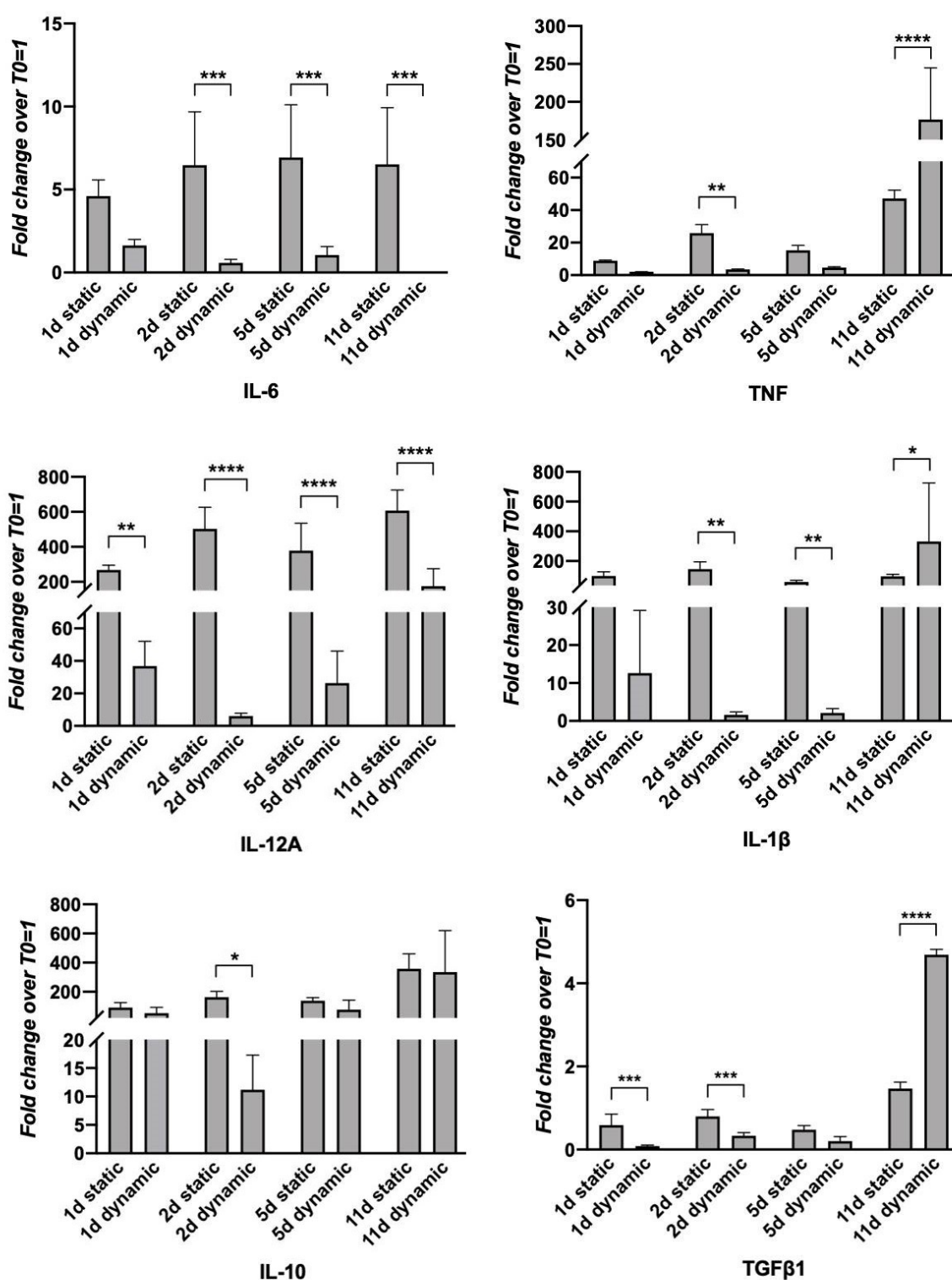


Figure 4-8. Cytokine markers expression in static vs dynamic culture. Gene expression profiles of pro-inflammatory (IL-6, TNF, IL-12A, IL-1β) and anti-inflammatory (IL-10, TGF-β1) cytokine markers of HY-FIB static vs. dynamic culture. * < 0.05; ** < 0.01; *** < 0.005; **** < 0.001.

4.4.7 Histological characterization of HY-FIB

Histological characterization of HY-FIB scaffold in both static and dynamic culture at Days 5 and 11 are reported in Figure 4-9; the overall scaffold structure was stained with Sirius Red for collagen highlighting. Despite fibrin hydrogel matrix, collected at Day 0, was only light pink stained, the same matrix was clearly stained in red at Day 5 and 11 in both samples taken from static and dynamic culture. However, a less homogeneous matrix organization and staining was observed in the samples taken from static culture. These data are in agreement with the behaviour of gene expression, and confirmed that both HY-FIB alone and HY-FIB plus cyclic strain had an effect on cells phenotype commitment.

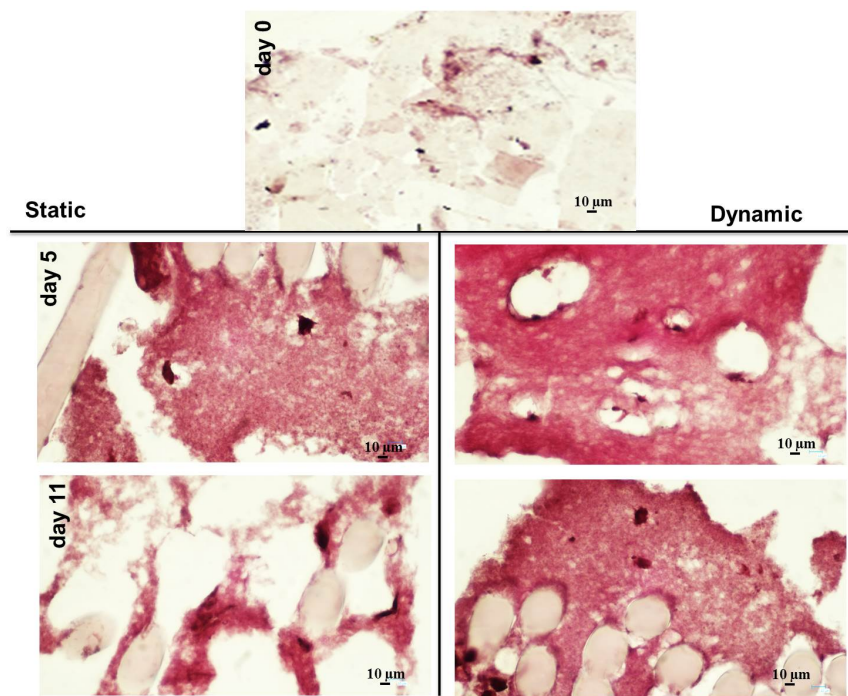


Figure 4-9. Histology characterization of the overall HY-FIB scaffold structure with Sirius Red staining. HY-FIB scaffolds in both static and dynamic culture at Days 5 and 11 are reported; the overall scaffold structure was stained with Sirius Red for collagen highlighting.

4.4.8 COL1A1 protein expression in dynamic culture

The expression of type I collagen, a tenogenic matrix-associated marker, was monitored by immunofluorescence over the culture time (Figure 4-10). At day 1, empty areas surrounding the cells are present, probably from the absence of uniform fibrin hydrogel. These spaces were then progressively filled with the protein, presumably via secretion into the extracellular environment. The level of staining observed under static conditions decreased after Day 1 and was maintained at ~50% of original levels thereafter while levels were maintained consistent to Day 0 in dynamic culture. Moreover, in the dynamic conditions, a

more uniform cells distribution was noted throughout the hydrogel matrix, especially at day 11.

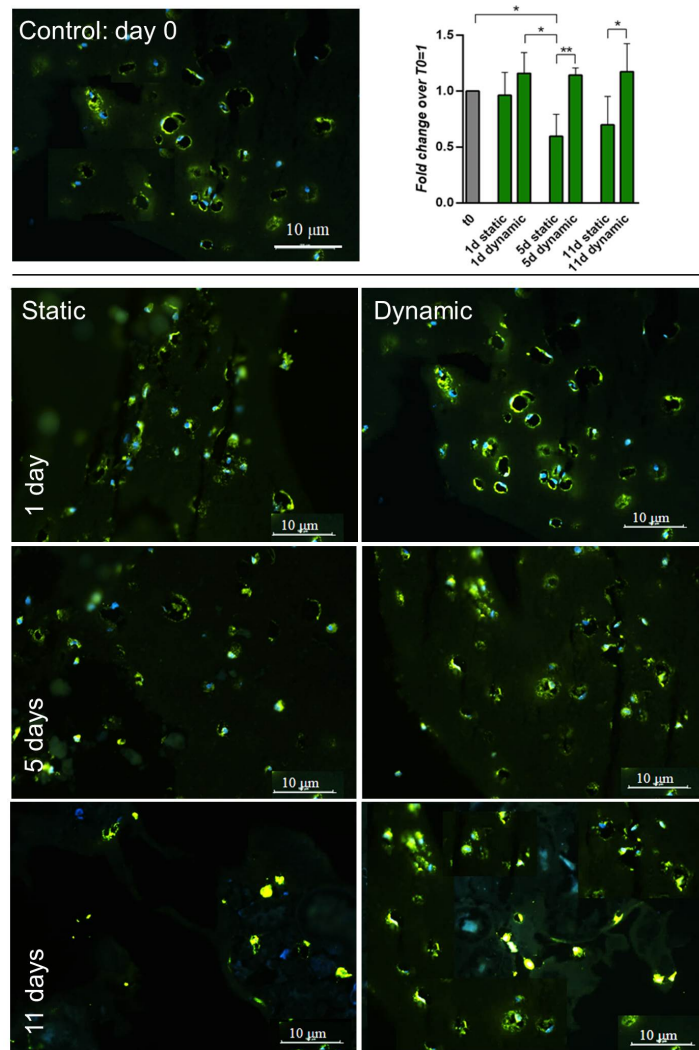


Figure 4-10. IF and quantitative-IF assays of type I collagen (COL1A1) in 3D static and dynamic culture of hBM-MSCs for 11 days. Fluorescence quantification was performed using ImageJ software. Signal intensity in each time point was normalized by cell number (e.g., by amount of cell nuclei revealed by DAPI staining). * ≤ 0.05 ; ** < 0.01 . N = 3 (biological replicates); n = 3 (technical replicates).

4.5 Discussion

The HY-FIB system is engineered to support delivery of PLGA-NCs within the hydrogel matrix, enabling controlled delivery of specific molecules within a 3D environment, e.g., drugs or other biological signals. The active form of hGDF-5 loaded into PLGA-NCs for controlled delivery within HY-FIB environment was investigated in the next study (see Chapter 5). Here, we investigated the effect of the HY-FIB 3D environment (hyaluronate band + PLGA carriers + fibrin gel) on hBM-MSCs tenogenic and cytokine marker gene expression in both static and dynamic, mechanical, input scenarios. We adopted the previous HY-FIB configuration including PLGA-NCs, but on this occasion, we delivered an

inactive form of hGDF5. In this manner, the biochemical input provided by the growth factor was excluded, but the complete HY-FIB configuration was maintained, and we were thus able to investigate the impact of mechanical input alone.

HY-FIB braided fibers enabled a well-defined mechanical stimulation of 9×10^{-2} Pa provided to hBM-MSCs during the 4h/day dynamic culture regime. The mean shear stress was calculated by FEM modeling³⁵⁰, assuming a homogeneous behavior of the system at a density of 1050 kg/m^3 and Young's modulus of 4.56 Mpa ¹³⁰. A Poisson ratio value of 0.25 was adopted³⁵⁰.

Further mechanical inputs with different intensities and durations were not investigated, not being the aim of the present work. Stress values resembling reduced physiological activity, similar that the ones used here, have been reported to direct stem cell commitment to a tenogenic phenotype^{330,331,351}.

COL1A1 is the major component of tendon tissue (75–85% of the dry mass of tendon), and is responsible for its mechanical strength²⁶¹. In the static group, COL1A1 showed a ≥ 3 -fold upregulation during the first and second day of cultivation. These data seem to suggest an overall effect of the 3D environment on cells behavior. The expression of COL1A1 was progressively reduced to a 2-fold upregulation at Day 11, in static environment. In dynamic conditions, its mRNA levels showed similar behavior during the first two days of cultivation (an increase up to 3-fold-changes, then reduced at Day 2). However, its expression was subsequently increased again to 2.8-fold at Day 11.

Decorin (DCN), a small leucine-rich proteoglycan implicated in the regulation of fibrillogenesis, is a fundamental component of the tendon extracellular matrix (ECM)³⁵². Compared to the static condition, a significant enhancement, up to 2.5-fold, of the mRNA level of DCN was shown when hBM-MSCs were cultured for 11 days with mechanical stimulation.

Scleraxis-A (SCX-A) is a neotendon marker, expressed in pro-tendon sites in the developing embryo. Specifically, SCX-A is a tendon-specific basic helix-loop-helix transcription factor responsible for the transition of MSCs into tendon progenitors²¹⁸. We observed substantial increases in SCX-A expression, up to 800-fold in static and 1600-fold in dynamic conditions after 11 days, demonstrating a stimulatory effect via the 3D system organization and consistent with previous observations^{219,115,220}.

The level of COL3A1 mRNA seems to be downregulated after 2 days in the static group and after 5 days in the dynamic group. Its downregulation can be considered a positive indication of proper cell differentiation; indeed, it seems that COL3A1 is the main responsible of fibrotic and scarred tissue arrangement and has been consistently reported at the rupture site of human tendons²⁶¹.

From both histology and immunofluorescence assays, we noted that the area surrounding the cells was progressively filled by type I collagen and, at Day 11, the extracellular matrix seemed to undergo remodeling (Figures 4-9 and 4-10). Moreover, in dynamic conditions a more homogeneous cell distribution within the hydrogel matrix was observed in the IF images. These findings support the

concept that 3D cultivation provides cues to the hBM-MSCs, and that dynamic signaling enables the adoption of a more uniform behavior including type I collagen protein deposition in the externally available space of the fibrin hydrogel. These data suggest that tenogenic commitment of hBM-MSCs cultured within the HY-FIB environment may be enhanced when controlled dynamic stretching is applied.

MSCs secrete a variety of cytokines and growth factors that promote cell recruitment, migration, proliferation, and differentiation. MSCs are also immunomodulatory, which may allow them to exert beneficial effects on the local immune cell population at the site of injury²⁵³. To better understand the hBM-MSCs inflammatory response when cultured within HY-FIB, cytokine expression was monitored over the 11 days of culture. The balance between pro- and anti-inflammatory soluble factors in the tendon healing process exerts a major impact on successful resolution of inflammation. Recent analysis of tendinopathy biopsies showed a distinct inflammatory infiltrate in the initial phase of tendinopathy with a high content of pro-inflammatory factors such as IL-6, TNF- α and IL-17²⁵².

To exclude a role for ihGDF5 in cytokine expression induction we evaluated their expression in hBM-MSCs undergoing 2D planar cultivation as a negative control. Indeed, in disc degeneration models using *in vitro* 3D cultures, human annulus cells display increased expression of pro-inflammatory cytokines, such as IL-1 β and TNF- α , while exposure to TNF- α and IL-1 β resulted in significant downregulation of GDF-5²⁵⁵. Therefore, it is plausible that GDF-5 may upregulate the expression of pro-inflammatory genes in hBM-MSCs leading to the maintenance of an autocrine feedback. However, when ihGDF-5 was added, no statistically significant expression of pro-inflammatory cytokines was observed; therefore, ihGDF-5 did not exert any effect on cytokines expression.

The addition of PLGA-NCs enabled an informed analysis of the inductive role of the HY-FIB overall structure. As described in Chapter 3, the cytotoxicity of SEE-fabricated PLGA-NCs on blood mononucleate viability, monitored with MTT assay³⁵³, was not affected after either 24 h or 48 h. Here, the overall HY-FIB system (loaded with SEE fabricated NCs) does not evidence any toxic effect on hBM-MSC cultivated within it for 11 days, providing an indirect indication about SEE technology as suitable process for the production of biomedical carriers.

In general, we observed that pro-inflammatory gene expression was higher in static than in dynamic conditions at all time points. On the contrary, the anti-inflammatory cytokines IL-10 was consistently upregulated in both static and dynamic conditions; TGF- β 1 was downregulated at all the time points tested except day 11, when it showed a marked increase (4-fold) only in dynamic environment. The described behavior confirmed that MSCs respond to a variety of biophysical cues; indeed, as suggested by Qazi *et al.*, 3D culture of MSCs on biomaterials can promote cell-cell interactions and enhance the paracrine effects of MSCs [77]. Moreover, as concluded by Ogle *et al.*, historically, biomaterial-

based therapies to promote tissue regeneration were designed to minimize the host inflammatory response. Recently, the roles that monocytes and macrophages can play in tissue repair have been highlighted. In this context, material properties and their capacity of controlled delivery of specific biomolecules has been engineered to achieve a given biological response that can be tuned not only to a better integration with biological systems but also in regulating the inflammatory response³¹⁶.

The overall and statistically significant balance of pro- vs. anti-inflammatory cytokines expressed by cells provided indications regarding the importance of dynamic culture for 3D *in vitro* model systems. For instance, IL-6, a well-known pleiotropic cytokine delivered by tissues in response to physio-pathological changes such as physical exercise, infection, and injury, was reported to deeply alter skeletal muscle milieu, by affecting the activity and quality of cellular interactors during tissue regeneration and leading to the fibrotic response³⁵⁴. In our 3D model system, IL-6 gene expression was considerably reduced in hBM-MSCs that underwent dynamic 3D HY-FIB cultivation when compared to the same cells cultivated in static condition.

There is no specific literature on cytokines response by hBM-MSCs cultivated within 3D scaffold. Almost all published studies described cell-specific differentiation toward a given phenotype, without considering how cytokines expression may be related to a 3D *in vitro* scaffold system. In this respect, the present investigation is the first study which suggests cytokines expression as a further variable to monitor cell behavior and reaction when loaded into a 3D *in vitro* model. Moreover, improved balance in anti-inflammatory cytokines observed for HY-FIB plus cyclic strain may be considered an indication of better cells response to the 3D *in vitro* system designed and proposed.

4.6 Conclusions

The 3D cell culture yielded evidence of type I collagen expression observed by both immunohistology and gene assay. When the same 3D system was cultivated under cyclic strain, the mechanical input stimulated a statistically significant increase in the expression of tenogenic markers when compared to the same cells assembled into the 3D system, but cultivated in a static culture. Further studies may involve a deeper understanding of the relationship between type I collagen production, cell commitment and mechanical input strain percentage or duration; hence, the HY-FIB system can be considered a good instrument for this study. The 3D culture system activated also the expression of pro-inflammatory cytokines, and, when cyclic strain was applied, pro-inflammatory cytokine gene over-expression by hBM-MSCs was better balanced against overexpression of anti-inflammatory cytokines. It remains to be determined what the involvement and the immunomodulatory activity of hBM-MSCs are, and the role of implantable biomaterials in the stimulation of inflammatory reactions. For instance, the stimulation of local inflammation is

reported as an important event in triggering repair in avascular tissues, such as cartilage and tendons³¹⁶.

On the other hand, the presence of PLGA-NCs within the fibrin hydrogel would allow the delivery of specific biomolecules that may be studied for the ability to further modulate inflammation reactions or promote regeneration/repair events (see Chapter 5). In this sense, HY-FIB provides a potential strategic approach to address a range of issues via the provision of a tightly controlled *in vitro* protocol. The 3D scaffold is a potential system to organize the sustained release of different biochemical signals and opens concrete perspectives to develop 3D bioengineered models to understand specific molecular and cellular composition of damaged systems.

Chapter 5

Study of the effect of biochemical and mechanical stimuli on the
tenogenic commitment of hWJ-MSCs

Ref: Ciardulli MC, Lovecchio J, Scala P et al. Submitted to Stem Cells International. 2021.

5.1 Introduction

As stated in Chapter 1, tendon injuries result in pain, swelling, loss of function of the tendon itself and nearby structures, and instability. Conservative management involves physical therapy and pharmacological treatment with non-steroidal anti-inflammatory drugs (FANS), corticosteroids, narcotics and viscosupplementation. Surgical procedures are performed when conservative modalities fail. Even though these approaches may lead to a relatively high rate of success, they present limitations³⁵⁵. Tendon tissue responds poorly to current treatments, resulting in permanent changes of the native tendon structures (with scar tissue formation and fibrosis) and biomechanics. The inability to complete regeneration derives from the nature of tendons: they are poorly cellularized and vascularized, and have a low metabolism^{6,29}.

In this context, *in vitro* models that allow the study of tenogenic events are important to improve pharmacological approaches and to develop advanced surgical devices. Human stem cells derived from bone marrow or adipose tissue aspirate were largely used for this purpose; those collected from cord blood and umbilical cord-derived Wharton's jelly had an increasing interest for tendon regenerative medicine studies. Stem cells, indeed, can produce sound healing, thanks to the production of cytokines, growth factors and extracellular vesicles (such as exosomes), all involved in regeneration processes^{356,357,358}. On the other hand, tissue engineering (TE) approaches, involving biopolymers and bioreactors, are capable to achieve biomimetic environment with specific microarchitectural and biomechanical inputs to appropriately stimulate cells toward a specific phenotype, allowing to understand tendon biology and related regenerative processes³⁵⁹.

Among the different types of stem cells adopted in TE approaches for tendon regeneration studies³⁶⁰, mesenchymal stem cells from the Wharton's Jelly of the human umbilical cord (hWJ-MSCs) appears to play a leading role in the future of regenerative medicine and can be also interesting for tenogenesis studies^{237,361}. Wharton's Jelly is a connective tissue of the umbilical cord located between the umbilical vessels and the amniotic epithelium. This gelatinous substance contains a relevant quantity of extracellular matrix components, such as collagen, hyaluronic acid, sulfated proteoglycans, but also growth factors, cytokines, extracellular vesicles and primitive mesenchymal stem cells³⁶². Compared to bone marrow- and adipose-derived collection procedures, the harvest of hWJ-MSCs do not pose donor site morbidity as every birth represent an opportunity to collect a large amount of hWJ-MSCs for research and clinical applications³⁶³. hWJ-MSCs resemble embryonic stem cells and have attractive expansive properties and immunomodulatory characteristics^{237,348}. hWJ-MSCs are able to differentiate along tenogenic lineage in response to signal transduction mediated by human Growth Differentiation Factor-5 (hGDF-5)³⁴⁸, a well-known growth factor belonging to the Transforming Growth Factor- β superfamily capable of triggering the expression of genes linked to neotendon phenotype^{159,136,131,249,248}.

Growth factors are naturally involved in tendon development and repair, and are secreted by a variety of cells, such as tendon progenitor cells, epithelial and vascular endothelial cells, fibroblasts, inflammatory cells. Following tissue damage, released growth factors bind to membrane receptors and activate intracellular signaling pathways involved in the transcriptional expression of genes linked to proliferation, differentiation and matrix synthesis, influencing the healing process¹⁴⁷. hGDF-5 seem to be involved in cytoskeleton reorganization, cell adhesion and extracellular matrix (ECM) remodeling during tenogenic differentiation¹⁶³.

Furthermore, tendon is a mechanosensitive tissue, and ECM remodeling is influenced also by mechanical stimulation^{364,365}: not surprisingly, prolonged rehabilitation is considered an efficient alternative to surgical procedures and pharmacological therapy¹². Tendon homeostasis, development and healing are driven by the mechanical forces applied to them; mechanotransduction processes translate mechanical loads into biochemical signals linked to key signaling pathways in tendon cells^{366,367,63}. Given these evidences, in tissue engineering approaches, mechanical stimulation has been delivered to stem cells in culture to promote tenogenic differentiation and matrix organization; specifically, strain showed to have a key role in tenogenic differentiation induction^{328,329,368}.

A biomimetic environment is achieved merging three-dimensional (3D) scaffolds and bioreactors as players to transfer biochemical stimuli and mechanical loads to cells in culture. Scaffolds have to reproduce the ECM by supporting cell growth and differentiation; they have to be totally bioresorbable and support required mechanical loads^{164,166,369}. Hydrogels are highly biocompatible but, to overcome their poor mechanical properties, they need to be merged with more force resistant biopolymers^{368,230}. Several bioreactors have been used to impart, in a controlled manner, mechanical forces to cells in culture, as tenogenic mechanical stimuli^{221,203,330,229,215,230,225,370,368}.

Furthermore, controlled delivery of biochemical stimuli, such as human growth factors, is still a challenge in TE protocols, but it is necessary to overcome the limits associated to standard culture medium supplementation³⁷¹. Poly-lactic acid (PLA) and poly-lactic-co-glycolic acid (PLGA) carriers (FDA-approved bioresorbable polymers) have been recently proposed for this purpose. These carriers may act as micro-environmental regulators within a 3D bioengineered scaffold, providing a spatio-temporally controlled delivery of several biomolecules^{371,371}; as already used in both pharmaceutical^{311, 372, 353} and biomedical^{373, 130, 282} fields.

5.2 Aim

In the present study, we proposed a bioengineered scaffold to study the tenogenic commitment of hWJ-MSCs, cultivated in a tenoinductive environment that ensured both biochemical and mechanical inputs. The 3D environment was

totally bioresorbable being assembled with a braided hyaluronate elastic band and a fibrin hydrogel to host hWJ-MSCs and, potentially, poly-lactic-co-glycolic acid nano-carriers (PLGA-NCs) loaded with hGDF-5. To understand the effect of hGDF-5 sustained delivery within the 3D fibrin hydrogel with respect to medium supplemented with the same growth factor, a different series of tests were performed. In both cases, the braided band transmitted a specific cyclic strain to the cells onboard along the 14 days of culture thanks to a custom-made bioreactor. Gene expression of type I collagen, Scleraxis-A, Decorin, Tenascin-C and type III collagen was evaluated to monitor cells tenogenic commitment. Picro-Sirius Red staining was used to understand collagen deposition and cells interaction with the synthetic extracellular matrix. Moreover, given the immunomodulatory properties of hWJ-MSCs, the expression of pro-inflammatory (IL-6, TNF, IL-12A, IL-1 β) and anti-inflammatory (IL-10, TGF- β 1) cytokines was also investigated under the best tenoinductive conditions.

5.3 Materials and Methods

5.3.1 hWJ-MSCs isolation and harvesting

Mesenchymal stem cells from the Wharton's Jelly of the human umbilical cord (hWJ-MSCs) were isolated from two donors (age 23 and 31) who gave written informed consent in accordance with the Declaration of Helsinki to use their umbilical cord for research purposes. The protocol was approved by Our Institutional Review Board (Ethic Committee "Campania Sud", Bruscianno, Naples, Italy; prot./SCCE n. 24988). hWJ-MSCs were prepared from fresh human umbilical cord obtained during normal spontaneous vaginal delivery. Briefly, umbilical cord sections, approximately 7.5 cm long, were placed in 0.9% NaCl physiological solution supplemented with Ampicillin-Sulbactam 1 g + 500 mg, stored at 4°C, and processed within 4 h of collection. The umbilical cord was cut into 2.5 cm segments, and washed in fresh transport media to remove blood and debris. Each umbilical cord segment was sectioned longitudinally with sterile scissors, and the visible arteries and veins removed. Each piece was transferred to a tissue culture flask 175 cm² (BD Falcon, Bedford, MA, USA) containing α -MEM (Corning Cellgro, Manassas, VA, USA) supplemented with 10% FBS (Corning Cellgro, Manassas, VA, USA), 1% GlutagroTM (Corning Cellgro, Manassas, VA, USA), and 1% Penicillin-Streptomycin solution. Cultures were incubated at 37°C in a humidified atmosphere containing 5% CO₂. Cell growth was monitored daily with changes of medium twice a week. Upon reaching 100% confluence, cells were detached using 0.05% trypsin-0.53 mM EDTA (Corning Cellgro, Manassas, VA, USA) and washed with PBS 1x (Corning Cellgro, Manassas, VA, USA), counted using Trypan Blue solution (Sigma-Aldrich, St. Louis, MO, USA), and sub-cultured at a concentration of 4 x 10³ cells/cm². For hWJ-MSCs immunophenotype characterization flow cytometry analysis was performed on cells obtained at Passage 1.

5.3.2 Flow cytometry and gating strategy

A minimum of 1×10^5 hWJ-MSCs were stained for mesenchymal phenotype analysis. Manufacturer's instructions of used antibodies (Beckman Coulter) were optimized as follows. For antibody mix 1, 2.5 μL of fluorescein isothiocyanate (FITC) - conjugated anti-CD90, 10 μL of phycoerythrin (PE) - conjugated anti-CD105, 5 μL of allophycocyanin (AOC) - conjugated anti-CD73, and 10 μL of phycoerythrin cyanin 7 (PC7) - conjugated anti-CD45 antibodies were added. For antibody mix 2, 10 μL of FITC - conjugated anti-HLA-DR, 10 μL of PE - conjugated anti-CD34, and 10 μL of PC7 - conjugated anti-CD14 antibodies were added. After 20 min incubation at room temperature, samples were washed twice with phosphate buffered saline (PBS) and resuspended in the same buffer for acquisition.

FACSVerse cytometer (BD Biosciences) equipped with 2 lasers (blue, 488 nm, and red laser, 628 nm) and BD FACSuite software (BD Biosciences) was used for sample acquisition. Compensation was calculated using single-color controls for each fluorochrome and an unstained sample was used as negative control for setting PMT voltages. All samples were run using the same PMT voltages. A minimum of 30,000 events were recorded.

FlowJo software (v.10.7.1, LLC, BD Biosciences) was employed for post-acquisition compensation and flow cytometric analysis. After post-acquisition compensation using FlowJo, hWJ-MSCs were first identified using linear parameters (forward scatter area [FSC-A] vs side scatter area [SSC-A], and double cells were excluded (FSC-A vs FSC-H). For antibody mix 1, CD90 and CD45 expression was investigated on single cells, and CD105 and CD73 expression was further studied on CD45-CD90+ cells. For antibody mix 2, HLA-DR and CD34 expression was first investigated on single cells, and CD14 was further studied on CD34-HLA-DR- cells. Expression of each marker on single cells was also reported using histograms and using unstained samples as negative controls.

5.3.3 3D system preparation and characterization

hGDF-5 loaded PLGA-NCs were fabricated as described in Chapter 3.

Hyaluronate band and overall 3D system elastic modulus was measured according to the ASTM 1708 by a CMT 6000 dynamometer (SANS, Shenzhen, China) equipped with a 100 N load cell. Samples were shaped to obtain specimens having a gauge length (L_0) of 22 mm and a width (W) of 5 mm; sample thickness (S) was 0.5 mm. A monoaxial deformation was applied to the sample with a speed of 22 mm/min, and force (F) and elongation (L) during traction was registered. The value of force (F) provided by the instrument was divided by the sample area ($A = W \times S$) to obtain the strength values ($\sigma = F/A$). The deformation values (L) during the run were compared to the initial length to obtain values of strain ($\varepsilon = (L - L_0)/L_0$); the ultimate tensile strength (σ_{max} ,

expressed in MPa) was calculated as load to failure/cross sectional area of the sample.

For each 3D scaffold sample, a mixture of 50 mg/mL fibrinogen from human plasma (Sigma-Aldrich, Milan, IT), 15,600 U/mL aprotinin (Sigma-Aldrich, Milan, IT), and α -MEM (Corning, NY, USA) supplemented with 10% FBS (referred to as growing media, GM) was added at a 1:1:1 ratio to 80 mg of PLGA-NCs (hGDF-5 loading: 3 μ g/g) and, then, to an average of 1×10^6 cells/mL. A homogeneous cells/PLGA-NCs/fibrinogen suspension was then embedded into a mold (30 x 20 x 4.5 mm) where the braided band had been previously positioned; free ends were left to enable scaffold fixation into the bioreactor. Upon addition of 100 U/mL thrombin (Sigma-Aldrich, Milan, IT), the mold was placed in a 37 °C humidified incubator for 30 min to allow fibrin polymerization. When the hydrogel was formed, the band was entrapped inside a uniformly distributed hydrogel.

The scaffold was then transferred from the mold to the bioreactor culture chamber, containing 20 mL of the culture media, and placed in an incubator at 37 °C in a 5% CO₂ atmosphere and 95% relative humidity. For the histochemical analysis, at different time points, a portion of the scaffold was fixed in 4% PFA (4°C, 4h), washed three times in PBS 1x (RT, 10 min), cryo-protected in 30% sucrose overnight, mounted in OCT embedding compound, frozen at -20°C and then cut in slices of 10 μ m of thickness using a cryostat. The remaining portion of the scaffold was placed in QIAzol[®] Lysis Reagent for total RNA extraction.

5.3.4 Cyclic strain bioreactor for dynamic culture and cytotoxicity

A cyclic deformation was applied to the 3D scaffold within a stand-alone culture chamber (maximum volume = 20 mL). The chamber was designed and 3D printed using a Dental Clear resin, a PMMA-like hard clear resin designed for printing models, used in dental application, where transparency is one of the main issues. The sample was held at one free end by a motionless arm and, at the other one, by a sliding one. The sliding arm presented a toothed clamp, connected to a rod, that was isolated from the inside of the culture chamber and driven by a linear motor (42BYGH48; 1.8, 1.2A, 0.4Nm, DFA) to transmit the motion. The motionless arm as well comprised a toothed clamp, attached to the side wall of the culture chamber. A custom-written software, developed with LabVIEW v. 8.2 (<http://www.ni.com/labview>), allowed to customize the system operations. The scaffold was deformed (40h of stretching followed by 6h of rest) at a frequency of 1 Hz with a mean load over the cycle of 0.1N and 10% of stretching of the initial total scaffold length (~3 mm when the total length of available for cell growth was 30 mm).

The 3D printed elements were tested for their cytotoxicity using CHO-K1 (P5) and HeLa (P14) cell lines. Cells were seeded on coverslips in 24-well plates at a density of 30,000 cells/well; after 24h, the coverslips were transferred in the

culture chamber of the bioreactor or in new standard well plates (control), both containing Dulbecco's Modified Eagle's Medium (DMEM) supplemented with 10% FBS (Corning Cellgro, Manassas, VA, USA), 1% Glutagro™ (Corning Cellgro, Manassas, VA, USA), and 1% Penicillin-Streptomycin solution. Cytotoxicity was evaluated after 24h and 48h using MTT assay. 500 µL of MTT was added (1 mg/mL final concentration) to each well, containing cells seeded on coverslips, and incubated at 37 °C for 4 h, protecting the plate from the light. Formazan salts were dissolved in 500 µL of DMSO. The experiments were performed in triplicate for each time point. The absorbance was measured at 490nm with UVvis system Tecan (mod. Infinite-M200 Pro). Cell viability was calculated as the percentage of the control group, considered as 100%. The percentage viability of cells was calculated according to equation (1):

$$\% \text{ Cell viability} = \frac{\text{Abs of sample} - \text{Abs blank}}{\text{Abs of control} - \text{Abs of blank}} \cdot 100 \quad (1)$$

For the cytotoxicity investigation on cells within the 3D scaffold, the bioengineered construct was assembled, as described above, using HeLa cell line. A cell density of about 1×10^6 /mL (P14) was used in the fibrin hydrogel. The scaffold was placed in the culture chamber of the bioreactor, containing 20 mL of DMEM supplemented with 10% FBS (Corning Cellgro, Manassas, VA, USA), 1% Glutagro™ (Corning Cellgro, Manassas, VA, USA), and 1% Penicillin-Streptomycin solution. The viability of cells into scaffolds was detected by fluorescence Live/Dead assay (Calcein AM solution 4µM and Ethidium homodimer I solution 2µM, Sigma-Aldrich, Milan, IT), after 24h and 72h. Cells were stained for 1 hour at 37°C, washed in PBS 1X and imaged using a fluorescence microscope (mod. Eclipse, Nikon, DE). Green emission of the Calcein dye stains the cytosol of live cells; red emission of cell membrane-impermeable ethidium homodimer-1 dye stains nuclei of dead cells. However, the braided band fibers resulted to retain red dye, overestimating the quantification of red channel. Consequently, only the green signal given by live cells was quantified.

Image quantification was performed in a blinded manner using image analysis software (ImageJ, National Institutes of Health, Bethesda, MD, USA) by measuring the green areas where live cells were present³⁷⁴. The original images were converted from RGB format into a gray scale (16-bit). Then, the average value of pixel intensity (within a range from 0-dark to 255-white) was calculated for each image. A minimum of 10 image fields were used for the analysis at each time point for each experiment. Data were expressed as fold change relative to $T_0 = 1$.

5.3.5 Gene expression profiles by qRT-PCR

Total RNA was extracted from hWJ-MSCs seeded into the 3D construct of each experimental group using QIAzol® Lysis Reagent (Qiagen, DE), chloroform (Sigma-Aldrich, Milan, IT) and the RNeasy Mini Kit (Qiagen, DE). For each

sample, 800-1000 ng of total RNA was reverse-transcribed using the iScript™ cDNA synthesis kit (Bio-Rad, Milan, IT). Relative gene expression analysis was performed in a LightCycler® 480 Instrument (Roche, IT), using the SsoAdvanced™ Universal SYBR® Green Supermix (Bio-Rad) with the validated primers for COL1A1, COL3A1, DCN, IL-1 β , IL-6, IL-10, IL-12A, SCX-A, TGF- β 1, TNF and TNC (Bio-Rad), and following MIQE guidelines²⁵⁶. Amplification was performed in a 10 μ L final volume, including 2 ng of complementary DNA (cDNA) as template. Specificity of the formed products was assessed via melting curve analysis. Triplicate experiments were performed for each condition explored, and data were normalized to glyceraldehyde-3-phosphate dehydrogenase (GAPDH) expression (reference gene), applying the geNorm method²⁵⁷ to calculate reference gene stability between the different conditions (calculated with CFX Manager software; M <0.5). The relative gene expression was calculated using the comparative Ct ($\Delta\Delta$ Ct) method, converted to relative expression ratio ($2^{-\Delta\Delta$ Ct}), and expressed as fold change over hWJ-MSCs T0 = 1.

5.3.6 Immunohistochemical assay

Sirius Red staining was performed using the Picro-Sirius Red Stain Kit (Polysciences, Inc., USA). Sections of 10 μ m of thickness were stained in hematoxylin for 8 min, then washed in water for 2 min. The sections were dipped into phosphomolybdic acid for 2 min and washed in water for 2 min. Then they were dipped into Picrosirius Red F3BA Stain for 60 min and dipped into HCl 0.1 M solution for 2 min. The sections were dehydrated in increasing ethanol gradient solutions (70–75–95–100%) and finally immersed into xylene for 5 min. Eukitt medium was used to mount the samples.

5.3.7 Statistical analysis

Statistical analysis was performed using GraphPad Prism software (6.0 for Windows). Data obtained from multiple experiments are expressed as mean \pm SD and analyzed for statistical significance using ANOVA test, for independent groups. Differences were considered statistically significant when $p \leq 0.05$ ³⁴⁷.

5.4 Results

5.4.1 Cytotoxicity of 3D printed cyclic strain bioreactor elements

The cyclic strain bioreactor was specifically designed and 3D printed; cytotoxicity of printed bioreactor elements was evaluated on CHO-K1 and HeLa cell lines before their use for stem cell cultures. The study revealed that bioreactor vessel and elements did not affect cells metabolic activity, which was of 80% for CHO-K1 cells and of 100% for HeLa cells at 24 h and 48 h (Figure 5-1a). Cytotoxicity was also evaluated on the 3D system assembled using 1 x

10^6 HeLa and placed in the bioreactor chamber for 72 h under cyclic strain, set at 10% deformation and 1 Hz of frequency. Live and Dead assay showed cells proliferation with a significant increase of green signal (live cells) of 2-fold after 24h and 5.5-fold after 72h of culture (Figure 5-1b). Overall data confirmed safety of bioreactor printed elements for cells culture.

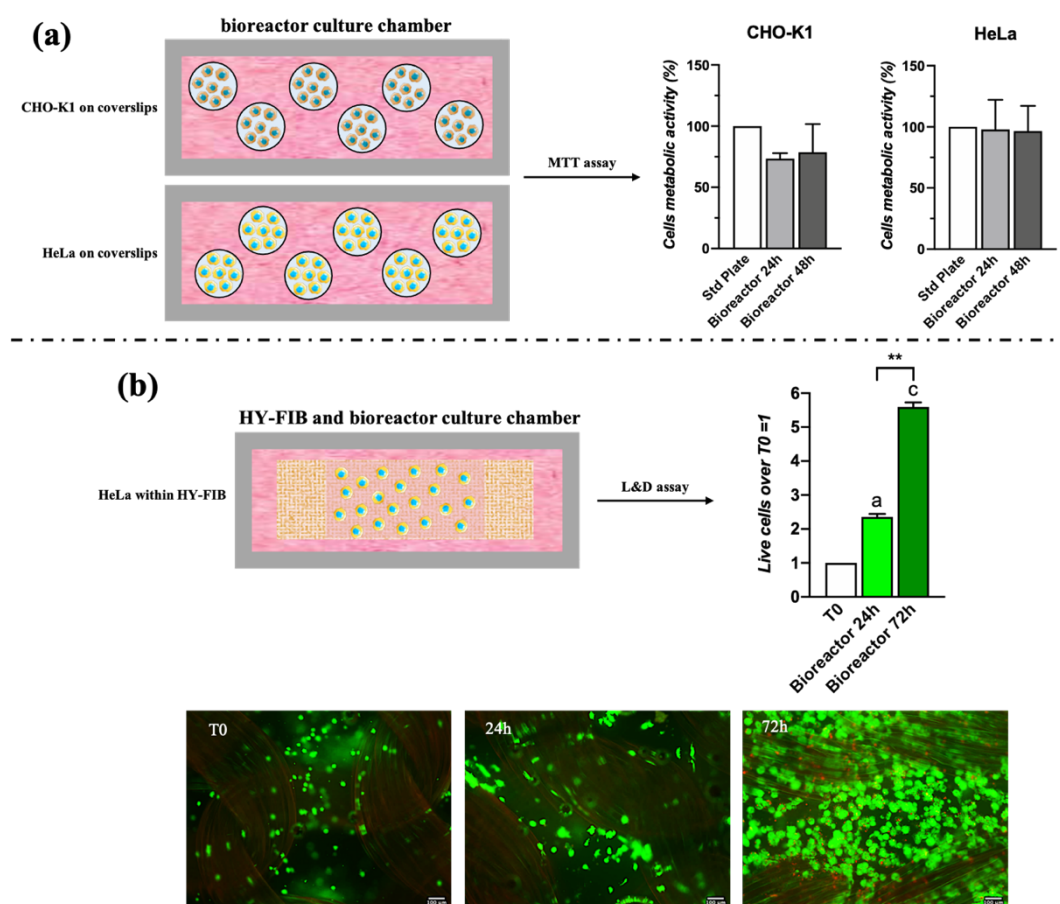


Figure 5-1. Cytotoxicity assay of 3D printed cyclic strain bioreactor with CHO-K1 and HeLa cells. (a) MTT assay on CHO-K1 and HeLa cells seeded on coverslips at 24 h and 48 h of culture in the bioreactor chamber. The histograms report the mean percentage of viable cells compared to control (cells cultured in a standard plate, 100%). (b) Live and Dead assay at 24h and 72h on HeLa cells embedded in the 3D fibrin hydrogel of the 3D scaffold. The green signal, indicating viable cells, was quantified using ImageJ software and presented as fold change over $T_0 = 1$. Statistically significant differences are shown as $** = p \leq 0.01$; $a = p \leq 0.05$, $c = \leq 0.005$ compared to T_0 . Scale bar = 100 μm.

5.4.2 3D scaffold assembly and its mechanical characterization

Flow cytometry characterization of hWJ-MSCs with data acquisition profiles is reported in Figure 5-2. Cells were positive for CD90, CD73, CD105 and negative for CD45, CD14, CD34, according to previously published data²⁵⁸. Each scaffold was assembled with 8×10^5 hWJ-MSCs.

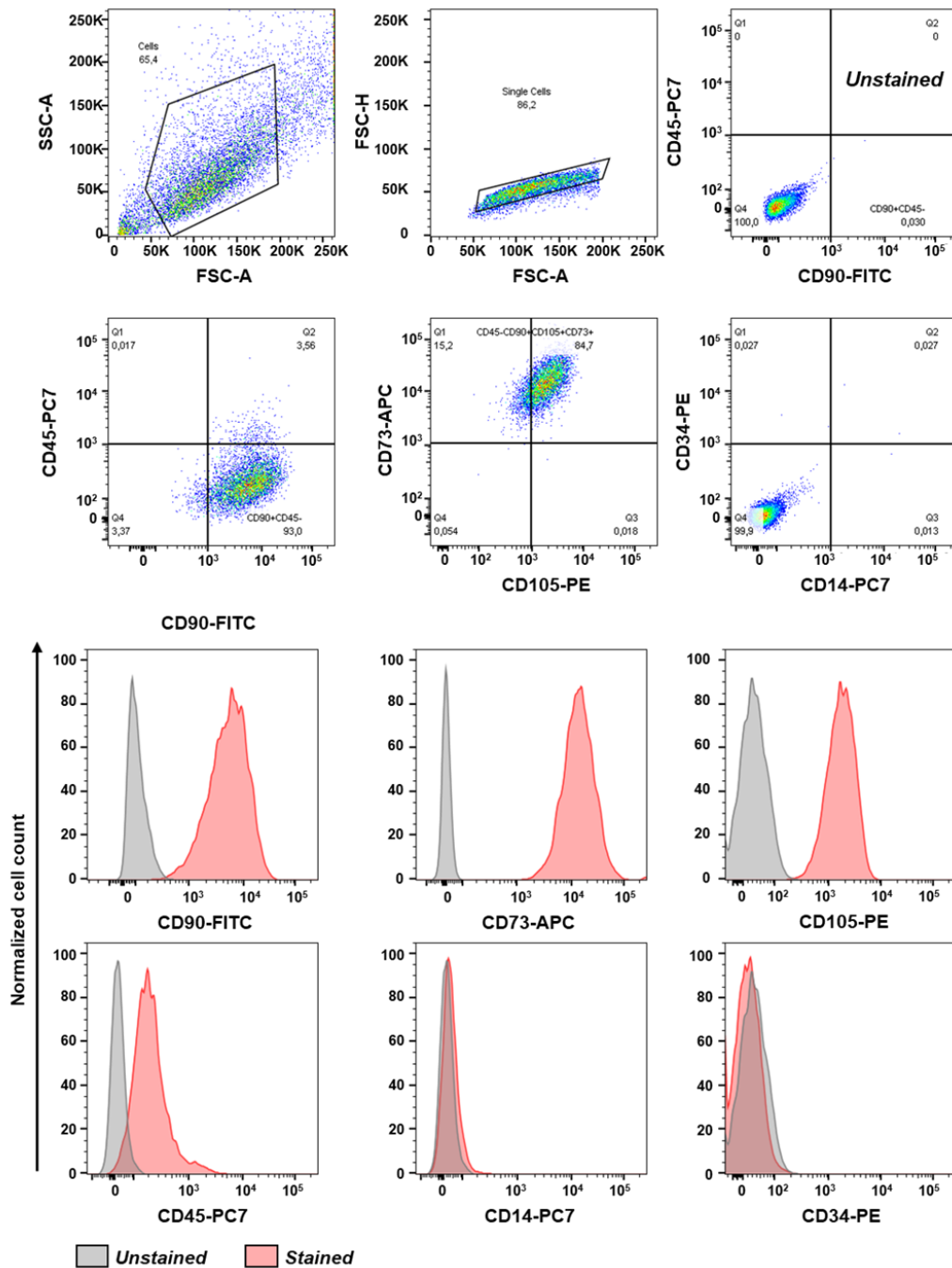


Figure 5-2. Flow cytometry characterization of hWJ-MSCs. The panel shows the representative flow cytometry events of forward scatter (FSC) vs. side scatter (SSC), excluding double cells (FSC-A vs FSC-H).

Within the 3D system, the hyaluronate band, coupled with the bioreactor, should be considered the main responsible of the mechanical strain. The braided band showed a tensile strength at break point of 2.8 MPa and a Young Modulus of 5.5 MPa. However, when the same measure was performed on the 3D assembled construct, the presence of fibrin environment reduced the tensile strength at break point of about one third (0.92 MPa), as well as the Young modulus of the 3D system, which was measured at 1.6 MPa, as indicated by the data reported in Table 5-1 and Figure 5-3.

| | Hyaluronate band | 3D construct |
|---------------------------------|------------------|--------------|
| Humidity (%) | 100 | 100 |
| Modulus of elasticity (MPa) | 5.5 | 1.6 |
| Elongation at break (%) | 85.71 | 78.75 |
| Tensile strength at break (MPa) | 2.8 | 0.92 |

Table 5-1. Mechanical characterization of hyaluronate braided band and bioengineered 3D construct.

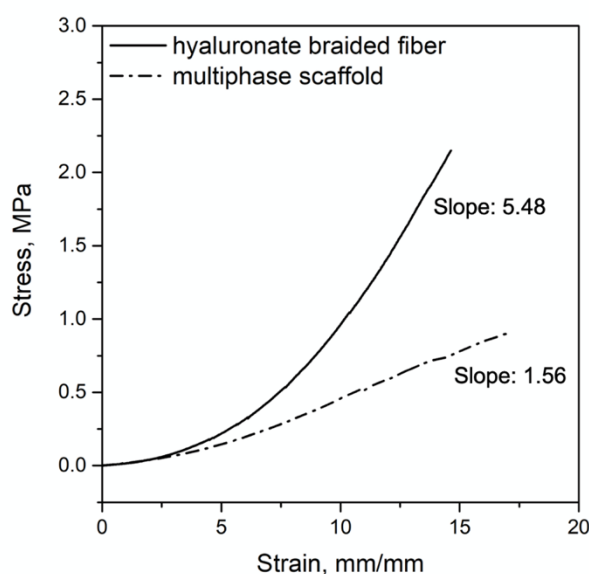


Figure 5-3. Mechanical characterization of the 3D scaffold. Stress–strain plot and elastic modulus values (a) and maximum load (b) of hyaluronate braided band (continuous line) and of multiphase stem cell-based scaffold (dashed line).

The mechanical behaviour of the overall system was adequate to deliver a cyclic deformation set at 10% with 1 Hz of frequency, as applied by the software control interface of the bioreactor (Figure 5-4a). The braided band of the scaffold was held at both free ends by a motionless arm and a sliding one, placed in the bioreactor chamber full of culture medium (Figure 5-4b) and exposed to mechanical stimulation for 40h (followed by 6h of rest). In these conditions, the braided band coupled with the applied strain assured a mean force distribution of 9×10^{-5} MPa to the 8×10^5 cells loaded within, as previously calculated³⁶⁸.

Under this mechanical strain force, two series of experiment were performed: (i) supplementing hGDF-5 in the external medium (Figure 5-4c) at 100 ng/mL and changing the medium every 4 days; (ii) assembling the 3D microenvironment adding, into the fibrin hydrogel, PLGA carriers able to ensure a controlled release of the growth factor within the 3D system (Figure 5-4d).

In the first series of runs, 100 ng/mL of hGDF-5 was supplemented in the external medium, as previously optimized^{368,130}. When carriers were loaded within the system, an amount of 80 mg was added in each 3D assembled system in order to ensure similar growth factor concentrations within the 3D system thanks to its sustained release from the carriers.

The multilevel scaffold structure was also investigated by Field Emission Scanning Electron Microscopy (FE-SEM) and the images collected displayed the braided band fibers of about 10 μm , uniformly covered by fibrin hydrogel, which represented an entrapment matrix for both hWJ-MSCs and PLGA carriers, when inserted (Figure 5-5).

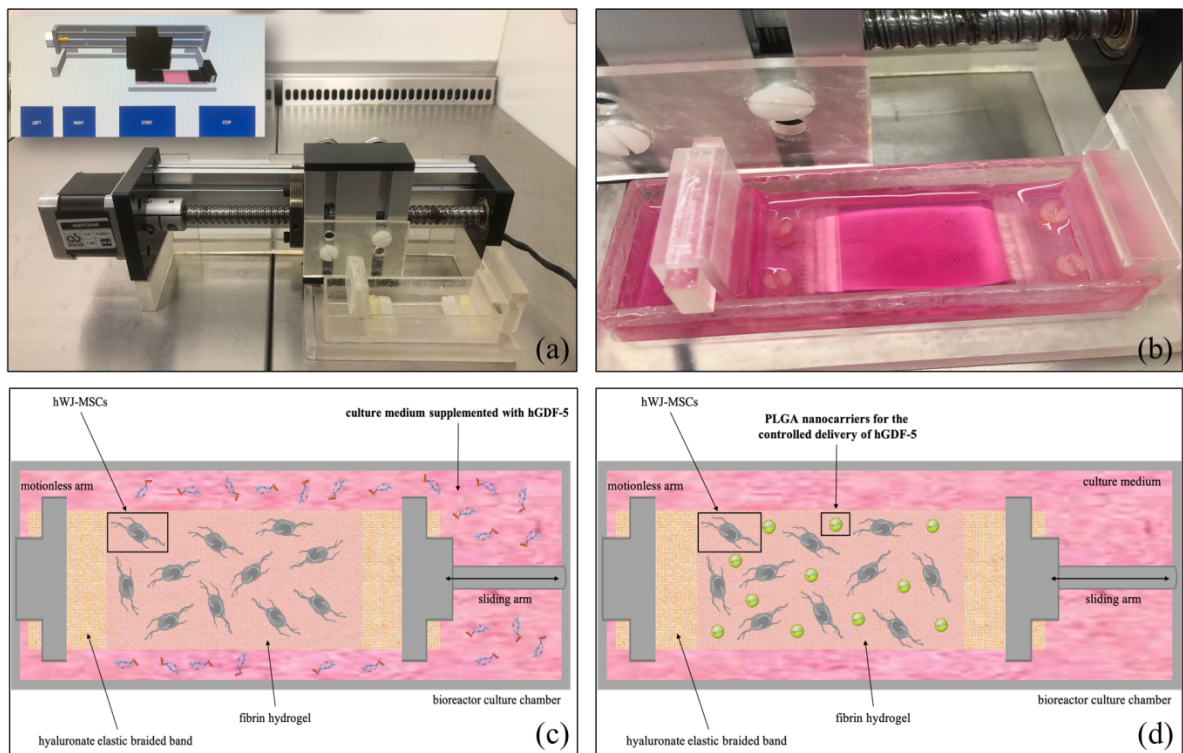


Figure 5-4. Cyclic strain bioreactor and experimental design (a) Image of the cyclic strain bioreactor and software interface. (b) 3D scaffold placed in the bioreactor culture chamber. Two series of experiments were performed: (c) hGDF-5 was supplemented in the culture medium or (d) encapsulated within PLGA carriers for growth factor controlled delivery.

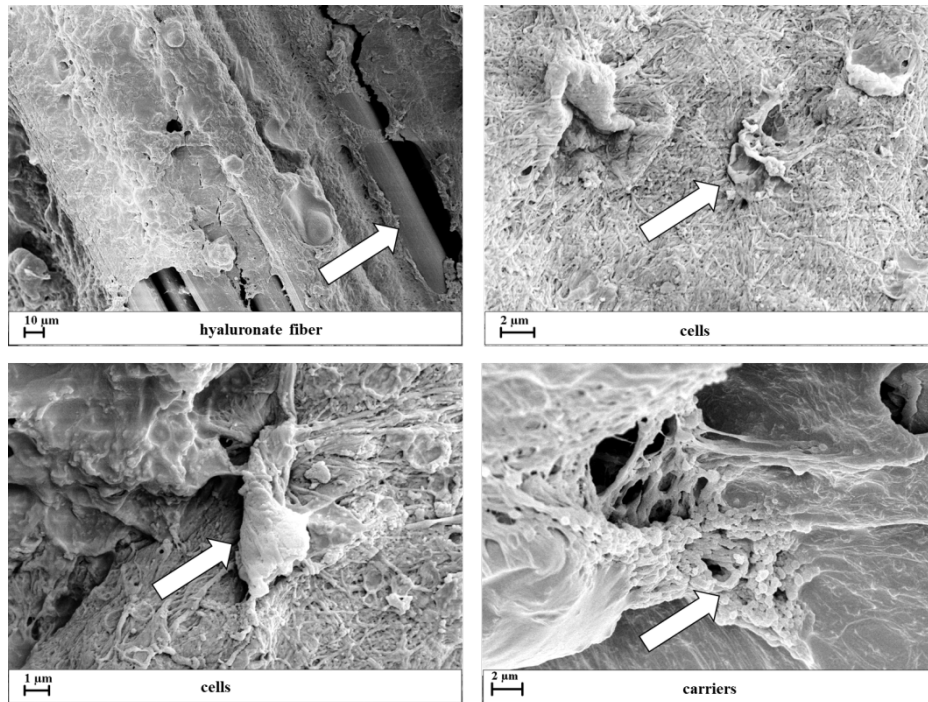


Figure 5-5. 3D scaffold structure monitored by FE-SEM images. FE-SEM images of 3D scaffold: hyaluronate fibers, cells entrapped within the fibrin matrix and PLGA carriers distributed within the fibrin network were observed.

5.4.3 Biomimetic system in dynamic culture coupled to hGDF-5 in the external medium

In the first experimental setting, hWJ-MSCs were seeded within the fibrin hydrogel of the system and cultured, under dynamic conditions, in a medium supplemented with 100 ng/mL of hGDF-5 for up to 14 days. Samples were collected after 7 days and 14 days to monitor tenogenic markers expression. However, in these conditions, only DCN displayed a slight and constant up-regulation of 1.4-fold at Day 7 and 1.5-fold at Day 14 (Figure 5-6).

Histological characterization was obtained by staining with Sirius Red for collagen highlighting at Days 7 and 14 of culture (Figure 5-7). An homogenous network of synthetic fibrin matrix at Day 0 was observed with cells immobilized within. The 3D fibrin matrix maintained its integrity during the culture, even though it showed small areas stained in darker red (arrowheads) probably filled with collagen; these areas were observed in the matrix especially Day 14 (Figure 5-7a). Further matrix characterization was performed with polarized microscope that revealed fine birefringent collagen fibers at Day 8 and Day 16 (Figure 5-7b).

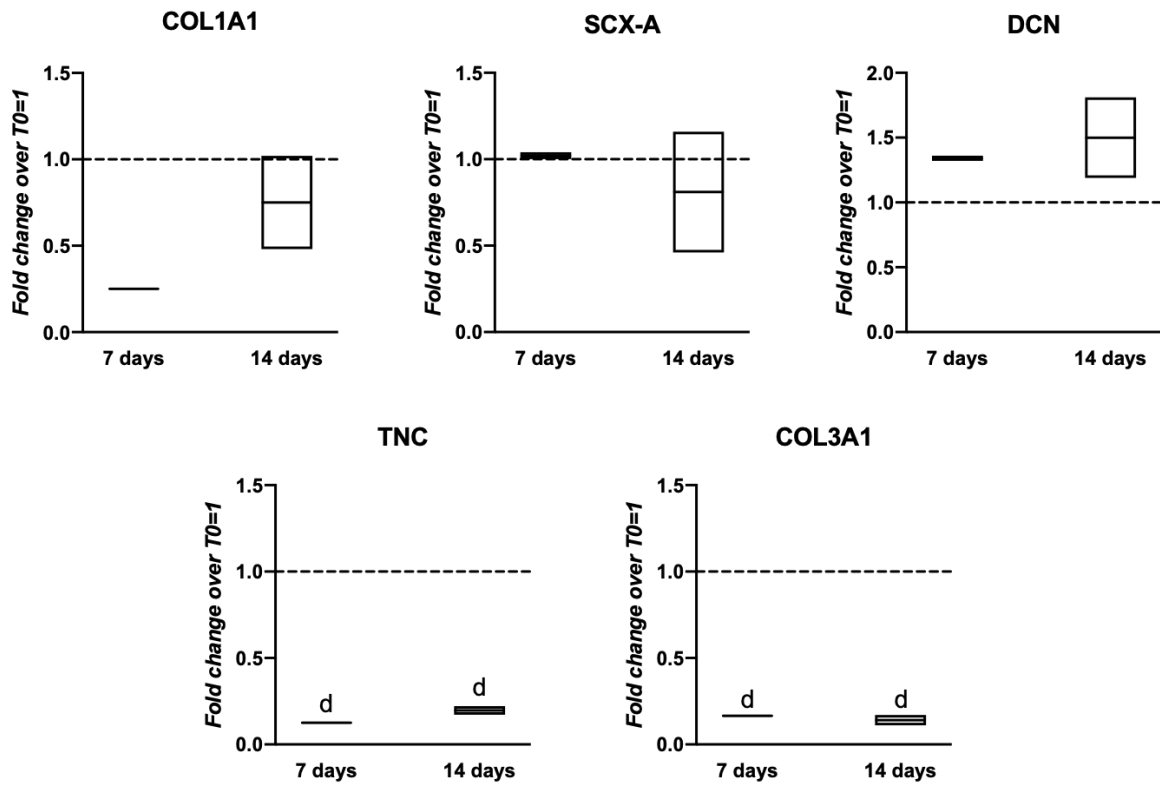


Figure 5-6. Gene expression profiles for tenogenic markers of hWJ-MSCs cultured within the 3D construct into an medium supplemented with hGDF-5. hWJ-MSCs were cultured in a medium supplemented with 100 ng/mL of hGDF-5 up to 14 days. The mRNA levels of different tenogenic markers (COL1A1, SCX-A, DCN, TNC and COL3A1) were monitored. Relative quantification of each mRNA gene expression normalized to endogenous GAPDH (internal control) was calculated using the $2^{-\Delta\Delta C_t}$ method and presented as fold change over hWJ-MSCs T0=1 (dashed line). Statistically significant differences are shown as d = $p \leq 0.001$ compared to T0; n = 2 (biological replicates).

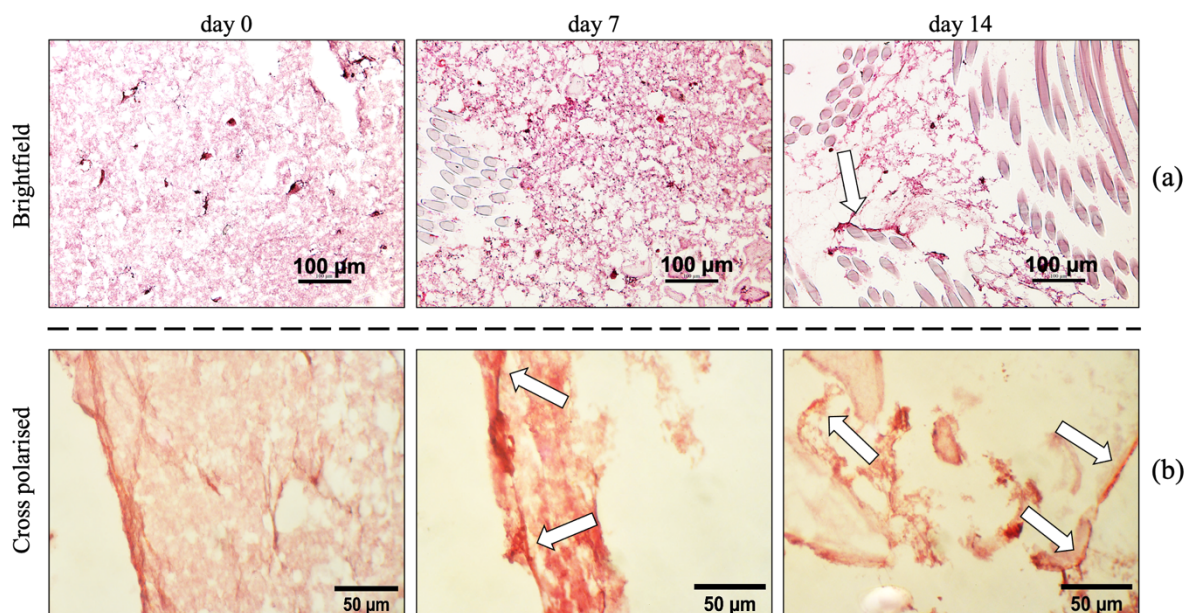


Figure 5-7. Histological characterization of the 3D bioengineered construct. hWJ-MSCs were cultured within 3D scaffold into a medium supplemented with hGDF-5. Samples at

different time-points (Days 7 and 14) under dynamic culture were subjected to Sirius Red staining for collagen highlighting. Brightfield (a; scale bar: 100 μm) and cross polarised (b; scale bar: 50 μm) images were acquired at each time-point.

5.4.4 Biomimetic system in dynamic culture coupled to hGDF-5 controlled delivery

On the basis of these results, we assembled a 3D system with an anisotropic nano-to-macro architecture observe if this configuration may enhance hWJ- MSCs tenogenic commitment. Indeed, functionalizing the fibrin hydrogel with polylactic-co-glycolic acid nanocarriers (PLGA-NCs) carrying human Growth Differentiation factor 5 (hGDF-5) and able to ensure a sustained delivery of the biochemical factor within the 3D scaffold, a better cells commitment was observed. hGDF-5 loaded PLGA-NCs were obtained using Supercritical Emulsion Extraction technology, as described in Chapter 3. Carriers exhibited a spherical morphology with a mean size of 450 (± 100) nm (Figure 5-8a to 5-8c) and a hGDF-5 loading of 3 $\mu\text{g/g}$, providing a daily released growth factor concentration of about 40 ng/mL when 80 mg of carriers were supplemented to the hydrogel component of the 3D system (Figure 5-8d).

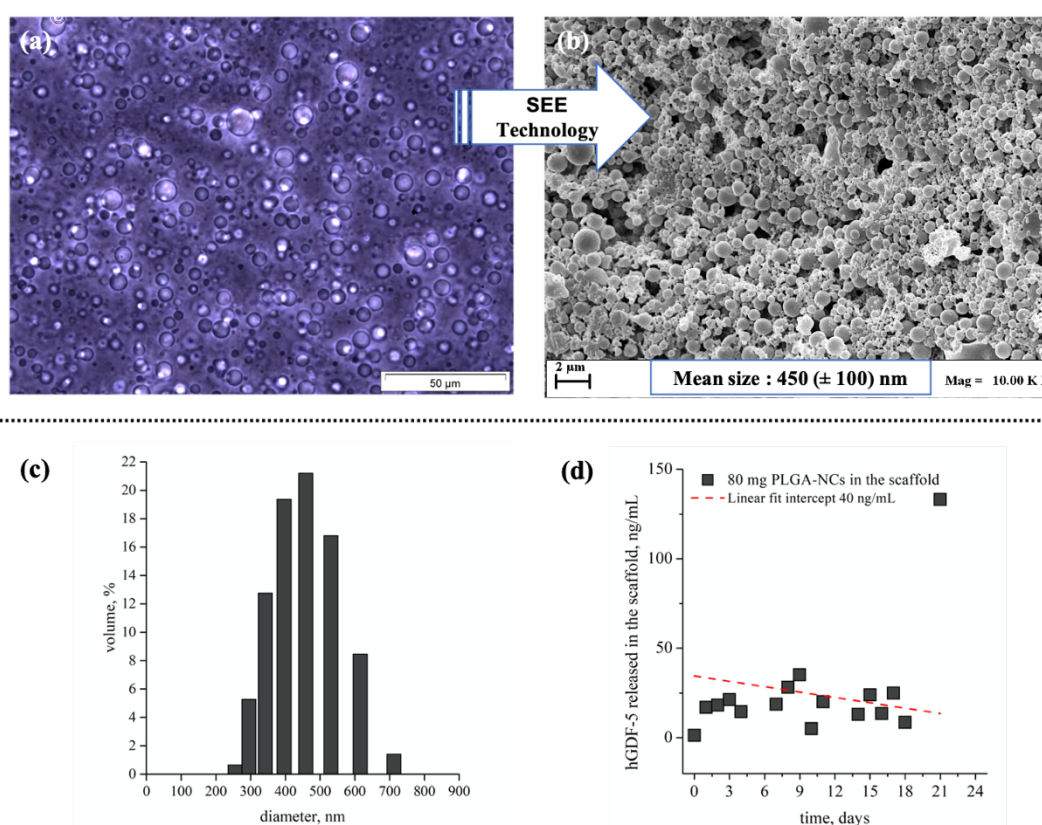


Figure 5-8. Images of emulsion and derived PLGA-NCs obtained by SEE technology, particle size distribution and hGDF-5 release profiles within 3D environment. Optical microscope image of emulsion (a) and electronic microscope image (b) of carriers obtained after emulsion processing by SEE technology; size distribution data of PLGA carriers expressed as volume percentage (c); *in vitro* hGDF-5 release profile (ng/mL/day) monitored at 37 $^{\circ}\text{C}$ and 100 rpm by ELISA-based assay from 80 mg of carriers, as loaded in each construct (d); $n = 2$.

Cells were cultured under dynamic conditions and time-points at Day 7 and Day 14 were chosen to monitor the gene expression of tenogenic markers. COL1A1 levels displayed a 7-fold overexpression at Day 7, rising slightly at Day 14 (8-fold). SCX-A levels were substantially elevated at Day 7 (100-fold), while an even stronger and significant increase (350-fold) was observed at Day 14. On the contrary, DCN displayed up-regulation of 4.5-fold at Day 7 before dropping to 2.5-fold at Day 14. TNC did not show significant up-regulation in both static and dynamic conditions, exhibiting expression levels close to T0. COL3A1 maintained a very slight up-regulation of 1.2-fold at Day 7 and 1.5-fold at Day 14 (Figure 5-9).

Collagen protein deposition within the 3D matrix was confirmed by Sirius Red staining (Figure 5-10). The homogenous network of synthetic fibrin matrix with cells (observed at Day 0), appeared progressively filled with new areas of matrix stained in darker red (arrowheads) suggesting collagen deposition within the matrix. Moreover, the overall matrix seemed clearly rearranged over time. (Figure 5-10a). Further matrix characterization was performed with polarized microscope that revealed a visible mass of birefringent collagen fibers at Days 7 and 14 of culture (Figure 5-10b).

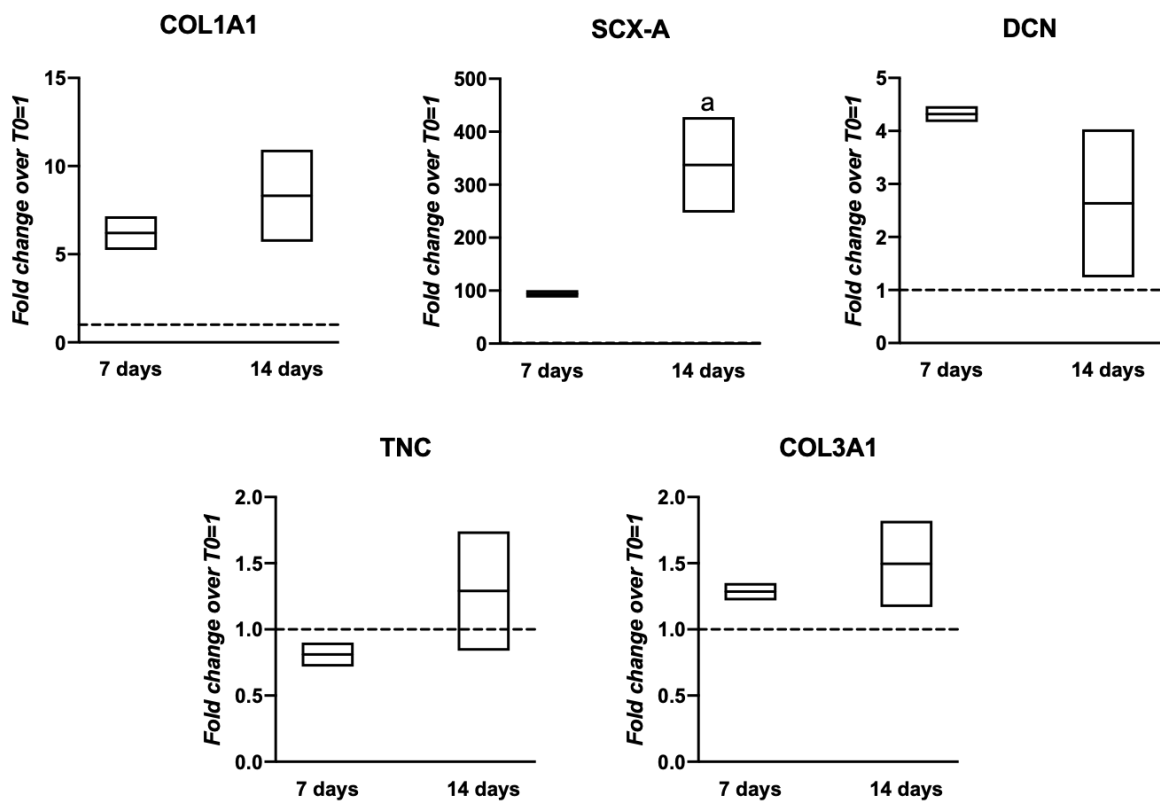


Figure 5-9. Gene expression profiles for tenogenic markers of hWJ-MSCs cultured within scaffold functionalized with PLGA-NCs for hGDF-5 controlled delivery. hWJ-MSCs were cultured in the 3D microenvironment for up to 14 days. The mRNA levels of different tenogenic markers (COL1A1, SCX-A, DCN, TNC and COL3A1) were monitored.

Relative quantification of each mRNA gene expression normalized to endogenous GAPDH (internal control) was calculated using the $2^{-\Delta\Delta C_t}$ method and presented as fold change over hWJ-MSCs T0=1 (dashed line). Statistically significant differences are shown as a = $p \leq 0.05$ compared to T0; n = 2 (biological replicates).

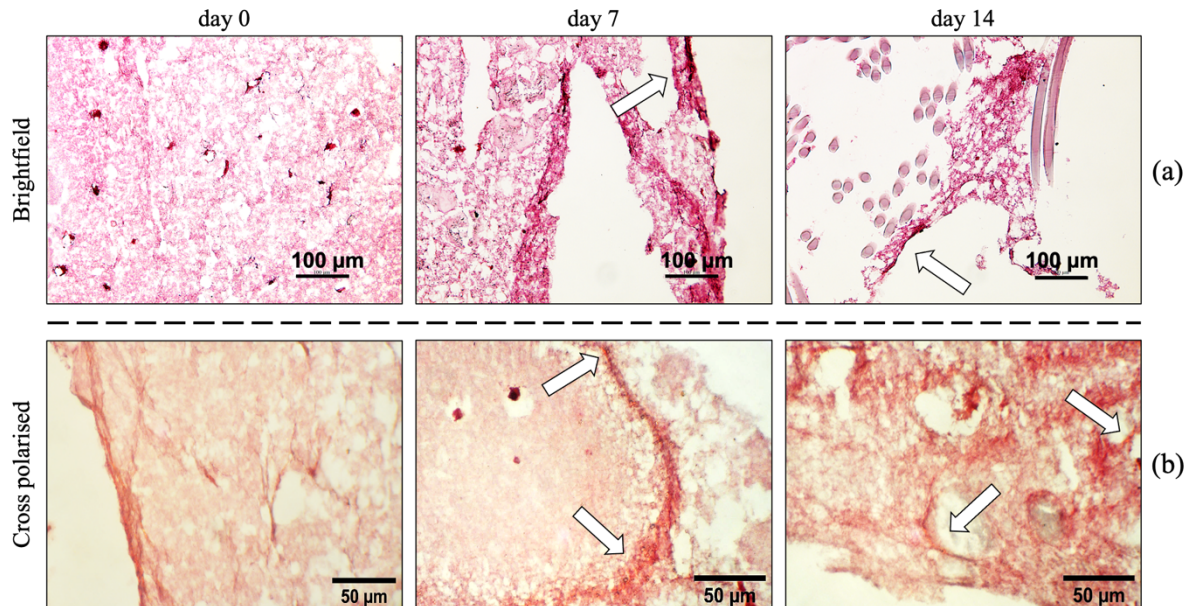


Figure 5-10. Histological characterization of the 3D bioengineered construct. hWJ-MSCs were cultured within the scaffold functionalized with PLGA-NCs for hGDF-5 controlled delivery. Samples at different time-points (Days 7 and 14) under dynamic culture were subjected to Sirius Red staining for collagen highlighting. Brightfield (a; scale bar: 100 µm) and cross polarised (b; scale bar: 50 µm) images were acquired at each time-point.

5.4.5 hWJ-MSCs immunomodulatory activity within the biomimetic system

Given the well-known hWJ-MSCs immunomodulatory activity^{237,375}, gene expression of several pro-inflammatory and anti-inflammatory cytokines along the culture was also considered for the set of culture that ensured the best tenogenic commitment.

The expression levels of IL-6 showed a slight and constant up-regulation (1.5-fold) across the time-points studied. At Day 7, TNF showed a 5-fold increase, followed by a strong and significant upregulation of 45-fold at Day 14. IL-12A showed no change (Day 7) and a slight overexpression of 1.4-fold at Day 14, while IL-1 β remained significantly downregulated for the entire duration of the experiment. IL-10 exhibited consistent upregulation with 30-fold and 120-fold increase at Day 7 and Day 14, respectively; TGF- β 1 upregulation was lower (2-fold) across the culture (Figure 5-11).

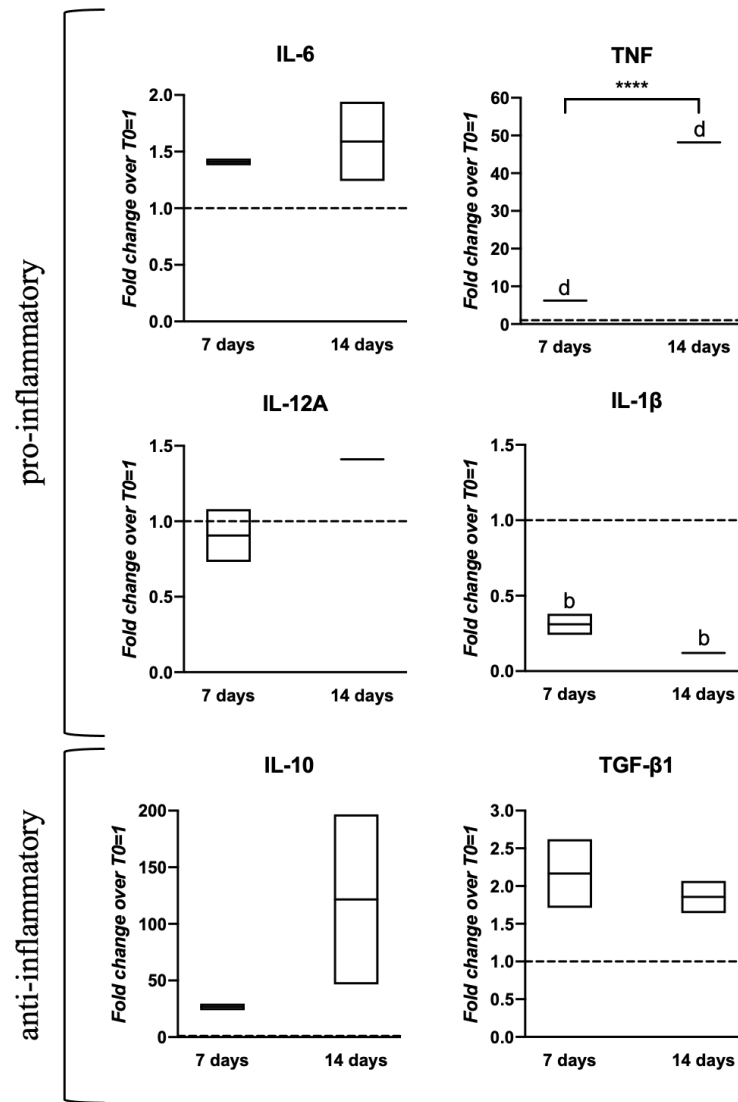


Figure 5-11. Gene expression profiles for cytokines by hWJ-MSCs cultured within scaffold assembled with PLGA-NCs for hGDF-5 controlled delivery. The mRNA levels of different pro-inflammatory (IL-6, TNF, IL-12A, IL-1 β) and anti-inflammatory (IL-10, TGF- β 1) cytokines were monitored. Relative quantification of each mRNA gene expression normalized to endogenous GAPDH (internal control) was calculated using the $2^{-\Delta\Delta C_t}$ method and presented as fold change over hWJ-MSCs Day 0 = 1. Statistically significant differences are shown as **** = $p \leq 0.001$; b = $p \leq 0.01$, d = $p \leq 0.001$ compared to T0; n = 2 (biological replicates).

5.5 Discussion

The work described in this chapter explored the behaviour of hWJ-MSCs cultured within a bio-functionalized 3D fibrous construct, as interactive teno-inductive graft model. The system was exposed, under cyclic strain, to a medium supplemented with hGDF-5, or functionalized with PLGA nanocarriers carrying hGDF-5 to commit cells toward tenogenic phenotype for up to 14 days. Thanks to the custom made bioreactor (extremely low cytotoxicity expressed on CHO-K1 and HeLa cell lines) and hyaluronate braided fibers with an elastic

modulus of 1.6 MPa, a mean force of 9×10^{-5} MPa was transmitted to the cells on it for 40h (followed by 6h of rest) during the entire culture.

Previous published investigations reported 100 ng/mL of hGDF-5 as the optimal concentration to induce stem cells commitment toward the tenogenic phenotype, when supplemented in the culture medium; these indications are mainly referred to 2D cultures in conventional flasks^{348,136,131}.

hWJ-MSCs behaviour is in contrast with previous work, in which the mechanical force distribution, provided by the cyclic strain of the braided band, triggered the tenogenic commitment of human bone marrow mesenchymal stem cells (hBM-MSCs) loaded on board, even in the absence of specific growth factors³⁶⁸. However, hWJ-MSCs are for the first time reported to be committed toward tenogenic phenotype. Also, no indication of their sensitiveness to mechanical inputs has ever been described in the literature. Therefore, comparison to previous data is extremely difficult. Indeed, hBM-MSCs are largely reported to express tenogenic markers by means of mechanical stimulation such as cyclic strain^{329,203,225}. hWJ-MSCs, on the contrary, resemble embryonic stem cells and are highly multipotent, even though they possess many properties of adult mesenchymal stem cells, and possibly would require a more complex environment to be committed toward a specific phenotype and could not be directly responsive to a specific mechanical cue.

Furthermore, hGDF-5 was already reported to commit these cells toward tenogenic phenotype; however, despite the mechanical input should improve the overall nutrient mass transfer within the 3D system³⁶⁹, overall data suggested that the hGDF-5 available in the external medium underwent a reduced mass transfer across the 3D fibrin hydrogel, which prevented the proper cells biochemical stimulation and subsequent proper commitment²⁸².

On the other hand, the data collected are largely favorable to the use of nanocarriers as drug delivery systems within the 3D scaffold to ensure the controlled delivery of biomolecules that can act as specific inputs. Furthermore, the use of carriers within a 3D environment cannot be useful in static environment, and always requires dynamic culture conditions to ensure the proper mass transfer, essential for the correct drug release profile always monitored *in vitro* in extremely diluted conditions (sink conditions), as previously described³⁶⁹. This aspect is fundamental and implies that mechanical input always exerts an important cooperative action, to provide not only a specific mechanical stimulation but also to ensure the proper mass transfer required for the correct release kinetics of drug delivery devices.

The 3D system had an effect also on hWJ-MSCs cytokines transcript expression. An inflammatory infiltrate with a high content of pro-inflammatory cytokines such as IL-6, TNF- α and IL-17 has been identified in tendon biopsies during the initial phase of the tendinopathy process^{376,103}. Indeed, inflammation is the first of the three main phases during the tendon healing process, followed by proliferation and remodeling. Each phase is influenced by a temporally and spatially controlled release of mediators by cells⁹⁶. Our data suggested the

expression of key immunomodulatory molecules by hWJ-MSCs when subjected to tenogenic differentiation *in vitro* and their capacity to modulate the inflammatory response. The overexpression of pro-inflammatory factors (IL-6, TNF) was evident, together with the upregulation of anti-inflammatory ones (IL-10, TGF β 1), probably suggesting an attempt by cells to support differentiation. In this sense, further investigations are required to better understand this finely tuned process.

5.6 Conclusions

The present work described an innovative biomimetic 3D elastomeric construct through the nano-functionalization and its *in vitro* evaluation for biosafety and improvement in teno-regenerative properties. The elastomeric 3D scaffold was fabricated using a hyaluronate band merged with fibrin hydrogel that allowed to assemble PLGA biopolymer microspheres carrying hGDF-5, and hWJ-MSCs. The 3D system was always cultured under cyclic strain to ensure a proper mechanical input and a system elongation of 10%. Compared to hGDF-5 supplemented in the culture medium, when PLGA/hGDF-5 carriers were used in the 3D system, hWJ-MSCs showed a better increase in tenogenic markers expression and collagen deposition within the fibrin matrix. We hypothesized a cooperative action between the mechanical and biochemical inputs, especially when the biomolecules were delivered in a controlled manner within the 3D environment, supporting the proper tenogenic activity of the scaffold.

hWJ-MSCs have been barely used in tendon tissue-engineering protocols; nevertheless, our data suggested that they can be an useful and advantageous alternative for *in vitro* studies about tendon regenerative protocols. An immunomodulatory activity, in relation to tenogenic commitment, was also observed.

The data confirmed the tenoinductive activity of the biomimetic *in vitro* model. Furthermore, methodologies to release multiple growth factors with independent release kinetics can mimic complex biomolecules patterns (spatial and temporal) of presentation to cells and can be useful for further studies and investigations.

Chapter 6

Conclusions and future perspectives

The work reported in the present thesis aimed to develop an innovative bioengineered multiphasic three-dimensional scaffold for tendon tissue engineering.

The theme of research presents a challenge of great value and relevance for the orthopaedic clinic; tendons are highly specialized tissues to perform the fundamental mechanical function of transferring the force useful for movement, or stability to the joints. Tendons can be subject to a wide range of lesions, with pathological conditions that can strongly influence joint movement up to major disabilities. The damaged tissue does not heal spontaneously, and will have significantly reduced mechanical properties. The need for research involving innovative repair and regeneration methodologies, such as the development of bio-engineered systems capable of regenerating the damaged structure, is clear.

The project achieved the goal of bio-functionalizing a complex 3D hierarchical fibrous construct, totally bioresorbable, intended to be used as an interactive scaffold with teno-inductive properties. The 3D multistage system, that we named HY-FIB, was designed with an anisotropic nano-to-macro architecture and it was functionalized with stem cells and biological active signals to study tenogenic differentiation process. HY-FIB guaranteed biophysical performances thanks to an internal structure of hyaluronate braided fibers, which are conventionally used in orthopedic surgery. The coupled pre-designed fibrin microenvironment represented the hydrogel microarchitecture in which to insert stem cells and PLGA carriers, engineered to ensure a controlled delivery of hGDF-5 within the synthetic extracellular matrix. The braided band allowed to give cyclic strain to the cells on board by specifically designed bioreactors.

The 3D bioengineered structure was a biomimetic system for tenogenesis studies and research. Indeed, the system allowed to improve the basic knowledge behind hBM-MSCs and hWJ-MSCs tenogenic differentiation. Even though most tissue engineering studies indicated hBM-MSCs as the gold standard to promote tendon regeneration, our data suggested that, given their properties, also hWJ-MSCs could be potentially used for this purpose.

On the other hand, the presence of PLGA nanocarriers within the fibrin hydrogel allowed the delivery of several growth factors, secretomes or specific biomolecules that may be studied for the ability to further promote regeneration/repair events or modulate inflammation. Indeed, nanocarriers can act as micro-environmental regulators within a 3D bioengineered scaffold, providing a wide range of spatio-temporally controlled biomolecules delivery.

Finally, the study of hBM-MSCs and hWJ-MSCs immunomodulatory activity and the understanding of their behaviour when incorporated into specific biomaterials opened novel perspectives for the development of scaffolds with specific functionalization able to stimulate anti-inflammatory responses. In any case, further studies are needed to better understand crosstalk between inflammation cues and stem cells, and the role of biomaterials in the stimulation of inflammatory reactions.

References

1. Benjamin M, Qin S, Ralphs JR. Fibrocartilage associated with human tendons and their pulleys. *J Anat.* 1995;187 (Pt 3):625-633.
2. Kannus P. Structure of the tendon connective tissue: Tendon connective tissue structure. *Scandinavian Journal of Medicine & Science in Sports.* 2000;10(6):312-320. doi:10.1034/j.1600-0838.2000.010006312.x
3. Thorpe CT, Birch HL, Clegg PD, Screen HRC. The role of the non-collagenous matrix in tendon function. *Int J Exp Path.* 2013;94(4):248-259. doi:10.1111/iep.12027
4. Thorpe CT, Udeze CP, Birch HL, Clegg PD, Screen HRC. Specialization of tendon mechanical properties results from interfascicular differences. *J R Soc Interface.* 2012;9(76):3108-3117. doi:10.1098/rsif.2012.0362
5. Kannus P. Structure of the tendon connective tissue: Tendon connective tissue structure. *Scandinavian Journal of Medicine & Science in Sports.* 2000;10(6):312-320. doi:10.1034/j.1600-0838.2000.010006312.x
6. Sharma P, Maffulli N. Tendon Injury and Tendinopathy: Healing and Repair. *The Journal of Bone & Joint Surgery.* 2005;87(1):187-202. doi:10.2106/JBJS.D.01850
7. Chuen FS, Chuk CY, Ping WY, Nar WW, Kim HL, Ming CK. Immunohistochemical Characterization of Cells in Adult Human Patellar Tendons. *J Histochem Cytochem.*
8. Russo V, Mauro A, Martelli A, *et al.* Cellular and molecular maturation in fetal and adult ovine calcaneal tendons. *J Anat.* 2015;226(2):126-142. doi:10.1111/joa.12269
9. McNeilly CM, Banes AJ, Benjamin M, Ralphs JR. Tendon cells *in vivo* form a three dimensional network of cell processes linked by gap junctions. *J Anat.* 1996;189 (Pt 3):593-600.
10. Willecke K, Eiberger J, Degen J, *et al.* Structural and Functional Diversity of Connexin Genes in the Mouse and Human Genome. *Biological Chemistry.* 2002;383(5). doi:10.1515/BC.2002.076
11. Tanji K, Shimizu T, Satou T, Hashimoto S, Bonilla E. Gap Junctions between Fibroblasts in Rat Myotendon. *Archives of Histology and Cytology.* 1995;58(1):97-102. doi:10.1679/aohc.58.97
12. Docheva D, Müller SA, Majewski M, Evans CH. Biologics for tendon repair. *Advanced Drug Delivery Reviews.* 2015;84:222-239. doi:10.1016/j.addr.2014.11.015
13. Giordano L, Porta GD, Peretti GM, Maffulli N. Therapeutic potential of microRNA in tendon injuries. *British Medical Bulletin.* 2020;133(1):79-94. doi:10.1093/bmb/ldaa002
14. Bi Y, Ehrchiou D, Kilts TM, *et al.* Identification of tendon stem/progenitor cells and the role of the extracellular matrix in their niche. *Nat Med.* 2007;13(10):1219-1227. doi:10.1038/nm1630
15. Józsa LG, Kannus P. *Human Tendons: Anatomy, Physiology, and Pathology.* Human Kinetics; 1997.
16. Salingcarnboriboon R. Establishment of tendon-derived cell lines exhibiting pluripotent mesenchymal stem cell-like property. *Experimental Cell Research.* 2003;287(2):289-300. doi:10.1016/S0014-4827(03)00107-1
17. Lui PPY. Identity of tendon stem cells - how much do we know? *J Cell Mol Med.* 2013;17(1):55-64. doi:10.1111/jcmm.12007
18. Mienaltowski MJ, Adams SM, Birk DE. Regional Differences in Stem Cell/Progenitor Cell Populations from the Mouse Achilles Tendon. *Tissue Engineering Part A.* 2013;19(1-2):199-210. doi:10.1089/ten.tea.2012.0182
19. Ruzzini L, Abbruzzese F, Rainer A, *et al.* Characterization of age-related changes of tendon stem cells from adult human tendons. *Knee Surg Sports Traumatol Arthrosc.* 2014;22(11):2856-2866. doi:10.1007/s00167-013-2457-4

20. Kirkendall DT, Garrett WE. Function and biomechanics of tendons. *Scandinavian Journal of Medicine & Science in Sports*. 2007;7(2):62-66. doi:10.1111/j.1600-0838.1997.tb00120.x
21. Kadler KE, Hojima Y, Prockop DJ. Collagen fibrils *in vitro* grow from pointed tips in the C- to N-terminal direction. *Biochemical Journal*. 1990;268(2):339-343. doi:10.1042/bj2680339
22. Riley G. The pathogenesis of tendinopathy. A molecular perspective. *Rheumatology*. 2004;43(2):131-142. doi:10.1093/rheumatology/keg448
23. Tuderman L, Kivirikko KI, Prockop DJ. Partial purification and characterization of a neutral protease which cleaves the N-terminal propeptides from procollagen. *Biochemistry*. 1978;17(15):2948-2954. doi:10.1021/bi00608a002
24. Grant TM, Thompson MS, Urban J, Yu J. Elastic fibres are broadly distributed in tendon and highly localized around tenocytes. *J Anat*. 2013;222(6):573-579. doi:10.1111/joa.12048
25. Flamia R, Zhdan PA, Martino M, Castle JE, Tamburro AM. AFM Study of the Elastin-like Biopolymer Poly(ValGlyGlyValGly). *Biomacromolecules*. 2004;5(4):1511-1518. doi:10.1021/bm049930r
26. Godinho MSC, Thorpe CT, Greenwald SE, Screen HRC. Elastin is Localised to the Interfascicular Matrix of Energy Storing Tendons and Becomes Increasingly Disorganised With Ageing. *Sci Rep*. 2017;7(1):9713. doi:10.1038/s41598-017-09995-4
27. Zhang G, Chen S, Goldoni S, *et al*. Genetic Evidence for the Coordinated Regulation of Collagen Fibrillogenesis in the Cornea by Decorin and Biglycan. *Journal of Biological Chemistry*. 2009;284(13):8888-8897. doi:10.1074/jbc.M806590200
28. Rigozzi S, Müller R, Stemmer A, Snedeker JG. Tendon glycosaminoglycan proteoglycan sidechains promote collagen fibril sliding—AFM observations at the nanoscale. *Journal of Biomechanics*. 2013;46(4):813-818. doi:10.1016/j.jbiomech.2012.11.017
29. O'Brien M. Structure and metabolism of tendons. *Scandinavian Journal of Medicine & Science in Sports*. 2007;7(2):55-61. doi:10.1111/j.1600-0838.1997.tb00119.x
30. Svensson L, Aszódi A, Heinegård D, *et al*. Cartilage Oligomeric Matrix Protein-Deficient Mice Have Normal Skeletal Development. *MCB*. 2002;22(12):4366-4371. doi:10.1128/MCB.22.12.4366-4371.2002
31. Jarvinen TAH. Mechanical loading regulates the expression of tenascin-C in the myotendinous junction and tendon but does not induce de novo synthesis in the skeletal muscle. *Journal of Cell Science*. 2003;116(5):857-866. doi:10.1242/jcs.00303
32. Kastelic J, Galeski A, Baer E. The Multicomposite Structure of Tendon. *Connective Tissue Research*. 1978;6(1):11-23. doi:10.3109/03008207809152283
33. Peacock EE. A Study of the Circulation in Normal Tendons and Healing Grafts*. *Annals of Surgery*. 1959;149(3):415-428. doi:10.1097/00000658-195903000-00011
34. Ahmed IM, Lagopoulos M, McConnell P, Soames RW, Sefton GK. Blood supply of the achilles tendon. *J Orthop Res*. 1998;16(5):591-596. doi:10.1002/jor.1100160511
35. Fenwick SA, Hazleman BL, Riley GP. The vasculature and its role in the damaged and healing tendon. *Arthritis Res*. 2002;4(4):252. doi:10.1186/ar416
36. Bidder M, Towler DA, Gelberman RH, Boyer MI. Expression of mRNA for vascular endothelial growth factor at the repair site of healing canine flexor tendon. *J Orthop Res*. 2000;18(2):247-252. doi:10.1002/jor.1100180212
37. Kuroda R, Kurosaka M, Yoshiya S, Mizuno K. Localization of growth factors in the reconstructed anterior cruciate ligament: immunohistological study in dogs. *Knee Surgery, Sports Traumatology, Arthroscopy*. 2000;8(2):120-126. doi:10.1007/s001670050198
38. Barboni B, Russo V, Gatta V, *et al*. Therapeutic potential of hAECs for early Achilles tendon defect repair through regeneration. *J Tissue Eng Regen Med*. 2018;12(3). doi:10.1002/term.2584

39. Ackermann PW, Salo P, Hart DA. Tendon Innervation. In: Ackermann PW, Hart DA, eds. *Metabolic Influences on Risk for Tendon Disorders*. Vol 920. Advances in Experimental Medicine and Biology. Springer International Publishing; 2016:35-51. doi:10.1007/978-3-319-33943-6_4
40. Nilsson J, von Euler AM, Dalsgaard C-J. Stimulation of connective tissue cell growth by substance P and substance K. *Nature*. 1985;315(6014):61-63. doi:10.1038/315061a0
41. Hong HS, Lee J, Lee E, *et al*. A new role of substance P as an injury-inducible messenger for mobilization of CD29+ stromal-like cells. *Nat Med*. 2009;15(4):425-435. doi:10.1038/nm.1909
42. Ackermann PW. Neuronal regulation of tendon homeostasis. *Int J Exp Path*. 2013;94(4):271-286. doi:10.1111/iep.12028
43. Alexander RM. Energy-saving mechanisms in walking and running. *J Exp Biol*. 1991;160:55-69.
44. Benjamin M, Ralphs JR. Tendons and ligaments--an overview. *Histol Histopathol*. 1997;12(4):1135-1144.
45. Kubo K, Kawakami Y, Kanehisa H, Fukunaga T. Measurement of viscoelastic properties of tendon structures *in vivo*: **Viscoelastic properties of tendon structures**. *Scandinavian Journal of Medicine & Science in Sports*. 2002;12(1):3-8. doi:10.1034/j.1600-0838.2002.120102.x
46. Gerard MP, Hodgson DR, Rose RJ, Walsh WilliamR. Effects of Recombinant Equine Growth Hormone on *In Vitro* Biomechanical Properties of the Superficial Digital Flexor Tendon of Standardbred Yearlings in Training. *Veterinary Surgery*. 2005;34(3):253-259. doi:10.1111/j.1532-950X.2005.00038.x
47. Ker R. Mechanics of tendon, from an engineering perspective. *International Journal of Fatigue*. 2007;29(6):1001-1009. doi:10.1016/j.ijfatigue.2006.09.020
48. Eyre DR, Paz MA, Gallop PM. Cross-Linking in Collagen and Elastin. *Annu Rev Biochem*. 1984;53(1):717-748. doi:10.1146/annurev.bi.53.070184.003441
49. Bailey AJ, Paul RG, Knott L. Mechanisms of maturation and ageing of collagen. *Mechanisms of Ageing and Development*. 1998;106(1-2):1-56. doi:10.1016/S0047-6374(98)00119-5
50. Avery NC, Bailey AJ. Enzymic and non-enzymic cross-linking mechanisms in relation to turnover of collagen: relevance to aging and exercise. *Scand J Med Sci Sports*. 2005;15(4):231-240. doi:10.1111/j.1600-0838.2005.00464.x
51. Fyfe I, Stanish WD. The Use of Eccentric Training and Stretching in the Treatment and Prevention of Tendon Injuries. *Clinics in Sports Medicine*. 1992;11(3):601-624. doi:10.1016/S0278-5919(20)30509-3
52. Diamant J, Keller A, Baer E, Litt M, Arridge RGC. Collagen; ultrastructure and its relation to mechanical properties as a function of ageing. *Proc R Soc Lond B*. 1972;180(1060):293-315. doi:10.1098/rspb.1972.0019
53. Kastelic J, Baer E. Deformation in tendon collagen. *Symp Soc Exp Biol*. 1980;34:397-435.
54. Sasaki N, Shukunami N, Matsushima N, Izumi Y. Time-resolved X-ray diffraction from tendon collagen during creep using synchrotron radiation. *Journal of Biomechanics*. 1999;32(3):285-292. doi:10.1016/S0021-9290(98)00174-2
55. Thorpe CT, Clegg PD, Birch HL. A review of tendon injury: Why is the equine superficial digital flexor tendon most at risk?: Why is the equine superficial digital flexor tendon most at risk? *Equine Veterinary Journal*. 2010;42(2):174-180. doi:10.2746/042516409X480395
56. Shearer T, Thorpe CT, Screen HRC. The relative compliance of energy-storing tendons may be due to the helical fibril arrangement of their fascicles. *J R Soc Interface*. 2017;14(133):20170261. doi:10.1098/rsif.2017.0261

57. Hooley CJ, McCrum NG, Cohen RE. The viscoelastic deformation of tendon. *Journal of Biomechanics*. 1980;13(6):521-528. doi:10.1016/0021-9290(80)90345-0
58. Riemersma DJ, Schamhardt HC. The cryo-jaw, a clamp designed for *in vitro* rheology studies of horse digital flexor tendons. *Journal of Biomechanics*. 1982;15(8):619-620. doi:10.1016/0021-9290(82)90073-2
59. Butler DL, Groot ES, Noyes FR, Zernicke RF. Biomechanics of ligaments and tendons. *Exerc Sport Sci Rev*. 1978;6:125-181.
60. Cohen RE, Hooley CJ, McCrum NG. Mechanism of the Viscoelastic Deformation of Collagenous Tissue. *Nature*. 1974;247(5435):59-61. doi:10.1038/247059a0
61. Arruda EM, Calve S, Dennis RG, Mundy K, Baar K. Regional variation of tibialis anterior tendon mechanics is lost following denervation. *Journal of Applied Physiology*. 2006;101(4):1113-1117. doi:10.1152/jappphysiol.00612.2005
62. Lavagnino M, Bedi A, Walsh CP, Sibilsky Enselman ER, Sheibani-Rad S, Arnoczky SP. Tendon Contraction After Cyclic Elongation Is an Age-Dependent Phenomenon: *In Vitro* and *In Vivo* Comparisons. *Am J Sports Med*. 2014;42(6):1471-1477. doi:10.1177/0363546514526691
63. Lavagnino M, Wall ME, Little D, Banes AJ, Guilak F, Arnoczky SP. Tendon mechanobiology: *Current knowledge and future research opportunities: TENDON MECHANOBIOLOGY*. *J Orthop Res*. 2015;33(6):813-822. doi:10.1002/jor.22871
64. Sensini A, Cristofolini L. Biofabrication of Electrospun Scaffolds for the Regeneration of Tendons and Ligaments. *Materials*. 2018;11(10):1963. doi:10.3390/ma11101963
65. Delgado Caceres M, Pfeifer CG, Docheva D. Understanding Tendons: Lessons from Transgenic Mouse Models. *Stem Cells and Development*. 2018;27(17):1161-1174. doi:10.1089/scd.2018.0121
66. Brent A. Developmental regulation of somite derivatives: muscle, cartilage and tendon. *Current Opinion in Genetics & Development*. 2002;12(5):548-557. doi:10.1016/S0959-437X(02)00339-8
67. Brent AE, Schweitzer R, Tabin CJ. A Somitic Compartment of Tendon Progenitors. *Cell*. 2003;113(2):235-248. doi:10.1016/S0092-8674(03)00268-X
68. Cserjesi P, Brown D, Ligon KL, *et al*. Scleraxis: a basic helix-loop-helix protein that prefigures skeletal formation during mouse embryogenesis. *Development*. 1995;121(4):1099-1110.
69. Schweitzer R, Chyung JH, Murtaugh LC, *et al*. Analysis of the tendon cell fate using Scleraxis, a specific marker for tendons and ligaments. *Development*. 2001;128(19):3855-3866.
70. Subramanian A, Schilling TF. Tendon development and musculoskeletal assembly: emerging roles for the extracellular matrix. *Development*. 2015;142(24):4191-4204. doi:10.1242/dev.114777
71. Espira L, Lamoureux L, Jones SC, Gerard RD, Dixon IMC, Czubryt MP. The basic helix-loop-helix transcription factor scleraxis regulates fibroblast collagen synthesis. *Journal of Molecular and Cellular Cardiology*. 2009;47(2):188-195. doi:10.1016/j.yjmcc.2009.03.024
72. Leéjard V, Brideau G, Blais F, *et al*. Scleraxis and NFATc Regulate the Expression of the Pro- α 1(I) Collagen Gene in Tendon Fibroblasts. *Journal of Biological Chemistry*. 2007;282(24):17665-17675. doi:10.1074/jbc.M610113200
73. Nourissat G, Berenbaum F, Duprez D. Tendon injury: from biology to tendon repair. *Nat Rev Rheumatol*. 2015;11(4):223-233. doi:10.1038/nrrheum.2015.26
74. Liu H, Zhu S, Zhang C, *et al*. Crucial transcription factors in tendon development and differentiation: their potential for tendon regeneration. *Cell Tissue Res*. 2014;356(2):287-298. doi:10.1007/s00441-014-1834-8
75. Wu M, Melichian DS, de la Garza M, *et al*. Essential Roles for Early Growth Response Transcription Factor Egr-1 in Tissue Fibrosis and Wound Healing. *The American*

- Journal of Pathology*. 2009;175(3):1041-1055. doi:10.2353/ajpath.2009.090241
76. Guerquin M-J, Charvet B, Nourissat G, *et al.* Transcription factor EGR1 directs tendon differentiation and promotes tendon repair. *J Clin Invest*. 2013;123(8):3564-3576. doi:10.1172/JCI67521
77. Lejard V, Blais F, Guerquin M-J, *et al.* EGR1 and EGR2 Involvement in Vertebrate Tendon Differentiation*. *Journal of Biological Chemistry*. 2011;286(7):5855-5867. doi:10.1074/jbc.M110.153106
78. Liu H, Zhang C, Zhu S, *et al.* Mohawk Promotes the Tenogenesis of Mesenchymal Stem Cells Through Activation of the TGF β Signaling Pathway: Mxk Promotes the Tenogenesis of MSCs. *Stem Cells*. 2015;33(2):443-455. doi:10.1002/stem.1866
79. Berthet E, Chen C, Butcher K, Schneider RA, Alliston T, Amirtharajah M. Smad3 binds scleraxis and mohawk and regulates tendon matrix organization: SMAD3 BINDS SCLERAXIS AND MOHAWK. *J Orthop Res*. 2013;31(9):1475-1483. doi:10.1002/jor.22382
80. Ito Y, Toriuchi N, Yoshitaka T, *et al.* The Mohawk homeobox gene is a critical regulator of tendon differentiation. *Proceedings of the National Academy of Sciences*. 2010;107(23):10538-10542. doi:10.1073/pnas.1000525107
81. Kimura W, Machii M, Xue X, *et al.* Irx11 mutant mice show reduced tendon differentiation and no patterning defects in musculoskeletal system development. *Genesis*. 2011;49(1):2-9. doi:10.1002/dvg.20688
82. Cong XX, Rao XS, Lin JX, *et al.* Activation of AKT-mTOR Signaling Directs Tenogenesis of Mesenchymal Stem Cells: mTOR Regulates Tenogenesis. *Stem Cells*. 2018;36(4):527-539. doi:10.1002/stem.2765
83. Shukunami C, Oshima Y, Hiraki Y. Molecular Cloning of tenomodulin, a Novel Chondromodulin-I Related Gene. *Biochemical and Biophysical Research Communications*. 2001;280(5):1323-1327. doi:10.1006/bbrc.2001.4271
84. Docheva D, Hunziker EB, Fässler R, Brandau O. Tenomodulin Is Necessary for Tenocyte Proliferation and Tendon Maturation. *MCB*. 2005;25(2):699-705. doi:10.1128/MCB.25.2.699-705.2005
85. Alberton P, Dex S, Popov C, Shukunami C, Schieker M, Docheva D. Loss of Tenomodulin Results in Reduced Self-Renewal and Augmented Senescence of Tendon Stem/Progenitor Cells. *Stem Cells and Development*. 2015;24(5):597-609. doi:10.1089/scd.2014.0314
86. Dex S, Alberton P, Willkomm L, *et al.* Tenomodulin is Required for Tendon Endurance Running and Collagen I Fibril Adaptation to Mechanical Load. *EBioMedicine*. 2017;20:240-254. doi:10.1016/j.ebiom.2017.05.003
87. Brandau O, Meindl A, Fässler R, Aszódi A. A novel gene, *tendin*, is strongly expressed in tendons and ligaments and shows high homology with chondromodulin-I: *Tendin* and Chondromodulin-I. *Dev Dyn*. 2001;221(1):72-80. doi:10.1002/dvdy.1126
88. Jelinsky SA, Archambault J, Li L, Seeherman H. Tendon-selective genes identified from rat and human musculoskeletal tissues: TENDON-SELECTIVE TRANSCRIPTS. *J Orthop Res*. 2010;28(3):289-297. doi:10.1002/jor.20999
89. Subramanian A, Schilling TF. Thrombospondin-4 controls matrix assembly during development and repair of myotendinous junctions. *eLife*. 2014;3:e02372. doi:10.7554/eLife.02372
90. Johnson M T. Proteomics of tendinopathy. *Front Biosci*. 2009;Volume(14):1505. doi:10.2741/3321
91. Mackie EJ, Ramsey S. Expression of tenascin in joint-associated tissues during development and postnatal growth. *J Anat*. 1996;188 (Pt 1):157-165.
92. Riley GP, Harrall RL, Cawston TE, Hazleman BL, Mackie EJ. Tenascin-C and human tendon degeneration. *Am J Pathol*. 1996;149(3):933-943.
93. Mehr D, Pardubsky PD, Martin JA, Buckwalter JA. Tenascin-C in tendon regions

- subjected to compression. *J Orthop Res.* 2000;18(4):537-545. doi:10.1002/jor.1100180405
94. Maffulli N, Ewen SWB, Waterston SW, Reaper J, Barrass V. Tenocytes from Ruptured and Tendinopathic Achilles Tendons Produce Greater Quantities of Type III Collagen than Tenocytes from Normal Achilles Tendons: An *in Vitro* Model of Human Tendon Healing. *Am J Sports Med.* 2000;28(4):499-505. doi:10.1177/03635465000280040901
 95. Stålmán A, Bring D, Ackermann PW. Chemokine expression of CCL2, CCL3, CCL5 and CXCL10 during early inflammatory tendon healing precedes nerve regeneration: an immunohistochemical study in the rat. *Knee Surg Sports Traumatol Arthrosc.* 2015;23(9):2682-2689. doi:10.1007/s00167-014-3010-9
 96. Thomopoulos S, Parks WC, Rifkin DB, Derwin KA. Mechanisms of tendon injury and repair: TENDON INJURY AND REPAIR. *J Orthop Res.* 2015;33(6):832-839. doi:10.1002/jor.22806
 97. Müller SA, Todorov A, Heisterbach PE, Martin I, Majewski M. Tendon healing: an overview of physiology, biology, and pathology of tendon healing and systematic review of state of the art in tendon bioengineering. *Knee Surg Sports Traumatol Arthrosc.* 2015;23(7):2097-2105. doi:10.1007/s00167-013-2680-z
 98. Vinhas A, Rodrigues MT, Gomes ME. Exploring Stem Cells and Inflammation in Tendon Repair and Regeneration. In: Turksen K, ed. *Cell Biology and Translational Medicine, Volume 2.* Vol 1089. Advances in Experimental Medicine and Biology. Springer International Publishing; 2018:37-46. doi:10.1007/5584_2018_258
 99. D'Addona A, Maffulli N, Formisano S, Rosa D. Inflammation in tendinopathy. *The Surgeon.* 2017;15(5):297-302. doi:10.1016/j.surge.2017.04.004
 100. Dakin SG, Dudhia J, Smith R KW. Resolving an inflammatory concept: The importance of inflammation and resolution in tendinopathy. *Veterinary Immunology and Immunopathology.* 2014;158(3-4):121-127. doi:10.1016/j.vetimm.2014.01.007
 101. Dean BJF, Dakin SG, Millar NL, Carr AJ. Review: Emerging concepts in the pathogenesis of tendinopathy. *The Surgeon.* 2017;15(6):349-354. doi:10.1016/j.surge.2017.05.005
 102. Rees JD, Stride M, Scott A. Tendons – time to revisit inflammation. *Br J Sports Med.* 2014;48(21):1553-1557. doi:10.1136/bjsports-2012-091957
 103. Millar NL, Murrell GAC, McInnes IB. Inflammatory mechanisms in tendinopathy – towards translation. *Nat Rev Rheumatol.* 2017;13(2):110-122. doi:10.1038/nrrheum.2016.213
 104. Del Buono A, Oliva F, Osti L, Maffulli N. Metalloproteases and tendinopathy. *Muscle Ligaments and Tendons J.* 2019;03(01):51. doi:10.32098/mltj.01.2013.08
 105. Andia I, Sanchez M, Maffulli N. Tendon healing and platelet-rich plasma therapies. *Expert Opinion on Biological Therapy.* 2010;10(10):1415-1426. doi:10.1517/14712598.2010.514603
 106. Tarafder S, Chen E, Jun Y, *et al.* Tendon stem/progenitor cells regulate inflammation in tendon healing via JNK and STAT3 signaling. *FASEB j.* 2017;31(9):3991-3998. doi:10.1096/fj.201700071R
 107. Shen H, Korpakakis I, Havlioglu N, *et al.* The effect of mesenchymal stromal cell sheets on the inflammatory stage of flexor tendon healing. *Stem Cell Res Ther.* 2016;7(1):144. doi:10.1186/s13287-016-0406-0
 108. Ackermann PW, Domeij-Arverud E, Leclerc P, Amoudrouz P, Nader GA. Anti-inflammatory cytokine profile in early human tendon repair. *Knee Surg Sports Traumatol Arthrosc.* 2013;21(8):1801-1806. doi:10.1007/s00167-012-2197-x
 109. Mobasher A, Shakibaei M. Is tendinitis an inflammatory disease initiated and driven by pro-inflammatory cytokines such as interleukin 1 β ? *Histology and Histopathology.* 2013;(28):955-964. doi:10.14670/HH-28.955
 110. da Silva Meirelles L, Fontes AM, Covas DT, Caplan AI. Mechanisms involved in the

- therapeutic properties of mesenchymal stem cells. *Cytokine & Growth Factor Reviews*. 2009;20(5-6):419-427. doi:10.1016/j.cytogfr.2009.10.002
111. Qi F, Deng Z, Ma Y, *et al.* From the perspective of embryonic tendon development: various cells applied to tendon tissue engineering. *Ann Transl Med*. 2020;8(4):131-131. doi:10.21037/atm.2019.12.78
112. Guillot PV, Cui W, Fisk NM, Polak DJ. Stem cell differentiation and expansion for clinical applications of tissue engineering. *Journal of Cellular and Molecular Medicine*. 2007;11(5):935-944. doi:10.1111/j.1582-4934.2007.00106.x
113. Crook JM, Peura TT, Kravets L, *et al.* The Generation of Six Clinical-Grade Human Embryonic Stem Cell Lines. *Cell Stem Cell*. 2007;1(5):490-494. doi:10.1016/j.stem.2007.10.004
114. Chen X, Song X-H, Yin Z, *et al.* Stepwise Differentiation of Human Embryonic Stem Cells Promotes Tendon Regeneration by Secreting Fetal Tendon Matrix and Differentiation Factors. *Stem Cells*. 2009;27(6):1276-1287. doi:10.1002/stem.61
115. Chen X, Yin Z, Chen J, *et al.* Force and scleraxis synergistically promote the commitment of human ES cells derived MSCs to tenocytes. *Sci Rep*. 2012;2(1):977. doi:10.1038/srep00977
116. Chen JL, Yin Z, Shen WL, *et al.* Efficacy of hESC-MSCs in knitted silk-collagen scaffold for tendon tissue engineering and their roles. *Biomaterials*. 2010;31(36):9438-9451. doi:10.1016/j.biomaterials.2010.08.011
117. Takahashi K, Yamanaka S. Induction of Pluripotent Stem Cells from Mouse Embryonic and Adult Fibroblast Cultures by Defined Factors. *Cell*. 2006;126(4):663-676. doi:10.1016/j.cell.2006.07.024
118. Takahashi K, Tanabe K, Ohnuki M, *et al.* Induction of Pluripotent Stem Cells from Adult Human Fibroblasts by Defined Factors. *Cell*. 2007;131(5):861-872. doi:10.1016/j.cell.2007.11.019
119. Bavin EP, Smith O, Baird AEG, Smith LC, Guest DJ. Equine Induced Pluripotent Stem Cells have a Reduced Tendon Differentiation Capacity Compared to Embryonic Stem Cells. *Front Vet Sci*. 2015;2. doi:10.3389/fvets.2015.00055
120. Komura S, Satake T, Goto A, *et al.* Induced pluripotent stem cell-derived tenocyte-like cells promote the regeneration of injured tendons in mice. *Sci Rep*. 2020;10(1):3992. doi:10.1038/s41598-020-61063-6
121. Parolini O, Soncini M, Evangelista M, Schmidt D. Amniotic membrane and amniotic fluid-derived cells: potential tools for regenerative medicine? *Regenerative Medicine*. 2009;4(2):275-291. doi:10.2217/17460751.4.2.275
122. Miki T. Amnion-derived stem cells: in quest of clinical applications. *Stem Cell Res Ther*. 2011;2(3):25. doi:10.1186/scrt66
123. Muttini A, Barboni B, Valbonetti L, Russo V, Maffulli N. Amniotic Epithelial Stem Cells: Salient Features and Possible Therapeutic Role. *Sports Medicine and Arthroscopy Review*. 2018;26(2):70-74. doi:10.1097/JSA.000000000000189
124. Miki T. Stem cell characteristics and the therapeutic potential of amniotic epithelial cells. *Am J Reprod Immunol*. 2018;80(4):e13003. doi:10.1111/aji.13003
125. Parolini O. From fetal development and beyond: A continued role for placenta in sustaining life? *Placenta*. 2011;32:S283-S284. doi:10.1016/j.placenta.2011.04.009
126. Barboni B, Curini V, Russo V, *et al.* Indirect Co-Culture with Tendons or Tenocytes Can Program Amniotic Epithelial Cells towards Stepwise Tenogenic Differentiation. Chin W-C, ed. *PLoS ONE*. 2012;7(2):e30974. doi:10.1371/journal.pone.0030974
127. Russo V, El Khatib M, di Marcantonio L, *et al.* Tendon Biomimetic Electrospun PLGA Fleeces Induce an Early Epithelial-Mesenchymal Transition and Tenogenic Differentiation on Amniotic Epithelial Stem Cells. *Cells*. 2020;9(2):303. doi:10.3390/cells9020303

128. Mohanty N, Gulati BR, Kumar R, *et al.* Immunophenotypic characterization and tenogenic differentiation of mesenchymal stromal cells isolated from equine umbilical cord blood. *In Vitro CellDevBiol-Animal*. 2014;50(6):538-548. doi:10.1007/s11626-013-9729-7
129. da Silva Meirelles L. Mesenchymal stem cells reside in virtually all post-natal organs and tissues. *Journal of Cell Science*. 2006;119(11):2204-2213. doi:10.1242/jcs.02932
130. Govoni M, Berardi AC, Muscari C, *et al.* An Engineered Multiphase Three-Dimensional Microenvironment to Ensure the Controlled Delivery of Cyclic Strain and Human Growth Differentiation Factor 5 for the Tenogenic Commitment of Human Bone Marrow Mesenchymal Stem Cells. *Tissue Engineering Part A*. 2017;23(15-16):811-822. doi:10.1089/ten.tea.2016.0407
131. Tan S-L, Ahmad RE, Ahmad TS, *et al.* Effect of Growth Differentiation Factor 5 on the Proliferation and Tenogenic Differentiation Potential of Human Mesenchymal Stem Cells *in vitro*. *Cells Tissues Organs*. 2012;196(4):325-338. doi:10.1159/000335693
132. Wang Q-W, Chen Z-L, Piao Y-J. Mesenchymal stem cells differentiate into tenocytes by bone morphogenetic protein (BMP) 12 gene transfer. *Journal of Bioscience and Bioengineering*. 2005;100(4):418-422. doi:10.1263/jbb.100.418
133. Dai L, Hu X, Zhang X, *et al.* Different tenogenic differentiation capacities of different mesenchymal stem cells in the presence of BMP-12. *J Transl Med*. 2015;13(1):200. doi:10.1186/s12967-015-0560-7
134. Harris MT, Butler DL, Boivin GP, Florer JB, Schantz EJ, Wenstrup RJ. Mesenchymal stem cells used for rabbit tendon repair can form ectopic bone and express alkaline phosphatase activity in constructs. *J Orthop Res*. 2004;22(5):998-1003. doi:10.1016/j.orthres.2004.02.012
135. Zarychta-Wisniewska W, Burdzinska A, Kulesza A, *et al.* Bmp-12 activates tenogenic pathway in human adipose stem cells and affects their immunomodulatory and secretory properties. *BMC Cell Biol*. 2017;18(1):13. doi:10.1186/s12860-017-0129-9
136. Park A, Hogan MV, Kesturu GS, James R, Balian G, Chhabra AB. Adipose-Derived Mesenchymal Stem Cells Treated with Growth Differentiation Factor-5 Express Tendon-Specific Markers. *Tissue Engineering Part A*. 2010;16(9):2941-2951. doi:10.1089/ten.tea.2009.0710
137. Haramshahi SMA, Bonakdar S, Moghtadaei M, *et al.* Tenocyte-imprinted substrate: a topography-based inducer for tenogenic differentiation in adipose tissue-derived mesenchymal stem cells. *Biomed Mater*. 2020;15(3):035014. doi:10.1088/1748-605X/ab6709
138. Sheyn D, Mizrahi O, Benjamin S, Gazit Z, Pelled G, Gazit D. Genetically modified cells in regenerative medicine and tissue engineering☆. *Advanced Drug Delivery Reviews*. 2010;62(7-8):683-698. doi:10.1016/j.addr.2010.01.002
139. Ni M, Rui YF, Tan Q, *et al.* Engineered scaffold-free tendon tissue produced by tendon-derived stem cells. *Biomaterials*. 2013;34(8):2024-2037. doi:10.1016/j.biomaterials.2012.11.046
140. Guo J, Chan K-M, Zhang J-F, Li G. Tendon-derived stem cells undergo spontaneous tenogenic differentiation. *Experimental Cell Research*. 2016;341(1):1-7. doi:10.1016/j.yexcr.2016.01.007
141. Mazzocca AD, Chowanec D, McCarthy MB, *et al.* *In vitro* changes in human tenocyte cultures obtained from proximal biceps tendon: multiple passages result in changes in routine cell markers. *Knee Surg Sports Traumatol Arthrosc*. 2012;20(9):1666-1672. doi:10.1007/s00167-011-1711-x
142. Yao L, Bestwick CS, Bestwick LA, Maffulli N, Aspden RM. Phenotypic Drift in Human Tenocyte Culture. *Tissue Engineering*. 2006;12(7):1843-1849. doi:10.1089/ten.2006.12.1843
143. Maffulli N. *Rotator Cuff Tear*. Karger; 2012. Accessed February 2, 2021. <http://site.ebrary.com/id/10568693>

144. Liu Y, Suen C-W, Zhang J, Li G. Current concepts on tenogenic differentiation and clinical applications. *Journal of Orthopaedic Translation*. 2017;9:28-42. doi:10.1016/j.jot.2017.02.005
145. Yan Z, Yin H, Nerlich M, Pfeifer CG, Docheva D. Boosting tendon repair: interplay of cells, growth factors and scaffold-free and gel-based carriers. *J EXP ORTOP*. 2018;5(1):1. doi:10.1186/s40634-017-0117-1
146. Schneider M, Angele P, Järvinen TAH, Docheva D. Rescue plan for Achilles: Therapeutics steering the fate and functions of stem cells in tendon wound healing. *Advanced Drug Delivery Reviews*. 2018;129:352-375. doi:10.1016/j.addr.2017.12.016
147. Sharma P, Maffulli N. Biology of tendon injury: healing, modeling and remodeling. *J Musculoskelet Neuronal Interact*. 2006;6(2):181-190.
148. James R, Kesturu G, Balian G, Chhabra AB. Tendon: Biology, Biomechanics, Repair, Growth Factors, and Evolving Treatment Options. *The Journal of Hand Surgery*. 2008;33(1):102-112. doi:10.1016/j.jhsa.2007.09.007
149. Havis E, Bonnin M-A, Olivera-Martinez I, et al. Transcriptomic analysis of mouse limb tendon cells during development. *Development*. 2014;141(19):3683-3696. doi:10.1242/dev.108654
150. Zhang Y-J, Chen X, Li G, et al. Concise Review: Stem Cell Fate Guided By Bioactive Molecules for Tendon Regeneration: Guided Stem Cell Fate for Tendon Regeneration. *STEM CELLS Translational Medicine*. 2018;7(5):404-414. doi:10.1002/sctm.17-0206
151. Gaut L, Duprez D. Tendon development and diseases: Tendon development and diseases. *WIREs Dev Biol*. 2016;5(1):5-23. doi:10.1002/wdev.201
152. Jones ER, Jones GC, Legerlotz K, Riley GP. Corrigendum to “Cyclical strain modulates metalloprotease and matrix gene expression in human tenocytes via activation of TGFβ” [Biochim. Biophys. Acta (2013) 2596–2607]. *Biochimica et Biophysica Acta (BBA) - Molecular Cell Research*. 2013;1833(12):3445-3446. doi:10.1016/j.bbamcr.2013.08.007
153. Dale TP, Mazher S, Webb WR, et al. Tenogenic Differentiation of Human Embryonic Stem Cells. *Tissue Engineering Part A*. 2018;24(5-6):361-368. doi:10.1089/ten.tea.2017.0017
154. Lee CH, Lee FY, Tarafder S, et al. Harnessing endogenous stem/progenitor cells for tendon regeneration. *J Clin Invest*. 2015;125(7):2690-2701. doi:10.1172/JCI81589
155. Lee JY, Zhou Z, Taub PJ, et al. BMP-12 Treatment of Adult Mesenchymal Stem Cells *In Vitro* Augments Tendon-Like Tissue Formation and Defect Repair *In Vivo*. Agarwal S, ed. *PLoS ONE*. 2011;6(3):e17531. doi:10.1371/journal.pone.0017531
156. Chai W, Ni M, Rui Y, et al. Effect of growth and differentiation factor 6 on the tenogenic differentiation of bone marrow-derived mesenchymal stem cells. *Chin Med J (Engl)*. 2013;126(8):1509-1516.
157. Violini S, Ramelli P, Pisani LF, Gorni C, Mariani P. Horse bone marrow mesenchymal stem cells express embryo stem cell markers and show the ability for tenogenic differentiation by *in vitro* exposure to BMP-12. *BMC Cell Biol*. 2009;10(1):29. doi:10.1186/1471-2121-10-29
158. Jiang D, Gao P, Zhang Y, Yang S. Combined effects of engineered tendon matrix and GDF-6 on bone marrow mesenchymal stem cell-based tendon regeneration. *Biotechnol Lett*. 2016;38(5):885-892. doi:10.1007/s10529-016-2037-z
159. Ozasa Y, Gingery A, Thoreson AR, An K-N, Zhao C, Amadio PC. A Comparative Study of the Effects of Growth and Differentiation Factor 5 on Muscle-Derived Stem Cells and Bone Marrow Stromal Cells in an *In Vitro* Tendon Healing Model. *The Journal of Hand Surgery*. 2014;39(9):1706-1713. doi:10.1016/j.jhsa.2014.05.005
160. Holladay C, Abbah S-A, O’Dowd C, Pandit A, Zeugolis DI. Preferential tendon stem cell response to growth factor supplementation: Growth factor supplementation of tendon stem cell culture. *J Tissue Eng Regen Med*. 2016;10(9):783-798. doi:10.1002/term.1852
161. Berasi SP, Varadarajan U, Archambault J, et al. Divergent activities of osteogenic

- BMP2, and tenogenic BMP12 and BMP13 independent of receptor binding affinities. *Growth Factors*. 2011;29(4):128-139. doi:10.3109/08977194.2011.593178
162. Shen H, Gelberman RH, Silva MJ, Sakiyama-Elbert SE, Thomopoulos S. BMP12 induces tenogenic differentiation of adipose-derived stromal cells. Awad HA, ed. *PLoS ONE*. 2013;8(10):e77613. doi:10.1371/journal.pone.0077613
163. Tan S-L, Ahmad TS, Ng W-M, *et al.* Identification of Pathways Mediating Growth Differentiation Factor5-Induced Tenogenic Differentiation in Human Bone Marrow Stromal Cells. Nurminsky DI, ed. *PLoS ONE*. 2015;10(11):e0140869. doi:10.1371/journal.pone.0140869
164. Chen J, Xu J, Wang A, Zheng M. Scaffolds for tendon and ligament repair: review of the efficacy of commercial products. *Expert Review of Medical Devices*. 2009;6(1):61-73. doi:10.1586/17434440.6.1.61
165. Moshiri A, Oryan A. Role of tissue engineering in tendon reconstructive surgery and regenerative medicine: Current concepts, approaches and concerns. *Hard Tissue*. 2012;1(2). doi:10.13172/2050-2303-1-2-291
166. Longo UG, Lamberti A, Petrillo S, Maffulli N, Denaro V. Scaffolds in Tendon Tissue Engineering. *Stem Cells International*. 2012;2012:1-8. doi:10.1155/2012/517165
167. Kishore V, Bullock W, Sun X, Van Dyke WS, Akkus O. Tenogenic differentiation of human MSCs induced by the topography of electrochemically aligned collagen threads. *Biomaterials*. 2012;33(7):2137-2144. doi:10.1016/j.biomaterials.2011.11.066
168. Alshomer F, Chaves C, Kalaskar DM. Advances in Tendon and Ligament Tissue Engineering: Materials Perspective. *Journal of Materials*. 2018;2018:1-17. doi:10.1155/2018/9868151
169. Dong C, Lv Y. Application of Collagen Scaffold in Tissue Engineering: Recent Advances and New Perspectives. *Polymers*. 2016;8(2):42. doi:10.3390/polym8020042
170. Zhi Y, Liu W, Zhang P, Jiang J, Chen S. Electrospun silk fibroin mat enhances tendon-bone healing in a rabbit extra-articular model. *Biotechnol Lett*. 2016;38(10):1827-1835. doi:10.1007/s10529-016-2158-4
171. Kwon S-Y, Chung J-W, Park H-J, Jiang Y-Y, Park J-K, Seo Y-K. Silk and collagen scaffolds for tendon reconstruction. *Proc Inst Mech Eng H*. 2014;228(4):388-396. doi:10.1177/0954411914528890
172. Seo Y-K, Kim J-H, Eo S-R. Co-effect of silk and amniotic membrane for tendon repair. *Journal of Biomaterials Science, Polymer Edition*. 2016;27(12):1232-1247. doi:10.1080/09205063.2016.1188349
173. Maghdouri-White Y, Petrova S, Sori N, *et al.* Electrospun silk–collagen scaffolds and BMP-13 for ligament and tendon repair and regeneration. *Biomed Phys Eng Express*. 2018;4(2):025013. doi:10.1088/2057-1976/aa9c6f
174. Sahoo S, Toh SL, Goh JCH. A bFGF-releasing silk/PLGA-based biohybrid scaffold for ligament/tendon tissue engineering using mesenchymal progenitor cells. *Biomaterials*. 2010;31(11):2990-2998. doi:10.1016/j.biomaterials.2010.01.004
175. Chen E, Yang L, Ye C, *et al.* An asymmetric chitosan scaffold for tendon tissue engineering: *In vitro* and *in vivo* evaluation with rat tendon stem/progenitor cells. *Acta Biomaterialia*. 2018;73:377-387. doi:10.1016/j.actbio.2018.04.027
176. Rodríguez-Vázquez M, Vega-Ruiz B, Ramos-Zúñiga R, Saldaña-Koppel DA, Quiñones-Olvera LF. Chitosan and Its Potential Use as a Scaffold for Tissue Engineering in Regenerative Medicine. *BioMed Research International*. 2015;2015:1-15. doi:10.1155/2015/821279
177. Leung M, Jana S, Tsao C-T, Zhang M. Tenogenic differentiation of human bone marrow stem cells via a combinatory effect of aligned chitosan–poly-caprolactone nanofibers and TGF- β 3. *J Mater Chem B*. 2013;1(47):6516. doi:10.1039/c3tb20825g
178. Beldjilali-Labro M, Garcia Garcia A, Farhat F, *et al.* Biomaterials in Tendon and

- Skeletal Muscle Tissue Engineering: Current Trends and Challenges. *Materials*. 2018;11(7):1116. doi:10.3390/ma11071116
179. Lee EJ, Kasper FK, Mikos AG. Biomaterials for Tissue Engineering. *Ann Biomed Eng*. 2014;42(2):323-337. doi:10.1007/s10439-013-0859-6
180. Lim WL, Liau LL, Ng MH, Chowdhury SR, Law JX. Current Progress in Tendon and Ligament Tissue Engineering. *Tissue Eng Regen Med*. 2019;16(6):549-571. doi:10.1007/s13770-019-00196-w
181. Shearn JT, Kinneberg KR, Dymont NA, *et al*. Tendon tissue engineering: progress, challenges, and translation to the clinic. *J Musculoskelet Neuronal Interact*. 2011;11(2):163-173.
182. El Khatib M, Mauro A, Wyrwa R, *et al*. Fabrication and Plasma Surface Activation of Aligned Electrospun PLGA Fiber Fleeces with Improved Adhesion and Infiltration of Amniotic Epithelial Stem Cells Maintaining their Teno-inductive Potential. *Molecules*. 2020;25(14):3176. doi:10.3390/molecules25143176
183. El Khatib M, Mauro A, Di Mattia M, *et al*. Electrospun PLGA Fiber Diameter and Alignment of Tendon Biomimetic Fleece Potentiate Tenogenic Differentiation and Immunomodulatory Function of Amniotic Epithelial Stem Cells. *Cells*. 2020;9(5):1207. doi:10.3390/cells9051207
184. Bashur CA, Shaffer RD, Dahlgren LA, Guelcher SA, Goldstein AS. Effect of Fiber Diameter and Alignment of Electrospun Polyurethane Meshes on Mesenchymal Progenitor Cells. *Tissue Engineering Part A*. 2009;15(9):2435-2445. doi:10.1089/ten.tea.2008.0295
185. Cardwell RD, Dahlgren LA, Goldstein AS. Electrospun fibre diameter, not alignment, affects mesenchymal stem cell differentiation into the tendon/ligament lineage: Ligament differentiation of C3H10T1/2 cells is enhanced on larger fibres. *J Tissue Eng Regen Med*. 2014;8(12):937-945. doi:10.1002/term.1589
186. Lee CH, Shin HJ, Cho IH, *et al*. Nanofiber alignment and direction of mechanical strain affect the ECM production of human ACL fibroblast. *Biomaterials*. 2005;26(11):1261-1270. doi:10.1016/j.biomaterials.2004.04.037
187. Zhang C, Wang X, Zhang E, *et al*. An epigenetic bioactive composite scaffold with well-aligned nanofibers for functional tendon tissue engineering. *Acta Biomaterialia*. 2018;66:141-156. doi:10.1016/j.actbio.2017.09.036
188. Nitti P, Gallo N, Natta L, *et al*. Influence of Nanofiber Orientation on Morphological and Mechanical Properties of Electrospun Chitosan Mats. *Journal of Healthcare Engineering*. 2018;2018:1-12. doi:10.1155/2018/3651480
189. Zhang C, Yuan H, Liu H, *et al*. Well-aligned chitosan-based ultrafine fibers committed teno-lineage differentiation of human induced pluripotent stem cells for Achilles tendon regeneration. *Biomaterials*. 2015;53:716-730. doi:10.1016/j.biomaterials.2015.02.051
190. Lavik E, Langer R. Tissue engineering: current state and perspectives. *Appl Microbiol Biotechnol*. 2004;65(1). doi:10.1007/s00253-004-1580-z
191. Rosso F, Marino G, Giordano A, Barbarisi M, Parmeggiani D, Barbarisi A. Smart materials as scaffolds for tissue engineering. *J Cell Physiol*. 2005;203(3):465-470. doi:10.1002/jcp.20270
192. Ahmed TAE, Dare EV, Hincke M. Fibrin: A Versatile Scaffold for Tissue Engineering Applications. *Tissue Engineering Part B: Reviews*. 2008;14(2):199-215. doi:10.1089/ten.teb.2007.0435
193. Jockenhoevel S, Zund G, Hoerstrup SP, *et al*. Fibrin gel -- advantages of a new scaffold in cardiovascular tissue engineering. *Eur J Cardiothorac Surg*. 2001;19(4):424-430. doi:10.1016/s1010-7940(01)00624-8
194. Ahmed TAE, Griffith M, Hincke M. Characterization and inhibition of fibrin hydrogel-degrading enzymes during development of tissue engineering scaffolds. *Tissue Eng*. 2007;13(7):1469-1477. doi:10.1089/ten.2006.0354

195. Mosesson MW. Fibrinogen and fibrin structure and functions. *J Thromb Haemost.* 2005;3(8):1894-1904. doi:10.1111/j.1538-7836.2005.01365.x
196. Mosesson MW, Siebenlist KR, Meh DA. The Structure and Biological Features of Fibrinogen and Fibrin. *Annals of the New York Academy of Sciences.* 2006;936(1):11-30. doi:10.1111/j.1749-6632.2001.tb03491.x
197. Horan JT, Francis CW. Fibrin Degradation Products, Fibrin Monomer and Soluble Fibrin in Disseminated Intravascular Coagulation. *Semin Thromb Hemost.* 2001;27(06):657-666. doi:10.1055/s-2001-18870
198. Schense JC, Hubbell JA. Cross-Linking Exogenous Bifunctional Peptides into Fibrin Gels with Factor XIIIa. *Bioconjugate Chem.* 1999;10(1):75-81. doi:10.1021/bc9800769
199. Smith JD, Chen A, Ernst LA, Waggoner AS, Campbell PG. Immobilization of Aprotinin to Fibrinogen as a Novel Method for Controlling Degradation of Fibrin Gels. *Bioconjugate Chem.* 2007;18(3):695-701. doi:10.1021/bc060265o
200. Baner AJ, Tsuzaki M, Yamamoto J, *et al.* Mechanoreception at the cellular level: the detection, interpretation, and diversity of responses to mechanical signals. *Biochem Cell Biol.* 1995;73(7-8):349-365. doi:10.1139/o95-043
201. Lavagnino M, Arnoczky SP, Tian T, Vaupel Z. Effect of Amplitude and Frequency of Cyclic Tensile Strain on the Inhibition of MMP-1 mRNA Expression in Tendon Cells: An *In Vitro* Study. *Connective Tissue Research.* 2003;44(3-4):181-187. doi:10.1080/03008200390215881
202. Screen HRC, Shelton JC, Bader DL, Lee DA. Cyclic tensile strain upregulates collagen synthesis in isolated tendon fascicles. *Biochemical and Biophysical Research Communications.* 2005;336(2):424-429. doi:10.1016/j.bbrc.2005.08.102
203. Govoni M, Muscari C, Lovecchio J, Guarnieri C, Giordano E. Mechanical Actuation Systems for the Phenotype Commitment of Stem Cell-Based Tendon and Ligament Tissue Substitutes. *Stem Cell Rev and Rep.* 2016;12(2):189-201. doi:10.1007/s12015-015-9640-6
204. Hannafin JA, Arnoczky SP, Hoonjan A, Torzilli PA. Effect of stress deprivation and cyclic tensile loading on the material and morphologic properties of canine flexor digitorum profundus tendon: An *in vitro* study. *J Orthop Res.* 1995;13(6):907-914. doi:10.1002/jor.1100130615
205. Archambault JM, Wiley JP, Bray RC. Exercise Loading of Tendons and the Development of Overuse Injuries: A Review of Current Literature. *Sports Medicine.* 1995;20(2):77-89. doi:10.2165/00007256-199520020-00003
206. Arnoczky SP, Lavagnino M, Egerbacher M. The mechanobiological aetiopathogenesis of tendinopathy: is it the over-stimulation or the under-stimulation of tendon cells?: *Mechanobiological aetiology of tendinopathy. International Journal of Experimental Pathology.* 2007;88(4):217-226. doi:10.1111/j.1365-2613.2007.00548.x
207. Magnusson SP, Langberg H, Kjaer M. The pathogenesis of tendinopathy: balancing the response to loading. *Nat Rev Rheumatol.* 2010;6(5):262-268. doi:10.1038/nrrheum.2010.43
208. Wang T, Gardiner BS, Lin Z, *et al.* Bioreactor Design for Tendon/Ligament Engineering. *Tissue Engineering Part B: Reviews.* 2013;19(2):133-146. doi:10.1089/ten.teb.2012.0295
209. Gonçalves AI, Rodrigues MT, Gomes ME. Tissue-engineered magnetic cell sheet patches for advanced strategies in tendon regeneration. *Acta Biomaterialia.* 2017;63:110-122. doi:10.1016/j.actbio.2017.09.014
210. Rinella L, Marano F, Paletto L, *et al.* Extracorporeal shock waves trigger tenogenic differentiation of human adipose-derived stem cells. *Connective Tissue Research.* 2018;59(6):561-573. doi:10.1080/03008207.2018.1424147
211. Abousleiman RI, Reyes Y, McFetridge P, Sikavitsas V. Tendon Tissue Engineering Using Cell-Seeded Umbilical Veins Cultured in a Mechanical Stimulator. *Tissue Engineering*

- Part A. 2009;15(4):787-795. doi:10.1089/ten.tea.2008.0102
212. Webb K, Hitchcock RW, Smeal RM, Li W, Gray SD, Tresco PA. Cyclic strain increases fibroblast proliferation, matrix accumulation, and elastic modulus of fibroblast-seeded polyurethane constructs. *Journal of Biomechanics*. 2006;39(6):1136-1144. doi:10.1016/j.jbiomech.2004.08.026
213. Cribb AM, Scott JE. Tendon response to tensile stress: an ultrastructural investigation of collagen:proteoglycan interactions in stressed tendon. *J Anat*. 1995;187 (Pt 2):423-428.
214. Juncosa-Melvin N, Shearn JT, Boivin GP, *et al*. Effects of Mechanical Stimulation on the Biomechanics and Histology of Stem Cell–Collagen Sponge Constructs for Rabbit Patellar Tendon Repair. *Tissue Engineering*. 2006;12(8):2291-2300. doi:10.1089/ten.2006.12.2291
215. Woon CYL, Kraus A, Raghavan SS, *et al*. Three-Dimensional-Construct Bioreactor Conditioning in Human Tendon Tissue Engineering. *Tissue Engineering Part A*. 2011;17(19-20):2561-2572. doi:10.1089/ten.tea.2010.0701
216. Saber S, Zhang AY, Ki SH, *et al*. Flexor Tendon Tissue Engineering: Bioreactor Cyclic Strain Increases Construct Strength. *Tissue Engineering Part A*. 2010;16(6):2085-2090. doi:10.1089/ten.tea.2010.0032
217. Butler DL, Hunter SA, Chokalingam K, *et al*. Using Functional Tissue Engineering and Bioreactors to Mechanically Stimulate Tissue-Engineered Constructs. *Tissue Engineering Part A*. 2009;15(4):741-749. doi:10.1089/ten.tea.2008.0292
218. Alberton P, Popov C, Prägert M, *et al*. Conversion of Human Bone Marrow-Derived Mesenchymal Stem Cells into Tendon Progenitor Cells by Ectopic Expression of Scleraxis. *Stem Cells and Development*. 2012;21(6):846-858. doi:10.1089/scd.2011.0150
219. Bagchi RA, Roche P, Aroutiounova N, *et al*. The transcription factor scleraxis is a critical regulator of cardiac fibroblast phenotype. *BMC Biol*. 2016;14(1):21. doi:10.1186/s12915-016-0243-8
220. Scott A, Danielson P, Abraham T, Fong G, Sampaio AV, Underhill TM. Mechanical force modulates scleraxis expression in bioartificial tendons. *J Musculoskelet Neuronal Interact*. 2011;11(2):124-132.
221. Doroski DM, Levenston ME, Temenoff JS. Cyclic Tensile Culture Promotes Fibroblastic Differentiation of Marrow Stromal Cells Encapsulated in Poly(Ethylene Glycol)-Based Hydrogels. *Tissue Engineering Part A*. 2010;16(11):3457-3466. doi:10.1089/ten.tea.2010.0233
222. Burk J, Plenge A, Brehm W, Heller S, Pfeiffer B, Kasper C. Induction of Tenogenic Differentiation Mediated by Extracellular Tendon Matrix and Short-Term Cyclic Stretching. *Stem Cells International*. 2016;2016:1-11. doi:10.1155/2016/7342379
223. Department of Orthopaedics, Dongguk University Ilsan Hospital, 814 Siksa-Dong, Goyang, 410-773, Republic of Korea, Im G-I. Clinical use of stem cells in orthopaedics. *eCM*. 2017;33:183-196. doi:10.22203/eCM.v033a14
224. Deniz P, Guler S, Çelik E, Hosseinian P, Aydin HM. Use of cyclic strain bioreactor for the upregulation of key tenocyte gene expression on Poly(glycerol-sebacate) (PGS) sheets. *Materials Science and Engineering: C*. 2020;106:110293. doi:10.1016/j.msec.2019.110293
225. Nam HY, Pingguan-Murphy B, Abbas AA, Merican AM, Kamarul T. Uniaxial Cyclic Tensile Stretching at 8% Strain Exclusively Promotes Tenogenic Differentiation of Human Bone Marrow-Derived Mesenchymal Stromal Cells. *Stem Cells International*. 2019;2019:1-16. doi:10.1155/2019/9723025
226. Cao D, Liu W, Wei X, Xu F, Cui L, Cao Y. *In Vitro* Tendon Engineering with Avian Tenocytes and Polyglycolic Acids: A Preliminary Report. *Tissue Engineering*. 2006;12(5):1369-1377. doi:10.1089/ten.2006.12.1369
227. Barkhausen T, van Griensven M, Zeichen J, Bosch U. Modulation of cell functions of human tendon fibroblasts by different repetitive cyclic mechanical stress patterns.

Experimental and Toxicologic Pathology. 2003;55(2-3):153-158. doi:10.1078/0940-2993-00302

228. Chen JL, Zhang W, Liu ZY, Heng BC, Ouyang HW, Dai XS. Physical regulation of stem cells differentiation into teno-lineage: current strategies and future direction. *Cell Tissue Res*. 2015;360(2):195-207. doi:10.1007/s00441-014-2077-4

229. Testa S, Costantini M, Fornetti E, *et al.* Combination of biochemical and mechanical cues for tendon tissue engineering. *J Cell Mol Med*. 2017;21(11):2711-2719. doi:10.1111/jcmm.13186

230. Rinoldi C, Fallahi A, Yazdi IK, *et al.* Mechanical and Biochemical Stimulation of 3D Multilayered Scaffolds for Tendon Tissue Engineering. *ACS Biomater Sci Eng*. 2019;5(6):2953-2964. doi:10.1021/acsbomaterials.8b01647

231. Dakin SG, Dudhia J, Smith RKW. Science in brief: Resolving tendon inflammation. A new perspective: Resolving tendon inflammation. *Equine Vet J*. 2013;45(4):398-400. doi:10.1111/evj.12030

232. Gaspar D, Spanoudes K, Holladay C, Pandit A, Zeugolis D. Progress in cell-based therapies for tendon repair. *Advanced Drug Delivery Reviews*. 2015;84:240-256. doi:10.1016/j.addr.2014.11.023

233. Veronesi F, Salamanna F, Tschon M, Maglio M, Nicoli Aldini N, Fini M. Mesenchymal stem cells for tendon healing: what is on the horizon?: Mesenchymal stem cells in acute and chronic tendon injuries. *J Tissue Eng Regen Med*. 2017;11(11):3202-3219. doi:10.1002/term.2209

234. Caplan AI, Bruder SP. Mesenchymal stem cells: building blocks for molecular medicine in the 21st century. *Trends in Molecular Medicine*. 2001;7(6):259-264. doi:10.1016/S1471-4914(01)02016-0

235. Baksh D, Yao R, Tuan RS. Comparison of Proliferative and Multilineage Differentiation Potential of Human Mesenchymal Stem Cells Derived from Umbilical Cord and Bone Marrow. *Stem Cells*. 2007;25(6):1384-1392. doi:10.1634/stemcells.2006-0709

236. Wang H-S, Hung S-C, Peng S-T, *et al.* Mesenchymal Stem Cells in the Wharton's Jelly of the Human Umbilical Cord. *Stem Cells*. 2004;22(7):1330-1337. doi:10.1634/stemcells.2004-0013

237. Marino L, Castaldi MA, Rosamilio R, *et al.* Mesenchymal Stem Cells from the Wharton's Jelly of the Human Umbilical Cord: Biological Properties and Therapeutic Potential. *IJSC*. 2019;12(2):218-226. doi:10.15283/ijsc18034

238. Ding D-C, Chang Y-H, Shyu W-C, Lin S-Z. Human Umbilical Cord Mesenchymal Stem Cells: A New Era for Stem Cell Therapy. *Cell Transplant*. 2015;24(3):339-347. doi:10.3727/096368915X686841

239. Fong C-Y, Chak L-L, Biswas A, *et al.* Human Wharton's Jelly Stem Cells Have Unique Transcriptome Profiles Compared to Human Embryonic Stem Cells and Other Mesenchymal Stem Cells. *Stem Cell Rev and Rep*. 2011;7(1):1-16. doi:10.1007/s12015-010-9166-x

240. Karahuseyinoglu S, Cinar O, Kilic E, *et al.* Biology of Stem Cells in Human Umbilical Cord Stroma: In Situ and *In Vitro* Surveys. *Stem Cells*. 2007;25(2):319-331. doi:10.1634/stemcells.2006-0286

241. Yea J-H, Bae TS, Kim BJ, Cho YW, Jo CH. Regeneration of the rotator cuff tendon-to-bone interface using umbilical cord-derived mesenchymal stem cells and gradient extracellular matrix scaffolds from adipose tissue in a rat model. *Acta Biomaterialia*. 2020;114:104-116. doi:10.1016/j.actbio.2020.07.020

242. Rak Kwon D, Jung S, Jang J, Park G-Y, Suk Moon Y, Lee SC. A 3-Dimensional Bioprinted Scaffold With Human Umbilical Cord Blood-Mesenchymal Stem Cells Improves Regeneration of Chronic Full-Thickness Rotator Cuff Tear in a Rabbit Model. *Am J Sports Med*. 2020;48(4):947-958. doi:10.1177/0363546520904022

243. Gonçalves AI, Rodrigues MT, Lee S-J, *et al.* Understanding the Role of Growth Factors in Modulating Stem Cell Tenogenesis. Neves NM, ed. *PLoS ONE*. 2013;8(12):e83734. doi:10.1371/journal.pone.0083734
244. Chang SC, Hoang B, Thomas JT, *et al.* Cartilage-derived morphogenetic proteins. New members of the transforming growth factor-beta superfamily predominantly expressed in long bones during human embryonic development. *J Biol Chem*. 1994;269(45):28227-28234.
245. Zhou S, Yates KE, Eid K, Glowacki J. Demineralized bone promotes chondrocyte or osteoblast differentiation of human marrow stromal cells cultured in collagen sponges. *Cell Tissue Banking*. 2005;6(1):33-44. doi:10.1007/s10561-005-4253-y
246. Wolfman NM, Hattersley G, Cox K, *et al.* Ectopic induction of tendon and ligament in rats by growth and differentiation factors 5, 6, and 7, members of the TGF-beta gene family. *J Clin Invest*. 1997;100(2):321-330. doi:10.1172/JCI119537
247. Forslund C, Rueger D, Aspenberg P. A comparative dose-response study of cartilage-derived morphogenetic protein (CDMP)-1, -2 and -3 for tendon healing in rats. *J Orthop Res*. 2003;21(4):617-621. doi:10.1016/S0736-0266(03)00010-X
248. Keller TC, Hogan MV, Kesturu G, James R, Balian G, Chhabra AB. Growth/differentiation factor-5 modulates the synthesis and expression of extracellular matrix and cell-adhesion-related molecules of rat Achilles tendon fibroblasts. *Connective Tissue Research*. 2011;52(4):353-364. doi:10.3109/03008207.2010.534208
249. Hogan M, Girish K, James R, Balian G, Hurwitz S, Chhabra AB. Growth differentiation factor-5 regulation of extracellular matrix gene expression in murine tendon fibroblasts. *J Tissue Eng Regen Med*. 2011;5(3):191-200. doi:10.1002/term.304
250. Wang D, Jiang X, Lu A, Tu M, Huang W, Huang P. BMP14 induces tenogenic differentiation of bone marrow mesenchymal stem cells in vitro. *Exp Ther Med*. Published online June 12, 2018. doi:10.3892/etm.2018.6293
251. Bottagisio M, Lopa S, Granata V, *et al.* Different combinations of growth factors for the tenogenic differentiation of bone marrow mesenchymal stem cells in monolayer culture and in fibrin-based three-dimensional constructs. *Differentiation*. 2017;95:44-53. doi:10.1016/j.diff.2017.03.001
252. Sugg KB, Lubardic J, Gumucio JP, Mendias CL. Changes in macrophage phenotype and induction of epithelial-to-mesenchymal transition genes following acute Achilles tenotomy and repair: TENDON MACROPHAGE PHENOTYPE AND EMT. *J Orthop Res*. 2014;32(7):944-951. doi:10.1002/jor.22624
253. Gao F, Chiu SM, Motan DAL, *et al.* Mesenchymal stem cells and immunomodulation: current status and future prospects. *Cell Death Dis*. 2016;7(1):e2062-e2062. doi:10.1038/cddis.2015.327
254. Kim D, Yoo K, Choi K, *et al.* Gene expression profile of cytokine and growth factor during differentiation of bone marrow-derived mesenchymal stem cell. *Cytokine*. 2005;31(2):119-126. doi:10.1016/j.cyto.2005.04.004
255. Gruber HE, Hoelscher GL, Ingram JA, Bethea S, Hanley EN. Growth and differentiation factor-5 (GDF-5) in the human intervertebral annulus cells and its modulation by IL-1 β and TNF- α *in vitro*. *Experimental and Molecular Pathology*. 2014;96(2):225-229. doi:10.1016/j.yexmp.2014.02.005
256. Bustin SA, Benes V, Garson JA, *et al.* The MIQE Guidelines: Minimum Information for Publication of Quantitative Real-Time PCR Experiments. *Clinical Chemistry*. 2009;55(4):611-622. doi:10.1373/clinchem.2008.112797
257. Hellemans J, Mortier G, De Paepe A, Speleman F, Vandesompele J. qBase relative quantification framework and software for management and automated analysis of real-time quantitative PCR data. *Genome Biol*. 2007;8(2):R19. doi:10.1186/gb-2007-8-2-r19
258. Mabuchi Y, Houlihan DD, Akazawa C, Okano H, Matsuzaki Y. Prospective Isolation of Murine and Human Bone Marrow Mesenchymal Stem Cells Based on Surface Markers.

- Stem Cells International*. 2013;2013:1-7. doi:10.1155/2013/507301
259. Donders R, Bogie JFJ, Ravanidis S, *et al*. Human Wharton's Jelly-Derived Stem Cells Display a Distinct Immunomodulatory and Proregenerative Transcriptional Signature Compared to Bone Marrow-Derived Stem Cells. *Stem Cells and Development*. 2018;27(2):65-84. doi:10.1089/scd.2017.0029
260. Liu L, Michowski W, Kolodziejczyk A, Sicinski P. The cell cycle in stem cell proliferation, pluripotency and differentiation. *Nat Cell Biol*. 2019;21(9):1060-1067. doi:10.1038/s41556-019-0384-4
261. Pajala A, Melkko J, Leppilahti J, Ohtonen P, Soini Y, Risteli J. Tenascin-C and type I and III collagen expression in total Achilles tendon rupture. An immunohistochemical study. *Histology and Histopathology*. 2009;(24):1207-1211. doi:10.14670/HH-24.1207
262. Jo CH, Lim H-J, Yoon KS. Characterization of Tendon-Specific Markers in Various Human Tissues, Tenocytes and Mesenchymal Stem Cells. *Tissue Eng Regen Med*. 2019;16(2):151-159. doi:10.1007/s13770-019-00182-2
263. Kundu J, Shim J-H, Jang J, Kim S-W, Cho D-W. An additive manufacturing-based PCL-alginate-chondrocyte bioprinted scaffold for cartilage tissue engineering: PCL-alginate-chondrocyte bioprinted scaffold for cartilage tissue engineering. *J Tissue Eng Regen Med*. 2015;9(11):1286-1297. doi:10.1002/term.1682
264. Lüthmann T, Hall H. Cell Guidance by 3D-Gradients in Hydrogel Matrices: Importance for Biomedical Applications. *Materials*. 2009;2(3):1058-1083. doi:10.3390/ma2031058
265. Vo TN, Kasper FK, Mikos AG. Strategies for controlled delivery of growth factors and cells for bone regeneration. *Advanced Drug Delivery Reviews*. 2012;64(12):1292-1309. doi:10.1016/j.addr.2012.01.016
266. Rahaman MN, Mao JJ. Stem cell-based composite tissue constructs for regenerative medicine. *Biotechnol Bioeng*. 2005;91(3):261-284. doi:10.1002/bit.20292
267. Ribeiro FO, Gómez-Benito MJ, Folgado J, Fernandes PR, García-Aznar JM. In silico Mechano-Chemical Model of Bone Healing for the Regeneration of Critical Defects: The Effect of BMP-2. Yamamoto M, ed. *PLoS ONE*. 2015;10(6):e0127722. doi:10.1371/journal.pone.0127722
268. Umulis D, O'Connor MB, Blair SS. The extracellular regulation of bone morphogenetic protein signaling. *Development*. 2009;136(22):3715-3728. doi:10.1242/dev.031534
269. Kim HKW, Oxendine I, Kamiya N. High-concentration of BMP2 reduces cell proliferation and increases apoptosis via DKK1 and SOST in human primary periosteal cells. *Bone*. 2013;54(1):141-150. doi:10.1016/j.bone.2013.01.031
270. Yamamoto M, Ikada Y, Tabata Y. Controlled release of growth factors based on biodegradation of gelatin hydrogel. *Journal of Biomaterials Science, Polymer Edition*. 2001;12(1):77-88. doi:10.1163/156856201744461
271. Park YJ, Lee YM, Lee JY, Seol YJ, Chung CP, Lee SJ. Controlled release of platelet-derived growth factor-BB from chondroitin sulfate-chitosan sponge for guided bone regeneration. *Journal of Controlled Release*. 2000;67(2-3):385-394. doi:10.1016/S0168-3659(00)00232-7
272. Holland TA, Bodde EWH, Cuijpers VMJI, *et al*. Degradable hydrogel scaffolds for *in vivo* delivery of single and dual growth factors in cartilage repair. *Osteoarthritis and Cartilage*. 2007;15(2):187-197. doi:10.1016/j.joca.2006.07.006
273. Wang X, Wenk E, Zhang X, Meinel L, Vunjak-Novakovic G, Kaplan DL. Growth factor gradients via microsphere delivery in biopolymer scaffolds for osteochondral tissue engineering. *Journal of Controlled Release*. 2009;134(2):81-90. doi:10.1016/j.jconrel.2008.10.021
274. Luginbuehl V, Wenk E, Koch A, Gander B, Merkle HP, Meinel L. Insulin-like

- Growth Factor I—Releasing Alginate-Tricalciumphosphate Composites for Bone Regeneration. *Pharm Res.* 2005;22(6):940-950. doi:10.1007/s11095-005-4589-9
275. Chung Y-I, Ahn K-M, Jeon S-H, Lee S-Y, Lee J-H, Tae G. Enhanced bone regeneration with BMP-2 loaded functional nanoparticle-hydrogel complex. *Journal of Controlled Release.* 2007;121(1-2):91-99. doi:10.1016/j.jconrel.2007.05.029
276. Gentile P, Chiono V, Carmagnola I, Hatton P. An Overview of Poly(lactic-co-glycolic) Acid (PLGA)-Based Biomaterials for Bone Tissue Engineering. *IJMS.* 2014;15(3):3640-3659. doi:10.3390/ijms15033640
277. Makadia HK, Siegel SJ. Poly Lactic-co-Glycolic Acid (PLGA) as Biodegradable Controlled Drug Delivery Carrier. *Polymers.* 2011;3(3):1377-1397. doi:10.3390/polym3031377
278. Faisant N, Akiki J, Siepmann F, Benoit JP, Siepmann J. Effects of the type of release medium on drug release from PLGA-based microparticles: Experiment and theory. *International Journal of Pharmaceutics.* 2006;314(2):189-197. doi:10.1016/j.ijpharm.2005.07.030
279. Faisant N, Siepmann J, Benoit JP. PLGA-based microparticles: elucidation of mechanisms and a new, simple mathematical model quantifying drug release. *European Journal of Pharmaceutical Sciences.* 2002;15(4):355-366. doi:10.1016/S0928-0987(02)00023-4
280. Klose D, Siepmann F, Elkharraz K, Krenzlin S, Siepmann J. How porosity and size affect the drug release mechanisms from PLGA-based microparticles. *International Journal of Pharmaceutics.* 2006;314(2):198-206. doi:10.1016/j.ijpharm.2005.07.031
281. Siepmann J, Siepmann F. Mathematical modeling of drug delivery. *International Journal of Pharmaceutics.* 2008;364(2):328-343. doi:10.1016/j.ijpharm.2008.09.004
282. Trucillo E, Bisceglia B, Valdrè G, *et al.* Growth factor sustained delivery from poly-lactic-co-glycolic acid microcarriers and its mass transfer modeling by finite element in a dynamic and static three-dimensional environment bioengineered with stem cells. *Biotechnology and Bioengineering.* 2019;116(7):1777-1794. doi:10.1002/bit.26975
283. Li M, Rouaud O, Poncelet D. Microencapsulation by solvent evaporation: State of the art for process engineering approaches. *International Journal of Pharmaceutics.* 2008;363(1-2):26-39. doi:10.1016/j.ijpharm.2008.07.018
284. Mao S, Shi Y, Li L, Xu J, Schaper A, Kissel T. Effects of process and formulation parameters on characteristics and internal morphology of poly(d,l-lactide-co-glycolide) microspheres formed by the solvent evaporation method. *European Journal of Pharmaceutics and Biopharmaceutics.* 2008;68(2):214-223. doi:10.1016/j.ejpb.2007.06.008
285. Yang Y-Y, Chia H-H, Chung T-S. Effect of preparation temperature on the characteristics and release profiles of PLGA microspheres containing protein fabricated by double-emulsion solvent extraction/evaporation method. *Journal of Controlled Release.* 2000;69(1):81-96. doi:10.1016/S0168-3659(00)00291-1
286. Rothstein SN, Federspiel WJ, Little SR. A unified mathematical model for the prediction of controlled release from surface and bulk eroding polymer matrices. *Biomaterials.* 2009;30(8):1657-1664. doi:10.1016/j.biomaterials.2008.12.002
287. Lichtenthaler RN. Gerd Brunner: Gas Extraction - An Introduction to Fundamentals of Supercritical Fluids and the Application to Separation Processes. Topics in Physical Chemistry, Vol. 4, eds. H. Baumgärtel, E. U. Franck, W. Grünbein. Steinkopff, Darmstadt/Springer, New Yo. *Berichte der Bunsengesellschaft für physikalische Chemie.* 1996;100(6):1090-1091. doi:10.1002/bbpc.19961000668
288. Ravi Kumar MNV, ed. *Handbook of Particulate Drug Delivery.* American Scientific Publishers; 2008.
289. Chattopadhyay P, Shekunov B, Yim D, Cipolla D, Boyd B, Farr S. Production of solid lipid nanoparticle suspensions using supercritical fluid extraction of emulsions (SFEE) for

- pulmonary delivery using the AERx system☆. *Advanced Drug Delivery Reviews*. 2007;59(6):444-453. doi:10.1016/j.addr.2007.04.010
290. Della Porta G, Reverchon E. Nanostructured microspheres produced by supercritical fluid extraction of emulsions. *Biotechnol Bioeng*. 2008;100(5):1020-1033. doi:10.1002/bit.21845
291. Kluge J, Fusaro F, Casas N, Mazzotti M, Muhrer G. Production of PLGA micro- and nanocomposites by supercritical fluid extraction of emulsions: I. Encapsulation of lysozyme. *The Journal of Supercritical Fluids*. 2009;50(3):327-335. doi:10.1016/j.supflu.2009.05.010
292. Della Porta G, Falco N, Reverchon E. NSAID Drugs Release from Injectable Microspheres Produced by Supercritical Fluid Emulsion Extraction. *Journal of Pharmaceutical Sciences*. 2010;99(3):1484-1499. doi:10.1002/jps.21920
293. Della Porta G, Castaldo F, Scognamiglio M, Paciello L, Parascandola P, Reverchon E. Bacteria microencapsulation in PLGA microdevices by supercritical emulsion extraction. *The Journal of Supercritical Fluids*. 2012;63:1-7. doi:10.1016/j.supflu.2011.12.020
294. Porta GD, Campardelli R, Falco N, Reverchon E. PLGA microdevices for retinoids sustained release produced by supercritical emulsion extraction: Continuous versus batch operation layouts. *Journal of Pharmaceutical Sciences*. 2011;100(10):4357-4367. doi:10.1002/jps.22647
295. Della Porta G, Falco N, Reverchon E. Continuous supercritical emulsions extraction: A new technology for biopolymer microparticles production. *Biotechnology and Bioengineering*. 2011;108(3):676-686. doi:10.1002/bit.22972
296. Falco N, Reverchon E, Della Porta G. Continuous Supercritical Emulsions Extraction: Packed Tower Characterization and Application to Poly(lactic- co -glycolic Acid) + Insulin Microspheres Production. *Ind Eng Chem Res*. 2012;51(25):8616-8623. doi:10.1021/ie300482n
297. Campardelli R, Espirito Santo I, Albuquerque EC, de Melo SV, Della Porta G, Reverchon E. Efficient encapsulation of proteins in submicro liposomes using a supercritical fluid assisted continuous process. *The Journal of Supercritical Fluids*. 2016;107:163-169. doi:10.1016/j.supflu.2015.09.007
298. Campardelli R, Della Porta G, Gomez L, Irusta S, Reverchon E, Santamaria J. Au-PLA nanocomposites for photothermally controlled drug delivery. *J Mater Chem B*. 2014;2(4):409-417. doi:10.1039/C3TB21099E
299. Tirado DF, Palazzo I, Scognamiglio M, Calvo L, Della Porta G, Reverchon E. Astaxanthin encapsulation in ethyl cellulose carriers by continuous supercritical emulsions extraction: A study on particle size, encapsulation efficiency, release profile and antioxidant activity. *The Journal of Supercritical Fluids*. 2019;150:128-136. doi:10.1016/j.supflu.2019.04.017
300. Gimenez-Rota C, Palazzo I, Scognamiglio MR, Mainar A, Reverchon E, Della Porta G. β -Carotene, α -tocopherol and rosmarinic acid encapsulated within PLA/PLGA microcarriers by supercritical emulsion extraction: Encapsulation efficiency, drugs shelf-life and antioxidant activity. *The Journal of Supercritical Fluids*. 2019;146:199-207. doi:10.1016/j.supflu.2019.01.019
301. Grasel F dos S, Behrens MC, Strassburger D, et al. SYNTHESIS, CHARACTERIZATION AND *in vitro* CYTOTOXICITY OF Acacia mearnsii PROANTHOCYANIDIN LOADED PLGA MICROPARTICLES. *Braz J Chem Eng*. 2019;36(1):239-250. doi:10.1590/0104-6632.20190361s20170154
302. Kang Y, Wu J, Yin G, et al. Preparation, characterization and *in vitro* cytotoxicity of indomethacin-loaded PLLA/PLGA microparticles using supercritical CO₂ technique. *European Journal of Pharmaceutics and Biopharmaceutics*. 2008;70(1):85-97. doi:10.1016/j.ejpb.2008.03.011
303. Santoro A, Bianco G, Picerno P, et al. Verminoside- and verbascoside-induced

- genotoxicity on human lymphocytes: Involvement of PARP-1 and p53 proteins. *Toxicology Letters*. 2008;178(2):71-76. doi:10.1016/j.toxlet.2008.02.006
304. Di Pietro P, D'Auria R, Viggiano A, *et al.* Bisphenol A induces DNA damage in cells exerting immune surveillance functions at peripheral and central level. *Chemosphere*. 2020;254:126819. doi:10.1016/j.chemosphere.2020.126819
305. Athanasiou K. Sterilization, toxicity, biocompatibility and clinical applications of polylactic acid/ polyglycolic acid copolymers. *Biomaterials*. 1996;17(2):93-102. doi:10.1016/0142-9612(96)85754-1
306. Palazzo I, Lamparelli EP, Ciardulli MC, *et al.* Supercritical emulsion extraction fabricated PLA/PLGA micro/nano carriers for growth factor delivery: Release profiles and cytotoxicity. *International Journal of Pharmaceutics*. 2021;592:120108. doi:10.1016/j.ijpharm.2020.120108
307. Bouissou C, Rouse JJ, Price R, van der Walle CF. The Influence of Surfactant on PLGA Microsphere Glass Transition and Water Sorption: Remodeling the Surface Morphology to Attenuate the Burst Release. *Pharm Res*. 2006;23(6):1295-1305. doi:10.1007/s11095-006-0180-2
308. Chandrapala J, Zisu B, Palmer M, Kentish S, Ashokkumar M. Effects of ultrasound on the thermal and structural characteristics of proteins in reconstituted whey protein concentrate. *Ultrasonics Sonochemistry*. 2011;18(5):951-957. doi:10.1016/j.ultsonch.2010.12.016
309. Zhang JX, Zhu KJ. An improvement of double emulsion technique for preparing bovine serum albumin-loaded PLGA microspheres. *Journal of Microencapsulation*. 2004;21(7):775-785. doi:10.1080/02652040400008465
310. Nihant N, Schugens C, Grandfils C, Jérôme R, Teyssié P. Polylactide Microparticles Prepared by Double Emulsion/Evaporation Technique. I. Effect of Primary Emulsion Stability. *Pharmaceutical Research*. 1994;11(10):1479-1484. doi:10.1023/A:1018912426983
311. Ciaglia E, Montella F, Trucillo P, *et al.* A bioavailability study on microbeads and nanoliposomes fabricated by dense carbon dioxide technologies using human-primary monocytes and flow cytometry assay. *International Journal of Pharmaceutics*. 2019;570:118686. doi:10.1016/j.ijpharm.2019.118686
312. Prota L, Santoro A, Bifulco M, Aquino RP, Mencherini T, Russo P. Leucine enhances aerosol performance of Naringin dry powder and its activity on cystic fibrosis airway epithelial cells. *International Journal of Pharmaceutics*. 2011;412(1-2):8-19. doi:10.1016/j.ijpharm.2011.03.055
313. Ahmed S, Chauhan VM, Ghaemmaghani AM, Aylott JW. New generation of bioreactors that advance extracellular matrix modelling and tissue engineering. *Biotechnol Lett*. 2019;41(1):1-25. doi:10.1007/s10529-018-2611-7
314. Mozafari M, Sefat F, Atala A. *Handbook of Tissue Engineering Scaffolds Volume One.*; 2019.
315. d'Angelo M, Benedetti E, Tupone MG, *et al.* The Role of Stiffness in Cell Reprogramming: A Potential Role for Biomaterials in Inducing Tissue Regeneration. *Cells*. 2019;8(9):1036. doi:10.3390/cells8091036
316. Ogle ME, Segar CE, Sridhar S, Botchwey EA. Monocytes and macrophages in tissue repair: Implications for immunoregenerative biomaterial design. *Exp Biol Med (Maywood)*. 2016;241(10):1084-1097. doi:10.1177/1535370216650293
317. Turksen K. *Approaches for Diverse Diseases and Conditions*. Springer; 2018. Accessed March 31, 2021. <https://link.springer.com/book/10.1007/978-3-030-04170-0>
318. Dakin SG, Martinez FO, Yapp C, *et al.* Inflammation activation and resolution in human tendon disease. *Sci Transl Med*. 2015;7(311):311ra173-311ra173. doi:10.1126/scitranslmed.aac4269
319. John T, Lodka D, Kohl B, *et al.* Effect of pro-inflammatory and immunoregulatory

- cytokines on human tenocytes. *J Orthop Res*. Published online 2010:n/a-n/a. doi:10.1002/jor.21079
320. Manning CN, Havlioglu N, Knutsen E, *et al*. The early inflammatory response after flexor tendon healing: A gene expression and histological analysis: EARLY INFLAMMATORY RESPONSE AFTER FLEXOR TENDON HEALING. *J Orthop Res*. 2014;32(5):645-652. doi:10.1002/jor.22575
321. Marsolais D, C??té CH, Frenette J. Neutrophils and macrophages accumulate sequentially following Achilles tendon injury. *J Orthop Res*. 2001;19(6):1203-1209. doi:10.1016/S0736-0266(01)00031-6
322. Chisari E, Rehak L, Khan WS, Maffulli N. The role of the immune system in tendon healing: a systematic review. *British Medical Bulletin*. 2020;133(1):49-64. doi:10.1093/bmb/ldz040
323. Oryan A, Moshiri A, Meimandi Parizi A, Maffulli N. Implantation of a Novel Biologic and Hybridized Tissue Engineered Bioimplant in Large Tendon Defect: An *In Vivo* Investigation. *Tissue Engineering Part A*. Published online October 12, 2013:131012175952003. doi:10.1089/ten.tea.2013.0053
324. Lui PPY, Wong OT. Tendon stem cells: experimental and clinical perspectives in tendon and tendon-bone junction repair. *Muscles Ligaments Tendons J*. 2012;2(3):163-168.
325. Lovecchio J, Gargiulo P, Vargas Luna JL, Giordano E, Sigurjónsson ÓE. A standalone bioreactor system to deliver compressive load under perfusion flow to hBMSC-seeded 3D chitosan-graphene templates. *Sci Rep*. 2019;9(1):16854. doi:10.1038/s41598-019-53319-7
326. Barber JG, Handorf AM, Allee TJ, Li W-J. Braided Nanofibrous Scaffold for Tendon and Ligament Tissue Engineering. *Tissue Engineering Part A*. 2013;19(11-12):1265-1274. doi:10.1089/ten.tea.2010.0538
327. Wang T, Lin Z, Day RE, *et al*. Programmable mechanical stimulation influences tendon homeostasis in a bioreactor system. *Biotechnol Bioeng*. 2013;110(5):1495-1507. doi:10.1002/bit.24809
328. Delaine-Smith RM, Reilly GC. Mesenchymal stem cell responses to mechanical stimuli. *Muscles Ligaments Tendons J*. 2012;2(3):169-180.
329. Chen Y-J, Huang C-H, Lee I-C, Lee Y-T, Chen M-H, Young T-H. Effects of Cyclic Mechanical Stretching on the mRNA Expression of Tendon/Ligament-Related and Osteoblast-Specific Genes in Human Mesenchymal Stem Cells. *Connective Tissue Research*. 2008;49(1):7-14. doi:10.1080/03008200701818561
330. Youngstrom DW, Rajpar I, Kaplan DL, Barrett JG. A bioreactor system for *in vitro* tendon differentiation and tendon tissue engineering: TENDON BIOREACTOR. *J Orthop Res*. 2015;33(6):911-918. doi:10.1002/jor.22848
331. Grier WG, Moy AS, Harley BA. Cyclic tensile strain enhances human mesenchymal stem cell Smad 2/3 activation and tenogenic differentiation in anisotropic collagen-glycosaminoglycan scaffolds. *Eur Cell Mater*. 2017;33:227-239. doi:10.22203/eCM.v033a14
332. Kay AG, Dale TP, Akram KM, *et al*. BMP2 repression and optimized culture conditions promote human bone marrow-derived mesenchymal stem cell isolation. *Regenerative Medicine*. 2015;10(2):109-125. doi:10.2217/rme.14.67
333. Correia SI, Pereira H, Silva-Correia J, *et al*. Current concepts: tissue engineering and regenerative medicine applications in the ankle joint. *J R Soc Interface*. 2014;11(92):20130784. doi:10.1098/rsif.2013.0784
334. Yang G, Rothrauff BB, Lin H, Gottardi R, Alexander PG, Tuan RS. Enhancement of tenogenic differentiation of human adipose stem cells by tendon-derived extracellular matrix. *Biomaterials*. 2013;34(37):9295-9306. doi:10.1016/j.biomaterials.2013.08.054
335. Lui PP. Stem cell technology for tendon regeneration: current status, challenges, and future research directions. *SCCAA*. Published online December 2015:163. doi:10.2147/SCCAA.S60832

336. MacLean S, Khan WS, Malik AA, Snow M, Anand S. Tendon Regeneration and Repair with Stem Cells. *Stem Cells International*. 2012;2012:1-6. doi:10.1155/2012/316281
337. Liu L, Hindieh J, Leong DJ, Sun HB. Advances of stem cell based-therapeutic approaches for tendon repair. *Journal of Orthopaedic Translation*. 2017;9:69-75. doi:10.1016/j.jot.2017.03.007
338. Akram KM, Samad S, Spiteri MA, Forsyth NR. Mesenchymal stem cells promote alveolar epithelial cell wound repair *in vitro* through distinct migratory and paracrine mechanisms. *Respir Res*. 2013;14(1):9. doi:10.1186/1465-9921-14-9
339. Pontikoglou C, Deschaseaux F, Sensebé L, Papadaki HA. Bone Marrow Mesenchymal Stem Cells: Biological Properties and Their Role in Hematopoiesis and Hematopoietic Stem Cell Transplantation. *Stem Cell Rev and Rep*. 2011;7(3):569-589. doi:10.1007/s12015-011-9228-8
340. Dominici M, Le Blanc K, Mueller I, *et al*. Minimal criteria for defining multipotent mesenchymal stromal cells. The International Society for Cellular Therapy position statement. *Cytotherapy*. 2006;8(4):315-317. doi:10.1080/14653240600855905
341. Chamberlain G, Fox J, Ashton B, Middleton J. Concise Review: Mesenchymal Stem Cells: Their Phenotype, Differentiation Capacity, Immunological Features, and Potential for Homing. *Stem Cells*. 2007;25(11):2739-2749. doi:10.1634/stemcells.2007-0197
342. Mosna F, Sensebé L, Krampera M. Human Bone Marrow and Adipose Tissue Mesenchymal Stem Cells: A User's Guide. *Stem Cells and Development*. 2010;19(10):1449-1470. doi:10.1089/scd.2010.0140
343. Kumar D, Gerges I, Tamplenizza M, Lenardi C, Forsyth NR, Liu Y. Three-dimensional hypoxic culture of human mesenchymal stem cells encapsulated in a photocurable, biodegradable polymer hydrogel: A potential injectable cellular product for nucleus pulposus regeneration. *Acta Biomaterialia*. 2014;10(8):3463-3474. doi:10.1016/j.actbio.2014.04.027
344. Bullough R, Finnigan T, Kay A, Maffulli N, Forsyth NR. Tendon repair through stem cell intervention: Cellular and molecular approaches. *Disability and Rehabilitation*. 2008;30(20-22):1746-1751. doi:10.1080/09638280701788258
345. Giordano R, Canesi M, Isalberti M, *et al*. Autologous mesenchymal stem cell therapy for progressive supranuclear palsy: translation into a phase I controlled, randomized clinical study. *J Transl Med*. 2014;12(1):14. doi:10.1186/1479-5876-12-14
346. Govoni M, Lotti F, Biagiotti L, *et al*. An innovative stand-alone bioreactor for the highly reproducible transfer of cyclic mechanical stretch to stem cells cultured in a 3D scaffold: A novel stand-alone bioreactor to induce cell muscle phenotype. *J Tissue Eng Regen Med*. 2014;8(10):787-793. doi:10.1002/term.1578
347. de Winter JCF. Using the Student's t-test with extremely small sample sizes. doi:10.7275/E4R6-DJ05
348. Ciardulli MC, Marino L, Lamparelli EP, *et al*. Dose-Response Tendon-Specific Markers Induction by Growth Differentiation Factor-5 in Human Bone Marrow and Umbilical Cord Mesenchymal Stem Cells. *IJMS*. 2020;21(16):5905. doi:10.3390/ijms21165905
349. Shukunami C, Yoshimoto Y, Takimoto A, Yamashita H, Hiraki Y. Molecular characterization and function of tenomodulin, a marker of tendons and ligaments that integrate musculoskeletal components. *Japanese Dental Science Review*. 2016;52(4):84-92. doi:10.1016/j.jdsr.2016.04.003
350. Duong H, Wu B, Tawil B. Modulation of 3D Fibrin Matrix Stiffness by Intrinsic Fibrinogen–Thrombin Compositions and by Extrinsic Cellular Activity. *Tissue Engineering Part A*. 2009;15(7):1865-1876. doi:10.1089/ten.tea.2008.0319
351. Wang T, Thien C, Wang C, *et al*. 3D uniaxial mechanical stimulation induces tenogenic differentiation of tendon-derived stem cells through a PI3K/AKT signaling

- pathway. *FASEB j.* 2018;32(9):4804-4814. doi:10.1096/fj.201701384R
352. Wagenhäuser MU, Pietschmann MF, Sievers B, *et al.* Collagen type I and decorin expression in tenocytes depend on the cell isolation method. *BMC Musculoskelet Disord.* 2012;13(1):140. doi:10.1186/1471-2474-13-140
353. Govoni M, Lamparelli EP, Ciardulli MC, *et al.* Demineralized bone matrix paste formulated with biomimetic PLGA microcarriers for the vancomycin hydrochloride controlled delivery: Release profile, cytotoxicity and efficacy against *S. aureus*. *International Journal of Pharmaceutics.* 2020;582:119322. doi:10.1016/j.ijpharm.2020.119322
354. Forcina L, Miano C, Scicchitano B, Musarò A. Signals from the Niche: Insights into the Role of IGF-1 and IL-6 in Modulating Skeletal Muscle Fibrosis. *Cells.* 2019;8(3):232. doi:10.3390/cells8030232
355. Aicale R, Oliviero A, Maffulli N. Management of Achilles and patellar tendinopathy: what we know, what we can do. *J Foot Ankle Res.* 2020;13(1):59. doi:10.1186/s13047-020-00418-8
356. Lamplot JD, Rodeo SA, Brophy RH. A Practical Guide for the Current Use of Biologic Therapies in Sports Medicine. *Am J Sports Med.* 2020;48(2):488-503. doi:10.1177/0363546519836090
357. Sezgin EA, Atik OŞ. Are orthobiologics the next chapter in clinical orthopedics? A literature review. *Eklemler Hastalıkları Cerrahisi.* 2018;29(2):110-116. doi:10.5606/ehc.2018.005
358. Ioannidou E. Therapeutic modulation of growth factors and cytokines in regenerative medicine. *Curr Pharm Des.* 2006;12(19):2397-2408. doi:10.2174/138161206777699007
359. Citeroni MR, Ciardulli MC, Russo V, *et al.* In Vitro Innovation of Tendon Tissue Engineering Strategies. *Int J Mol Sci.* 2020;21(18). doi:10.3390/ijms21186726
360. Citeroni MR, Mauro A, Ciardulli MC, *et al.* Amnion-Derived Teno-Inductive Secretomes: A Novel Approach to Foster Tendon Differentiation and Regeneration in an Ovine Model. *Front Bioeng Biotechnol.* 2021;9:649288. doi:10.3389/fbioe.2021.649288
361. Gupta A, El-Amin SF, Levy HJ, Sze-Tu R, Ibim SE, Maffulli N. Umbilical cord-derived Wharton's jelly for regenerative medicine applications. *J Orthop Surg Res.* 2020;15(1):49. doi:10.1186/s13018-020-1553-7
362. Taghizadeh RR, Cetrulo KJ, Cetrulo CL. Wharton's Jelly stem cells: future clinical applications. *Placenta.* 2011;32 Suppl 4:S311-315. doi:10.1016/j.placenta.2011.06.010
363. Vangsnæs CT, Sternberg H, Harris L. Umbilical Cord Tissue Offers the Greatest Number of Harvestable Mesenchymal Stem Cells for Research and Clinical Application: A Literature Review of Different Harvest Sites. *Arthroscopy.* 2015;31(9):1836-1843. doi:10.1016/j.arthro.2015.03.014
364. Maeda E, Sugimoto M, Ohashi T. Cytoskeletal tension modulates MMP-1 gene expression from tenocytes on micropillar substrates. *Journal of Biomechanics.* 2013;46(5):991-997. doi:10.1016/j.jbiomech.2012.11.056
365. Maeda E, Shelton JC, Bader DL, Lee DA. Differential regulation of gene expression in isolated tendon fascicles exposed to cyclic tensile strain *in vitro*. *Journal of Applied Physiology.* 2009;106(2):506-512. doi:10.1152/jappphysiol.90981.2008
366. Zhang C, Zhu J, Zhou Y, Thampatty BP, Wang JH-C. Tendon Stem/Progenitor Cells and Their Interactions with Extracellular Matrix and Mechanical Loading. *Stem Cells International.* 2019;2019:1-10. doi:10.1155/2019/3674647
367. Galloway MT, Lally AL, Shearn JT. The Role of Mechanical Loading in Tendon Development, Maintenance, Injury, and Repair: *The Journal of Bone and Joint Surgery-American Volume.* 2013;95(17):1620-1628. doi:10.2106/JBJS.L.01004
368. Ciardulli MC, Marino L, Lovecchio J, *et al.* Tendon and Cytokine Marker Expression by Human Bone Marrow Mesenchymal Stem Cells in a Hyaluronate/Poly-Lactic-Co-Glycolic Acid (PLGA)/Fibrin Three-Dimensional (3D) Scaffold. *Cells.* 2020;9(5):1268. doi:10.3390/cells9051268

369. Lamparelli EP, Lovecchio J, Ciardulli MC, *et al.* Chondrogenic Commitment of Human Bone Marrow Mesenchymal Stem Cells in a Perfused Collagen Hydrogel Functionalized with hTGF- β 1-Releasing PLGA Microcarrier. *Pharmaceutics*. 2021;13(3):399. doi:10.3390/pharmaceutics13030399
370. Grier WK, Sun Han Chang RA, Ramsey MD, Harley BAC. The influence of cyclic tensile strain on multi-compartment collagen-GAG scaffolds for tendon-bone junction repair. *Connective Tissue Research*. 2019;60(6):530-543. doi:10.1080/03008207.2019.1601183
371. Della Porta G, Ciardulli MC, Maffulli N. Microcapsule Technology for Controlled Growth Factor Release in Musculoskeletal Tissue Engineering: *Sports Medicine and Arthroscopy Review*. 2018;26(2):e2-e9. doi:10.1097/JSA.0000000000000188
372. Cricchio V, Best M, Reverchon E, *et al.* Novel Superparamagnetic Microdevices Based on Magnetized PLGA/PLA Microparticles Obtained by Supercritical Fluid Emulsion and Coating by Carboxybetaine-Functionalized Chitosan Allowing the Tuneable Release of Therapeutics. *Journal of Pharmaceutical Sciences*. 2017;106(8):2097-2105. doi:10.1016/j.xphs.2017.05.005
373. Porta GD, Nguyen B-NB, Campardelli R, Reverchon E, Fisher JP. Synergistic effect of sustained release of growth factors and dynamic culture on osteoblastic differentiation of mesenchymal stem cells: Sustained Growth Factor Release for Osteoblastic Differentiation. *J Biomed Mater Res*. 2015;103(6):2161-2171. doi:10.1002/jbm.a.35354
374. Jensen EC. Quantitative Analysis of Histological Staining and Fluorescence Using ImageJ: Histological Staining/Fluorescence Using ImageJ. *Anat Rec*. 2013;296(3):378-381. doi:10.1002/ar.22641
375. La Rocca G, Lo Iacono M, Corsello T, Corrao S, Farina F, Anzalone R. Human Wharton's Jelly Mesenchymal Stem Cells Maintain the Expression of Key Immunomodulatory Molecules When Subjected to Osteogenic, Adipogenic and Chondrogenic Differentiation *In Vitro*: New Perspectives for Cellular Therapy. *CSCR*. 2013;8(1):100-113. doi:10.2174/1574888X11308010012
376. Millar NL, Akbar M, Campbell AL, *et al.* IL-17A mediates inflammatory and tissue remodelling events in early human tendinopathy. *Sci Rep*. 2016;6(1):27149. doi:10.1038/srep27149

Figures

| | |
|---|----|
| Figure 1-1. Hierarchical arrangement of the structure of tendons..... | 3 |
| Figure 1-2. Typical stress–strain curve for tendon tissue..... | 8 |
| Figure 1-3. Image of a fibrin hydrogel..... | 18 |
| Figure 1-4. <i>In vitro</i> strategies for tendon tissue engineering..... | 22 |
| Figure 2-1. Flow cytometry events illustrate hBM-MSCs and hWJ-MSCs characterization..... | 31 |
| Figure 2-2. Proliferation rate of hBM-MSCs and hWJ-MSCs with the human Growth Differentiation Factor 5 (hGDF-5) dose-dependent effect..... | 32 |
| Figure 2-3. Morphometric analysis of hBM-MSCs and hWJ-MSCs with the hGDF-5 dose-dependent effect..... | 33 |
| Figure 2-4. Brightfield images of hBM-MSCs and hWJ-MSCs with the hGDF-5 dose-dependent effect..... | 34 |
| Figure 2-5. Quantitative Real-Time Polymerase Chain Reaction (qRT-PCR) on the expression of tenogenic markers by hBM-MSCs and hWJ-MSCs with the hGDF-5 dose-dependent effect..... | 35 |
| Figure 2-6. Immunofluorescence (IF) images and quantitative immunofluorescence (q-IF) data illustrating the effect of different hGDF-5 dose on hBM-MSCs..... | 36 |
| Figure 2-7. IF images illustrating the type 1 collagen expression at different hGDF-5 dose on hWJ-MSCs..... | 37 |
| Figure 2-8. Immunofluorescence (IF) images and quantitative immunofluorescence (q-IF) data illustrating the effect of different hGDF-5 dose on hWJ-MSCs..... | 38 |
| Figure 2-9. RT-PCR on the expression of cytokine by hBM-MSCs and hWJ-MSCs with the hGDF-5 concentration-dependent effect..... | 39 |
| Figure 3-1. Biopolymer microspheres for controlled drug delivery..... | 45 |
| Figure 3-2. Schematic comparison between solvent evaporation (SE) and supercritical emulsion extraction (SEE) technologies..... | 47 |
| Figure 3-3. Schematic illustration of SEE process..... | 50 |
| Figure 3-4. Optical image of emulsions and SEM image of carriers loaded with growth factor..... | 54 |
| Figure 3-5. Release profiles of growth factors measured in α -MEM at 37°C for up to 25 days..... | 54 |
| Figure 3-6. Carriers cytotoxicity evaluated using Chinese Hamster Ovary cell line (CHO-K1) that were treated with empty and loaded PLGA carriers for 24 h and 48 h..... | 55 |
| Figure 3-7. Carrier cytotoxicity evaluated using human peripheral blood mononuclear cells (hPBMCs)..... | 56 |
| Figure 4-1. Gene expression profiles for tenogenic markers and pro-inflammatory and anti-inflammatory cytokines..... | 66 |

| | |
|--|----|
| Figure 4-2. IF and quantitative-IF assays of type 1 Collagen (COL1A1) and type 3 Collagen (COL3A1) monitored along hBM-MSCs treatment with 1.6 ng/ and 100 ng/mL of ihGDF-5 for 16 days..... | 67 |
| Figure 4-3. ihGDF-5 loaded PLGA-NCs characterization..... | 68 |
| Figure 4-4. HY-FIB three-dimensional (3D) scaffold features and cyclic strain bioreactor..... | 69 |
| Figure 4-5. Gene expression profiles of tenogenic markers..... | 71 |
| Figure 4-6. Tenogenic markers expression in static vs dynamic culture..... | 71 |
| Figure 4-7. Gene expression profiles of pro-inflammatory and anti-inflammatory cytokines..... | 72 |
| Figure 4-8. Cytokine markers expression in static vs dynamic culture..... | 73 |
| Figure 4-9. Histology characterization of the overall HY-FIB scaffold structure with Sirius Red staining..... | 74 |
| Figure 4-10. IF and quantitative-IF assays of type 1 Collagen (COL1A1) in 3D static and dynamic culture of hBM-MSCs for 11 days..... | 75 |
| Figure 5-1. Cytotoxicity assay of 3D printed cyclic strain bioreactor with CHO-K1 and HeLa cells..... | 88 |
| Figure 5.2. Flow cytometry characterization of hWJ-MSCs..... | 89 |
| Figure 5.3. Mechanical characterization of the 3D scaffold..... | 90 |
| Figure 5-4. Cyclic strain bioreactor and experimental design..... | 91 |
| Figure 5-5 3D scaffold structure monitored by FE-SEM images..... | 92 |
| Figure 5-6. Gene expression profiles for tenogenic markers of hWJ-MSCs cultured within the 3D construct into an medium supplemented with hGDF-5..... | 93 |
| Figure 5-7. Histological characterization of the 3D bioengineered construct..... | 93 |
| Figure 5-8. Images of emulsion and derived PLGA-NCs obtained by SEE technology, particle size distribution and hGDF-5 release profiles within 3D environment..... | 94 |
| Figure 5-9. Gene expression profiles for tenogenic markers of hWJ-MSCs cultured within scaffold functionalized with PLGA-NCs for hGDF-5 controlled delivery..... | 95 |
| Figure 5-10. Histological characterization of the 3D bioengineered construct..... | 96 |
| Figure 5-11. Gene expression profiles for cytokines by hWJ-MSCs cultured within scaffold assembled with PLGA-NCs for hGDF-5 controlled delivery..... | 97 |

Tables

| | |
|--|----|
| Table 2-1. Flow cytometry statistics data of all the main events considered for the population of hBM-MSCs and hWJ-MSCs used in the experiments..... | 30 |
| Table 3-1. A summary of emulsion formulations processed with SEE technology..... | 53 |
| Table 5-1. Mechanical characterization of hyaluronate braided band and bioengineered 3D construct and | 90 |

Abbreviations

| | |
|----------|--|
| ADSCs | Adipose derived stem cells |
| AECs | Amniotic epithelial stem cells |
| AKT-mTOR | Protein kinase B-mammalian target of rapamycin |
| BMP-12 | Bone Morphogenetic Protein-12 |
| BMP-13 | Bone Morphogenetic Protein-13 |
| BMP-14 | Bone Morphogenetic Protein-14 |
| BSA | Bovine serum albumin |
| CDMP-1 | Cartilage-derived morphogenetic protein-1 |
| CGRP | Calcitonin gene-related peptide |
| CHO-K1 | Chinese hamster ovary cells sub-clone K1 |
| COL14A1 | Collagen alpha-1(XIV) chain |
| COL1A1 | Collagen alpha-1(I) chain |
| COL1A2 | Collagen alpha-2(I) chain |
| COL3A1 | Collagen alpha-1(III) chain |
| COMP | Cartilage oligomeric protein |
| CTGF | Connective tissue growth factor |
| DCN | Decorin |
| DMEM | Dulbecco's Modified Essential Medium |
| DMSO | Dimethyl sulfoxide |
| DSDs | Droplet size distributions |
| EA | Ethyl acetate |
| ECM | Extracellular matrix |
| Egr 1/2 | Early growth response 1 and 2 factors |
| ELISA | Enzyme Linked Immunosorbent Assay |
| EMT | Epithelial-to-mesenchymal transition |
| FANS | Non-steroidal anti-inflammatory drugs |
| FBS | Fetal bovine serum |
| FE-SEM | Field emission-scanning electron microscopy |
| FEM | Finite element modeling |
| FGF-2 | Fibroblast growth factor-2 |
| FSC | Forward scatter |
| GAGs | Glycosaminoglycans |
| GAPDH | Glyceraldehyde-3-phosphate dehydrogenase |
| GFs | Growth factors |
| hBM-MSCs | Human bone marrow mesenchymal stem cells |
| hESCs | Human embryonic stem cells |
| hGDF-5 | Human growth differentiation factor-5 |
| hMSCs | Human mesenchymal stem cells |
| hPBMCs | Human peripheral blood mononuclear cells |
| HSA | Human serum albumin |

| | |
|--------------------|---|
| hWJ-MSCs | Human Wharton's Jelly mesenchymal stem cells |
| IGF-1 | Insulin-like growth factor-1 |
| ihGDF-5 | Inactive human growth differentiation factor-5 |
| IL-10 | Interleukin-10 |
| IL-1 β | Interleukin-1 β |
| IL-4 | Interleukin-4 |
| IL-6 | Interleukin-6 |
| iPSCs | Induced pluripotent stem cells |
| MAP-K | Mitogen-activated protein kinase |
| Mkx | Mohawk |
| MTT | 3-(4,5-Dimethylthiazol-2-yl)-2,5-diphenyl-tetrazolium bromide |
| o/w | Oil-in-water |
| OPF | Oligo (poly (ethylene glycol) fumarate |
| PBS | Phosphate buffered saline |
| Pc | Critical pressure |
| PCL | Polycaprolactones |
| PDGF | Platelet-derived growth factor |
| PEO | Polyethylene oxide |
| PEUUR | Poly (ester urethane) urea |
| PFA | Paraformaldehyde |
| PGA | Polyglycolic acids |
| PGS | Poly(glycerol-sebacate) |
| PLA | Poly lactic acid |
| PLCL | Poly (lactic-co-caprolactone) acids |
| PLGA | Poly lactic co-glycolic acid |
| PLGA-NCs | Poly lactic co-glycolic acid nanocarriers |
| PSDs | Particle size distributions |
| PU | Polyurethane |
| PVA | Poly-vinylalcohol |
| qIF | Quantitative immunofluorescence |
| RPMI | Roswell park memorial institute medium |
| RT | Room temperature |
| SC-CO ₂ | Supercritical carbon dioxide |
| SCX-A | Scleraxis-A |
| SE | Solvent evaporation |
| SEE | Supercritical emulsion extraction |
| SF | Shrinkage factor |
| SP | Substance P |
| SSC | Side scatter |
| Tc | Critical temperature |
| TE | Tissue engineering |
| TGF- β 1 | Transforming growth factor- β 1 |
| TGF- β 2 | Transforming growth factor- β 2 |

| | |
|----------------|---------------------------------------|
| TGF- β 3 | Transforming growth factor- β 3 |
| THBS | Thrombospondin |
| TNC | Tenascin-C |
| TNF- α | Tumor necrosis factor- α |
| TNMD | Tenomodulin |
| TPSCs | Tendon progenitor stem cells |
| UB | Umbilical cord |
| VEGF | Vascular endothelial growth factor |
| w1/o/w2 | Water-in-oil-in-water |
| α MEM | Minimum essential medium alpha |

Publications in International Peer Review Journals

1. **Ciardulli MC**, Lovecchio J, Scala P, Lamparelli EP, Giudice V, Giordano E, Selleri C, Forsyth NR, Maffulli N, Della Porta G. 3D biomimetic construct with hGDF-5 sustained delivery and cyclic strain bioreactor to study *in vitro* the tenogenic commitment of human Wharton's Jelly Mesenchymal Stem Cells. *Submitted to Nanomedicine*. **2021**.
2. Lamparelli EP, Lovecchio J, **Ciardulli MC**, Giudice V, Dale TP, Selleri C, Forsyth NR, Giordano E, Maffulli N, Della Porta G. Chondrogenic Commitment of Human Bone Marrow Mesenchymal Stem Cells in a Perfused Collagen Hydrogel Seeded with hTGF- β 1-Releasing PLGA Microcarrier. *Pharmaceutics*. 13(3):399. **2021** March 17. doi.org/10.3390/pharmaceutics13030399.
3. Citeroni MR, Mauro A, **Ciardulli MC**, Di Mattia M, El Khatib M, Russo V, Turriani M, Santer M, Della Porta G, Maffulli N, Forsyth NR, Barboni B. Amnion-derived teno-inductive secretomes: a novel approach to foster tendon differentiation and regeneration in an ovine model. *Front Bioeng Biotechnol*. 9: 649288. **2021** March 11. doi.org/10.3389/fbioe.2021.649288.
4. Palazzo I, Lamparelli EP, **Ciardulli MC**, Scala P, Reverchon E, Forsyth NR, Maffulli N, Santoro A, Della Porta G. Supercritical emulsion extraction fabricated PLA/PLGA micro/nano carriers for growth factor delivery: release profiles and cytotoxicity. *Int J Pharm*. 592:120108. **2021** Jan 5. doi:10.1016/j.ijpharm.2020.120108.
5. Citeroni MR, **Ciardulli MC**, Russo V, Della Porta G, Mauro A, El Khatib M, Di Mattia M, Galesso D, Barbera C, Forsyth NR, Maffulli N, Barboni B. *In vitro* innovation for tendon tissue engineering strategies. *Int J Mol Sci*. 21(18):E6726. **2020** September 14. Review. doi: 10.3390/ijms21186726.
6. **Ciardulli MC**, Marino L, Lamparelli EP, Guida M, Forsyth NR, Selleri C, Della Porta G, Maffulli N. Dose-Response Tendon-Specific Markers Induction by Growth Differentiation Factor-5 in Human Bone Marrow and Umbilical Cord Mesenchymal Stem Cells. *Int J Mol Sci*. 21(16):5905. **2020** August 17. doi:10.3390/ijms21165905.
7. Govoni M, Lamparelli EP, **Ciardulli MC**, Santoro A, Oliviero A, Palazzo I, Reverchon E, Vivarelli L, Maso A, Storni, E, *et al*. Demineralized bone matrix paste formulated with biomimetic PLGA microcarriers for the Vancomycin Hydrochloride controlled delivery: release Profile, cytotoxicity and efficacy against *S. aureus*. *Int J Pharm*. 582:119322. **2020** May 30. doi:10.1016/j.ijpharm.2020.119322.

8. **Ciardulli MC**, Marino L, Lovecchio J, Giordano E, Forsyth NR, Selleri C, Maffulli N, Della Porta G. Tendon and Cytokine marker expression by human Bone Marrow Mesenchymal Stem Cells in a Hyaluronate/Poly-Lactic-Co-Glycolic Acid(PLGA)/Fibrin Three-Dimensional (3D) scaffold. *Cells*. 9(5):E1268. **2020** May 20. doi: 10.3390/cells9051268.
9. Cipollaro L, **Ciardulli MC**, Della Porta G, Peretti GM, Maffulli N. Biomechanical issues of tissue-engineered constructs for articular cartilage regeneration: *in vitro* and *in vivo* approaches. *Br Med Bull*. pii: ldz034. **2019** Dec 11. Review. doi:10.1093/bmb/ldz034.
10. Ciaglia E, Montella F, Trucillo P, **Ciardulli MC**, Di Pietro P, Amodio G, Remondelli P, Vecchione C, Reverchon E, Maffulli N, Puca AA, Della Porta G. “A bioavailability study on microbeads and nanoliposomes fabricated by dense carbon dioxide technologies using human-primary monocytes and flow cytometry assay”. *Int J Pharm*. 570:118686. **2019** Oct 30. doi:10.1016/j.ijpharm.2019.118686.
11. Della Porta G, **Ciardulli MC**, Maffulli N. “Microcapsule technology for controlled growth factor release in musculoskeletal tissue engineering”. *Sports Med Arthrosc Rev*. 26(2):e2-e9. **2018** Jun 26. Review. doi:10.1097/JSA.000000000000188.

Book chapters

1. **Ciardulli MC**, Aicale R, Maffulli N, Della Porta G. Chapter 15: Scaffolds for regeneration of meniscus lesions. In: *Handbook of Tissue Engineering scaffold*. Vol One. 2019 Eds. Elsevier, ISBN 978-0-08-102563-5, pp. 329. **2019** June 18. Book Chapter.

Oral presentations at International Conferences

1. “Tenogenic commitment of hBM-MSCs cultivated into a 3D scaffold under dynamic conditions by means of a cyclic strain bioreactor”. **9° I.S.MuL.T. Congress**. “Open mind and new technologies in muscles, ligaments and tendons”. Verona, 29th – 30th November **2019**.
2. “Tenogenic commitment of hBM-MSCs induced by controlled delivery of hGDF-5 and cyclic strain within a 3D multiphase microenvironment”.

- TERMIS EU 2019 meeting.** “Tissue engineering therapies: from concept to clinical translation & commercialization”. Rhodes, 27th – 31st May **2019**.
3. “hGDF-5 and cyclic strain controlled delivery for the tenogenic commitment of hBM-MSCs in a 3D microenvironment”. **8° I.S.MuL.T. Congress.** “Open mind and new technologies in muscles, ligaments and tendons”. Salerno, 30th November – 1st December **2018**.

Poster presentations at International Conferences

Ciardulli MC, Marino L, LoVecchio J, Palazzo I, Santoro A, Reverchon E, Giordano E, Selleri C, Maffulli N, Della Porta G. “hGDF-5 and cyclic strain controlled delivery for the tenogenic commitment of hBM-MSCs in a 3D microenvironment”. **8° I.S.MuL.T. Congress.** “Open mind and new technologies in muscles, ligaments and tendons”. Salerno, 30th November – 1st December 2018.

Awards

I.S.MuL.T. & IBSA Foundation “Award 2018” for the best poster.

Acknowledgements

There are many people whom I would like to thank for their contribution, both directly and indirectly, to this thesis.

I would first like to sincerely thank my supervisors, professor Nicola Maffulli and professor Giovanna Della Porta for the esteem and the trust placed in me and in my work. Furthermore, I am especially grateful to professor Giovanna Della Porta for allowing me to fully express my personality and my ideas, being optimistic in the face of my moments of negativity and supportive when I needed it.

I would like to acknowledge professor Emanuele D. Giordano and Dr. Joseph Lovecchio for their essential contribution to bioreactors realization, for all the nice scientific discussions and for their good advices.

My gratitude also goes to the Supercritical Fluids group, professor Ernesto Reverchon, Dr. Mariarosa Scognamiglio and Dr. Ida Palazzo, for the valuable support to my work and for the availability demonstrated at every turn.

It is my privilege to thank professor Nicholas R. Forsyth and his research team for greeting me in his laboratories at Keele University, for his precious suggestions, for sharing his knowledge and for contributing to improve my cultural and professional background.

I am extremely thankful also to my tutor, Dr. Devis Galesso, and his team at Fidia Farmaceutici S.p.A. for the keen interest in my project, for the kindness, enthusiasm and for the sacrifice of their time for the training lessons. I am really sorry about the impossibility of working with them in person.

Sincere thanks to my laboratory colleagues, Erwin and Pasqualina, with whom I have shared moments of deep anxiety but also of big excitement and happiness. Thank you for supporting me in my research activity and for putting up with my stresses and moans!

Some special words of thanks go to my friends, Federica, Sara, Chiara, Rita, Antonella and Giuseppe who have always been a major source of encouragement. Thank you guys for always being there for me in my bad and good times.

I would like to express my deepest gratitude to my uncles, Carmine and Nicla, for being my second family, for having always pushed me to go ahead in my professional career, cheering for me and truly rejoicing in my successes.

The last word goes to my parents, Gino and Annamaria, and my sister, Laura, for their unconditional love and endless patience, for always showing how proud they are of me and for giving me the extra strength and motivation to get things done. They are the reason for who I am today, so this thesis is dedicated to them.